IAEA-TECDOC-491

NUCLEAR DATA FOR THE CALCULATION OF THERMAL REACTOR REACTIVITY COEFFICIENTS

PROCEEDINGS OF AN ADVISORY GROUP MEETING
ORGANIZED BY THE
INTERNATIONAL ATOMIC ENERGY AGENCY
AND HELD IN VIENNA, 7–10 DECEMBER 1987

A TECHNICAL DOCUMENT ISSUED BY THE
INTERNATIONAL ATOMIC ENERGY AGENCY, VIENNA, 1989

The IAEA does not normally maintain stocks of reports in this series. However, microfiche copies of these reports can be obtained from

INIS Clearinghouse
International Atomic Energy Agency
Wagramerstrasse 5
P.O. Box 100
A-1400 Vienna, Austria

Orders should be accompanied by prepayment of Austrian Schillings 100,– in the form of a cheque or in the form of IAEA microfiche service coupons which may be ordered separately from the INIS Clearinghouse.

PLEASE BE AWARE THAT
ALL OF THE MISSING PAGES IN THIS DOCUMENT
WERE ORIGINALLY BLANK

NUCLEAR DATA FOR THE CALCULATION OF
THERMAL REACTOR REACTIVITY COEFFICIENTS
IAEA, VIENNA, 1989
IAEA-TECDOC-491
ISSN 1011–4289

Printed by the IAEA in Austria
January 1989

FOREWORD

On its 15th meeting in Vienna, 16-20 June 1986, the International Nuclear Data Committee (INDC) considered it important to review the accuracy with which changes in thermal reactor reactivity resulting from changes in temperature and coolant density can be predicted. It was noted that reactor physicists in several countries had to adjust the thermal neutron cross-section data base in order to reproduce measured reactivity coefficients. Consequently, it appeared to be essential to examine the consistency of the integral and differential cross-section data and to make all the information available which has a bearing on reactivity coefficient prediction. Following the recommendation of the INDC, the Nuclear Data Section of the International Atomic Energy Agency, therefore, convened the Advisory Group Meeting on Nuclear Data for the Calculation of Thermal Reaction Reactivity Cofficients, in Vienna, Austria, 7-10 Dec. 1987. The Conclusions and Recommendations of the meeting together with the papers presented, are submitted in the present document.

The Agency wishes to express its sincere thanks to J.L. Rowlands not only for his excellent chairmanship during the meeting but also for the final wording of the conclusions. The Agency also thanks all participants for coming to Vienna and for contributing to the success of the meeting.

EDITORIAL NOTE

In preparing this material for the press, staff of the International Atomic Energy Agency have mounted and paginated the original manuscripts as submitted by the authors and given some attention to the presentation.

The views expressed in the papers, the statements made and the general style adopted are the responsibility of the named authors. The views do not necessarily reflect those of the governments of the Member States or organizations under whose auspices the manuscripts were produced.

The use in this book of particular designations of countries or territories does not imply any judgement by the publisher, the IAEA, as to the legal status of such countries or territories, of their authorities and institutions or of the delimitation of their boundaries.

The mention of specific companies or of their products or brand names does not imply any endorsement or recommendation on the part of the IAEA.

Authors are themselves responsible for obtaining the necessary permission to reproduce copyright material from other sources.

CONTENTS

NUCLEAR DATA FOR THE CALCULATION OF THERMAL REACTOR REACTIVITY COEFFICIENTS — A BRIEF INTRODUCTION

J.L. ROWLANDS
Winfrith Atomic Energy Establishment,
United Kingdom Atomic Energy Authority,
Dorchester, Dorset,
United Kingdom

Abstract

Several reactor physics groups have been unable to reproduce the measured values of thermal reactor reactivity coefficients using current evaluations of nuclear data. Consequently they have used modified data in the thermal energy region. In response to this problem differential cross section measurements have been made at Geel and Harwell. This paper briefly summarises the nuclear data changes made by these reactor physics groups and also summarises the assumptions made by some reactor physicists about the effect of crystalline structure on Doppler reactivity coefficients.

---

1. SHAPES OF ACTINIDE CROSS-SECTIONS AT THERMAL ENERGIES

As a consequence of the analysis of thermal reactor reactivity coefficient measurements changes have been proposed to the shapes of cross sections for the primary actinides in the thermal energy range (that is, from about 0.01 eV to 0.1 eV). In particular, changes have been proposed for the energy dependence of:

(a) Eta for uranium-235

and (b) Capture for uranium-238

In ENDF/B-V 235U eta varies by less than about 0.2% below 0.1 eV whereas Santamarina, Golinelli and Erradi (1984) [1] propose a value which increases by about 2% from 0.01 eV to a maximum value at about 0.08 eV. In JENDL-2 (JEF-1) the 238U capture cross section decreases slightly less rapidly than a 1/v form (being about 2% higher than this at 0.1 eV) whereas Santamarina et al propose a more rapid decrease than the 1/v form, the variation being about 20% greater between 0.01 and 0.1 eV. These changes are based on measurements of temperature coefficients in light water moderated lattices.

In his earlier study of the reactivity temperature coefficient in light water reactors Edenius (1976) [2] recommended a similar adjustment to the shape of the 238U capture cross section in order to improve the agreement between calculation and measurement of reactivity coefficients.

A similar adjustment to 235U eta to that of Santamarina et al was adopted in the 1981 Version of the WIMS library [3] (Halsall, 1982). The value of eta increases to a maximum at an energy of about 0.09 eV, the value at the maximum being about 2.4% higher than the value at 0.01 eV. This adjustment had been proposed earlier by Askew (1971) [4] to make calculated moderator temperature coefficients less negative and also help to improve the agreement between the values of effective multiplication, keff, calculated for different types of thermal system: the well-thermalised ORNL uranyl nitrate spheres, lattices of natural uranium with D_2O moderation and lattices of enriched uranium with H_2O moderation.

As a consequence of these proposals requests for measurements of the energy dependence of eta and of cross sections at thermal energies were included in the NEA High Priority Nuclear Data Request List. Measurements have now been carried out at Geel and at Harwell and it is possible to reconsider the validity of these adjustments.

Information about the shapes of cross sections at thermal energies can also be obtained from the reaction rate measurements made for a range of moderator temperatures (from about -200°C to 300°C) by Okazaki and Jones [5]. The measurements give the values of the cross sections averaged over a Maxwellian spectrum, with a temperature corresponding to that of the moderator. Measurements have been made for fission in 233U, 235U and 239Pu and capture in 232Th and 238U (relative to 55Mn capture).

Changes to the shapes of actinide cross sections at thermal energies could have implications for the values of 2200 m/sec parameters derived from a simultaneous fit to 2200 m/sec measurements and Thermal Maxwellian Average values.

2. INFLUENCE OF SOLID STATE EFFECTS ON DOPPLER COEFFICIENT CALCULATIONS

The revisions to the shapes of cross-sections at thermal energies are made to improve the calculation of the variation of reactivity with changes in the thermal neutron spectrum. The fuel temperature coefficient is dominated by the 238U Doppler effect. So as to improve the agreement between calculated and measured fuel temperature, or power coefficients, both Edenius and Santamarina et al have assumed that solid state effects have a significant effect on Doppler coefficients measured at room temperature. The gas model of Doppler broadening is used with an effective temperature which is higher than the actual temperature by an amount which is determined by the Debye temperature, θ_D. At temperatures above the Debye temperature the effective temperature is given, approximately, by:

$$T^* = T(1 + 0.05\ (\frac{\theta_D}{T})^2)$$

and the effective temperature is about 5% higher than the actual temperature when the temperature equals the Debye temperature. At lower temperatures the effective temperature is relatively higher than the actual temperature. In some studies a Debye temperature of about 620^{0}K is assumed for UO_2 whereas analyses of resonance shapes and neutron diffraction studies are consistent with an effect corresponding to a Debye temperature of about 250^{0}K, (see for example, Butland, 1974 [6]). The adoption of a high value for the Debye temperature, as is done by both Edenius and by Santamarina et al, reduces the magnitude of the negative fuel temperature coefficient calculated for measurements starting at room temperature but has only a very small effect on values calculated for a reactor at operating temperatures. Consequently, if this assumption of a high Debye temperature is incorrect and there is a different reason for the overestimation of the magnitude of the fuel temperature coefficient at low temperatures the fuel temperature ocefficient might be overestimated in calculations for operating reactors.

3. OTHER POSSIBLE EXPLANATIONS FOR DISCREPANCIES

A number of possible alternative explanations for the discrepancies between calculated and measured temperature coefficients have been investigated by Edenius.

Edenius concluded that approximations in the representation of nuclear data in lattice cell calculations were not a significant source of error. However, it is important to verify that the approximations used in each analysis are acceptable. In particular, it is necessary to ensure that the number of energy groups used in the thermal range, the neglect of temperature dependence of cross-sections in this range and the usual neglect of solid state effects on total and partial cross sections are not introducing errors. The treatment of the resonance region also requires validation by comparison with lattice slowing down calculations made using a very fine energy representation.

The effect of using different thermal scattering models for light water was also examined by Edenius and he concluded that the use of an altenative model would not reproduce the measured reactivity coefficients more accurately. However, the use of alternative thermal scattering models for D_20 and graphite might reduce the discrepancies for the values of keff and reactivity coefficients for systems with different moderators.

4. OTHER ANALYSES RELATING TO REACTIVITY COEFFICIENTS

Williams et al (1985) [7] have carried out an analysis of thermal reactor benchmarks using ENDF/B-V data and the reactor design code EPRI-CELL. Resonance integrals have been calculated to compare with Hellstrand's measurements for UO_2 pins in D_20 moderator. The comparison is made for two valus of the fuel pin radius (0.52 and 1.04cm) and two temperatures, 300 and 900K. Calculation overestimates the measured resonance

integrals by between about 1 and 3%. The change with temperature is overestimated by 6% and 8%, respectively, for the two sizes of fuel pin. These differences are within the uncertainties on the measurements.

The results of calculations for twenty-one UO_2 fuelled, H_2O moderated lattices are also presented. The uranium enrichments range from 1.3% to 4.02%. The calculated values of keff are, on average, 0.2% high and, with only 2 exceptions, all the values lie within 0.25% of this mean value (the other two differing by + 0.38% and -0.54%).

Ozer [8] describes Monte Carlo calculations made using ENDF/B-V data and the comparison of these with the results obtained using the design code, CELL-2. These include U-metal and UO_2 temperature coefficients. Calculation is within a few percent of the measured values. Using ENDF/B-V improved the accuracy of prediction of the hot critical reactivity by about 0.5% $d\rho$ for the ZION 2 reactor, largely eliminating the earlier discrepancy.

Selected thermal reactor benchmark experiments have been analysed by Bernnat et al (1986) [9] using JEF-1 data and the RSYST/CGM calculational scheme. JEF-1 uses the ENDF/B-V evaluation for 235U but the 238U evaluation is different from ENDF/B-V. The JEF-1 values of the 238U capture at 2200 m/sec and the capture resonance integral are the same as ENDF/B-V but the Maxwellian average is 0.3% higher. For the five ORNL nomogeneous uranyl nitrate solutions, (1 to 4 and 10) the three UO_2 fuelled, water moderated, BAPL lattices (1, 2 and 3) and the four tight lattices (HI-C, UO_2, 3, 10, 11 and 13) the calculated values of keff are all within 0.15% of unity. For the metal fuelled, water moderated lattices (TRX-1, 2, 3 and 4) the calculated values of keff are not in such good agreement, the value for TRX-1 being underestimated by 0.4%, TRX-2 by 0.27% and TRX-4 by 0.21%. For the series of three lattices consisting of natural uranium rods with D_2O moderation (MIT-1, 2 and 3) the underestimation of keff is larger, being about 0.7%. Changes both to the absolute values of thermal cross-sections and to the energy shapes of the cross sections would alter these relative differences.

REFERENCES

[1] SANTAMARINA, A., GOLINELLI, C., ERRADI, L., Temperature Effects Analysis in Light Water Reactor Lattices ANS Topical Meeting on Reactor Physics, Chicago (1984).

[2] EDENIUS, M., Studies of the Reactivity Temperature Coefficient in Light Water Reactors. AE-RF-76-3160 (1976).

[3] HALSALL, M. J., Recent Adjustments to the WIMS Nuclear Data Library. AEEW-R1492 (1982)

[4] ASKEW, J. R., A Proposed Adjustment of the U235 Thermal Cross-Section.
Internal AEE Winfrith Document (1971).

[5] OKAZAKI, A., JONES, R. T., Measured Dependence of Some Effective Cross Sections on Thermal Neutron Temperatures in the Range -195°C to 297°C.
(Paper to this Meeting)

[6] BUTLAND, A. T. D., Annals of N.S & E.1, p.575 (1974)

[7] WILLIAMS, M. L., ERRADI, L., Analysis of Thermal Reactor Benchmarks with Design Codes based on ENDF/B-V Data.
Nuclear Technology, 71, 2, p.386 (1985).

[8] OZER, O., LWR Analysis Experience with ENDF/B-V Data.
Proc. Topical Meeting on Reactor Physics and Safety
p. 1101, Saratoga Springs, N.Y. (1986)

[9] BERNNAT, W., et al. Analysis of Selected Thermal Reactor Benchmark Experiments based on the JEF-1 Evaluated Nuclear Data File.
IKE 6-157, JEF Report 7 (1986)

CONCLUSIONS AND RECOMMENDATIONS

1 TEMPERATURE COEFFICIENTS OF REACTIVITY

1.1 Accuracy requirements

Participants at the Advisory Group Meeting considered the following calculational target accuracies to be appropriate:

$$(C - E) = \pm 1 \text{ to } 2 \text{ pcm}/^0C \text{ (2 s.d.)}$$

for the moderator temperature coefficient, and

$$(C-E)/E = \pm 10\% \text{ (2 s.d.)}$$

for the fuel temperature coefficient,

where (C-E) is the difference between calculation, C, and experiment, E.

1.2 Current status

The agreement between calculation and measurement, (C-E), differs in different countries and for different reactor types. It also differs for the comparison with measurements made on critical facilities and on operating reactors. In some countries (for example, France, Sweden and the UK) nuclear data have been modified so as to improve the agreement between calculation and experiment.

For isothermal measurements:

a) Using unmodifed data

For light water reactor critical facilities (Sweden, France and UK)

$$(C - E) \simeq -2 \text{ to } -8 \text{ pcm}/^0C$$

For operating light water reactors (France, Sweden)

$$(C - E) \simeq -2.5 \text{ pcm}/^0C \ (\sim 100^0C \text{ to } 300^0)$$

Using some calculational schemes there is a discrepancy of about 0.5% to 1.0% dK in the change in keff on going from cold to hot critical.

The use of unmodifed ENDF/B-V data in LWR design codes has been shown to give results within the experimental uncertainty for a large LWR (USA).

For gas cooled graphite moderated critical facilities (UK)

$$(C - E) \simeq -1 \text{ to } -2 \text{ pcm}/^0C \text{ for uranium fuel}$$

and there is agreement between C and E for plutonium fuel.

For 235U/Th gas cooled graphite moderated reactors there is no significant discrepancy, neither for reactors nor critical

facility measurements, when the standard design calculational methods are used. However, ENDF/B-V Version 1 data for thorium were not so satisfactory (USA).

There is very little information openly available for MOX fuel. Some experiments have been carried out in Sweden and France.

b) Using modified data

France:

For light water reactors

$(C - E) \simeq -1$ pcm/^{0}C (cold)

$(C - E) \simeq -1$ to -2 pcm/^{0}C (hot)

Sweden:

For the light water reactor critical facilities

$(C - E) \simeq 0$ pcm/^{0}C (20^0C to 245^0C)

For light water reactors

$(C - E) \simeq 0$ to $+ 0.5$ pcm/^{0}C (hot)

UK:

Using modified 235U η data, (C-E) for all systems is increased by 1 pcm/^{0}C (ie becomes less negative). There is now believed to be no significant error for graphite or water reactors (ie (C-E) $\simeq$ 0 to -1 pcm/^{0}C), although (C - E) for low enriched critical LWR facilities remains about -4 ± 2 pcm/^{0}C.

1.3 Modifications made to data to improve predictions of temperature coefficients

These have been made in France, Sweden and the UK.

a) Shapes of cross sections in the thermal energy range: (ie below about 0.1 eV)

i) 235U σ_f (France)

ii) 235U eta (France, UK)

iii) 238U capture (France, Sweden)

b) Other changes:

iv) A high Debye temperature of about 620^0K has been adopted for U in UO_2. This reduces the calculated Doppler effect particularly at low temperatures (300^0K) (France and Sweden). This value was adopted

in France in order to improve the agreement between calculation and measurement of Doppler worth in MINERVE.

v) Adoption of an improved graphite thermal scattering model in 1972 improved the calculation of moderator temperature coefficients (UK). (This revision predated the studies leading to the change in 235U eta described above).

These changes were not uniquely determined by the integral measurements. They were chosen to be consistent with the uncertainties in the differential nuclear data (and in the Debye temperature) and also with possible resonance parameter representations (France, Sweden). It is believed by the groups making these changes that changes must be applied to nuclear data for the fuel isotopes in order to correct for the discrepancies although it cannot be excluded that approximations in the representation of nuclear data and in the calculational methods are contributing to the discrepancies.

Concerning the void reactivity effect in normal light water reactors, the experimental information is meagre. The void coefficient is related to the coolant density component of the temperature coefficient and the uncertainties can be related.

2 RESULTS OF RECENT NUCLEAR DATA MEASUREMENTS AND STUDIES

Measurements have been carried out at CBNM Geel of energy shapes at thermal energies for fission of 233U, 235U and 239Pu, for eta of 235U, and for capture of 238U. The results are preliminary pending the completion of measurements below about 20 meV being made at ILL Grenoble. Measurements of 235U eta have also been made at Harwell.

Studies of solid state effects in Doppler broadening have been made at Harwell and in the USA.

Measurements of Maxwellian spectrum averaged cross sections have been made for a range of moderator temperatures (-200°C to 300°C) at Chalk River (Canada).

2.1 235U fission.

The high precision shape measurement made at Geel is consistent with ENDF/B-V above about 20 meV but is about 1.5% lower below about 20 meV. The Chalk River Maxwellian spectrum measurements are consistent with these measurements and also with ENDF/B-V. The shape adopted in the French cross section set is consistent with the Geel measurement.

2.2 238U capture.

The Geel curve is consistent with a 1/v dependence or with the slightly less rapid variation adopted in ENDF/B-V, both being consistent with the Chalk River measurements. The measurements are not consistent with the more rapid variation adopted by the French group (a 20% reduction relative to 1/v between 10 meV and 100 meV) nor the variation proposed by Edenius (Sweden) in 1976.

(The current Swedish thermal reactor data library contains 238U capture data in the thermal range which was revised by Edenius and which has a smaller variation through the thermal range).

2.3 235U eta.

Sample size corrections have been found to be important in the analysis of the Geel measurements. Below 70 meV the resulting preliminary data are consistent with the variation adopted by the French group rather than with the constant value adopted in ENDF/B-V. The measurements to be made at ILL will provide an independent check on the data below 20 meV. The measurements made at Harwell have a larger uncertainty particularly below 10 meV, and are not accurate enough to distinguish between the constant value adopted in ENDF/B-V and the data adopted by the French group. There is an indication of a structure in the energy dependence at about 70 meV which could be due to solid state effects. This is seen in both the Harwell and the Geel measurements. Some of the structure in the Geel measurements could be due to the use of beryllium to tailor the neutron spectrum. The energy dependence adopted in the UK (WIMS) data set between 50 meV and 150 meV is not supported by the measurements.

2.4 Crystalline binding effects in Doppler broadening

Studies of the energy shapes of resonances and of the temperature dependence of thick sample transmission made at Harwell are consistent with the recommendation of Butland which proposes that an acceptable approximation is the use of the gas model with an effective temperature of the form:

$$T_{eff} = T\left(1 + 0.05\left(\frac{T_0}{T}\right)^2\right)$$

where $T_0 \propto 250^0K$ for U in UO_2

A study has also been made by Sher (1984 ANS Meeting in New Orleans). He points out that the lower frequency vibrations are carried by the uranium nuclei and the higher frequency vibrations by the oxygen nuclei. Although the crystalline binding effects result in a small asymmetry in the cross-section shape in a resonance Sher concludes that the recommendation of Butland should be satisfactory.

The Harwell group see some evidence of crystalline structure effects in low energy resonances and consider that more work is desirable, bearing in mind the importance of the Doppler effect and the conflicting conclusions drawn from some thick sample measurements (eg Brugger and Aminfar). Effective temperatures can be deduced from thick sample transmission measurements made at a range of temperatures and the Harwell group recommend more measurements of this type.

2.5 Conclusions drawn from the results of the recent differential cross section measurements

Following the completion of the measurements described in this section a reanalysis of the integral measurements, using the new

data, is required. It would be preferable to include measurements made using different moderators (H_2O and graphite) in these reanalyses. Meeting participants considered that it would be valuable if an accurate benchmark temperature coefficient measurement could be carried out for a regular lattice. Spectral indicator measurements in the thermal range could help to determine the variation of the thermal spectrum with temperature.

Even though the modifed data in some current data sets are not now within the uncertainties of the differential nuclear data it is considered that the continued use of these data sets (in the associated calculational schemes) is preferable to the adoption of the new data until extensive validation (and consequent modification of other items of data) has been carried out. In some cases it might be necessary to increase the uncertainties of predictions for systems and properties which lie outside the range of validation of the current data sets.

3 CALCULATIONAL METHODS APPROXIMATIONS AND METHODS DEVELOPMENT

Ishiguro pointed out problems with the F-Table method (based on homogeneous-medium slowing-down calculations) when applied in Advanced Light Water Reactor studies. He considered this to be a consequence of the rapid flux attenuation through the resonance energy range.

Some groups take account of the temperature dependence of all cross sections in the thermal energy range whereas others treat this dependence only for the 1 eV 240Pu resonance. It is considered that an investigation is needed of the accuracy of the current data and methods used to treat the 240Pu resonance, the temperature dependence of the absorption and its influence on void coefficients. It is not usual to allow for crystalline effects in the cross sections for the fuel isotopes at thermal energies. The effect of these should be examined.

Tebin described his Generalised Subgroup Method. In the SAPHIRE code the variation of temperature across a fuel pin and the variation of the composition (such as plutonium build-up near the surface of the pin) is allowed for. The subgroup parameters are interpolated in temperature (in the form $a + b\ T + c.T$). The method includes a treatment of the correlation between subgroups.

New calculational systems are being developed in several countries. In particular methods for treating new designs of PWR are being developed.

4 REQUIREMENTS FOR THE DESIGN OF ADVANCED LIGHT WATER REACTORS

These reactors aim to have a high conversion ratio and to recycle plutonium. The thermal component of the spectrum is small and the resonance range assumes greater importance.

The results of more recent critical experiments are proprietary and so the status of validation of methods and data is different in different countries. The NEACRP has organised a calculational

benchmark intercomparison to enable participants to form a view on the status of their methods. There are significant differences between the results of calculations made using different nuclear data libraries.

The prediction of the void coefficient for different void fractions, different stages of burnup and different absorber configurations has an uncertainty which it is desirable to reduce. There is a need for more data for intermediate coolant fractions. Treatment of the Doppler effect could require improved calculational methods and experimental validation. It is also considered desirable to improve the accuracy of prediction of burnup characteristics.

Self-shielding effects become more important not only for the primary actinides but also for fission product isotopes (a 5% effect) and for the 242Pu resonance at 2.67 eV, for example. Self-shielding is also important for resonances in the thermal energy range.

It is not only the infinite dilute cross section of 238U which must be known, but the parameters affecting the resonance shielding (which is calculated to be significantly different using different evaluations). It is recommended that as well as providing data on the uncertainty in the infinite dilute cross section of 238U evaluators should provide an estimate of the accuracy of the shielded cross section (calculated for a background cross section of σ_b = 10 barns) and the variation with temperature between 300°K and 1000°K.

5 RECOMMENDATIONS

5.1 Nuclear data measurement and evaluation requirements

The importance of completing the low energy measurements of 235U eta and 235U fission planned for ILL Grenoble is emphasized. These measurements must be followed by evaluations of the data. A revision of the 235U g-factors input to the Axton 2200 m/sec data evaluation is required. These factors will now have lower uncertainties.

Additional measurements should be carried out to improve the accuracy of 235U eta and alpha in the thermal and epithermal range. There is also a need for corresponding measurements for 239Pu.

Further measurements to clarify crystalline binding effects in Doppler broadening are considered to be important.

Evaluators are requested to provide information on shielded cross-sections as well as infinite dilution values. In particular, for 238U the uncertainty in the capture cross-section calculated with shielding corresponding to σ_b = 10 barns and in the difference between the values at 300°K and 1000°K (averaged over broad energy intervals) is requested.

5.2 Reactivity coefficient measurements and analyses

There is a requirement for reference benchmark temperature coefficient measurements carried out in uniform lattices (between

about 10°C and 80°C, for example) to an accuracy of ± 1 pcm/°C. Data are required for both uranium and plutonium lattices. If such measurements have already been carried out it is requested that participants enquire if the descriptions can be made available to the IAEA NDS and other participants. Data for tight lattices are considered to be of particular interest. Reference Doppler, or fuel temperature coefficient measurements, are also requested for both UO_2 and MOX lattices. Benchmark experiments on the void coefficient in tight pitched lattices are also required. One set of benchmark results which is available is for the KRITZ-1 core. This consists of an array of UO_2 pins in water, the uranium enrichment being 1.1882%. The temperature range of the experiments is 20°C to 210°C and the uncertainty in the change of keff with trmperature is less than 100 pcm (see EPRI NP-2855, p 25-6).

Following the reanalysis of reactivity coefficient measurements, made using evaluations which take into account the new differential measurements, participants are asked to exchange information about data modifications made and the accuracy of prediction of measured reactivity coefficients.

Participants are requested to collaborate on work to resolve differences between the conclusions drawn from reactivity coefficient measurements made on different systems. Participants are asked to keep the IAEA NDS informed of progress.

5.3 Internationally available calculational systems

There is a requirement for an internationally available thermal reactor neutronics calculational scheme and associated nuclear data library which could be made available through the IAEA for reference calculations, reactor studies and training purposes. Such a scheme is also required for studies relating to the conversion of research reactors which at present use high enrichment fuel to the use of low enrichment fuel.

There is also a requirement for a compilation of references to integral data available for testing such a library, including reactivity coefficient measurements.

Participants were asked to provide the IAEA NDS with information on availability of calculational schemes and also to provide references to suitable integral measurements.

5.4 Proposed benchmark intercomparison

A benchmark intercomparison exercise is recommended for comparison of calculations of moderator and fuel temperature coefficients and coolant density coefficients for a conventional PWR.

5.5 NEACRP benchmark intercomparison for high conversion light water reactors

Members of NEACRP who attended the AGM were asked to enquire if the IAEA NDS and participants can be kept informed of the results of the NEACRP HCLWR benchmark intercomparison.

PAPERS PRESENTED AT THE MEETING

EFFECT OF FUEL BURNUP AND CROSS-SECTIONS ON MODULAR HTGR REACTIVITY COEFFICIENTS

W. LEFLER, A. BAXTER, D. MATHEWS
GA Technologies, Inc.,
San Diego, California,
United States of America

Abstract

The temperature dependence of the reactivity coefficient in a prismatic block Modular High-Temperature Gas-Cooled Reactor (MHTGR) design is examined and found to be large and negative. Temperature coefficient results obtained with the ENDF/B-V data library were almost the same as results obtained with the earlier versions of the ENDF/B data library usually used at GA Technologies Inc. (GA) in spite of a significant eigenvalue increase with the ENDF/B-V data. The effects of fuel burnup and arbitrarily assumed cross section variations were examined and tabulated.

1. INTRODUCTION

The active core of the 350 MW(t) MHTGR is annular in configuration, shaped to provide a large external surface-to-volume ratio for the transport of heat radially to the reactor vessel in case of a loss of coolant flow [1]. For a given fuel temperature limit, the annular core provides approximately 40% greater power output over a typical cylindrical configuration. The reactor core is made up of columns of hexagonal blocks, each 793-mm high and 360-mm wide. The active core is 3.5 m in o.d., 1.65 m in i.d., and 7.93-m tall. Fuel elements contain coated microspheres of 19.8% enriched uranium oxycarbide and of fertile thorium oxide. The core is controlled by 30 control rods which enter the inner and outer side reflectors from above.

A significant feature of the Standard MHTGR design is its capability for passive decay heat rejection. In the unlikely event that both the normal and shutdown cooling systems are unavailable, decay heat must be rejected by radiation, conduction, and natural convection from the core to the reactor vessel wall and outward to air-cooled panels within the reactor cavity structure. These passive decay heat rejection requirements influence the shape and size of the reactor core. A relatively tall core with a high surface-to-volume ratio provides acceptable fuel temperatures during a total loss of coolant flow, whether the primary coolant system is pressurized or depressurized. At the rated core thermal power of 350 MW, the peak fuel temperature is approximately 1600°C for the most severe loss-of-forced circulation case. This temperature is well within the limits for high retention of fission products by the all-ceramic coated fuel particles.

2. MHTGR REACTIVITY COEFFICIENTS

Whenever there is a change in the operating condition or configuration of a reactor, a change in reactivity may be induced. Such changes are important for controlling heat generation and thus for reactor safety. They influence the course of a reactivity transient and determine the degree of stability during reactor operation. These reactivity changes are defined in terms of coefficients, i.e., the reactivity change produced by a unit change in the variable of interest. For analytical purposes, a coefficient can be quantified by partial coefficients each depending on separate reactor changes to the variable of interest. For example, a core temperature coefficient of reactivity is composed of contributions from changes in the resonance energy range neutron cross section of fuel compact nuclides (Doppler effect) and in thermal neutron energy spectrum (moderator effect) as functions of temperature, i.e.,

$$\frac{dk_{eff}}{k_{eff}} = \frac{1}{k_{eff}} \frac{\partial k_{eff}}{\partial T_f} dT_f + \frac{1}{k_{eff}} \frac{\partial k_{eff}}{\partial T_m} dT_m$$

where K_{eff} = effective reactivity,
T_f = fuel temperature,
T_m = moderator temperature.

Normally the reactivity changes are quantified by combining all the individual feedback effects into one overall coefficient called the power coefficient. The power coefficient of reactivity is defined as the change in reactivity resulting from a unit change in reactor power level. It is the sum of the reactivity effects caused by a power change, i.e., the reactivity feedback due to temperature change, the reactivity feedback due to changes in coolant density, and the reactivity feedback due to changes in graphite volume and density. Considering the operational or configurational changes in the MHTGR core, only the temperature component of the power coefficient is significant.

The helium coolant is inert and essentially transparent to neutrons. Thus, coolant density or phase changes are insignificant in affecting reactivity of the MHTGR. (In contrast, liquid cooled reactors normally have significant reactivity coefficients associated with the coolant density.) The total loss of helium from the MHTGR core is worth less than 0.01% $\Delta\rho$ in reactivity.

Graphite dimensional changes also have only small reactivity effects, either positive or negative. Graphite expansion with temperature reduces reactivity by reducing the average moderator density, but it also increases reactivity by decreasing core leakage, thus the net effect is small. The thermal neutron absorption cross section for graphite is very small, of the order of only a few millibarns.

The main reactivity feedback effects in the MHTGR are a prompt, instantaneous negative fuel feedback (Doppler), a large negative thermal neutron spectrum feedback (moderator) that is also relatively prompt and a secondary small delayed positive reflector feedback (hours or days to

heatup reflector). The Doppler feedback is due to an increase in the effective cross section for neutron capture in the fertile nuclides (U-238 and Th-232) as the fuel temperature increases. The negative moderator coefficient results from an increase in the mean of thermal neutron energy which increases the effective neutron capture rate compared to the fission rate at higher temperatures.

The MHTGR reactivity change with temperature varies depending on cycle [initial core (IC) or equilibrium] and time in cycle. This change reflects the varying contributions of the fixed burnable poison (FBP), fission products, and the important nuclides which build up from transmutation, such as Pu-239 and Pu-240. The calculated reactivity change, $\Delta\rho = (k_2 - k_1)/(k_1 \cdot k_2)$ with temperature change of the active core at the beginning of cycle (BOC) of the IC and at the end-of-cycle (EOC) of a typical equilibrium (equil) core is shown in Fig. 1. These two cases represent the extremes in reactivity change, and thus in the temperature coefficient curves for the MHTGR core, since the BOC initial core case has no fission product or plutonium buildup, and the EOC equilibrium core case has no FBP and the maximum level of fission products and plutonium. The slope of these curves, when plotted as a function of core temperature, yields the active core temperature coefficient of reactivity, as shown in Fig. 2.

The reactivity change with temperature, as well as the reactivity coefficient as a function of temperature, are shown as a function of the mean fuel temperature in all figures in this paper. In developing these figures, a somewhat lower moderator temperature was assumed at each fuel temperature. The reactivity values were calculated at nominal steady-state full power temperature conditions. The control rod position is assumed to be withdrawn as appropriate for achieving criticality, for calculations of temperature coefficients. If control rods were inserted, the negative coefficients would be stronger.

The active core isothermal temperature coefficient is different in both magnitude and shape (as a function of temperature) for BOC conditions compared to EOC conditions as shown in Fig. 2. The difference is

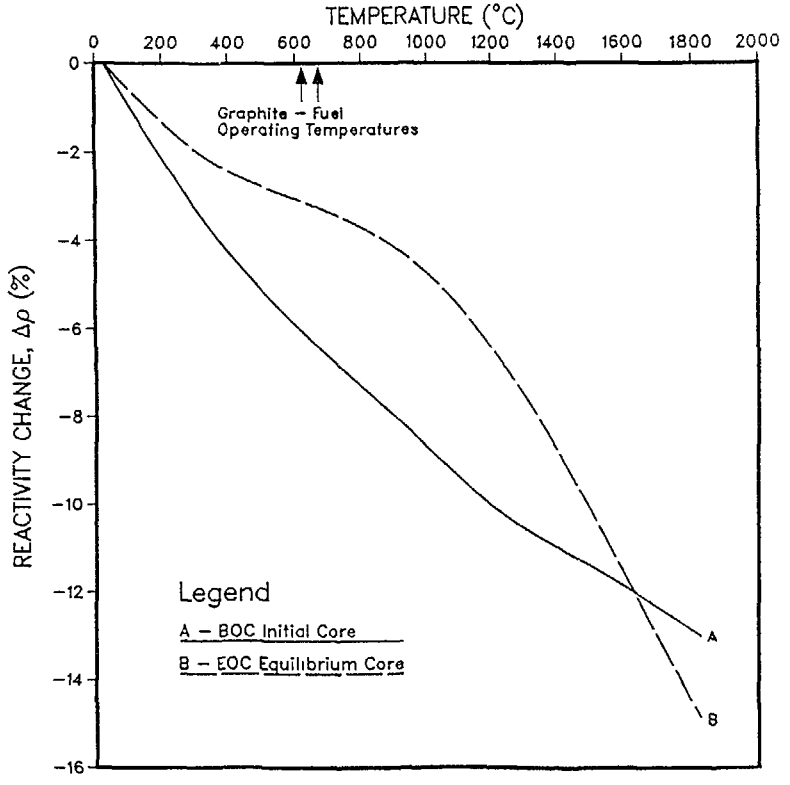

Fig. 1. MHTGR reactivity change with temperature (constant reflector temperature)

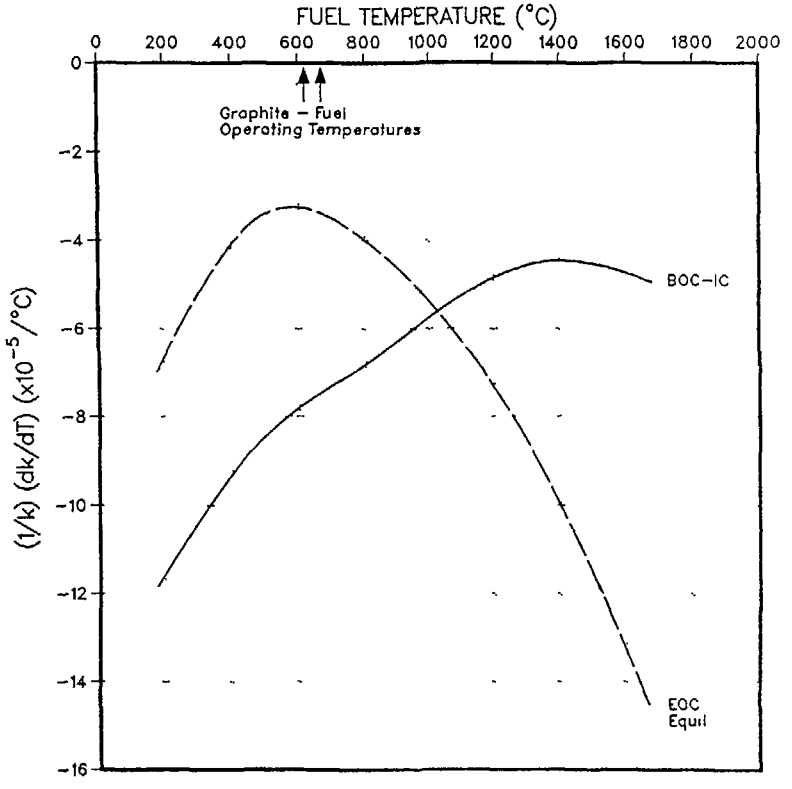

Fig. 2. Core isothermal temperature coefficient at beginning of initial cycle and end of equilibrium cycle

due to differences in the important contributors to the coefficient as shown in Figs. 3 and 4. At IC-BOC conditions, the prompt Doppler coefficient (due to U-238 and Th-232) and the FBP (due to shielded B-10 poison pins) are significant contributors (along with U-235) to the overall coefficient. As shown in Fig. 3, Xe-135 is the only important nuclide which contributes a small positive component to the very negative total coefficient.

At the EC-EOC condition, the FBP loading is depleted and plays no role in the coefficient. The prompt Doppler, and the Xe-135 contributions are essentially the same as for the BOC condition and were not plotted in the Fig. 4 results. Two major contributors of particular interest to the EOC coefficient are Pu-239 (a positive contributor at full power and accident temperatures up to approximately 1300°C) and Pu-240 (a strong negative contributor at accident conditions) although other nuclides, such as U-235, also contribute to the EOC coefficient.

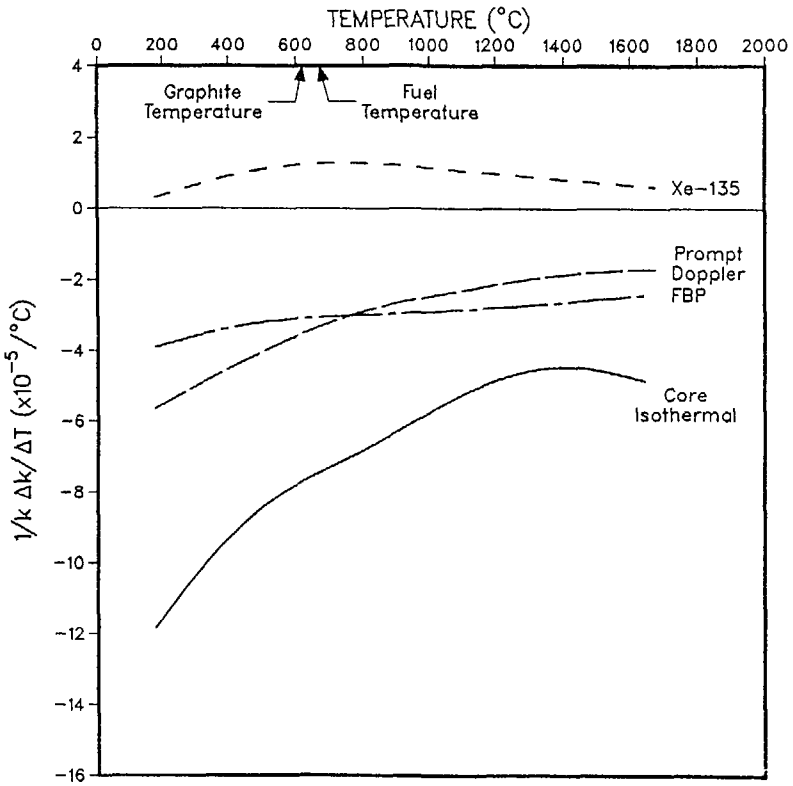

Fig. 3. Principal contributors to isothermal temperatures coefficient (initial core - BOC)

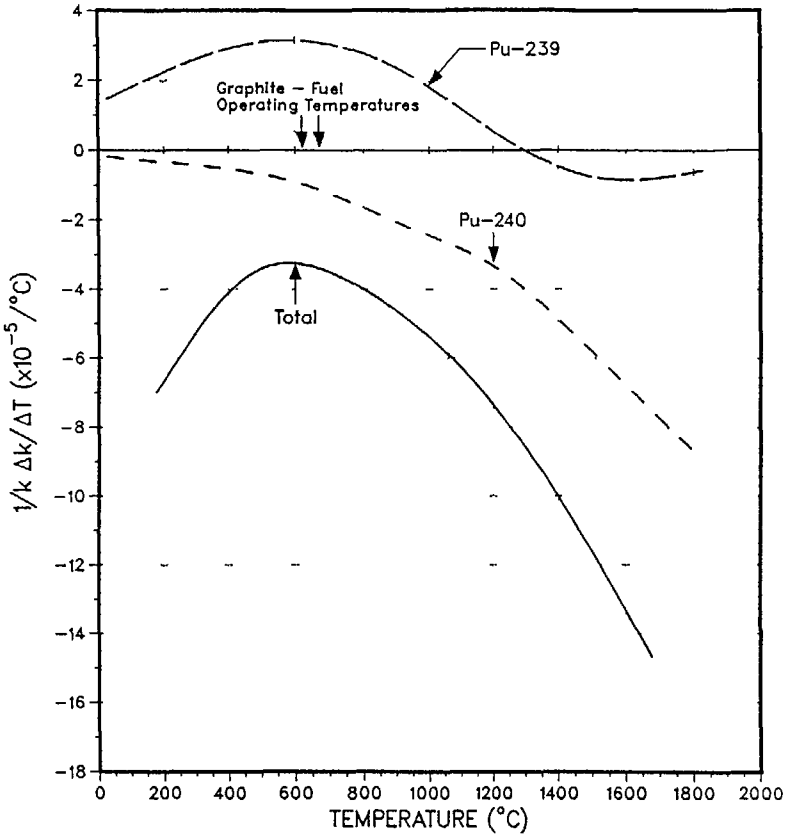

Fig. 4. Plutonium contributors to the temperature coefficient (EOC - equilibrium core)

The Doppler feedback effect is prompt acting and negative at all times in the cycle. The feedback due to FBP, Xe-135, Pu-239, and Pu-240, and essentially all other isotopes in the core, except U-238 and Th-232, is due to temperature changes in the moderator graphite which typically occur 5 to 10 sec later than fuel compact temperature changes following a power level change. The moderator coefficient is a negative feedback for any transients involving fuel temperature increases from nominal full power conditions.

The reactivity defect and temperature coefficient data discussed above refer to the active core temperature coefficient. The reflector temperature coefficient for the MHTGR is positive and this effect reduces the overall reactivity temperature defect from cold to hot conditions. The temperature response of the reflectors greatly lags

that of the active core (typically by hours) and the reflector effect can be neglected in any short-term transient analysis and/or in any events terminated by a reactor trip.

3. EFFECT OF CROSS SECTION DATA

The impact of uncertainty in the cross section of selected nuclides has been evaluated to determine the effects of such uncertainties on the equilibrium EOC isotopics and neutron balance and to quantify their expected impact on the EOC temperature coefficient and k_{eff} of the core. These uncertainty analyses have also included the assessment of the use of the ENDF/B-V cross sections in comparison to the earlier ENDF/B versions normally used in HTGR design calculations at GA.

Concerns related to neutron cross section and plutonium buildup uncertainties have been previously related to the possible effect of such uncertainties on the EOC temperature coefficient of reactivity.

Sensitivity analyses have been completed to quantify the impact of cross section uncertainties on both the core k_{eff} values and EOC isotopic quantities, with a particular emphasis on the EOC isotopic changes and the resultant potential impact of such changes on the EOC temperature coefficient. The sensitivity analyses have consisted of the following:

Step 1: Zero-dimensional (0-D) k_{eff} values and EOC isotopic compositions were compared to the same results calculated from detailed two-dimensional (2-D) depletion estimates using the MHTGR reference cross sections. This comparison established the validity of using the simpler and more readily computed point burnup model results which were then used for further cross section sensitivity studies.

Step 2: Additional 0-D depletion calculations were run for nominal assumed uncertainties in the cross sections (σ) or loadings of selected nuclides (U-238, total U, Pu-239, and Pu-240) to determine the impact of cross section variations on BOC, MOC, and EOC k_{eff} and on EOC reactor isotopics. Compensating effects and/or nonrandom trends were identified, e.g., a higher U-238 resonance cross section would increase the negative fuel Doppler effect due to U-238, but would also increase the plutonium production and thus the positive moderator temperature coefficient contribution due to enhanced Pu-239 buildup, for example. Some interesting compensating effects, due to Pu-239 and Pu-240 buildup effects were identified from the results of these sensitivity studies.

Step 3: The multigroup cross sections of selected nuclides from the GA reference sets used above (ENDF/B-I, II, and III) were compared to current ENDF/B-V data values in the MHTGR spectrum. The reference fuel depletion was repeated with all ENDF/B-V values to assess the magnitude of changes in the EOC compositions and in the calculated EOC temperature coefficient of reactivity due to the use of older cross sections in the GA reference calculations. This comparison eliminated any concerns regarding uncertainties related to the use of older cross section sets since the ENDF/B-V cross sections produced essentially the same temperature coefficient at EOC as was produced with the older cross section sets. The ENDF/B-V coefficients were 2% less negative at normal operating temperatures and 5% more negative at accident temperatures than the coefficients calculated with the older data sets.

Step 4: From the sensitivities developed in Step 2 above, and with the realization that there were essentially no important cross section uncertainties relating to the use of older ENDF/B data as demonstrated in Step 3 above, a highly conservative estimate of the impact of large uncertainties related to individual contributors to the EOC temperature coefficient was developed. This estimate assumed conservative and nuclide specific estimates of the uncertainty in the temperature coefficient contribution due to the particular nuclide. These uncertainties were assumed to be independently random and RMS combined to yield an overall uncertainty in the temperature coefficient.

Preliminary sensitivity study results for k_{eff} and EOC isotopics were compared from a detailed 2-D depletion result and a 0-D depletion result in Step 1. In these, and all other 0-D or point-burnup sensitivity studies and/or one-dimensional (1-D) temperature coefficient calculations, a nine-neutron group (five fast, four thermal) cross section library was used.

In addition to the reference 2-D and point-depletion comparisons based on the use of the reference GA cross section set, six additional point-depletion estimates were performed with modified cross sections (or loadings) for selected isotopes. The purpose of performing the modified point-depeletion runs was to determine the change in the EOC isotopics, k_{eff}, and in certain neutron balance information needed to estimate the impact of such changes on the EOC temperature coefficient or to determine these effects due to the use of the ENDF/B-V data. In all, eight depletion cases were used to complete Steps 1 and 2 above and to provide the ENDF/B-V verification required in Step 3 above.

These cases were:

A - 2-D; reference cross sections.
B - 0-D; reference cross sections.
C - 0-D; U-238 fast microscopic capture cross section (σ_c^f) increased by 5%.
D - 0-D; Pu-240 thermal microscopic capture cross section (σ_c^{th}) for the 1.05 eV capture resonance was increased by 10%.
E - 0-D; Pu-239 thermal microscopic absorption cross section ($\sigma_c^{th} + \sigma_f^{th}$) increased by 10%.
F - 0-D; kg U loaded (N_{U-235} and N_{U-238}) increased by 3%.
G - 0-D; Pu-239 thermal microscopic fission cross section (σ_f^{th}) increased by 10%.
H - 0-D; ENDF/B-V cross sections used.

It should be noted that no special significance should be attributed to the magnitude of the modifications made in Cases C through G. These were arbitrarily chosen in order to obtain the sensitivity to these arbitrary changes.

Table I summarizes the EOC core isotopic loadings (kg) for the heavy metals of most significance for each of these cases. The total EOC heavy metal includes typically 6 or 7 kg (13 to 15 lb) of heavy

TABLE I
MHTGR SENSITIVITY STUDY RESULTS HEAVY METAL (HM) LOADING (kgs) AT EOC

	Case							
	A	B	C	D	E	F	G	H
	Reference 2-D	Reference 0-D	1.05 x^{f} U-238 σ_c	1.10 x^{th} Pu-240 σ_c	1.10 x^{th} Pu-239 σ_a	1.03 x N_u Loading	1.10 x^{th} Pu-239 σ_f	ENDF/B-V
U-235	141.06	136.77	138.83	137.05	137.68	147.63	137.88	136.75
U-236	44.57	44.88	44.61	44.84	44.76	45.35	44.72	43.73
U-238	1550.7	1552.5	1549.4	1552.5	1552.6	1600.7	1553.1	1553.8
Pu-239	14.67	14.25	15.12	14.29	13.09	15.19	13.45	13.72
Pu-240	7.86	7.98	8.32	7.56	8.07	8.13	7.55	8.08
Pu-241	4.99	4.87	5.10	4.98	4.97	5.01	4.63	4.59
Pu-242	2.51	2.38	2.44	2.45	2.43	2.30	2.26	2.69
Th-232	1357.8	1360.2	1360.4	1360.2	1360.3	1360.5	1360.6	1360.8
Pa-233	2.86	2.75	2.72	2.74	2.74	2.67	2.72	2.72
U-233	24.63	24.91	24.99	24.92	24.93	24.92	24.83	24.68
Total HM	3158.6	3158.1	3158.5	3158.1	3158.1	3218.8	3158.2	3158.1

metals such as Np-237, Np-239, Pu-238, and U-232 not specifically listed but which were included in the depletion chains. Table II summarizes the EOC unrodded k_{eff} values predicted for each case at the end of the equilibrium cycle and also the EOC fractional absorptions in U-238, Pu-239, and Pu-240 for each case. The fractional absorptions in U-238 and Pu-240 from the depletion code EOC neutron balance is a measure of the reactivity worth and/or the temperature coefficient contribution magnitude for those specific isotopes. The fractional absorption rate in Pu-239 is also an indicator of its relative contribution to the temperature coefficient for those cases in which the Pu-239 capture to fission cross section ratio remains a constant, i.e., except for Case G. comparison of Cases A and B shows very good agreement in the EOC k_{eff} and also very good agreement (~≤3%) in plutonium and other heavy metal isotopes. This comparison clearly shows that the 0-D model is sufficiently accurate for use in determining the sensitivity effects of interest.

Comparison of Cases C and B results show that a 5% U-238 fast capture cross section increase produces only a 0.003 Δk reduction in core k_{eff} at EOC while increasing the fractional absorptions in Pu-239 by 6% and in Pu-240 by 4%.

Since the effect of a 5% U-238 resonance cross section increase is to increase both the Pu-239 and Pu-240 concentration by about 5%, the result would be to possibly increase the Doppler coefficient (more U-238 capture) and the Pu-240 contribution to the temperature coefficient at accident temperatures by about 2% while the temperature coefficient at normal full power conditions would be somewhat reduced due to the 6% higher Pu-239 loading.

Increasing the Pu-240 resonance cross section for the large 1.05 eV capture resonance by 10% makes essentially no change in the k_{eff} at EOC but, due to saturation effects, results in a 5.3% reduction

TABLE II
EOC CYCLE k_{eff} VALUES AND FRACTIONAL ABSORPTIONS

	Case							
	A	B	C	D	E	F	G	H
	Reference 2-D	Reference 0-D	1.05 x^{f} U-238 σ_c	1.10 x^{th} Pu-240 σ_c	1.10 x^{th} Pu-239 σ_a	1.03 x N_u Loading	1.10 x^{th} Pu-239 σ_f	ENDF/B-V
K_{eff} (EOC)	1.0022	1.0030	0.9991	1.0027	1.0033	1.0086	1.0131	1.0103
Fractional absorptions (% of total)								
U-238	13.4	13.3	13.8	13.3	13.3	13.5	13.4	13.2
Pu-239	14.1	14.3	14.7	14.4	14.4	14.4	14.4	14.2
Pu-240	4.53	4.56	4.66	4.63	4.61	4.53	4.32	4.49

in the Pu-240 loading at EOC. However, there is almost no change in the reactivity worth of Pu-240 nor in its contribution to the temperature coefficient. On net, large Pu-240 cross section uncertainties would appear to only result in modest changes in the EOC k_{eff} or in the temperature coefficient at accident temperatures. The base case Pu-240 worth at EOC was 6.1% Δk while the 10% increase in Pu-240 cross section (Case D) yielded a change to only a 6.2% Δk value. These %Δk values result from the Pu-240 fractional absorptions of 4.56% (Case B) and 4.63% (Case D) as shown in Table II.

In Case E, both the Pu-239 fission and capture cross sections in the thermal range (≤2.38 eV) were increased by 10%. This perturbation results in an 8% reduction in the Pu-239 loading at EOC and an increase in Pu-240 of only 1%. Saturation effects result in only very modest k_{eff} changes, i.e., k_{eff} increased by 0.0003 Δk. Since the macroscopic reaction rates in both Pu-239 and Pu-240 differ by only 2%, or less, the effect on the EOC temperature coefficient is insignificant. Therefore, the Pu cross section uncertainty would have negligible effect on fuel temperatures or fission product release.

A 3% change in total uranium loading, which is three times the expected loading uncertainty factor based on fuel manufacturing experience, shows that the EOC k_{eff} is increased by 0.0056 Δk. From the result, the actual uranium loading uncertainty of ±1% would be expected to produce ~±0.002 Δk uncertainty and a ±2.3% change in Pu-239 loading at EOC.

In Case G, only the Pu-239 thermal fission cross section was increased by 10% so that this case represents a change in the Pu-239 thermal σ_f/σ_c ratio, and would tend to produce an increase in the positive contribution to the temperature coefficient due to Pu-239.

The reference MHTGR cross sections are based on earlier evaluations and on selected cross sections for the more important nuclides which GA believes are accurate for MHTGR calculations. The impact of the possible uncertainties due to the use of the GA reference set compared to the use of ENDF/B-V cross sections has been evaluated. Table III lists the source of the cross section data for the GA reference set.

TABLE III
SOURCE OF CROSS SECTION DATA FOR GA REFERENCE

Nuclide	Data Source		
	Fast	Resonance	Thermal
Th-232	ENDF/B-III	ENDF/B-II	ENDF/B-III
U-233	ENDF/B-III	ENDF/B-III	ENDF/B-III
U-235	ENDF/B-III	ENDF/B-I	ENDF/B-II
U-238	ENDF/B-III	ENDF/B-I	ENDF/B-III
Pu-239	ENDF/B-III	ENDF/B-III	ENDF/B-II
Pu-240	ENDF/B-III	ENDF/B-II	ENDF/B-II

The reference point depletion burnup study was repeated through initial cycles to an equilibrium reload based on the use of ENDF/B-V cross section in Case H. The fissile loading at each reload was held at the reference value and the burnup dependent k_{eff} values were compared. The use of the ENDF/B-V cross section increased the equilibrium EOC k_{eff} by 0.7% $\Delta\rho$ compared to the reference GA case result.

A comparison of the EOC plutonium compositions and fractional absorption rates in Pu-239 and Pu-240 show only trivial differences due to the use of the ENDF/B-V data. For example, the GA reference data showed that the Pu-239 and Pu-240 fractional absorptions were 14.3% and 4.56%, respectively. With the ENDF/B-V data the respective values were 14.2% and 4.49%.

The fractional absorptions for each case, expressed as a percent of all neutron absorptions, show that the Pu-239 fractional absorptions vary by less than ±3% from the Case B reference value. Maximum variations for Pu-240 absorption rate at EOC are the same to within ~±2%. These results indicate that, in general, very high cross section uncertainties would be required to make modest uncertainties in the EOC temperature coefficient contribution due to Pu-239 and Pu-240, the two most dominant nuclides.

Figure 5 shows the buildup of Pu-239 and Pu-240 in one fuel segment (one-half of the core fuel elements) as a function of exposure out to the equilibrium exposure of 964 equivalent full power days (EFPDs). As shown, the Pu-239 concentration saturates before the end of an equilibrium cycle exposure, while Pu-240 is nearly saturated by the end of the design burnup cycle. The change in the buildup rate of Pu-239, and Pu-240, that occurs at 482 days is due to the refueling that occurs for the other core segment at that time. The refueling results in a change in the core thermal flux and thus the Pu-239 absoprtion rate.

The total core plutonium loading, corresponding to the plutonium loading in both of the two core segments, when plotted over an equilibrium cycle exposure shows that Pu-239 is equilibrated by about 250 EFPDs while Pu-240 is ~71% of its EOC value at 250 EFPDs. An equilibrium cycle is based on 482 EFPDs exposure between reloads.

These saturating effects, which result in an EOC reaction rate in the nuclide that is nearly independent of cross section uncertainty for that nuclide, explain why ±10% cross section uncertainties produce only ~±2.5% changes in the EOC reaction rates for these two plutonium isotopes as given in Table II. Reasonable modeling and cross section

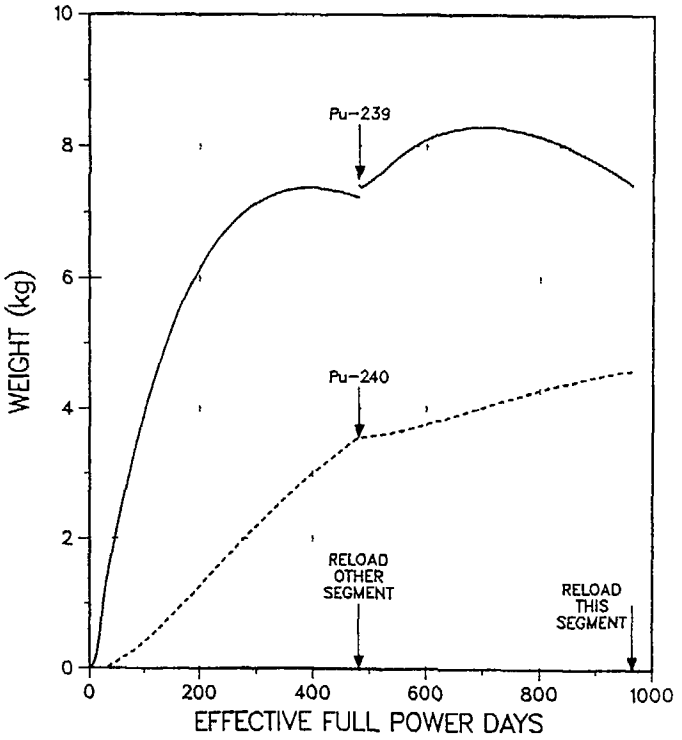

Fig. 5. MHTGR - Pu-239 and Pu-240 building in one refueling segment of the core

uncertainties can only produce modest uncertainties in the EOC temperature coefficient contributions due to either Pu-239 or Pu-240 unless the cross section uncertainties involve fairly large changes in the Pu-239 fission-to-capture ratio.

An important feature in the sensitivity analysis (Step 3) was the assessment of the impact of using ENDF/B-V cross sections rather than the reference GA cross section (ENDF/B-I to -III). For example, the ENDF/B-V U-235 is more reactive than the earlier version normally used by GA while the U-238 resonance capture is ~1.5% lower with the newer data. The Pu-239 fission and capture cross sections, as well as the σ_c/σ_f ratios are nearly the same in the all-important two bottom thermal groups. Finally, the Pu-240 resonance cross section is 5% lower than the value used in the reference set. The assessment of very conservative uncertainties in the temperature coefficient described below involves uncertainties much larger than indicated from the comparisons of the GA reference cross sections and the newer ENDF/B-V results.

Figure 6 compares the ECC temperature coefficient of reactivity for the reference MHTGR cross sections and EOC isotopics, the ENDF/B-V

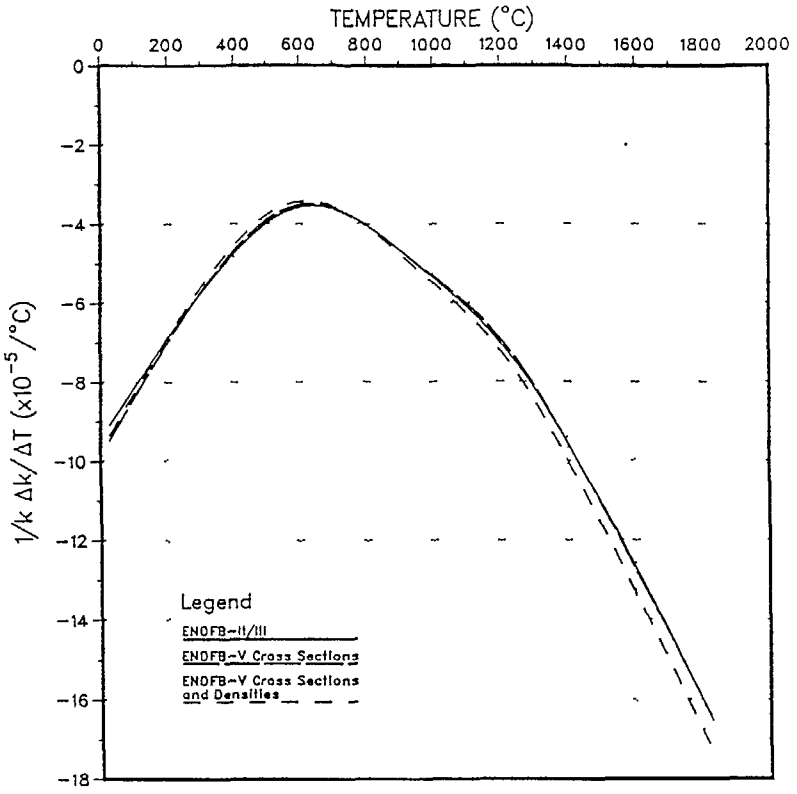

Fig. 6. Total temperature coefficient (constant reflector temperature, EOC equilibrium core)

cross sections with reference EOC isotopics, and also with ENDF/B-V cross sections and isotopics (Case H isotopics). These results show convincingly that the GA use of the older cross section data sets have very little impact on the EOC temperature coefficient and if anything, the coefficient at higher temperature is slightly more negative with the newer data.

The depletion sensitivity analyses for arbitrarily assumed cross section uncertainties (Step 2) indicated that, for example, ±10% cross section changes in Pu-239 and Pu-240 tended to produce only ~±2.5% changes in the EOC reaction rates in these nuclides and, by deduction, only relatively small changes in the contributions to the EOC temperature coefficient is expected due to these plutonium cross section changes.

Further confirmation of the probable accuracy of the GA reference cross sections (Step 3) demonstrated that the use of ENDF/B-V cross sections would change the temperature coefficient predictions by less than about 5% over the whole range of temperatures with the ENDF/B-V results slightly more negative than the reference calculation results.

In the evaluation of very large uncertainties (Step 4), the approach was to define a conservative estimate of the possible temperature coefficient uncertainty due to assumed random uncertainties in the temperature coefficient contribution for all of the significant contributors to the overall coefficient. Other "worst case" estimates assuming nonrandom uncertainties have also been made for the licensing authorities. Since the results are qualitatively similar, they will not be discussed here.

One-sigma cross section uncertainties for the thermal (E = 0.0253 eV) fission or capture cross sections (σ_f or σ_γ) and also for the epithermal (E > 0.5 eV) cross section integrals (I_f or I_γ) are given in [2]. A summary of these data for U-238, Pu-239, Pu-240, and Xe-135 cross sections and their one-sigma uncertainties are summarized in Table IV.

In the MHTGR neutron spectrum, the majority of Pu-239 neutron capture and fission takes place in the thermal range so the uncertainty in those rates is related to the cross section uncertainty given for the 0.0253 eV cross section rather than to the uncertainty given for the integrals at E > 0.50 eV. For example, the four thermal neutron groups used for the depletion studies have upper limit energies of 0.13, 0.825, 1.275, and 2.38 eV. Approximately 19% of all Pu-239 captures and 26% of all fissions occur in the lowest group (≤0.13 eV) while ~97% of all captures and fissions in Pu-239 are predicted to occur at ≤0.825 eV.

For Pu-240, essentially all of the absorptions occur at E > 0.5 eV, and the I_γ uncertainty of ±12% is an appropriate one-sigma estimate for sensitivity studies for example. For Xe-135, for example, the

TABLE IV
ONE-SIGMA CROSS SECTION UNCERTAINTIES

	Description	Uncertainty (%)
U-238	σ_γ = 2.70 ± 0.02 barns (0.0253 eV)[a]	--
	I_γ = 275 ± 5 barns (E > 0.5 eV)	±1.8
Pu-239	σ_f = 742.5 ± 3.0 barns (0.0253 eV)	±0 4
	σ_γ = 268.8 ± 3.0 barns (0.0253 eV)	±1.1
	I_f = 301 ± 10 barns (E > 0.5 eV)	±3.3
	I_γ = 200 ± 20 barns (E > 0.5 eV)	±10.0
Pu-240	σ_γ = 289.5 ± 1.4 barns (0.0253 eV)	±0.5
	I_γ = 8013 ± 960 barns (E > 0.5 eV)	±12.0
Xe-135	σ_γ = (2.65 ± 0.20) x 10^6 barns (0.0253 eV)	±7.5
	I_γ = 7634 barns (E > 0.5 eV)	--

[a] σ_γ = capture cross section
σ_f = fission cross section
I_γ = capture cross section integral
I_f = fission cross section integral

σ_γ uncertainty at 0.0253 eV is estimated to be typical of the total cross section uncertainty.

To illustrate the possible effect of combined modeling, burnup, or cross section uncertainties on the core isothermal temperature coefficient, an uncertainty analysis was performed as part of Step 4 in which random uncertainties were assumed in the reference calculated temperature coefficient contributions due to all the key nuclides. These uncertainties, which represent estimates of a conservative uncertainty for the coefficient contribution due to selected nuclides, are summarized in Table V. The magnitude of the indicated temperature coefficient contribution uncertainty for the various nuclides except Pu-239 and Pu-240 is consistent with the correlations of measured and predicted temperature coefficient and xenon worths for both Peach Bottom and Fort St. Vrain. The indicated ±25% uncertainty due to Pu-239 and Pu-240 is much higher than indicated in the HTLTR experiment with plutonium fuels and is higher than would be expected based on the EOC plutonium buildup uncertainty analysis and temperature coefficient changes due to cross section changes discussed earlier.

TABLE V
TEMPERATURE COEFFICIENT
UNCERTAINTY EFFECTS

Contributor	Assumed Coefficient Uncertainty (%)
Pu-239	±25
Pu-240	±25
U-238	±10
Th-232	±10
Xe-135	±20
U-235	±5
All other	±5

The core isothermal temperature coefficient was calculated combining all these assumed coefficient uncertainties in a root mean square fashion; and the resulting error limits in the core isothermal temperature coefficient are shown as error bars in Fig. 7. This combination of large calculational errors results in an overall temperature coefficient uncertainty of only about ±15% at accident temperatures while the coefficient at operating temperature is reduced by ~30% with this very conservative approach.

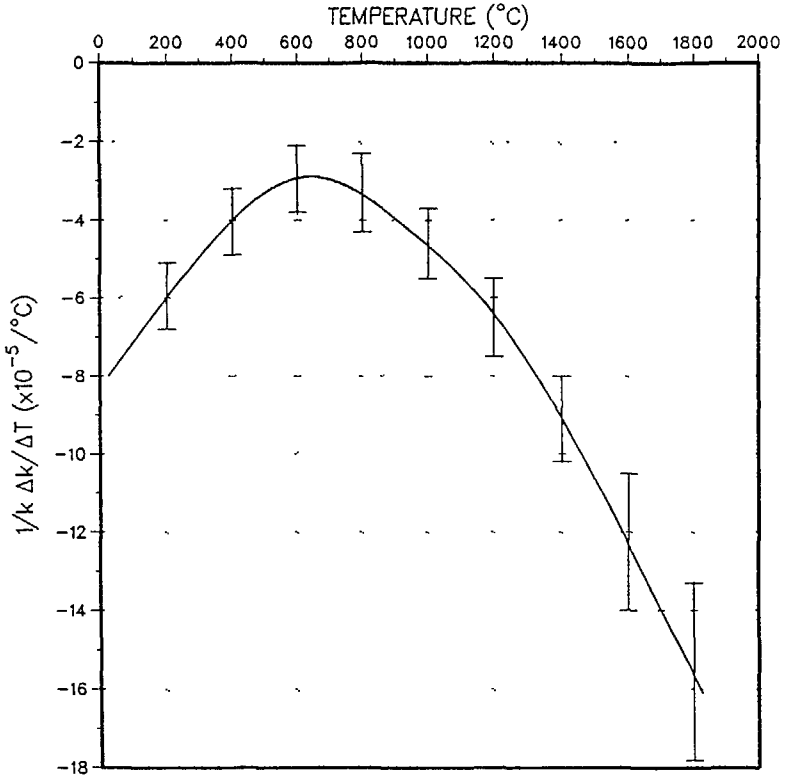

Fig. 7. Temperature coefficient uncertainty due to random uncertainty in key nuclide contributors (EOC equilibrium core)

4. CONCLUSIONS

In the MHTGR, only the temperature component of the power coefficient is significant. The overall temperature coefficient is large and negative.

The use of the GA reference cross section set has very little impact on the EOC temperature coefficient when compared to the EOC temperature coefficient calculated with ENDF/B-V cross section data.

An estimate of the potential uncertainty in the overall core temperature coefficient was evaluated by conservatively estimating uncertainties in the predicted contribution to the overall coefficient from individual nuclides. In this case, it was assumed that such nuclide contribution uncertainties were random. This uncertainty estimate yielded an uncertainty of ~±30% at normal operating temperature but a lower average uncertainty of ~±15% over typically evaluated accident temperatures.

This conservative uncertainty analyses assumed uncertainties due to Pu-239 and Pu-240 which were much larger than indicated due to the saturating effects of those nuclides as assessed and described in these sensitivity studies.

ACKNOWLEDGEMENTS

Work on this paper supported by U.S. Department of Energy contract DE-AC03-84SF11963.

The authors wish to thank R. K. Lane for his efforts in the cross section uncertainty evaluation.

REFERENCES

[1] BREHER, W., NEYLAN, A., SHENOY, A., Modular High-Temperature Gas-Cooled Reactor (MHTGR) Status, Intersociety Energy Conversion Engineering Conference, Philadelphia, PA, August 10-14, 1987.

[2] MUGHABGHAB, S. F., GARBER, D. I., Neutron Cross Sections Volume I, Resonance Parameters, BNL-325, 3rd ed., Vol. I, 1973.

COMPARISON OF CALCULATED AND MEASURED REACTIVITY COEFFICIENTS FOR LIGHT WATER REACTOR LATTICES

E. JOHANSSON
Studsvik Energiteknik AB,
Nyköping, Sweden

Abstract

The cell and assembly multigroup transport theory burnup code CASMO in its latest version, CASMO-3, combined with a 70-group nuclear data library, a modified variant of an earlier CASMO library, has been tested against data from experimental facilities. The tests reported deal with reactivity coefficients for light water reactor lattices and, to some extent, with related parameters, in particular the resonance absorption in U238.

I. INTRODUCTION

The cell and assembly multigroup transport theory burnup code CASMO is used by many utilities world wide. Over the years the code combined with various multigroup nuclear data libraries has been tested extensively against data from experimental facilities as well as against results from power reactors. This is so also for the latest version of the code, labeled CASMO-3, and its 70-group library being a modified version of a previous library.

The tests of CASMO-3 and its library reported here are based on data from experimental facilities. The emphasis in the study is on reactivity coefficients for lattices moderated with light water. Some tests for the resonance absorption in U238 are also included in this context. The reactivity measurements were performed in the high temperature reactor KRITZ at Studsvik, whereas the resonance absorption measurements were carried out at the reactor R1 in Stockholm. Some of the tests included in this paper have been done by other investigators and the results have also been reported elsewhere, some tests were done quite recently by the present author.

II. THE CALCULATIONAL MODEL AND ITS APPLICATION

The CASMO code first solves the one-dimensional integral transport theory equation for each pin cell type involved. This calculation is carried out in the microgroup energy structure, consisting of 70 groups in the work presented

here. There are 14 groups above 9118 eV and 13 groups in the resonance region between 4 eV and 9118 ev. For BWR assemblies and (as an option) for single pin cell cases the microgroup calculation is followed by a calculation in the macrogroup energy structure, here in 23 groups, the default value for a 70-group library. The subsequent two-dimensional calculation needed for BWR and PWR assemblies is performed with a transmission probability routine COXY in 12 groups or less. The default value, 7 groups, was used in this work. Finally, a fundamental mode calculation is carried out, in the macrogroup structure, accounting for the leakage. Shielded resonance absorption data based on the equivalence theorem are used in the region from 4 eV to 9118 eV for U235, U236, U238, and Pu239. The important resonances in Pu239 at 0.296 eV and in Pu240 at 1.056 eV are adequately treated by a tight group structure around these energies. More detailed information on CASMO, in particular on CASMO-3 used in the present work, can be found in Refs 1, 2, and 3.

The burnup process in burnable absorber (BA) rods can not be handled directly in CASMO. Such cases are first treated with the code MICBURN (Ref 4), producing homogenized cross sections to be used in CASMO. The present work does not include any such burnup, but MICBURN had to be used anyway, namely for the so called grey BA rods having a non-uniform axial BA distribution, in the present work a pattern of pellets with and without Gd. The rods with a uniform (homogeneous) Gd distribution on the other hand, could be treated directly in CASMO.

The 70-group nuclear data library labeled E4LBG70 (Ref 5) used in the CASMO calculations is based on data from several sources, in particular ENDF/B-3, 4, and 5. It is equivalent to or almost equivalent to the library versions presently applied in CASMO by many users around the world.

Cross section data obtained from CASMO were used in the core calculations for the various KRITZ cases. These calculations were performed with the diffusion theory code DIXY, applied in x,y geometry, with the axial leakage represented by a buckling term. Separate cross section data were used for each pin-cell type, water hole, and gap. The DIXY calculations were throughout performed in the 4-group energy structure 10 MeV - 0.821 Mev - 5530 ev - 0.625 eV - 0. Cross section data for the KRITZ water reflector were generated in special CASMO calculations. In some cases, particularly for pin cells with Gd, the cross section data from CASMO had to be adjusted to outweigh the errors in diffusion theory calculations for such rods. The correction factors needed in that context were obtained from CASMO.

The main results from the calculation for each KRITZ core is the k_{eff} value, to be compared with the experimental result of unity. As mentioned, calculations were also done for the resonance absorption in U238. These calculations, performed on pin cells, are presented below in connection with the reactivity effect due to fuel temperature changes. Some other calculations are also presented.

III. REACTIVITY EFFECT OF A FUEL TEMPERATURE CHANGE

As an introduction some results from calculations of the fuel temperature reactivity effects in a power reactor will be presented. These calculations (Ref 6), performed with CASMO for the first reload fuel batch in the Swedish BWR Forsmark 1, refer to an 8x8 rod assembly with 4 Gd rods. These CASMO calculations, using a 40-group variant of the library, were done for the fuel temperatures T_f = 540 K, 840 K, 1140 K, 1640 K, and 2140 K for each combination of the burnup degrees E = 0, 5, 10, 20, and 30 MWd/kgHMi and the void fractions V = 0, 50, and 75 %. HMi means Heavy Metal initially and V refers to the volume fraction of dry steam. Core calculations were not needed for the present survey. It can be mentioned in this context that the span of the migration area as a function of T_f is less than 0.3 cm^2 for any of the E, V pairs.

The reactivity effect due to a fuel temperature change from T_f' to T_f'' was obtained as

$$\Delta\rho = 2 \cdot 10^5 (k_\infty'' - k_\infty')/(k_\infty'' + k_\infty') = 10^5 \, \Delta k_\infty / \bar{k}_\infty$$

CASMO also calculates the components of k_∞ in two energy groups. The following relations are given in Ref 3.

$$k_\infty = (1-P_1)\eta_1 f_1 + P_1 \eta_2 f_2$$

where $\eta_1 f_1 = \nu_1 \Sigma_{f1}/\Sigma_{a1}$, $\eta_2 f_2 = \nu_2 \Sigma_{f2}/\Sigma_{a2}$

and $P_1 = \Sigma_r/(\Sigma_r + \Sigma_{a1})$ with $\Sigma_r = (\phi_1 \Sigma_{1\to2} - \phi_2 \Sigma_{2\to1})/\phi_1$

The boundary between the two groups is at 0.625 eV in this work.

From the expressions just given one can estimate the thermal component of $\Delta\rho$ as

$$\Delta\rho_2 = 10^5 \bar{P}_1 \Delta(\eta_2 f_2)/\bar{k}_\infty + a \quad \Delta(\phi_2 \Sigma_{2\to1}) \text{ term}$$

The last term can be neglected here because the upscattering is fairly small. Values of $\Delta\rho_2$ and of $\Delta\rho_1 = \Delta\rho - \Delta\rho_2$ for a change of T_f from 540 K to 1140 K are given in Fig 1. In addition, results for $d\rho_1/dT_f$ and $d\rho_2/dT_f$ as a function of T_f are presented in Fig 2.

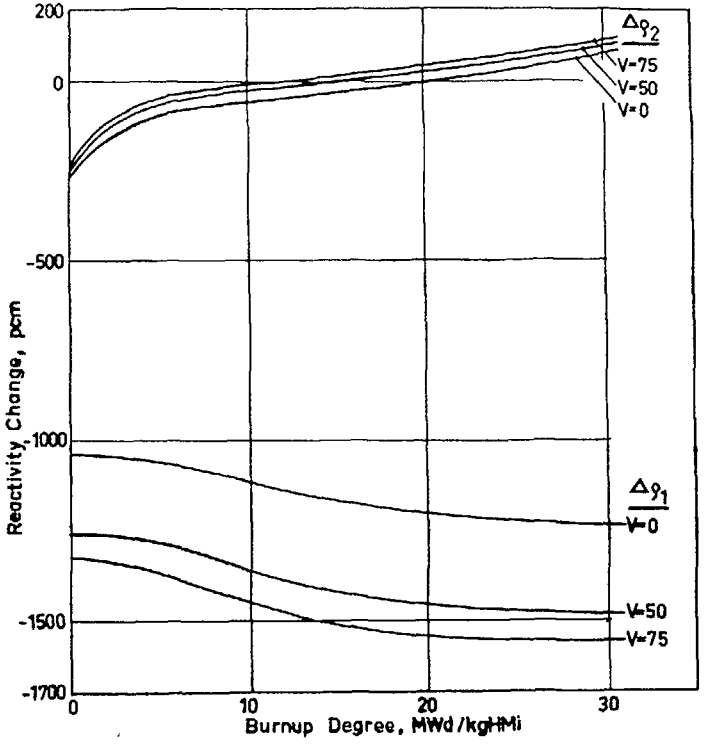

Fig.1 Reactivity changes calculated with CASMO for an increase of the fuel temperature in typical BWR fuel from 540 K to 1140 K.

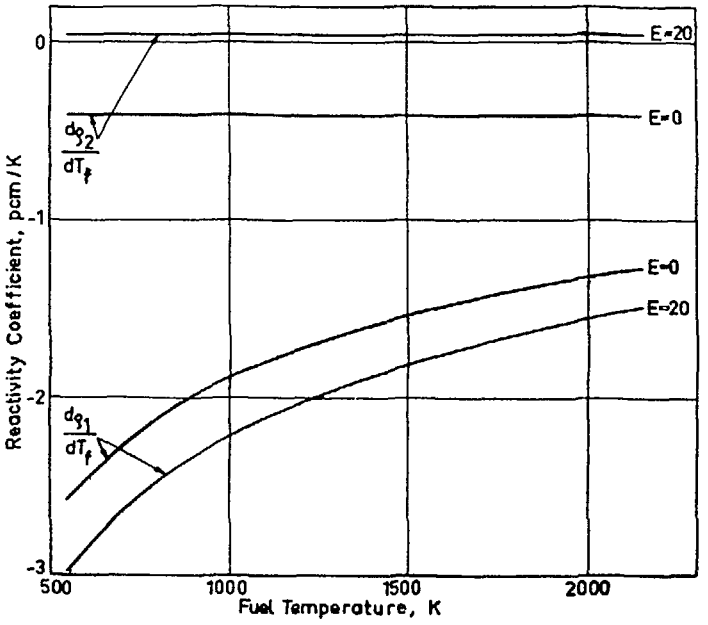

Fig. 2 The reactivity coefficients $d\rho_1/dT_f$ and $d\rho_2/dT_f$ versus the fuel temperature T_f from CASMO calculations for typical BWR fuel. Void, V = 50 %.

The minor reactivity component $\Delta\rho_2$, the thermal one, given in Fig 1 shows an obvious dependence on the degree of burnup, with a span of more than 300 pcm. The net effect in a reactor would, however, be small for this particular example because of compensating effects between negative and positive contributions. The corresponding coefficient $d\rho_2/dT_f$ in Fig 2 seems to be about constant as a function of T_f. The thermal component shown could be due to many causes, such as influence from Pu239 and Pu241, gradually growing with burnup, as well as influence from the Gd absorber, present up to about E = 6 MWd/kgHMi in the BWR calculations referred to.

The thermal component is associated with the spectrum hardening occurring when the fuel oxide is heated. This hardening has been demonstrated in measurements of the neutron spectrum in a UO_2 tube at 50°C and at 750°C. The results, obtained with a time-of-flight spectrometer analysing the neutron beam from a

lead scatterer located in the centre of the UO_2 tube, are shown in Fig 3. Also shown are some results from THERMOS calculations - with the oxygen treated as a free gas of mass 16. Such a treatment seems to be adequate.

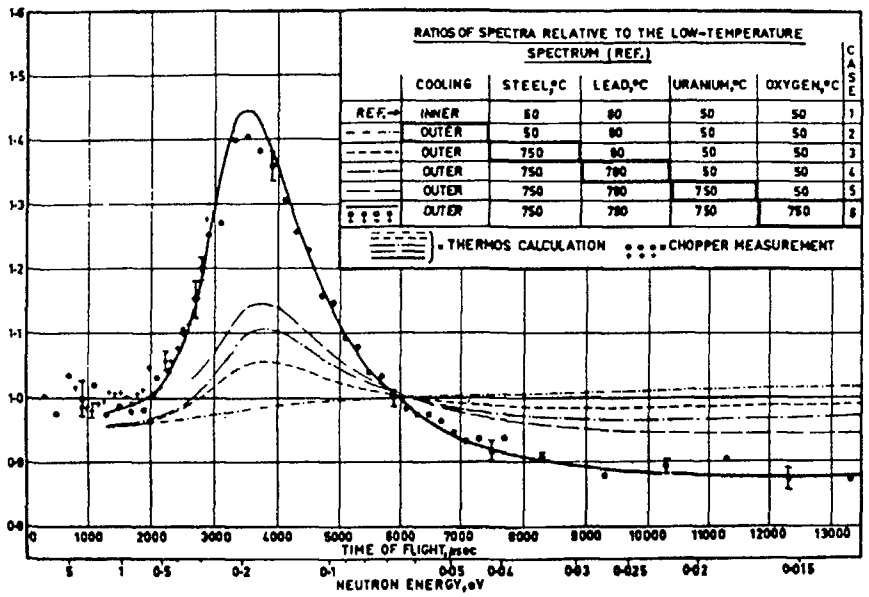

Fig. 3 Measured and calculated neutron spectra in a UO_2 tube relative to the low-temperature spectrum. Normalization to equal neutron density from 0.012 eV to 2.34 eV. From Ref 7.

The epithermal reactivity component $\Delta\rho_1$, the major one, to some extent depends on the void fraction and on the degree of burnup, as shown by the curves in Fig 1, a behaviour that seems reasonable. This component is mainly due to the resonance absorption in U238. It is shown experimentally in Ref 8 that the effective resonance integral $RI(T_f)$ of this nuclide could be written as

$$RI(T_f) = RI(T_0)\ (1+\beta(\sqrt{T_f}-\sqrt{T_0}))$$

This result refers to uranium oxide and uranium metal rods for fuel temperatures T_f in the region from 300 K to 1000 K. T_0 is a reference temperature, e.g. 300 K. The parameter β depends on the fuel type and on the rod radius. The small 1/v contribution is not included in RI. The behaviour of $d\rho_1/dT_f$ would follow a curve proportional to the derivative dRI/dT_f, i.e. $1/\sqrt{T_f}$.

CASMO calculations for single rods in water (Ref 9) combined with experimental data for β and RI based on Refs 8 and 10, led to the results given in Table I. $\Delta RI/RI$ is the change of the effective resonance integral between T_f = 300 K and T_f = 1000 K. The experimental uncertainties (1 σ) are $\pm$3.5 % for RI and $\pm$8 % for $\Delta RI/RI$.

TABLE I

Comparison of Calculated and Experimental Resonance Integrals and Temperature Effects for the Resonance Integral of U238. In this Comparison the 1/v Contribution Was Included. The Library Used Is Equivalent to E4LBG70. RI = RI(300), ΔRI = RI(1000) - RI(300)

	Fuel	Rod Radius cm	$(\frac{C}{E} - 1)\ 100$, %
RI	UO_2	0.40	+0.1
		0.52	-0.4
		0.80	+0.4
		1.04	0.0
		1.60	-0.8
	U metal	0.50	-4.2
		1.00	-1.0
$\frac{\Delta RI}{RI}$	UO_2	0.40	+0.6
		0.52	+3.5
		0.80	-2.1
		1.04	-0.2
		1.60	-0.9
	U metal	0.50	+4.8
		1.00	-4.8

IV. REACTIVITY EFFECT OF A MODERATOR TEMPERATURE CHANGE

The experiments referred to in this section were all performed in the zero-power high-temperature reactor KRITZ used at Studsvik up to the mid-seventies. A great variety of light water moderated lattices, including several cases with plutonium, were investigated in this reactor in the temperature range from 300 K to 520 K. The measurements deal with criticality combinations of temperature, boron content, and water level (and the associated axial buckling) as well as with fission rate distributions.

The tests of CASMO-3 and its library E4LBG70 discussed in this section concentrate on the criticality states around 300 K and 500 K for various cores fueled with enriched uranium. So far the present calculational model has not been tested thoroughly against the Pu-bearing lattices. One such test, dealing with a small, regular lattice of PuO_2UO_2 rods from an early KRITZ project, is, however, included here. The purpose of the tests is to compare calculated k_{eff} values with the measured ones, which are unity throughout. As this is done both at low and high temperature the calculation of the reactivity effect of a moderator temperature change is also tested - or, to be more accurate the effect of a uniform temperature change as the fuel effect is also included.

In addition to regular pin lattices the present study deals with PWR lattices with large or small water holes and with BWR lattices with or without burnable absorbers (Gd rods). The layout for the BWR lattices is shown in Fig 4.

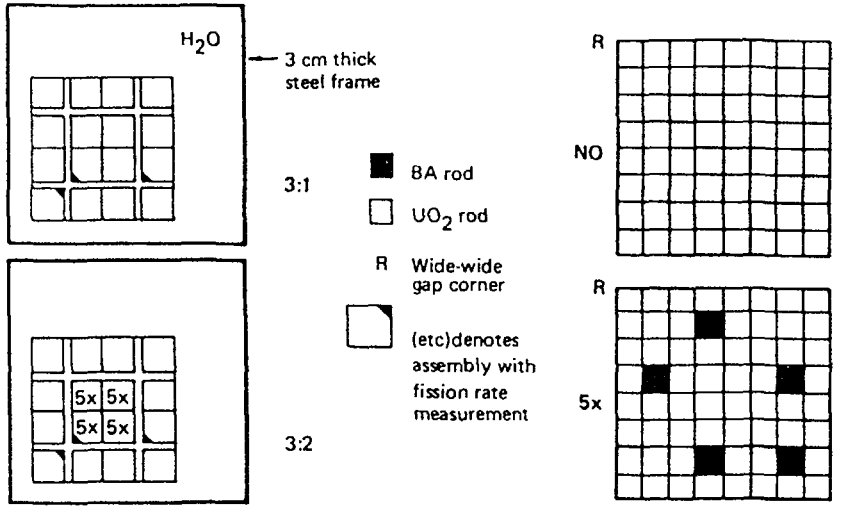

Fig. 4 Two cores from the BWR/BA measurements in KRITZ. The outer dimension of the steel frame, approximating the real steel configuration, is 115 x 115 cm.

CASMO-3/DIXY calculations were carried out as outlined in Section II. For the BA cores 3:3 and 3:4, not shown in Fig 4, MICBURN calculations were done (Ref 11) because of the presence of grey BA rods. A set of k_{eff} values obtained in the calculations is given in Table II. Some of these values were first given in Ref 12 and later on cited in Ref 1.

TABLE II

CASMO-3/DIXY Calculated k_{eff} Values for Critical Cores in the KRITZ Reactor. Cold and Hot Refer to the Uniform Temperature, Being about 300 K and 500 to 520 K, Respectively. Data Library E4LBG70.

Core		Calculated k_{eff} Cold	Hot	Ref
KRITZ-2 Pin Cell Cores				
2:1	UO_2(1.9 % enr U), V_m/V_f = 1.2	1.0000	1.0007	12, 1
2:13	UO_2(1.9 % enr U), V_m/V_f = 1.7	0.9989	0.9990	12, 1
2:19[a]	PuO_2UO_2(1.5 % PuO_2), V_m/V_f = 3.3	1.0026	1.0030	This work
KRITZ-3 PWR Cores				
U-WH1	Small water holes	0.9998	0.9999	This work, 12
U-WH2	Large water holes	1.0003	1.0002	12, 1
KRITZ-4 BWR Cores				
3:1	No Gd	1.0010 1.0009	1.0016 1.0010	12, 1 This work
3:2	5 hom Gd rods in each of 4 central assemblies	1.0016 1.0009	1.0015 1.0007	12, 1 This work
3:3	5 grey Gd rods (type Y)	1.0006	0.9992	This work
3:4	5 grey Gd rods (type Z)	1.0005	0.9999	This work

a) A correction, somewhat uncertain, of -500 pcm and -380 pcm, respectively, related to shielding effects in the PuO_2 grains has been applied to the k_{eff} values given.

The experimental uncertainties (1σ) of k_{eff} for the cases in Table II can be expressed as follows, according to Ref 13. For each single case the uncertainty is ± 80 pcm for the pin cell cores in KRITZ-2, ± 140 pcm for the PWR cores in KRITZ-3, and ± 60 pcm for the BWR cores in KRITZ-4. The uncertainty for a hot case relative to the corresponding cold case is ± 60 pcm for the PWR cases and ± 40 pcm for the BWR cases. The uncertainty values given do not include any

uncertainty in geometry or fuel composition. Essentially they account for uncertainties in the criticality measurement, mainly those for the boron content and for the axial buckling.

The reactivity effect $\Delta\rho$ (Cold→Hot) due to a temperature change is not measured explicitly in the experiments, which, as has been mentioned, primarily give critical states. Neither are numerical values for this $\Delta\rho$ parameter needed in the tests. However, a few estimates have been done anyway, by use of the expression

$$\Delta\rho(\text{Cold}\rightarrow\text{Hot}) = -\Delta\beta\,\frac{d\rho}{d\beta} - \Delta B_z^2\,\frac{d\rho}{dB_z^2},$$

where β means the boron content and B_z^2 the axial buckling. $\Delta\beta$ and ΔB_z^2 were obtained in the measurements and average values of $d\rho/d\beta$ and $d\rho/dB_z^2$ were estimated from calculations. The results obtained for $\Delta\rho$(Cold→Hot) are -3100 pcm for core 2:19, + 500 pcm for core 3:1, and - 700 pcm for core 3:2. Obviously the results vary strongly. To some extent this depends on large differences in boron content among the various cases.

The outcome of the tests for the reactivity effect of a uniform temperature increase can be expressed as $10^5(k_{eff}(\text{Hot}) - k_{eff}(\text{Cold}))$. For the cores in Table II the largest deviation from the ideal value zero is - 140 pcm, referring to core 3:3, a core with grey Gd rods. The average value of $10^5|k_{eff}(\text{Hot}) - k_{eff}(\text{Cold})|$ for all 9 cores is (70+10+40+10+10+(60+10)/2+(10+20)/2+140+60)/9 = 43 pcm, a value of the same order as the experimental uncertainty. The average deviation means about 0.2 pcm/K, a very small value in this context.

V. REACTIVITY EFFECT OF A VOID CHANGE

Special measurements concerning the effect of void were carried out in the BWR/BA project in KRITZ. The void was created either by air bubbles or by empty zircaloy tubes inserted in the central assembly. In the present study the zircaloy tube variant has been analysed. One of the pertinent cores is shown in Fig 5. Altogether there were 45 tubes in the central assembly, occupying, walls included, 36.9 % of the normal coolant volume. Measurements were carried out also with a voided assembly without BA in the centre, a NO assembly - see Fig 4, as well as for cores without any tubes.

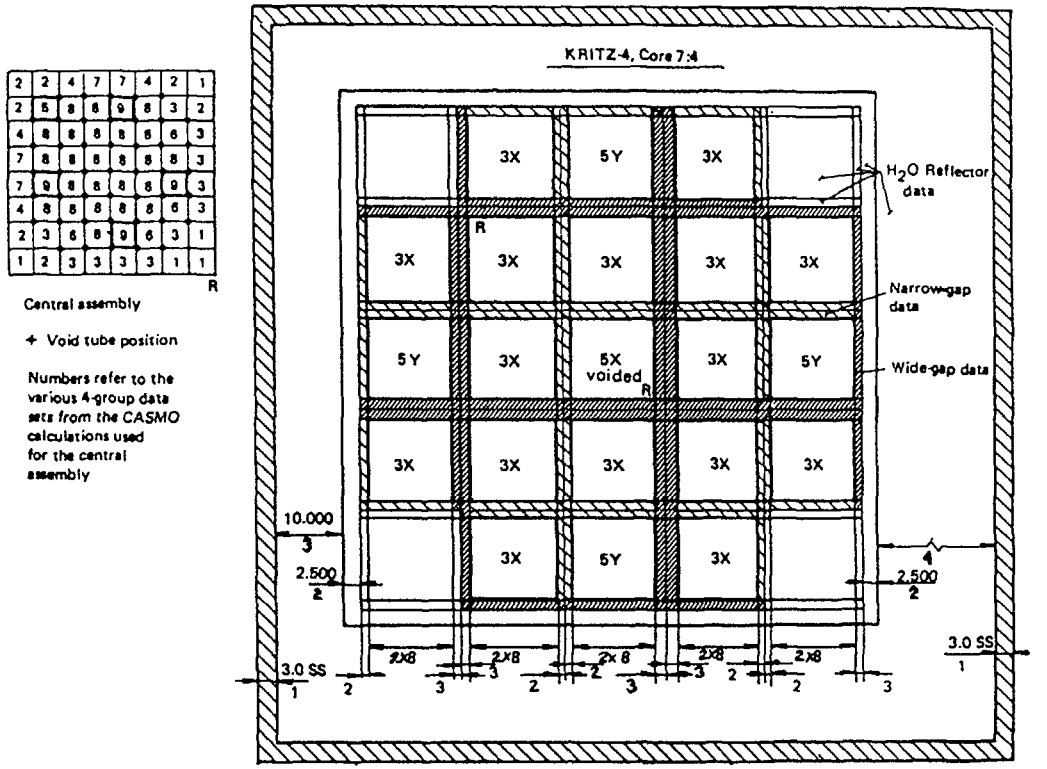

Fig. 5 One of the KRITZ cores used in the void reactivity studies. Some details concerning the core calculations are also given. 2x8 means 2 micromeshes in this direction for each of 8 pin cells. The total mesh number is 118x118.

The average void fraction, representing dry, saturated steam, to be used in the CASMO input was found to be 37.7 %. A non-uniform distribution of this void across the assembly was needed in the CASMO input. Some information on the core calculations is given in Fig 5. The k_{eff} results obtained are presented in Table III, also showing the estimated void reactivity, obtained in a manner similar to the one for the temperature effect in Section IV. The k_{eff} level is somewhat lower than for the corresponding cases in Table II. To some extent this depends on a less severe flux convergence criterion in the calculations for the cores in Table III.

TABLE III

CASMO-3/DIXY Calculated k_{eff} Values for Critical Cores in the KRITZ Reactor With or Without Void in the Central Assembly. Data Library E4LBG70.

Core	Temp K	Central Assembly	k_{eff}	Void Reactivity pcm
KRITZ-4 BWR Cores				
7 1	515.6	NO, no void	0.99681	
7.2	517.1	5X, no void	0.99728	
7.3	515.1	NO, voided	0.99612	-790
7:4	517.4	5X, voided	0.99696	-344

As the k_{eff} values in Table III for the voided cases are lower than for the corresponding cases without void, the calculations overestimate the numerical value of the void reactivity. The overestimate is 69 pcm for the NO case and 32 pcm for the 5X case, or about 9 % of the estimated void reactivity. The experimental uncertainty for a case with void relative to the corresponding case without void is given as $\pm$ 40 pcm in Ref 13.

VI. DISCUSSION

The 70-group nuclear data library, E4LBG70, used in the CASMO calculations in the present work, is not based on one single evaluated compilation. Instead, as mentioned in Section II, several data sources have been used, in particular the compilations ENDF/B-3,4, and 5.

The shielded resonance data for U238 in the library E4LBG70 have been obtained after adjustment downwards of values originally calculated from the basic resonance parameters. This adjustment (Refs 5,9), particularly noticeable for large diameter rods with their pronounced selfshielding, was chosen temperature dependent. It was governed by the experimental results (Refs 8, 10) used in the comparison shown in Table II. The adjustment means an obvious shift in the calculation of the fuel temperature effect for all rods examined. On the other hand, it is not very important for RI(300) for UO_2 rods with radii of about 0.5 cm, i.e. normal LWR rods. It should be noted that the shifts discussed are of the order of the standard deviation in the experimental results, i.e. $\pm$3.5 % for RI(300) and +8 % for the temperature (Doppler) effect. However, if there is no special preference, it is generally justified to try to reproduce nominal measured results - also for changes within the experimental uncertainty limits. It is not clear if the need for the adjustment is associated with basic resonance data or with the method - for instance, does the equivalence theorem really give results accurate to the order of 1 %?

The fuel temperature reactivity effect in an LWR is not only due to the Doppler effect in the resonances in U238 and, to a lesser extent, in other resonances, such as the one at 1.056 eV in Pu240. There is also an effect in the thermal region in the first place caused by the hot oxygen in UO_2 fuel leading to a hardening of the neutron spectrum. In this work the thermal and nonthermal reactivity components have been estimated separately on the basis of CASMO calculations for a typical BWR fuel assembly. Furthermore, reference has been made to an experimental demonstration of the spectrum hardening in heated UO_2 as well as to calculations showing that the oxygen could be treated as a free gas of mass 16. Probably the cross section data presently available are adequate for a calculation of the thermal region reactivity effect as well as of the effect in Pu240.

Concerning the resonance absorption in U238 it can be noted that CASMO uses a temperature, T_D, somewhat higher than the physical temperature. A free gas model using such an elevated temperature is expected to give an adequate approximation of the influence of atomic vibrations in the UO_2 lattice. Another problem, of a more practical nature, is to find the correct physical temperature for the fuel in a power reactor.

For the Doppler effect in U238 we finally present in Table IV the relative importance of various energy regions. These data have been obtained from very recent calculations with CASMO for an LWR pin cell and should be regarded as somewhat preliminary.

In the thermal region a slight non 1/v dependence has been adopted for the absorption cross section of U238. This adjustment (Refs 5, 9) associated with an assumed bound level (resonance at negative energy) has contributed to the good outcome of the reactivty effect for a change of the uniform temperature as shown in Tabel II. Not only this differential effect but also the individual k_{eff} values are very well calculated. The outcome of the calculations is also quite good for the void reactivity effect as shown in Table III.

TABLE IV

Relative Doppler Reactivity in U238 in Various Energy Regions for an LWR Pin Cell for a Fuel Temperature Increase from 840 K to 940 K.

Energy Region, eV	Relative Effect, %
9118.0 -906.898	9
906.898 -367.262	11
367.262 -148.728	14
148.728 - 75.5014	11
75.5014- 48.052	7
48.052 - 27.700	8
27.700 - 15.968	15
15.968 - 9.877	-
9.877 - 4.00	25

So far, only few sensitivity studies have been performed in the analysis of the KRITZ experiments. The results from one such study (from Ref 13), showing the effect of an error in the resonance absorption in U238 is presented in Table V. Even a 1 % error in the resonance integral causes significant changes for the individual k_{eff} values whereas the influence on the "Cold to Hot" effect is fairly small. One reason for further study of the resonance integral of U238 would be the calculation of the Doppler effect. A study of the accuracy of the equivalence theorem might also be valuable. Another important parameter is the thermal absorption cross section of U238 for which a high accuracy measurement would be very valuable. For the rest it is, on the basis of the present tests, difficult to select any particular cross section or other parameter, the values of which seem to be doubtful with respect to the calculation of reactivity coefficients. Nevertheless, such values might exist, in spite of the very good outcome of the tests, because of possible compensating effects. Also, there are so far very few applications of the library in calculations on cores containing plutonium. Several such cores were studied in the KRITZ experiments. Finally, the calculational model has been tested against measured results for tight lattices. The outcome of these tests, presented in Ref 14, is reasonably good, though far from the very good outcome for normal thermal light water moderated lattices.

TABLE V

Errors in Calculated k_{eff} Values for Some of the KRITZ Cores due to an Error in the Effective Resoncance Integral of U238, as an Example Chosen Equal to +1 %.

Core	Error in k_{eff}, pcm	
	Cold	Hot
KRITZ-2 Pin Cell Cores		
2·1 UO_2 (1.9 % enr U) V_m/V_f=1.2	-244	-295
2.13 UO_2(1.9 % enr U) V_m/V_f= 1.7	-182	-222
2:19 PuO_2UO_2(1.5 % PuO_2) V_f = 3.3	-107	-133
KRITZ-3 PWR Cores		
U-WH1 Small water holes	-156	-185
KRITZ-4 BWR Cores		
3·1 No Gd	-124	-149

REFERENCES

1. M. EDENIUS and Å. AHLIN, "CASMO-3 New Features, Benchmarking, and Advanced Applications," Proc. Int. Topl. Mtg. Advances in Reactor Physics, Mathematics and Computation, Paris, April 27-30, 1987, Volume 3, 1497(1987).

2. M. EDENIUS, Å. AHLIN, and B.H. FORSSEN, "CASMO-3, A Fuel Assembly Burnup Program, User's Manual," STUDSVIK/NFA-86/7, Studsvik Energiteknik AB (1986)

3. M. EDENIUS, Å. AHLIN, and H. HÄGGBLOM, "CASMO-3, A Fuel Assembly Burnup Program, Methodology," STUDSVIK/NFA-86/8, Studsvik Energiteknik AB (1986).

4. M. EDENIUS, Å. AHLIN, and C. GRÄGG, "MICBURN-3, Microscopic Burnup in Burnable Absorber Rods," STUDSVIK/NFA-86/26, Studsvik Energiteknik AB (1986).

5. H. HÄGGBLOM, "The CASMO-3 Nuclear Data Library," STUDSVIK/NFA-86/12, Studsvik Energiteknik AB (1986).

6. S. LUNDBERG, Priv. Comm.

7. E. JOHANSSON, E. JONSSON, M. LINDBERG, and J. MEDNIS, "The Neutron Spectrum in a UO_2 Tube at Different Temperatures," Nucl. Sci. Eng., 26, 47(1966).

8. E. HELLSTRAND, P. BLOMBERG, and S. HÖRNER, "The Temperature Coefficient of the Resonance Integral for Uranium Metal and Oxide," Nucl. Sci. Eng., 8, 497(1960).

9. H. HÄGGBLOM, "The CASMO Library Versions E3LI69G, E3LI69H, E3LI69I, and E3LI70I," Internal Report, NR-85/86, Studsvik Energiteknik AB (1985).

10. E. HELLSTRAND, "Measurement of Resonance Integrals, "Reactor Physics in the Resonance and Thermal Regions, Volume II, 151. Editors A.J. Goodjohn and G.C. Pomraning,The M.I.T. Press, Cambridge Mass. and London (1966).

11. E. JONSSON, Priv. Comm.

12. P. JERNBERG, "CASMO-3 Benchmark against Critical Experiments," STUDSVIK/NFA-86/11, Studsvik Energiteknik AB (1986).

13. E. JOHANSSON and M. EDENIUS, "Benchmarking of a CASMO/CPM 69-Group Library Based on ENDF/B-5," Proc. Thermal Reactor Benchmark Calculations, Techniques, Results, and Applications," Brookhaven National Laboratory, Upton, New York, May 17-18, 1982, EPRI NP-2855, Electric Power Research Institute (1983).

14. E. JOHANSSON, "Reactor Physics Calculations for Alternative Fuel Recycling Strategies Using Tight Pressurized Water Reactor Lattices," Nucl.Technol., to be published.

TEMPERATURE EFFECT ANALYSIS IN LWR LATTICES — THERMAL CROSS-SECTION SHAPES AND QUALIFICATION THROUGH FRENCH INTEGRAL EXPERIMENTS

A. SANTAMARINA
Département des réacteurs à eau,
CEA, Institut de recherche technologique
et de développement industriel,
Saint-Paul-lez-Durance, France

Abstract

The reactivity temperature coefficient is analyzed for light water reactor lattices. Qualification through French integral experiments leads to adjustments in the thermal cross-section curve shapes for U-235 and U-238.

1. INTRODUCTION

Reactivity Temperature Coefficient (RTC) is a very important parameter for design studies, safety and operation of Light Water Reactors (LWR).

The calculation of this parameter is a delicate problem, as RTC is the result of the sum of several negative and positive contributions of different physical phenomena linked to the fuel and moderator temperature change : theoretical considerations on RTC neutron calculation and the main effects involved in LWR moderator temperature coefficient are summarized in section 2.

For several years, an important disagreement about 4 pcm/°C (10^{-5} in $\Delta K/K$) between calculation and the available RTC experimental data has arisen /1, 2, 3/ ; start-up operations in French PWRs confirmed the existence of a large discrepancy between measured RTC values (nominal conditions) and core calculations performed with the APOLLO French neutron code /4/. Most of the data basis was critical experiments limited to the room

temperature conditions, and RTC measurements in UO_2 - PuO_2 lattices were scarce. In order to obtain an accurate and exhaustive experimental information, the CREOLE experiment was conceived in 1978 /5/ ; differential RTC measurements up to 300°C and integral water density effect measurement aimed to point out the origin of the calc/exp discrepancy. The description and the interpretation of this PWR RTC experiment performed in the EOLE reactor is detailed in the third section.

Complementary RTC experiments were utilised to complete the experimental basis for our sensitivity studies : Calculation - Experiment Comparison on RTC start-up measurements in large French PWRS (operation feedback experience) and on French critical experiments in slab lattices are presented in the fourth section.

We then investigated the sensitivity of the temperature coefficient to the different nuclear data and to the cell parameters ; in the fifth section the results of the sensitivity studies are presented in the UO_2 lattices where the tendancies are the most meaningful.

In order to reduce the calculation-experiment discrepancy, some identified wrong data were modified : new evaluations /6/ of the ^{235}U and ^{238}U thermal cross-sections were presented /7/ at the 1982 International Conference on Nuclear Data. We performed the final evaluations in 1984 and presented the proposed cross-section shapes at the CHICAGO Conference /8/ ; we shall point-out in the sixth section that these new-cross sections were consistent with uncertainties and values of available differential cross-section measurements. These evaluations were implemented in the up-dated APOLLO multigroup library /9/ : this 1986 APOLLO library is qualified through french LWR integral experiments /10/and enabled us to perform accurate reactor calculations.

2. THEORETICAL ANALYSIS OF THE MAIN TEMPERATURE EFFECTS CONTRIBUTING TO THE LWR REACTIVITY COEFFICIENT

Reactor temperature variations modify the neutron balance through a nuclear mechanism and through a macroscopic physical phenomena :

- the thermal move of the target nuclei increases with the temperature : fuel temperature induces U/Pu resonance broadening (Doppler effect), and moderator temperature variation leads to the modification in the "thermalized neutron temperature" (Thermal Spectrum Shift effect) ;

- the temperature increase induces a thermal expansion of the core materials ; the main neutron effect, due to the Water Density decrease, is linked to the moderation ratio modification (K_∞ contribution) and the migration area M^2 increase (leakage contribution).

2.1 Neutron balance breakdown

The core effective multiplication factor depends on non-leakage probability P :

$$Keff = K_\infty \cdot P$$

We shall use the following breakdown pattern :

$$K_\infty = \chi \cdot \varepsilon^f \cdot \varepsilon^{epith} \cdot p \cdot f \cdot \eta^{th}$$

χ : (n, 2n) factor

ε^f : "fast" fission factor (^{238}U, ^{240}Pu)

ε^{epith} : epithermal fission factor (^{235}U, ^{239}Pu, ^{241}Pu fissions above the thermal cut-off Ec = 0.625 eV)

p : resonance escape probability (^{238}U, ^{240}Pu)

1-f : parasitic thermal capture probability (moderator and clad capture)

η : neutron yield per absorption in fuel.

In a fundamental mode the P leakage factor is patterned by the formula :

$P = \frac{e^{-\tau B^2}}{1+L^2B^2}$ where τ, L^2 and B^2 are respectively the Fermi age, the diffusion area and the core geometrical buckling. For non-homogeneous core, the P factor is computed as $P = A^{core} / (A^{core} + A^{reflector})$ where A stands for the neutron absorption rate.

The Temperature Coefficient is defined as :

$$\alpha = \frac{1}{Keff} \cdot \frac{dKeff}{dT} \qquad \text{then,}$$

$$\alpha = \frac{1}{\chi}\frac{d\chi}{dT} + \frac{1}{\varepsilon^f}\frac{d\varepsilon^f}{dT} + \frac{1}{\varepsilon^{ep}}\frac{d\varepsilon^{ep}1}{dT\ p}\frac{dp}{dT} + \frac{1}{f}\frac{df}{dT} + \frac{1}{\eta}\frac{d\eta}{dT} + \frac{1}{P} \cdot \frac{dP}{dT}$$

2.2 K_∞ contribution to α (RTC) value

A PWR ⌀1.26 cm square pitch lattice is used.

A UO_2 cell 3.1 % ^{235}U enriched and a MOX cell (UO_2 - PuO_2 with 3.2 % fissile Pu enrichment) are studied.

Table I shows the results in the UO_2 fueled lattice. The main contributions to K_∞ reactivity change are linked to water density effect :

- the fast and epithermal fission factors produce a strong positive contribution, up to + 50 pcm/°C in hot conditions,
- the ^{238}U resonance escape factor gives a strong stabilizing component around - 100 pcm/°C in operating conditions,
- parasitic capture in water contributes positively with + 15 pcm/°C.

TABLE I: K_∞ COMPONENT BREAKDOWN WITH THE TEMPERATURE CHANGE IN A PWR CELL (UO_2e^{235} = 3.1%)
(in pcm/°C)

Temperature Range	$\frac{1}{\chi} \cdot \frac{d\chi}{dT}$	$\frac{1}{\varepsilon_1} \cdot \frac{d\varepsilon_1}{dT}$	$\frac{1}{\varepsilon_2} \cdot \frac{d\varepsilon_2}{dT}$	$\frac{1}{p} \cdot \frac{dp}{dT}$	$\frac{1}{f} \cdot \frac{df}{dT}$	$\frac{1}{\eta} \cdot \frac{d\eta}{dT}$	$\frac{1}{k_\infty} \cdot \frac{dk_\infty}{dT}$
20°C - 115°C	+ 0.046	+ 2.912	+ 7.681	- 21.835	+ 4.960	- 3.379	- 10.762
115°C - 190°C	+ 0.092	+ 5.259	+ 14.245	- 37.879	+ 7.621	- 3.207	- 15.290
190°C - 245°C	+ 0.103	+ 7.980	+ 22.345	- 56.961	+ 10.084	- 3.174	- 21.371
245°C - 290°C	+ 0.149	+ 12.127	+ 35.474	- 85.068	+ 13.403	- 3.339	- 29.737
20°C - 290°C	+ 0.088	+ 6.169	+ 17.416	- 42.093	+ 8.218	- 3.272	- 17.042

With a 1200 ppm soluble boron poisoning level (BOC), the 1/f . df/dT component amounts to + 45 pcm/°C in PWR nominal conditions ; then the overall K_∞ RTC value becomes slightly negative and constant $\alpha \simeq -4$ pcm/°C for every temperature and limits drastically the moderator poisoning.

The η contribution is very weak (- 3 pcm/°C) and appears as constant with the temperature because it corresponds to the Thermal Spectral Shift effect.

Table II gives the results in the Pu fueled cell. The fast and epithermal effects are increasing because of the larger Resonance Integral of ^{239}Pu and ^{241}Pu ; the resonance escape factor component increases by 40 % due to the ^{240}Pu 1 eV resonance. In the thermal range, the f contribution is heavily reduced by the strong absorption of the Pu fuel rod ; the spectrum effects are more important, around - 7 pcm/°C, due to the high contribution level of ^{239}Pu production and absorption cross-sections.

2.3 Detailed temperature effect analysis in the thermal neutron range

In fact, the weak η contribution in the K_∞ variation with temperature change is the result of the cancelling of large positive and negative components linked to thermal cross-sections. In order to point-out the cross-section shape components, the η . f breakdown was performed with separate reaction rates normalized to a $\sigma = \beta/v$ reaction rate.

Results are presented in table III and IV for UO_2 and PuO_2 lattices. This breakdown of the thermal RTC components stresses the importance of the ^{235}U and ^{239}Pu thermal cross-sections : although the final effect on η is some few pcm/°C, it results from absorption and production compo-

TABLE II: K_∞ COMPONENT BREAKDOWN WITH THE TEMPERATURE CHANGE IN A PWR/MOX CELL (3.2% Pu ENRICHED) (in pcm/°C)

Temperature Range	$\frac{1}{X} \cdot \frac{dX}{dT}$	$\frac{1}{\epsilon_1} \cdot \frac{d\epsilon_1}{dT}$	$\frac{1}{\epsilon_2} \cdot \frac{d\epsilon_2}{dT}$	$\frac{1}{p} \cdot \frac{dp}{dT}$	$\frac{1}{f} \cdot \frac{df}{dT}$	$\frac{1}{\eta} \cdot \frac{d\eta}{dT}$	$\frac{1}{k_\infty} \cdot \frac{dk_\infty}{dT}$
20°C - 130°C	+ 0.050	+ 2.865	+ 11.998	- 29.383	+ 4.810	- 7.018	- 16.426
130°C - 200°C	+ 0.133	+ 6.739	+ 23.831	- 53.746	+ 5.700	- 6.760	- 25.004
200°C - 254°C	+ 0.140	+ 10.175	+ 37.380	- 79.858	+ 6.338	- 6.839	- 34.174
254°C - 296°C	+ 0.269	+ 15.749	+ 60.863	- 121.200	+ 7.487	- 7.401	- 47.354
20°C - 296°C	+ 0.122	+ 7.292	+ 28.172	- 55.887	+ 5.776	- 6.928	- 26.048

TABLE III: TEMPERATURE EFFECT IN THE NEUTRON THERMAL RANGE (in pcm/°C)

		20°C - 115°C	115°C - 190°C	190°C - 245°C	245°C - 290°C
UO_2 fuel	σ_a^{238}	- 0.260	- 0.246	- 0.250	- 0.288
	σ_a^{235}	+ 11.204	+ 8.723	+ 7.409	+ 6.908
	$(\nu\sigma_f)^{235}$	- 15.249	- 12.410	- 10.873	- 10.386
	Total	- 4.305	- 3.933	- 3.714	- 3.766
Clad	$\sigma_a Zr$	+ 0.027	+ 0.019	+ 0.015	+ 0.012
	f_g	+ 0.041	+ 0.033	+ 0.029	+ 0.039
	Total	+ 0.068	+ 0.052	+ 0.044	+ 0.051
Moderator	$\sigma_a^{H_2O}$	+ 0.702	+ 0.483	+ 0.372	+ 0.316
	d_{H_2O}	+ 4.001	+ 6.877	+ 9.407	+ 12.664
	f_m	+ 1.192	+ 0.959	+ 0.834	+ 0.797
	Total	+ 5.895	+ 8.319	+ 10.613	+ 13.777
Total = $\frac{1}{\eta f} \cdot \frac{d(\eta f)}{dT}$		+ 1.658	+ 4.438	+ 6.943	+ 10.062

nents around 10-15 pcm/°C for ^{235}U and 60 pcm/°C for ^{239}Pu. The ^{239}Pu cross section components to RTC value are larger than ^{235}U cross-section components because of a more pronounced non-1/v shape ; the opposite sign of the ^{235}U and ^{239}Pu components comes from a slopy σ235 (first negative resonance) compared to standard 1/v law and from a σ239 (E) increase lower than 1/v due to the large 0.3 eV resonance.

We have to note that cross-section contributions (as does disadvantage factor fm = Φmod/Φfuel) are slightly decreasing with Temperature because they originate from Spectrum Shift effect, whereas other thermal components linked to water expansion (N_{H2O}, N_B) give increasing contributions with temperature.

2.4 Leakage component to the RTC value

The τ and L^2 migration area components ($M^2 = \tau + L^2$) enable us to separate fast and thermal leakage contributions to the RTC value :

$$\frac{1}{P} \cdot \frac{dP}{dT} = - \left(\frac{M^2B^2}{1+M^2B^2}\right) \cdot \left[W^{fast} \cdot \frac{1}{\tau}\frac{d\tau}{dT} + W^{th} \cdot \frac{1}{L^2}\frac{dL^2}{dT} \right]$$

As the thermal area L^2 represents about 8 % of the migration area in a UO_2 lattice, the weight of the fast neutron range $W^{fast} = \tau/M^2$ induces a fast contribution ten times larger than the thermal leakage components. In a MOX assembly, the fast/thermal ratio is roughly thirty as shown in table V ; this table points out that the CREOLE leakage contribu-

TABLE IV: TEMPERATURE EFFECT IN THE NEUTRON THERMAL RANGE WITH A UO_2–PuO_2 FUEL (in pcm/°C)

		20°C - 130°C	130°C - 200°C	200°C - 254°C	254°C - 296°C
UO_2-PuO_2 fuel	σ_a^{235}	+ 0.966	+ 0.811	+ 0.770	+ 0.835
	$(\nu\sigma_f)^{235}$	- 1.262	- 1.066	- 1.011	- 1.076
	σ_a^{238}	- 0.101	- 0.096	- 0.105	- 0.119
	σ_a^{239}	- 60.685	- 63.660	- 65.540	- 69.757
	$(\nu\sigma_f)^{239}$	+ 57.425	+ 60.890	+ 62.907	+ 67.033
	σ_a^{240}	- 1.485	- 1.726	- 2.034	- 2.590
	σ_a^{241}	- 1.223	- 1.144	- 1.036	- 0.907
	$(\nu\sigma_f)^{241}$	+ 1.316	+ 1.193	+ 1.039	+ 0.847
	Total	- 5.049	- 4.798	- 5.010	- 5.734
Clad	σ_a^{Zr}	+ 0.017	+ 0.010	+ 0.007	+ 0.004
	f_g	+ 0.006	- 0.001	- 0.003	- 0.001
	Total	+ 0.023	+ 0.009	+ 0.004	+ 0.003
Moderator	σ_a^{H2O}	+ 0.391	+ 0.243	+ 0.164	+ 0.107
	d_{H_2O}	+ 1.955	+ 3.263	+ 4.199	+ 5.488
	f_m	+ 0.254	+ 0.144	+ 0.101	+ 0.124
	Total	+ 2.600	+ 3.650	+ 4.464	+ 5.719
Total = $\frac{1}{nf} \cdot \frac{d(nf)}{dT}$		- 2.130	- 1.139	- 0.542	- 0.012

TABLE V: LEAKAGE CONTRIBUTION TO THE REACTIVITY TEMPERATURE COEFFICIENT (UO_2–PuO_2 lattice)

	$\frac{1}{P_{th}} \cdot \frac{dP_{th}}{dT}$ (pcm/°C)		$\frac{1}{P_r} \cdot \frac{dP_r}{dT}$ (pcm/°C)		$\frac{1}{P} \cdot \frac{dP}{dT}$ (pcm/°C)	
	CREOLE	PWR	CREOLE	PWR	CREOLE	PWR
20°C - 130°C	- 0.697	- 0.096	- 16.918	- 2.342	- 17.615	- 2.438
130°C - 200°C	- 1.061	- 0.149	- 34.056	- 4.799	- 35.117	- 4.948
200°C - 254°C	- 1.471	- 0.213	- 51.566	- 7.478	- 51.574	- 7.691
254°C - 296°C	- 2.058	- 0.322	- 76.198	- 11.916	- 78.256	- 12.238

tion to RTC measured value is overestimated by a factor 7 compared to the leakage contribution in a 1000 MWe PWR.

The severe increase with temperature of the leakage component demonstrates that RTC leakage contribution is mainly linked to water density effect.

3. THE CREOLE EXPERIMENT

The objective of the CREOLE experimental program was to respond to the nead for accurate and differential information spanning the 20-300°C temperature range.

CREOLE experiment aims to point out the origin of the Calculation - Experiment discrepancy : temperature effect measurements and overclad experiments were performed in order to uncouple water density effects from nuclei temperature effects.

During this experimental program, the following measurements were performed :

- continuous differential measurements of the temperature coefficient of reactivity in UO_2 clean and Boron poisoned lattices and UO_2 - PuO_2 lattices, ranging from room temperature up to 300°C,
- an integral measurement to calibrate the average temperature coefficient between 20°C and 300°C using the equivalence with the Boron poisoning effect of the moderator : this experiment enabled us to qualify the βeff value used in the RTC measurement by doubling time method,
- measurements of the reactivity effects due to the change in water density has been simulated by the use of Aluminium overcladding in order to remove the moderator.

All these measurements were carried out in a PWR fuel type zone contained in a pressurized cylindrical loop located in the center of the Zero power reactor EOLE.

3.1 Description of the CREOLE facility

The CREOLE experimental facility consists of a pressurized central test loop in which it is possible to achieve the moderator temperature and the pressure of a large PWR power reactor, a large air gap separation zone and a peripheral driver core zone surrounded by a water reflector. Starting from the center, the experimental loop contains the following concentric zones (see figure 1) :

- A central tube made of Zirconium alloy (9.8 mm i.d. ; 1 mm thickness), intended for axial distribution of fission rate measurements using fission chambers.
- A PWR type assembly of 200 UO_2 or UO_2-PuO_2 fuel pins with Zircalloy cladding. The fuel rods were arranged in a 1.26 cm square lattice pitch. The main characteristics of the fuel rods used are summarized below :
  - Pellet diameter : 8 mm
  - o.d. of cladding : 9.4 mm
  - Uranium enrichment : 3.1 % for UO_2 fuel rods and natural UO_2 for mixed oxide (UO_2-PuO_2) fuel rods.
  - Plutonium characteristics : two enrichments were used, 2 % and 3.2 % on fissile Plutonium.
- A zirconium alloy filler to prevent water gaps next to the peripheral cells of the lattices studies in the central loop.
- An annular tube made of Zirconium alloy, designed in such a way that it can withstand the maximum pressure conditions in the experimental zone (120 bars for the 300°C temperature).

The driver core was loaded with UO_2 (3.5 % enrichment) fuel pins with Aluminium cladding. The fuel rods were arranged in a 1.43 cm square lattice pitch. The criticality was obtained by raising the moderator

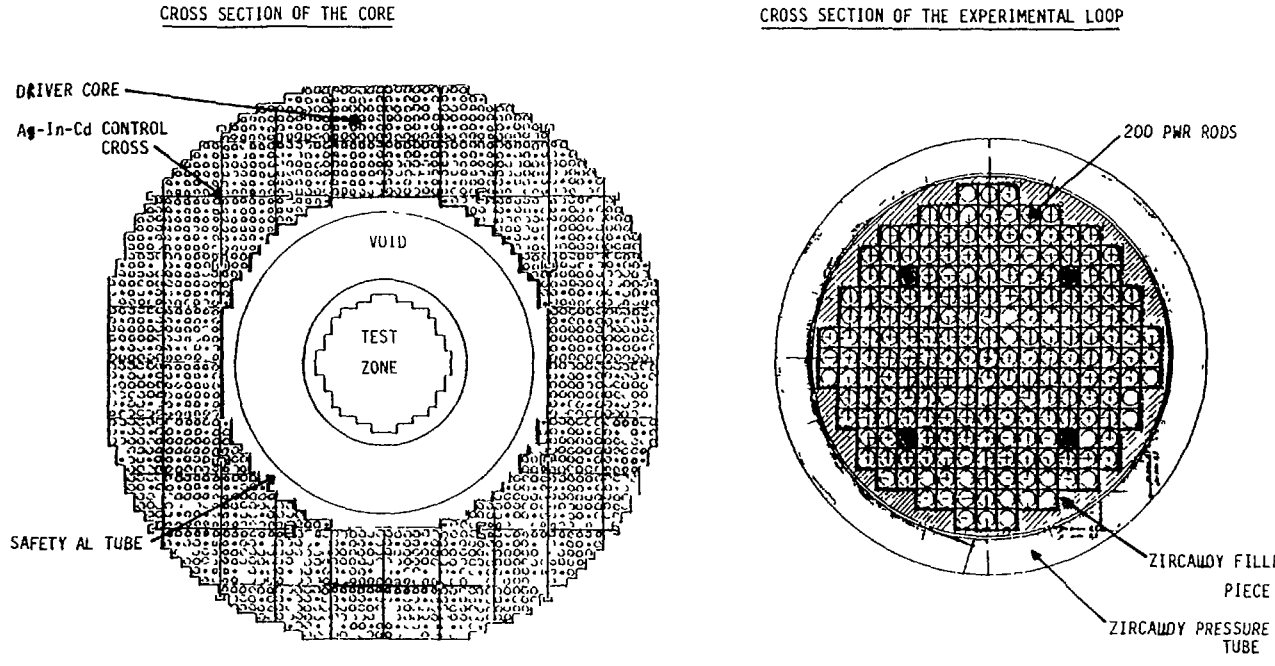

FIG 1 Radial cross-section of the CREOLE experiment

(light water) level in the reactor tank. For safety reasons the driver core was isolated from the experimental loop by a tank made of Aluminium alloy and a large air gap zone which contains a stainless-steel heat reflector intended to prevent the heat leakage from the central loop to the driver core. The driver core sizes were adjustable according to the investigated lattice type and the operating conditions in the central loop.

The driver core was surrounded by a radial reflector made of water. Except for the control rod system which was located above the reactor core, all the other auxiliary systems intended either for operating or for safety purposes were located under the reactor tank. Figure 2 shows a longitudinal section of the CREOLE core.

Measurements were performed in the four following configurations of the experimental loop :

- configuration 1 : In this configuration the experimental loop was loaded with 200 UO_2 (3.1 % ^{235}U enriched) fuel rods and a clean water moderator.

- configuration 2 : In this configuration the experimental loop was loaded with 200 UO_2-PuO_2 fuel rods (80 rods 2 % fissile Pu enriched and 120 central rods with 3.2 % fissile Pu enrichment).

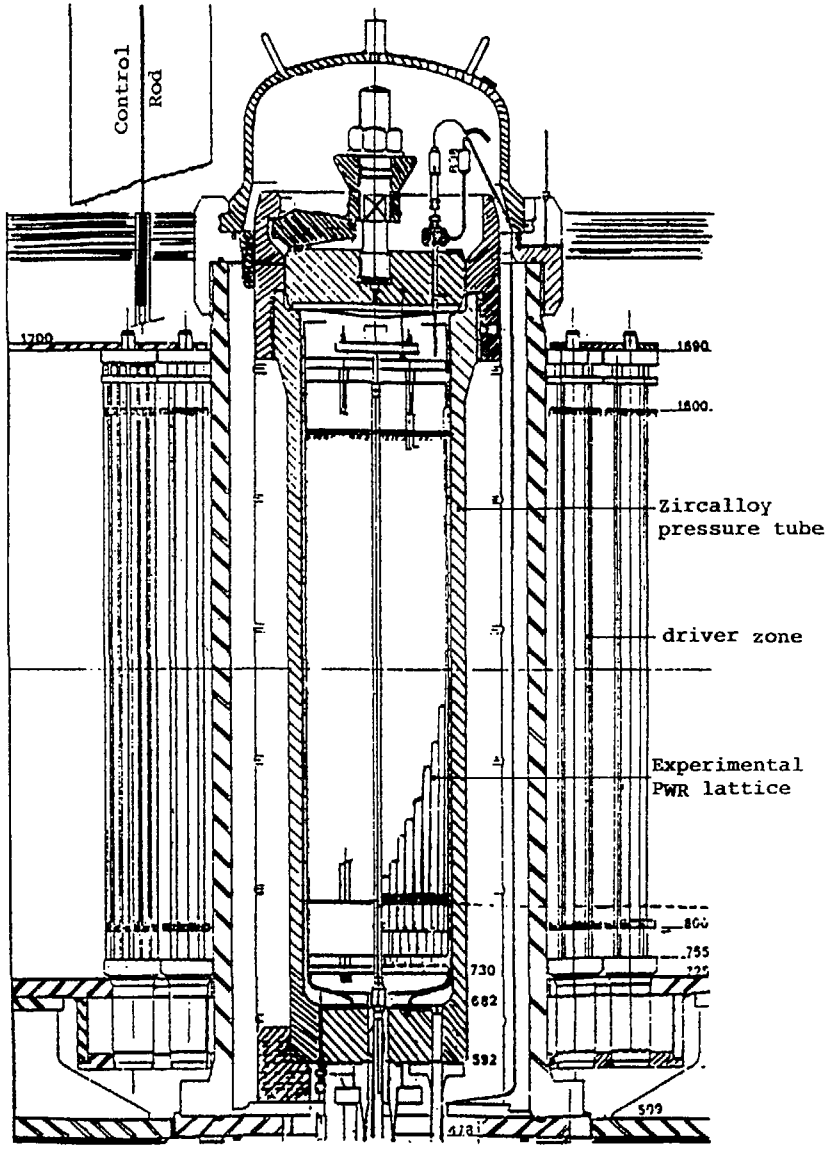

FIG. 2. Longitudinal cross-section of the CREOLE core.

- configuration 3 : This configuration is different from the configuration 1 by the addition of 1200 ppm of Boron in the moderator.

- configurations 4 : Aluminium overclads are placed around experimental fuel rods.

3.2 Measurements Techniques and Experimental Results

3.2.1 Reactivity and Temperature measurements

Starting from a core with a reactivity excess of about 300 pcm, the moderator temperature in the experimental loop was raised using an electric heater placed in a water storage tank located below the reactor tank. The resultant reactivity change was measured by the usual positive reactor period method.

The temperature was measured with a platinium resistance thermometer located in the top, just under the cover, of the experimental loop. The temperature homogeneity has been proved experimentally using the indications given by 7 thermocouples located in different spot levels inside the experimental loop. The relative uncertainty in the measured temperatures was estimated at 0.2°C.

In the configurations 1 and 2, the reactivity loss due to the temperature change from 20°C to 300°C was much greater than the core reactivity excess (300 pcm). This led us to perform the reactivity measurements for these configurations in four temperature ranges, with corresponding driver core loadings (see figure 3) :

- 1^{t} range : 20°C - 120°C
- 2^{d} range : 110°C - 200°C
- 3^{d} range : 190°C - 250°C
- 4^{th} range : 245°C - 300°C

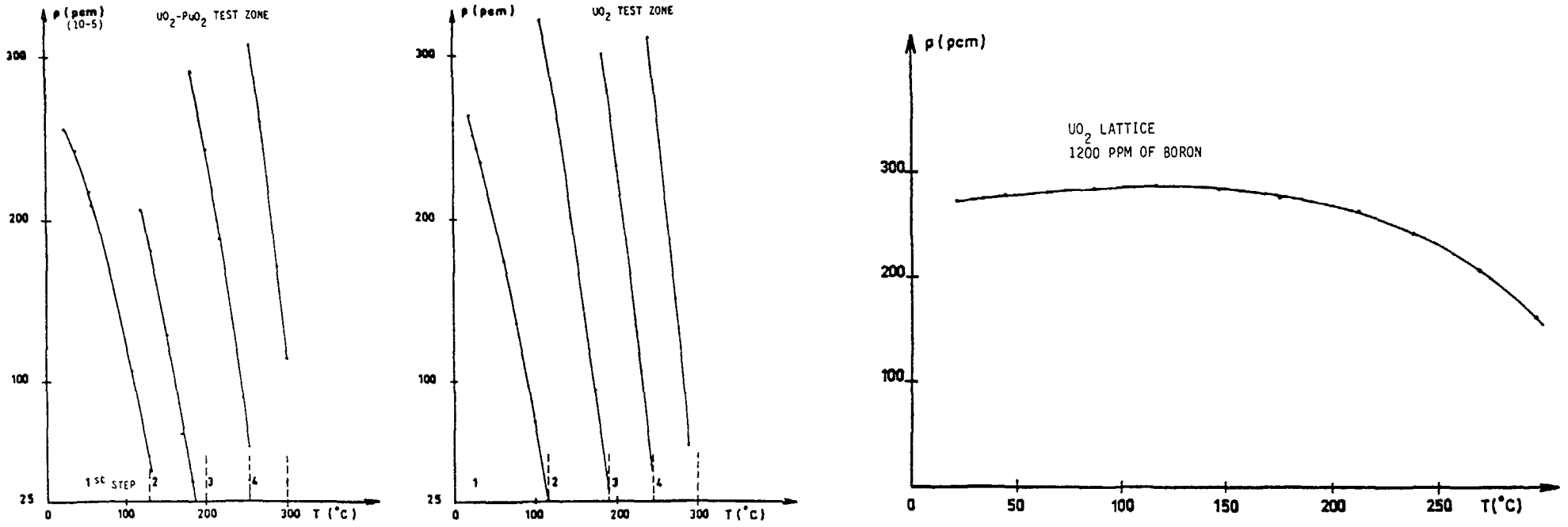

FIG. 3. Core reactivity effects as a function of the loop temperature.

The passage from one to the next range required to reload the driver core in order to achieve a core reactivity excess of 300 pcm. The reactivity measurements were carried out by steps of ΔT = 5°C in each temperature range.

In the configuration 3, where the Boron was added to the moderator (1200 ppm), the reactivity loss corresponding to the temperature change from 20°C to 300°C, was less than the core reactivity excess (figure 3). Consequently, all the reactivity measurements were performed with the same driver core loading ; moreover the light reactivity variations lead to accurate RTC measurements because the experimental value is independant of the βeff.

In addition to these differential measurements, the following integral reactivity measurements have also been carried out : determination of the integral temperature effect between 20°C and 300°C by equivalence with the Boron effect.

3.2.2 Overclad experiments

Water density effects on the temperature coefficient were simulated in the configuration 4 by the use of three sets of Aluminium overclads to remove moderator. The simulated values of the water density were : 0.6, 0.8 and 0.9 g/cm^3.

3.2.3 Fission rate distribution measurements

The aim of these measurements is to achieve the qualification of the 3D core calculation.

Several measurements of radial power distribution have been carried out in both experimental loop and driver core. For the experimental loop these measurements have been performed in room temperature as well as in 300°C. Various techniques were applied in these measurements, including gamma-spectrometry on fuel rods, fission chambers and activation foils.

Axial buckling measurements were performed in the central thimble with miniature fission chambers.

3.3 Experimental data analysis

In order to condense the experimental results (fig. 3) in a pratical form and to avoid the experimental fluctuations, we introduced a least square polynomial fitting of the measured core reactivity versus the loop temperature in the overall 20-300°C experimental range (see fig. 4a). For the clean water configurations 1 and 2, this was achieved by joining the results in the four temperature steps through characteristic smoothing fit inside each temperature range.

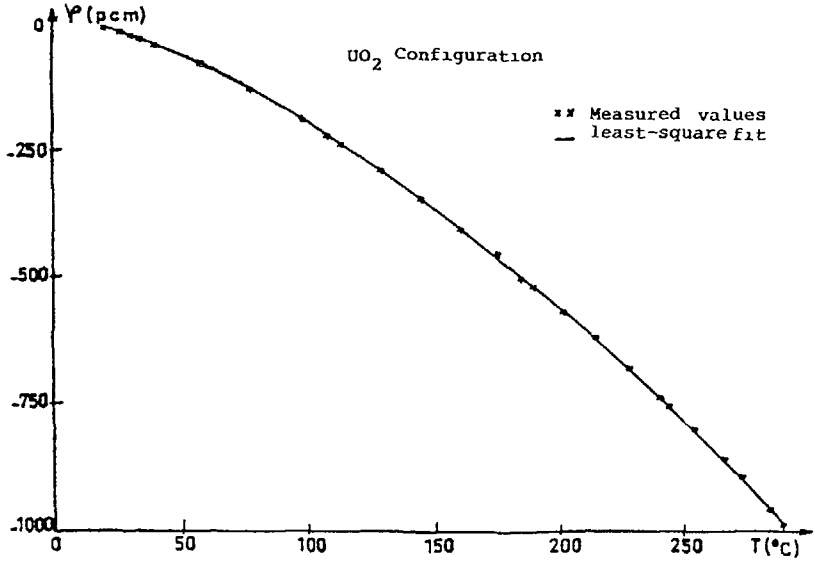

FIG. 4a. Core reactivity with temperature

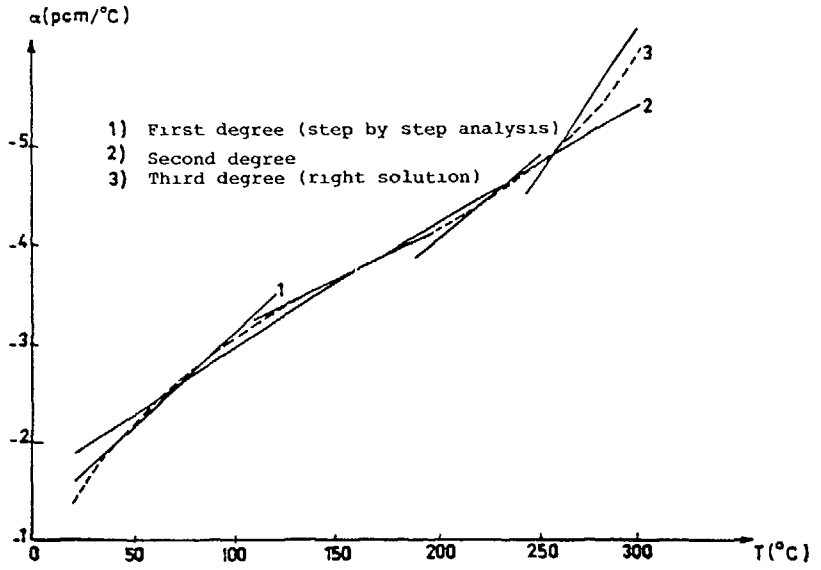

FIG. 4b. Various fitted shapes of the RTC core measurements.

It became obvious that a fourth degree polynomial fit must be used to smooth (see fig 4a and 4b) the overall core reactivity variation ; the derivative of this fit supplies the experimental differential RTC core value versus loop temperature ; these analytical forms are given in the following table :

	$\alpha_{core} = \frac{d\rho_{core}}{dT}$ in pcm/°C
1 UO_2 lattice 0 ppm Boron	$- 0.794 - 3.429 \times 10^{-2}.T + 1.552 \times 10^{-4}.T^2 - 3.239 \times 10^{-7}.T^3$
2 UO_2-PuO_2 lattice 0 ppm Boron	$- 0.258 - 3.250 \times 10^{-2}.T + 1.665 \times 10^{-4}.T^2 - 3.596 \times 10^{-7}.T^3$
3 UO_2 lattice 1200ppm of Boron	$0.0189 + 1.539 \times 10^{-3}.T - 1.385 \times 10^{-5}.T^2 - 2.805 \times 10^{-9}.T^3$

As shown in the corresponding figure 4b for the UO_2 lattice, the core RTC in clean water configurations is negative for the whole 20°C - 300°C range and increases almost linearly with the temperature.

3.4 CREOLE core calculation

In order to determine the infinite medium calculation/experiment discrepancy, it was necessary to define an accurate calculation scheme of the CREOLE core. The high leakage level, and the axial streaming effect due to the large air gap zone, requires transport theory utilisation. Then, the 3D core calculation was performed in a RZ pattern (see figure 5) with a S_N code.

Due to the mismatched spectrum at the test loop/feeder zone boundary, we needed to elaborate a sophisticated group-constant collapsing pattern : the few group cross-sections were obtained with the French APOLLO transport code in the following sequence :

- the space homogeneization for each reactor lattice (test and driver zone) was performed in 99-energy groups through cell or multicell calculations,

- the spectrum used to collapse cross-sections was derived from a one dimensional calculation model of the core.

In order to define the optimum discretization of each variable in the Boltzmann equation, an important preliminary study has been carried out leading to the following pattern :

- S_4 quadrature,
- 10 energy-group (6 thermal groups),
- Radial mesh-point - 1 cm (for the asymptotic regions)
- Axial mesh-point ≤ 1.5 cm.

The absolute error in the corresponding computed core Keff is about 100 pcm.

The overall calculation sequence summarized in figure 6 was reproduced for every computed loop temperature Ti.

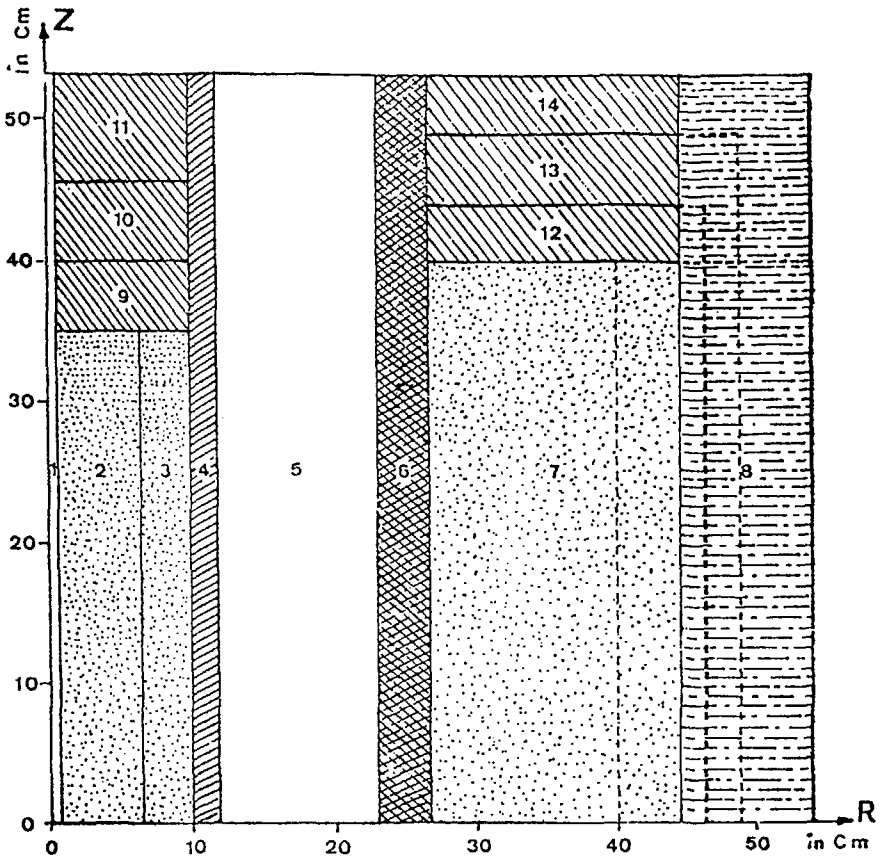

1. Thimble
2. UO_2-PUO_2 3.2 %
3. UO_2-PUO_2 2 %
4. Zircalloy pressure tube
5. Void
6. Safety tube : AG5
7. Feeder zone
8. H_2O
9. Axial reflector (CREOLE loop)
10. " " "
11. " " "
12. Axial reflector (Driver core)
13. " " "
14. " " "

FIG. 5. CREOLE RZ representation in S_N core calculation.

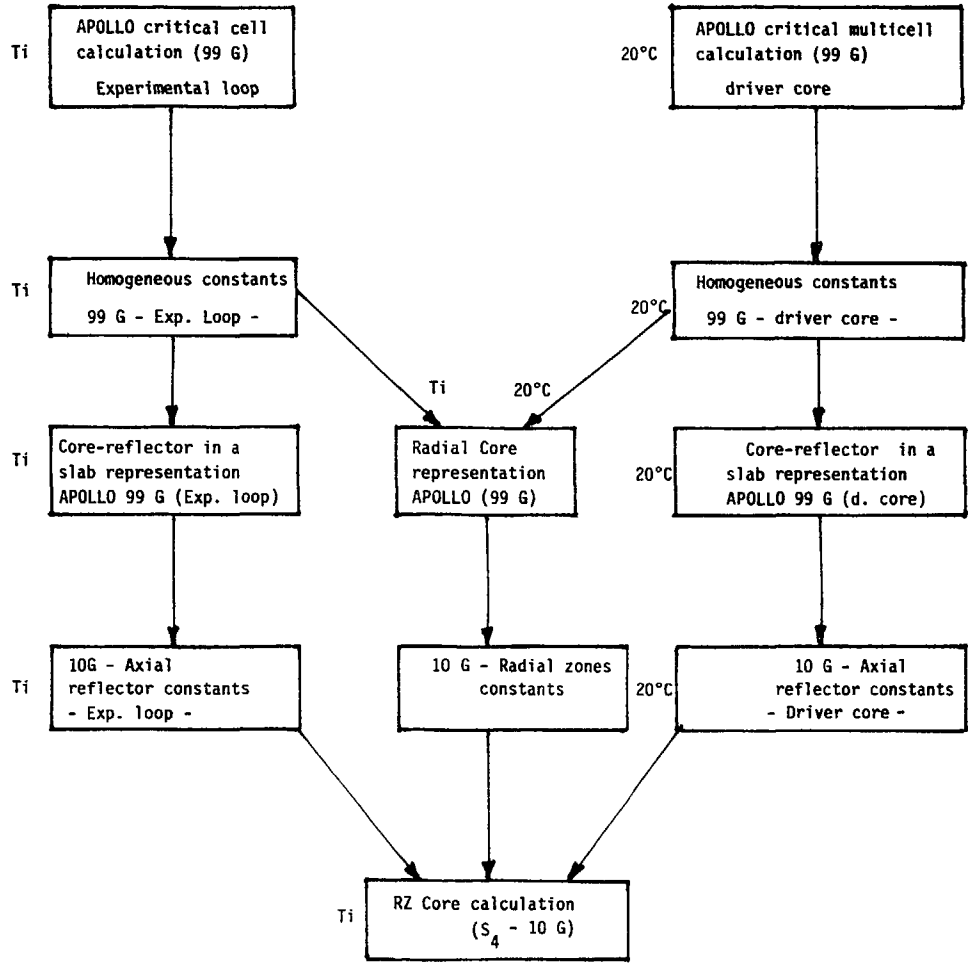

FIG. 6. CREOLE core calculation pattern.

This core calculation scheme was validated through 3D flux measurements. Figures 7 et 8, respectively for ^{235}U fission chamber activities in UO_2 and UO_2-PuO_2 lattices, point-out that axial buckling and streaming effect are accurately computed ; the good calc/experiment agreement in cold and hot conditions demonstrate that the measured axial leakage variation, linked to the reflector gain increase with water density expansion, is correctly reproduced.

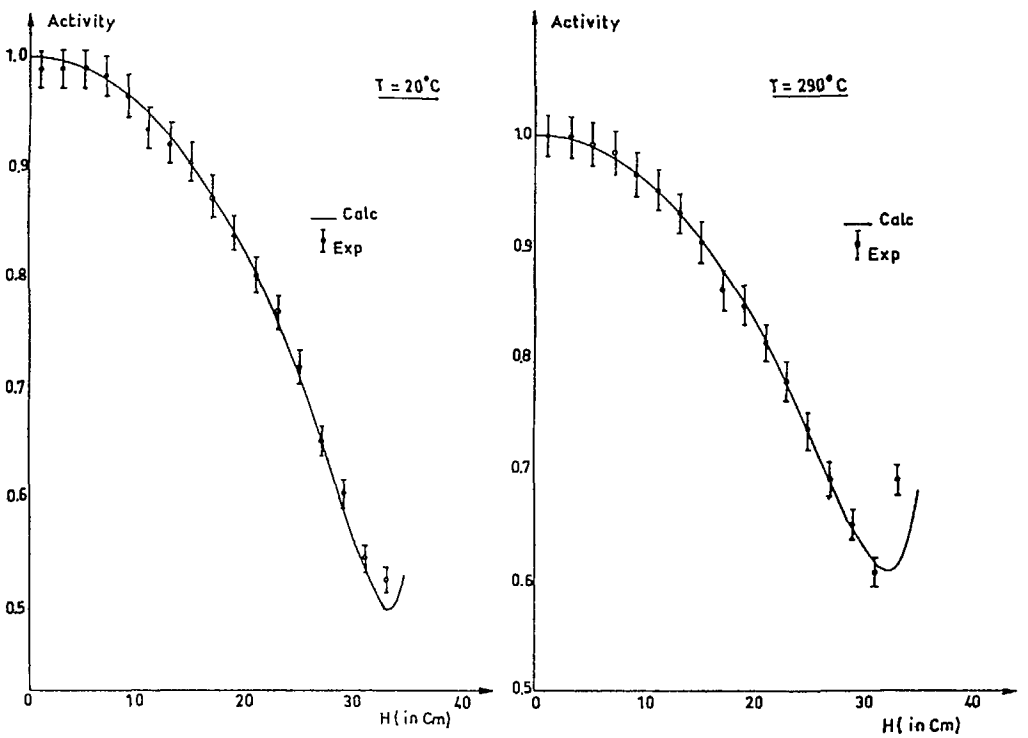

FIG. 7. Axial ^{235}U fission rate measurements in the CREOLE loop (UO_2 lattice).

Fission rate measurements on the experimental fuel rods are plotted on figures 9 and 10 (UO_2 and UO_2-PuO_2 lattice) : computed values are consistent with experimental radial power-maps within uncertainty margins. This results demonstrate that mismatched spectrum at the loop/driver zone boundary are well mocked-up ; figure 10 points out that strong thermal neutron gradients in the Pu test lattice are accurately reproduced.

The experimental-calculation comparaison of the radial distribution in the driver zone is graphed on the figure 11 : our RZ core calculation supplies a satisfactory flux shape at the core/water-reflector interface.

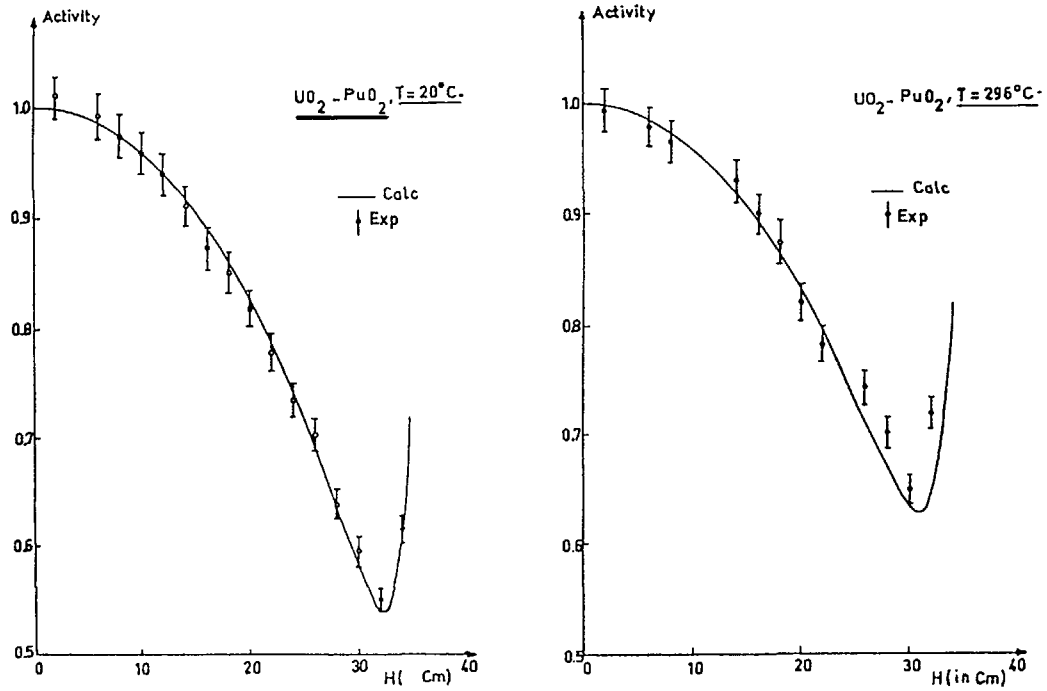

FIG. 8. Axial ^{235}U fission rate measurements in the CREOLE experiment.

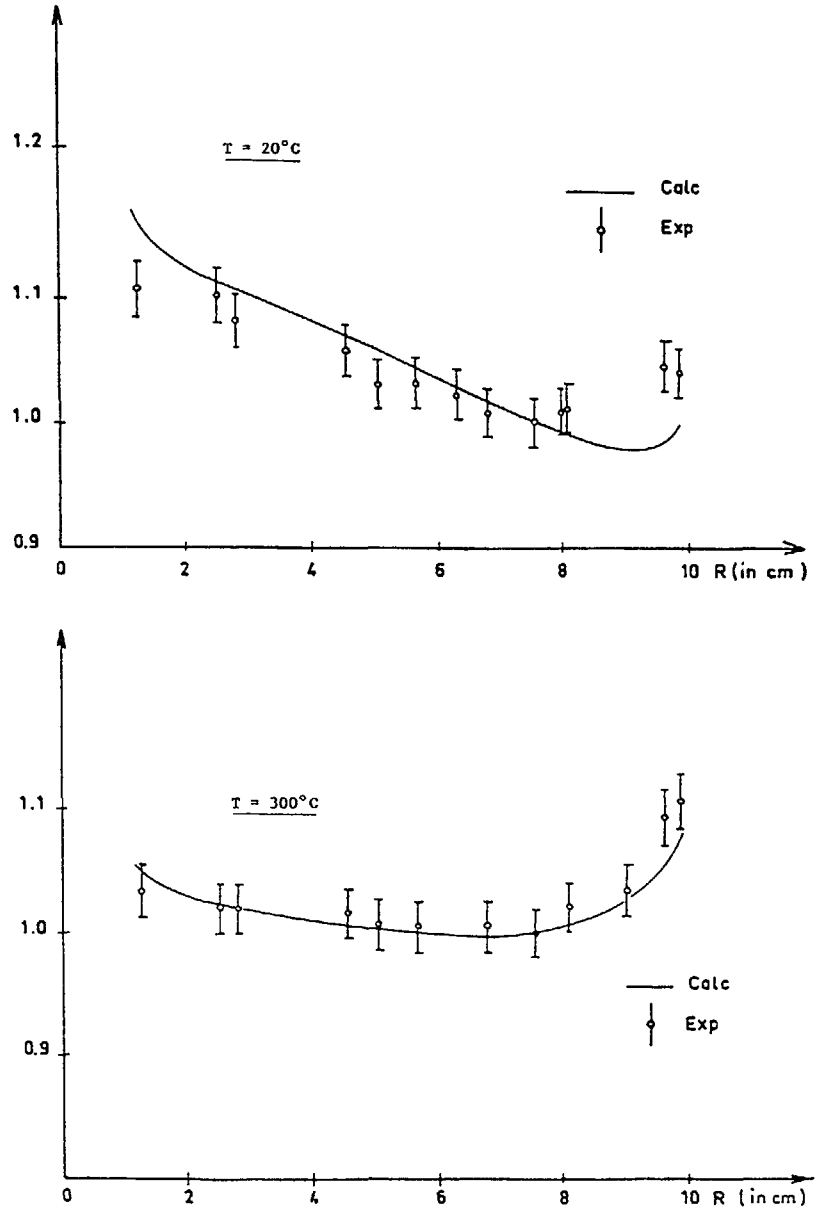

FIG. 9. Radial power maps in the UO_2 lattice.

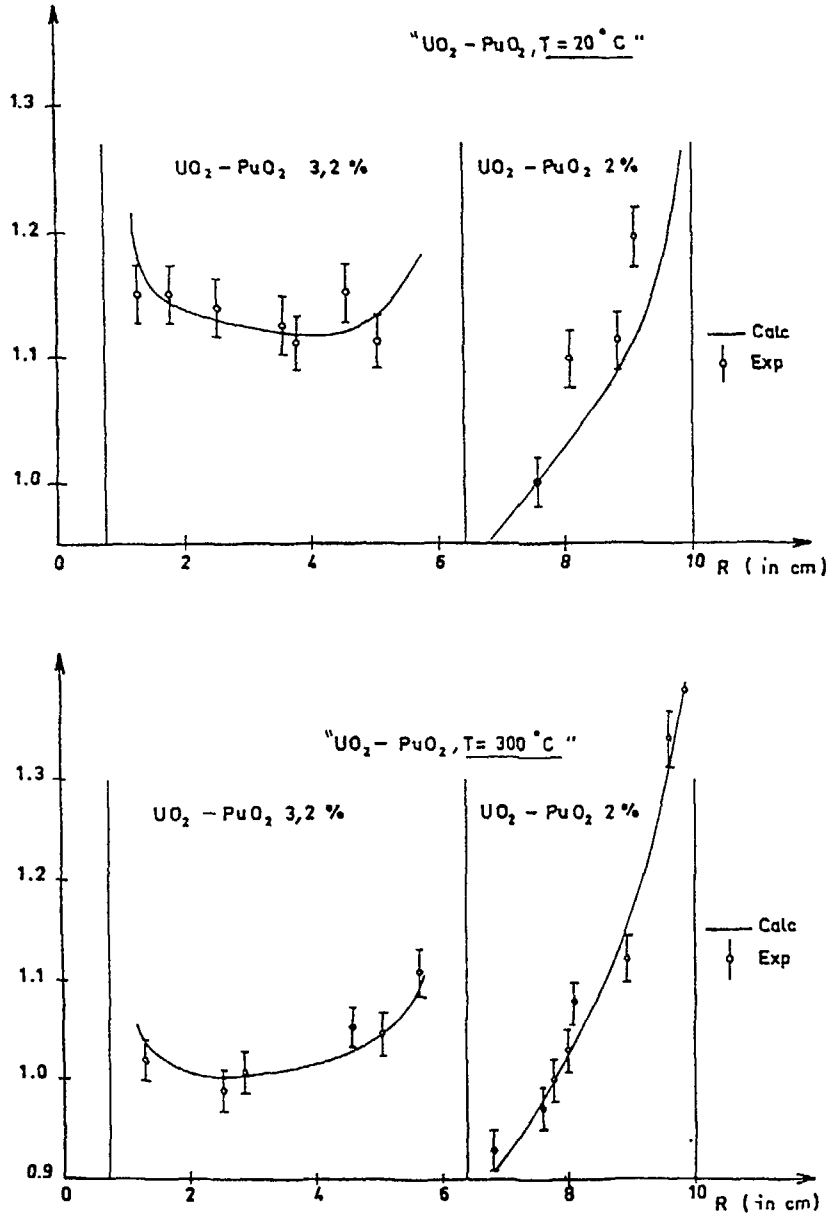

FIG. 10. Radial power map in the CREOLE loop.

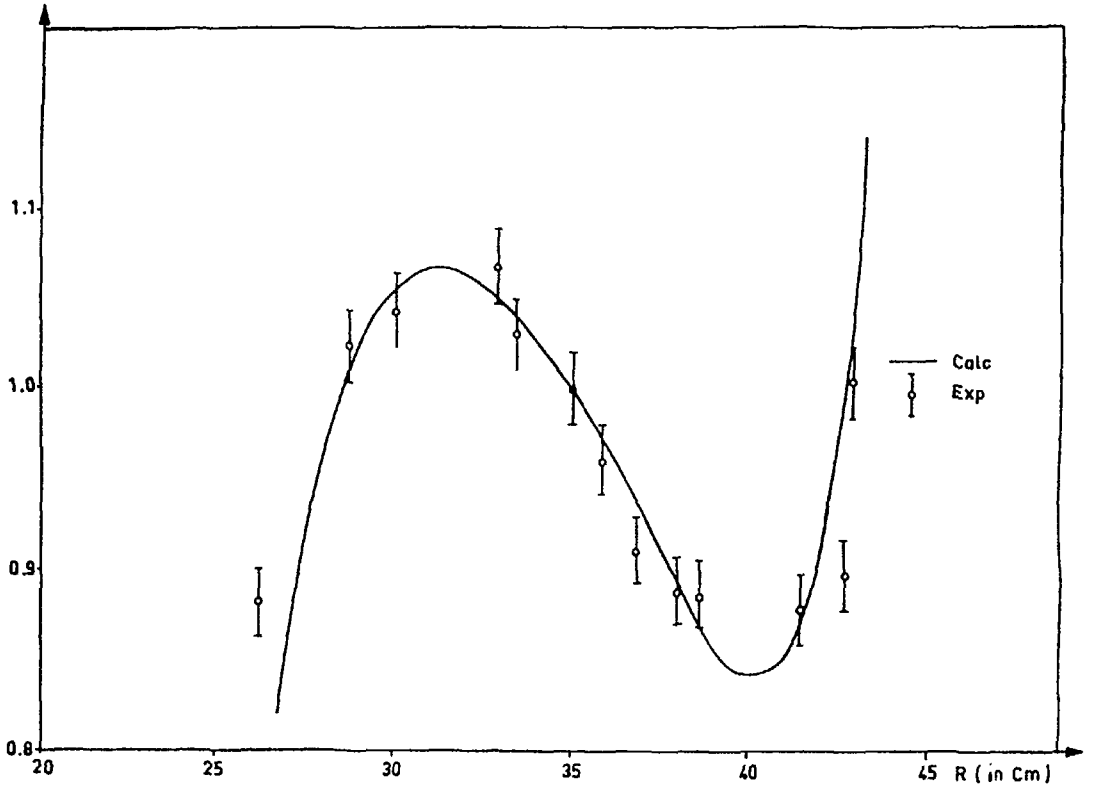

FIG. 11. Radial fission rate measurements in the feeder core.

3.5 Experiment-Calculation comparison of the core RTC measurements

. Differential core RTC values are graphed on figure 12 : the calculation-experiment comparaison stresses the commun trends to compute too negative 20-90°C RTC values in UO_2 lattices ; this discrepancy tends to be reduced in the 90°C - 250°C intermediary temperature range and it is slightly reversed for the hot conditions (T > 250°C). The experiment-calculation comparaison in the MOX lattice (figure 12) supplies less meaningful trends.

The interpretation of the overclad reactivity worth measurements is shown on the figure 13 in the UO_2-PuO_2 lattice configuration ; from

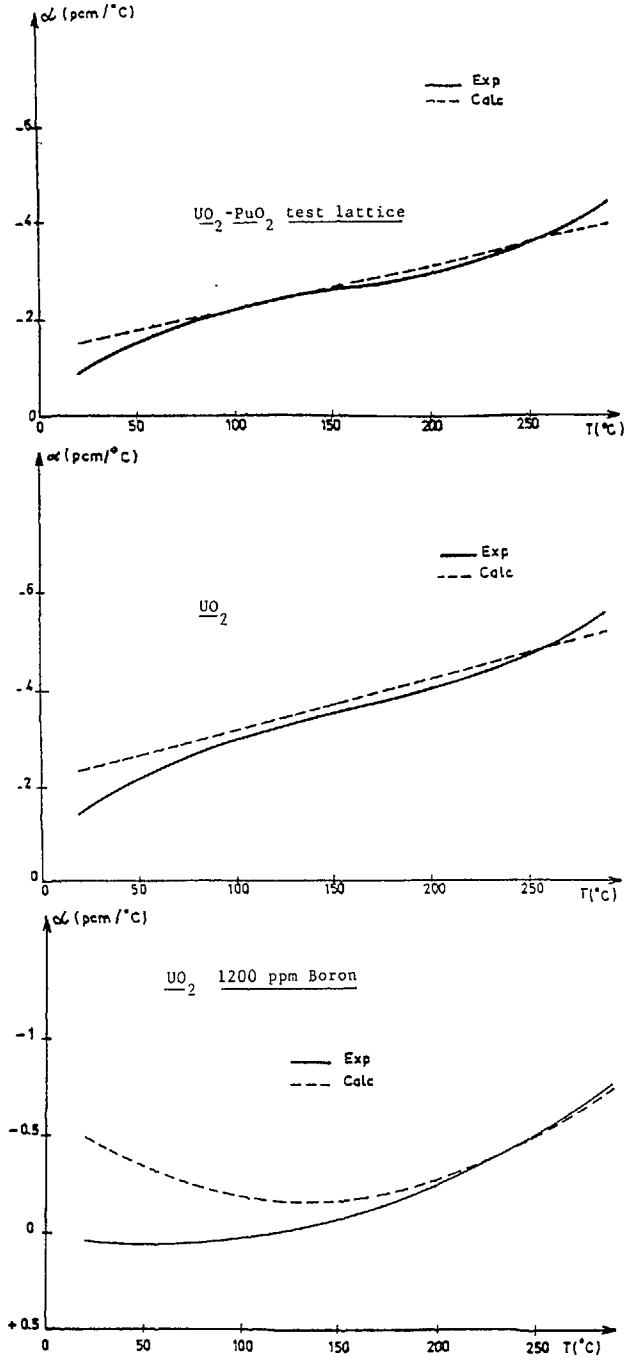

FIG. 12. RTC measurements in CREOLE.

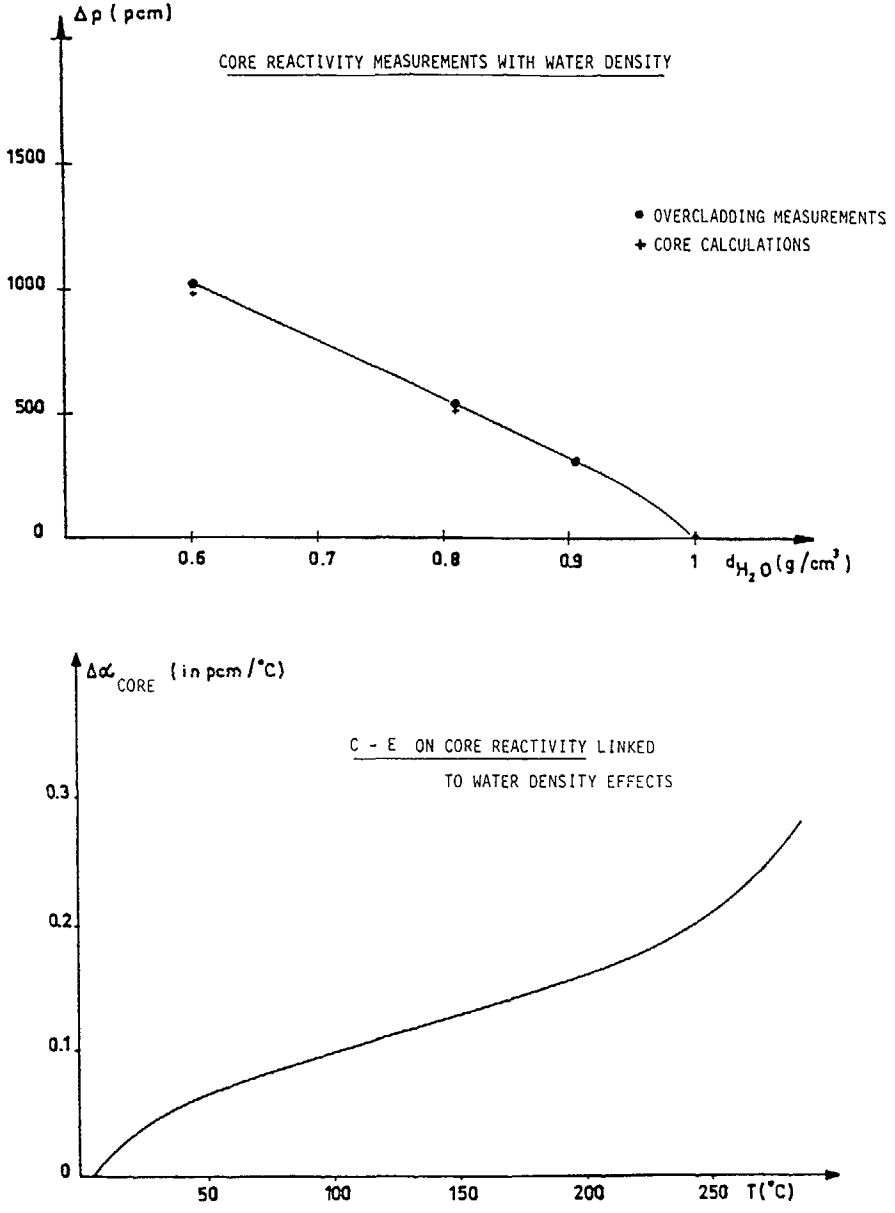

FIG. 13. Water density experiments.

these integral measurements in the various test lattices, we deduced that our S_N core calculation underestimates by 4 % ± 3 % the water-density effects ; this bias infers a contribution to the αcore RTC which presents a specific shape with temperature : figure 13b shows that this water density error is the main component to the inversion of the core RTC discrepancy in the high temperature range.

. In order to make these CREOLE results useful for a sensitivity study, it is necessary to derive the measured RTC discrepancy in a PWR lattice (independant of the specific coupled core CREOLE). This conversion of the $\Delta\alpha^{core}$ (T) CREOLE discrepancies at every T temperature is obtained through the following pattern :

$$\Delta\alpha\ (T)^{\infty}_{PWR} = \Delta\alpha\ (T)_{core}\ /W\ (T)$$

W (T) represents the reactivity weight of the experimental zone and was derived from core calculations.

. The deduced RTC Calculation - Experiment disagreement in fundamental mode is summarized in table VI ; the discrepancy shapes versus temperature are graphed on figure 14.

. The interpretation leading to these results includes two approximations in the Doppler effect calculation : the UO_2 crystalline binding effect and the countinuous variation of the Bell factor with fuel temperature change were neglected. The improved calculations were performed with a θDebye = 600°K correction to represent the crystalline binding effect ; this Debye temperature was deduced from Doppler measurements /11/ in the Minerve reactor through heated UO_2 sample oscillations in a PWR experimental lattice (figure 15). Figure 16 presents the comparison between these two CREOLE interpretations and points out that Doppler corrections reduce the calculation-experiment disagreement.

3.6 Spectral shift effect information

The above α Calc-Exp discrepancy involves the leakage contribution. We have shown in section 2.4 that leakage component in CREOLE RTC

TABLE VI: CALCULATION EXPERIMENT BIAS IN CREOLE C-E in pcm/°C ($10^{-5}\frac{\Delta K}{K}$/°C)

Temperature range T in °C	Measured effect	UO_2-PuO_2	UO_2	UO_2 1200 ppm of Boron
(20, 90)	Temperature coefficient	- 2.3 ± 1.8	- 4.2 ± 1.7	- 4.9 ± 1.2
	Water density effect	+ 0.4 ± 0.4	+ 0.5 ± 0.5	-
(90, 245)	Temperature coefficient	- 0.4 ± 2.5	- 1.9 ± 2.2	- 1.1 ± 1.7
	Water density effect	+ 1.1 ± 1.1	+ 1.4 ± 1.4	-
(245, 290)	Temperature coefficient	+ 2.2 ± 3.8	+ 1.1 ± 3.5	+ 0.3 ± 2.4
	Water density effect	+ 2.0 ± 2.0	+ 2.5 ± 2.5	-

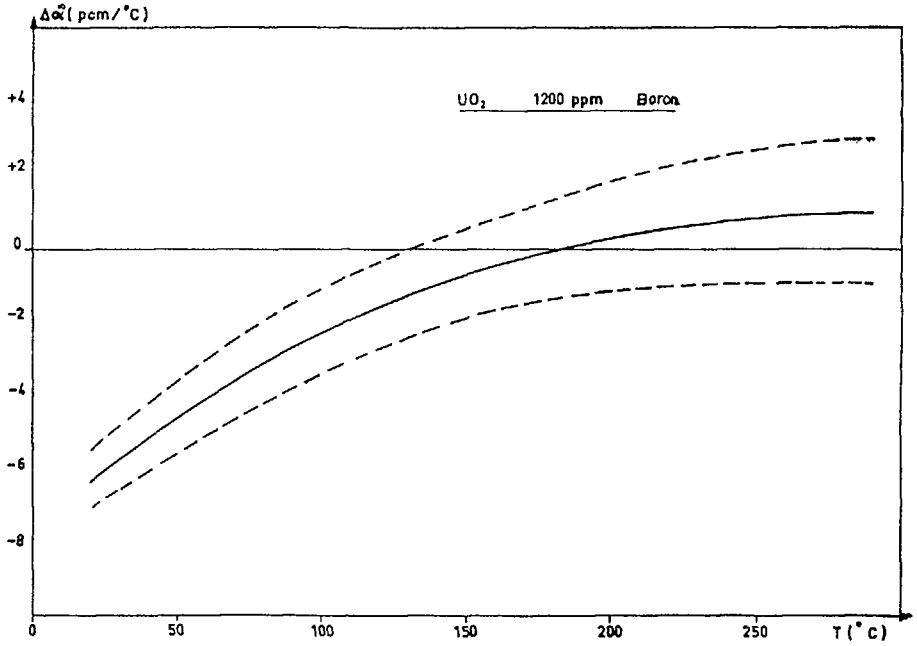

FIG. 14.

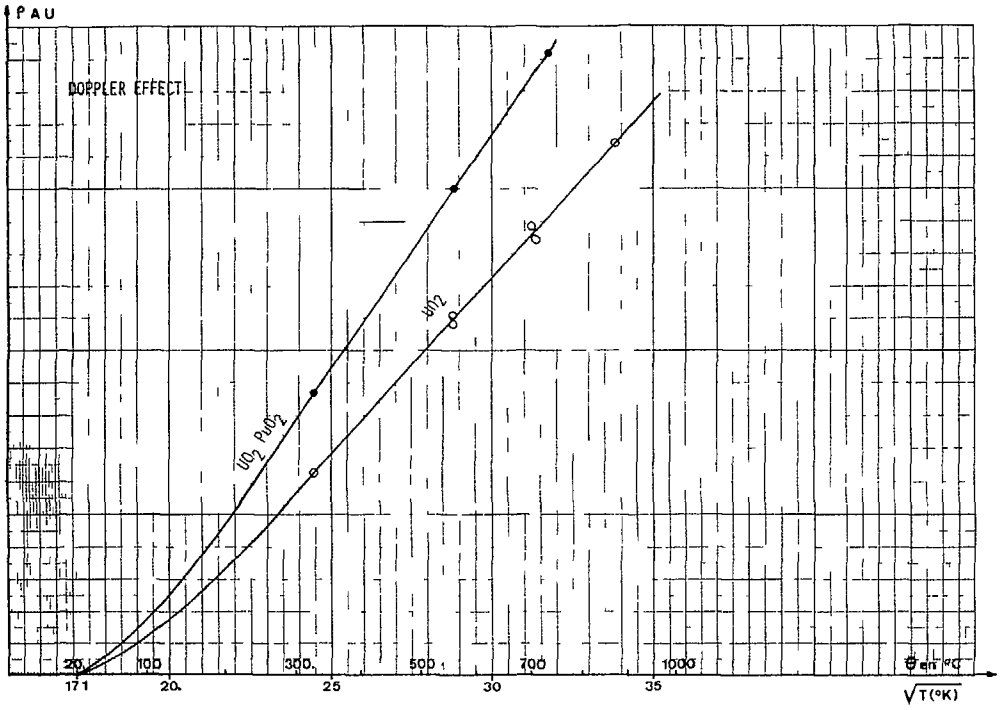

FIG 15 Doppler worth measurements in the MINERVE experiment

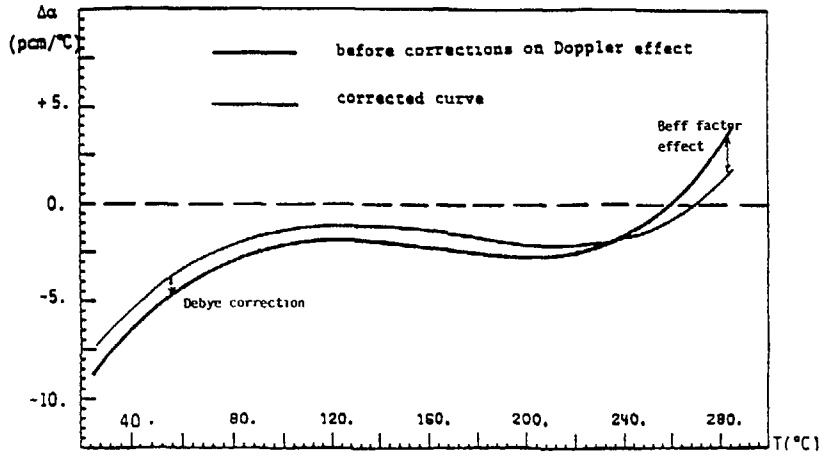

FIG 16 Calculation-experiment comparison on UO_2 RTC measurement

measurement is overestimated compared to the PWR leakage component ; moreover our S_N core calculation with P0 and P1 cross-sections induces a M^2 migration area 6 % smaller than the APOLLO B1 value.

Consequently we substracted from the α (T) core measurement, the water density effect (involving leakage component) measured through the overclad experiments (fig 13). Then we obtained an accurate experimental information on thermal spectrum shift effect (plus Doppler efect) with water temperature increase ; the corresponding Calculation - Experiment comparison (average discrepancy on the 1 and 3 UO_2 test lattices) is shown on figure 17 : the Δα (T) discrepancy is ranging continuously from

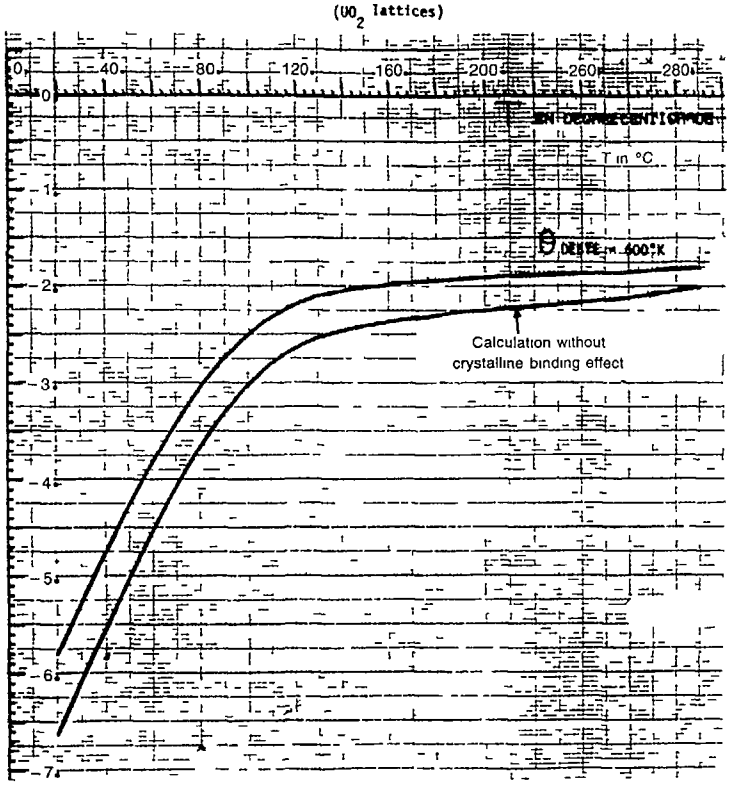

FIG 17 Calculation-experiment comparison on thermal spectrum shift effect and Doppler components in CREOLE RTC measurements

- 5 pcm/°C (room temperature) to - 2 pcm/°C at PWR operating conditions. We can verify that this $\Delta\alpha$ (T) bias shape is consistent with spectral shift effect versus moderator temperature variation (see section 2.3).

4. INTERPRETATION OF COMPLEMENTARY RTC EXPERIMENTS

To complete and confirm the results obtained in CREOLE, we calculated the quasi-totality of available experiments on RTC measurements in LWR lattices. Calculation - Experiment comparison on RTC start-up measurements in large French PWRs was also used.

4.1 RTC critical experiments

Interpretation results of RTC critical experiments are summarized in Table VII and Table VIII : investigated lattices are presented in an increasing ^{235}U enrichment order (^{235}U enrichment and moderation ratio are the main parameters involved in the LWR α value). In spite of the high leakage component in these critical experimental, tables VII and VIII points out the 3-7 pcm/°C overestimation trend on the computed cold RTC absolute value.

TABLE VII: INTERPRETATION RESULTS OF COMPLEMENTARY RTC CRITICAL EXPERIMENTS (low enrichment)

	UO_2 1.311 %		UO_2 2.02 %	UO_2 2.35 %	UO_2 2.49 %	UO_2 3.003 %	UO_2 4.95 %	
EXPERIMENT	BAPL/1RX		NAIG/NCA	BATTELLE	AERI/OLF	AEEW/DIMPLE	ANL/ZPR7	
Référence								
GEOMETRY/PITCH(cm)	Hexag/2.205	Hexag/2.36	⊞ /1.84	⊞ /1.90	⊞ 1.77	⊞ /1.32	Hexag./1.27	
V_m/V_{UO_2}	1.071	1.405	2.918	2.390	2.500	1.001	1.141	1.504
B^2_{meas} (20°C) cm^{-2}	$2.837.10^{-3}$	$3.017.10^{-3}$	$6.972.10^{-3}$	$4.17.10^{-3}$	$8.55.10^{-3}$	$6.60.10^{-3}$	$9.147.10^{-3}$	$1.076.10^{-2}$
k^{cal}_{eff} (20°C)	1.00139	1.00610	1.01967	1.00607	1.01474	1.00393	1.00437	1.00726
α^{meas} pcm/°C	- 8.2	- 7.6	- 6.2 ± 0.6	- 1.6	- 4.1	- 1.8 ± 2.	-10.1 ± 0.5	-12.8 ± 0.5
Temperature Range	10°C - 50°C		10°C - 30°C	20°C - 60°C	20°C - 30°C	20°C - 80°C	20°C - 46°C	
Measurement technique	Doubling Time		D.T.	D.T.	D.T.	Buckling	Doubling Time	
$(\frac{1}{k_\infty} \cdot \frac{dk_\infty}{dT})$ pcm/°C	- 9.9	- 7.5	- 3.8	+ 2.3	- 4.8	- 13.6	- 10.3	- 8.7
$(\frac{M^2}{1+M^2B^2} \cdot \frac{dB^2g}{dT})$ pcm/°C	+ 1.7	+ 1.6	+ 4.1	+ 1.7	+ 5.5	+ 4.4	+ 5.6	+ 6.
$\alpha^{cal} = \frac{1}{k_{eff}} \cdot \frac{dk_{eff}}{dT}$ (pcm/°C)	- 14.7	- 13	- 9.5	- 5	- 12	- 20.7	- 15.3	- 15.6
$\Delta\alpha = \alpha^{cal} - \alpha^{meas}$ (pcm/°C)	- 6.5	- 5.4	- 3.3	- 3.4	- 8	- 2.7	- 5.2	- 2.8

TABLE VIII: INTERPRETATION RESULTS OF COMPLEMENTARY RTC CRITICAL EXPERIMENTS (high enrichment)

	UO_2 3.042 %				UO_2 3.41 %			UO_2 5.1 %
EXPERIMENT	ANL/ZPR7				NPY/NORA			AZUR
Reference								
GEOMETRY/PITCH (cm)	Hexag/1.166	Hexag./1.27	⌀ /1.24	⌀ /1.349	⌀ /1.90	⌀ /2.314	⌀ /2.687	Slab /1.382
V_m/V_{UO_2}	0.4347	0.7544	0.962	1.371	1.660	3.030	4.510	2.440
B^2_{meas}(20°C) (cm^{-2})	$2.436.10^{-3}$	$5.538.10^{-3}$	$4.747.10^{-3}$	$9.182.10^{-3}$	$8.18.10^{-3}$	$9.88.10^{-3}$	$8.64.10^{-3}$	$7.816.10^{-3}$
k^{cal}_{eff} (20°C)	0.99841	0.99752	0.99799	0.99491	1.01418	1.02377	1.02925	1.01074
α_{meas}(pcm/°C)	- 9.5 ± 0.5	-10.1 ± 0.7	-10.6 ± 0.4	- 7.6 ± 0.4	- 9.8	- 5.3	+ 2.7	- 2.75
Temperature Range	20°C - 46°C				20°C - 60°C			20°C - 88°C
Measurement Technique	**Doubling Time**				**Moderator Critical Height**			**Soluble Boron**
$(\frac{1}{k_\infty} \cdot \frac{dk_\infty}{dT})$ pcm/°C	- 15.9	- 13.7	- 11.9	- 10.2	- 6.89	+ 0.3	+ 6.2	+ 6.6
$\frac{M^2}{1+M^2B^2} \cdot \frac{dB_g^2}{dT}$ (pcm/°C)	+ 1.4	+ 3.8	+ 2.6	+ 6.5	+ 5.7	+ 5.9	+ 4.8	+ 4.5
$\alpha^{cal} = \frac{1}{k_{eff}} \cdot \frac{dk_{eff}}{dT}$ (pcm/°C)	- 18	- 17.9	- 15.7	- 17.4	- 15.1	- 10.9	- 5.7	- 7.65
$\Delta\alpha = \alpha^{cal} - \alpha^{meas}$ (pcm/°C)	- 8.5	- 7.8	- 5.1	- 9.8	- 5.3	- 5.6	- 8.4	- 4.9

The interpretation results of the KRITZ RTC measurements are the following :

T : 20 - 90°C αcalc - αmeas = - 4.9 pcm/°C
T : 90 - 160°C - 4.9 pcm/°C
T : 160 - 210°C - 3.3 pcm/°C

The average Calc - Exp. in the above 17 α isothermal measurements below T = 90°C is $\Delta\alpha$ = - 5.7 ± 2.1 pcm/°C (spread in one standard deviation).

This average discrepancy on RTC measurements at room temperature in LWR critical experiments is consistent with CREOLE results.

4.2 PWR start-up measurements

Calculations /12/ of large fresh PWR cores by EDF (Electricité de France) based on the APOLLO code gave the following Calculation - Experiment disagreement on the RTC isothermal value (around T = 295°C).

$$\overline{(\alpha_c - \alpha_m)}^{900\ MWe} = - 2.5 \pm 1.5\ pcm/°C$$

$$\overline{(\alpha_c - \alpha_m)}^{1300\ MWe} = - 2.8 \pm 1.5\ pcm/°C$$

Measurements spanning the 140°C - 290°C temperature range were carried out in the CRUAS plant (900 MWe PWR) : calculation/experiment comparison shown in figure 18 indicates a constant $\alpha_c - \alpha_m$ = - 3 pcm/°C disagreement with moderator temperature.

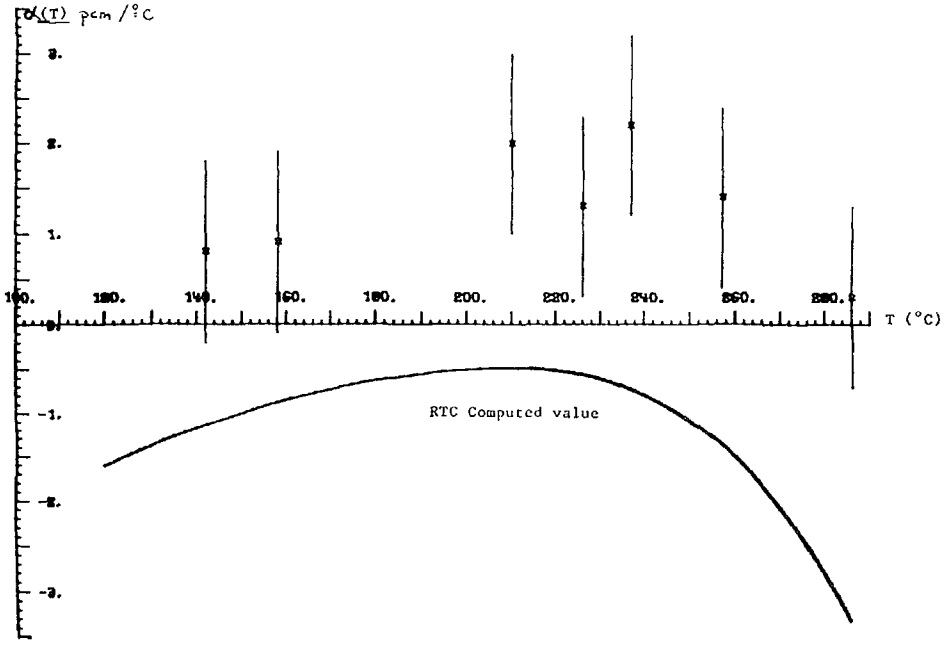

FIG. 18. Temperature coefficient measurements in a 900 MW(e) PWR.

Experience feedback from equilibrium 900 MWe PWR cores (e^{235} = 3.25 %) is summarized below below for 58 PWR cycles between January 1986 and November 1987 /13/ :

- without control rods in the core :

  $(\overline{\alpha calc - \alpha meas})$ = - 3.1 pcm/°C

  spread : σ = 1.05 pcm/°C

- with Ag - In - Cd control clusters :

  $(\overline{\alpha calc - \alpha meas})$ = - 3.4 pcm/°C

  σ = 1.24 pcm/°C.

These results, corresponding to irradiated UO_2 assemblies (and consequently with 1 % Pu content), are consistent with fresh core results.

5. SENSITIVITY STUDIES

The APOLLO interpretation of RTC experiments, based on standard thermal cross-section shapes, has pointed out a Calculation-Experiment discrepancy ranging from - 5 pcm/°C at room temperature to - 3 pcm/°C at PWR operating conditions. The integral measurements specifically the CREOLE experiment, confirmed that the disagreement is not linked to the water expansion with the moderator temperature increase. The main goal of the sensitivity study is to determine the neutronics parameters capable to explain the high level in α discrepancy, specifically at room temperature conditions.

5.1 Thermal scattering and crystal structure effects

In order to assess the maximum discrepancy linked to the water thermalization model, we compared the reference APOLLO results based on the Haywood /14/ model to APOLLO calculations in the gas model (no accounting for the chemical binding effect in the H_2O molecule) : the gas model overestimates the absolute RTC value by 1.5 pcm/°C. Thus, the Crystal structure effect cannot contribute by more than 1 pcm/°C in the C/E disagreement ; this conclusion is confirmed by the consistency of the various scattering models :

αNELKIN - αHAYWOOD = - 0.1 pcm/°C.

5.2 Thermal expansion

Although material thermal expansion was accounting for in CREOLE calculations, we analyzed the neutronic effects linked to radius modifications with temperature. We pointed out that the main effects are linked to clad and grid expansion through a moderation ratio modification : clad expansion effect amounts in a $\Delta\alpha$ = - 0.2 pcm/°C modification, whereas the lattice pitch expansion induces a positive contribution $\Delta\alpha$ = + 0.6 pcm/°C to the RTC value.

The $\Delta\alpha$ = - 0.08 component due to fuel radius expansion is cancelled by the corresponding fuel density decrease effect amounting to $\Delta\alpha$ = + 0.15 pcm/°C.

5.3 Modification of cross-section level

Modifications of cross-section level in APOLLO code were performed in the fast and thermal energy range (E < 0.625 eV). Table IX investigates realistic modifications of the main cross-sections : Ieff^{238}U Resonance Integral and fast $\sigma_s^{H_2O}$ level are the unique cross-sections contributing significantly to the RTC value, but their α component is linked to water density effect and cannot reduce the calc/exp discrepancy at room temperature.

5.4 Modification of thermal cross-section shapes

The sensitivity study demonstrated that the discrepancy on RTC calculation can only originate from thermal spectrum shift effect. The assumption of a calculational bias due to APOLLO code is eliminated : as a matter of fact, too negative RTC values are also calculated in graphite

TABLE IX: SENSITIVITY OF THE UO_2 REACTIVITY TEMPERATURE COEFFICIENT TO NUCLEAR DATA
Average $\Delta\alpha$ effect in the 20°C-290°C temperature range

	Uncert	Modification	$\frac{\Delta k_\infty}{k_\infty}$ (20°C) (pcm)	$\Delta\left[\frac{B^2}{1+M^2B^2}\cdot\frac{dM^2}{dT}\right]$ (pcm/°C)	$\Delta\left[\frac{1}{k_\infty}\cdot\frac{dk_\infty}{dT}\right]$ (pcm/°C)	$\Delta\left[\frac{1}{k_{eff}}\cdot\frac{dk_{eff}}{dT}\right]$ (pcm/°C)
thermal fission σ_f ^{235}U	∿ 1 % (σ_{2200})	+ 1 %	+ 848	0.	- 0.19	- 0.19
thermal absorption ^{235}U	1 à 1.5 % (σ_{2200})	+ 1 %	- 695	+ 0.03	+ 0.14	+ 0.17
thermal capture ^{238}U	≤ 2 % (σ_{2200})	+ 1 %	- 96	+ 0.003	+ 0.003	+ 0.009
thermal capture H_2O	∿ 1 %	+ 1 %	- 66	+ 0.001	+ 0.07	+ 0.071
I_{eff} ^{238}U	∿ 0.7 barns	+ 0.7 barns	- 701	+ 0.28	- 0.87	- 0.59
η épitherm ^{235}U	∿ 4 %	+ 2 %	+ 148	+ 0.03	+ 0.15	+ 0.18
Fast fission ^{238}U	∿ 0.02barns	∿ - 0.02barns	- 153	+ 0.04	- 0.22	- 0.18
Fast Scattering	G1* : 3 à 5 %	- 1%		- 0.03	- 0.02	- 0.05
	G2 : 3 à 5 %	- 1%		- 0.05	- 0.24	- 0.29
	G3 : 3 à 5 %	- 1 %		- 0.06	- 0.44	- 0.50
H_2O	3 à 5 %	- 1 %	-	- 0.14	- 0.70	- 0.84

* G1 : 10 MeV - 0.9 MeV G2 : 0.9 MeV-5 KeV G3 : 5 KeV-2.8 eV

moderated experiments ; moreover similar calc-exp discrepancies on RTC measurements were obtained with different codes in Sweden /3/ and United Kingdom /2, 15/.

Tables III and IV shawn that the thermal shapes of heavy nuclide cross-sections, compared to the 1/v law, give large components to the α value ; then a slight modification of the uranium cross-section slopes, consistent with σ differential measurements, can strongly reduce the calc-exp disagreement in the integral experiments.

The $\Delta\alpha/\Delta\sigma$ sensitivity coefficient was obtained through APOLLO calculations performed with the maximum shape modifications defined in the *ERRADI* thesis : the corresponding η^{235} multigroup set is plotted on figure 19, and the σ_C ^{238}U capture cross-section is graphed on figure 20. These modified cross-sections supply large modification of the temperature coefficient, as shown in figure 21 for a 3.1 % enriched UO_2 lattice ; this figure points out that the RTC effect of ^{235}U cross-section modification is strongly increasing with the moderation ratio of the LWR lattice. Figure 22 indicates that the α value is very sensitive to the $^{238}\sigma$ capture slope for LWR fuel with low enrichment. In a standard fresh PWR core (V_{H_2O}/V_{fuel} = 2), these modifications amounts to a + 5 pcm/°C increase of the calculated RTC value.

6. EVALUATION OF ^{238}U AND ^{235}U CROSS-SECTIONS

The overall Calculation-Experiment discrepancies on RTC measurements were involved in our experimental data base for sensitivity studies (as well as Keff measurements and spent fuel analyses /10/) ; cross-sections modifications are derived from tendancy research method based on this experimental data.

6.1 Rebuilding of thermal cross-sections

Instead of arbitrarily fitting the supposed wrong data in order to minimize the error on the calculation of the temperature coefficient, we have defined an evaluation of the thermal cross-sections based on the consideration of the basic nuclear data : resonance parameters and associated statistic laws. This procedure is divided into three steps :

- Reconstruction of the concerned thermal cross-section from resonance parameters.
- Sensitivity study of the temperature coefficient with the parameters of negative-energy resonances.
- The result of the study allowed us to define the appropriate modifications on the cross section shapes, according to the lightest variations of the negative-energy resonance parameters ; these variations are found to be consistent with the statistic distributions related to these parameters.

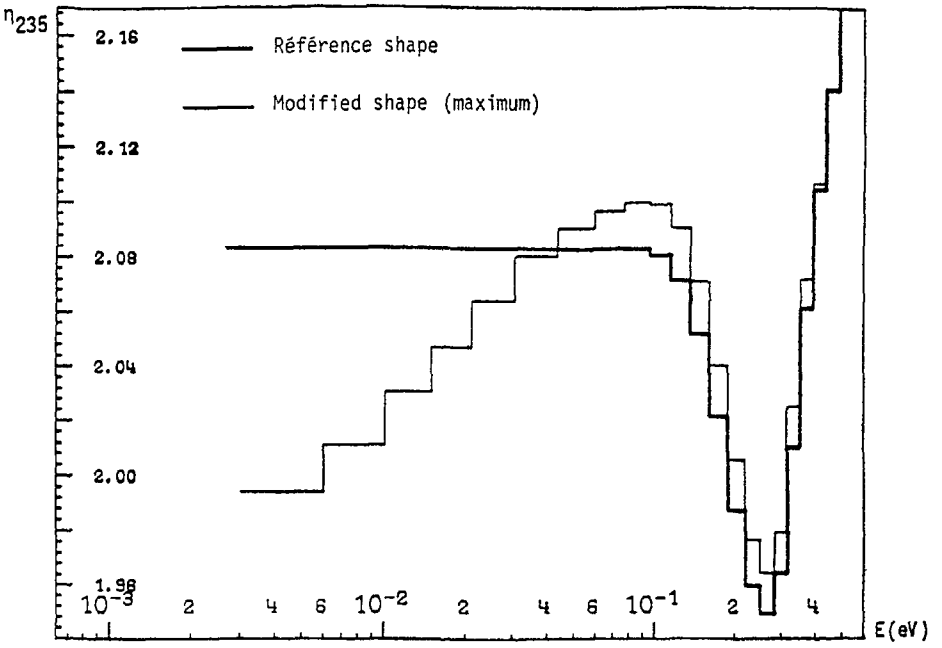

FIG. 19. η_{235} thermal shape.

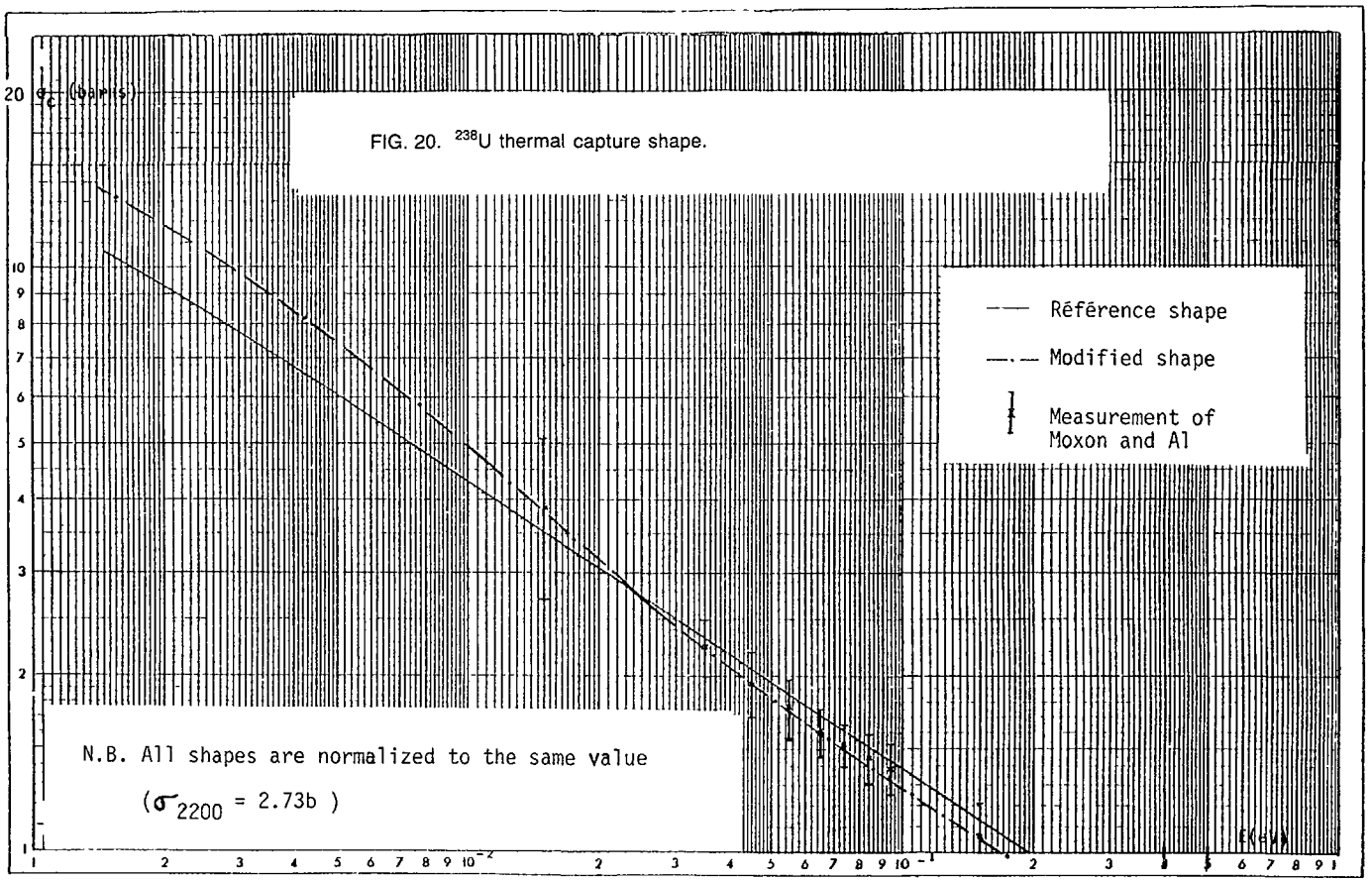

FIG. 20. ^{238}U thermal capture shape.

6.2 ^{235}U cross-section evaluation

We first calculate the contribution of the positive resonances to the ^{235}U capture and fission cross-sections : figure 23 points out that positive resonances give a weak contribution σ^+ to the ^{235}U cross-sections in the thermalized neutron range (v/vo ≤ 2). Negative energy resonances were rebuilt with a <D> = 1 eV constant spacing and Γ_γ = 31 meV (σ_R^- component in figure 23).

We verified that it is necessary to adopt a high Γ_f fission width for the first bound level, i.e. Γ_f = 230 meV, in order to reproduce the reference σ^{2200} value. Figure 23 demonstrates that the thermal ^{235}U cross-section shapes are uniquely linked to this first negative resonance (σ_1^- component). The adjusted energy for this resonance is E_1^- = - 0.80 eV.

The difference in the energy location of this first bound level amounts to ΔE_R = - 0.25 eV between the ENDF/BIV σf^5 shape and our proposi-

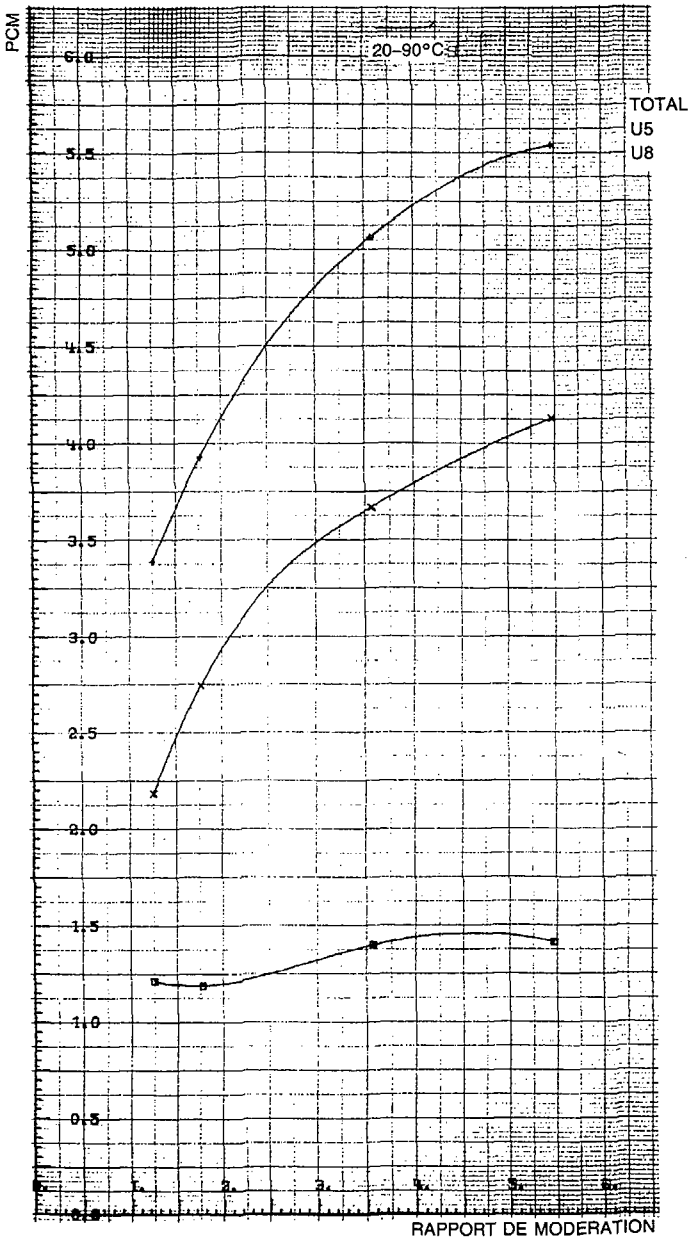

FIG. 21. RTC modifications with ^{235}U and ^{238}U cross-section shapes.

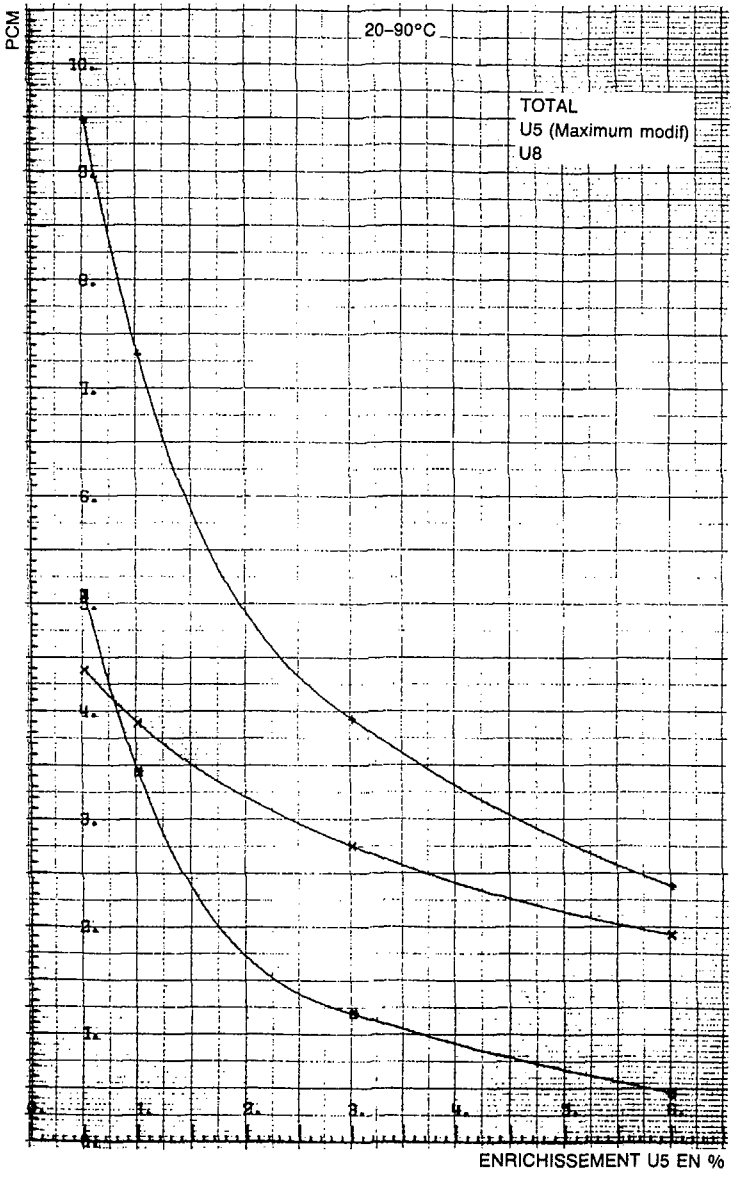

FIG. 22. RTC modification linked to ^{235}U and ^{238}U cross-section shapes.

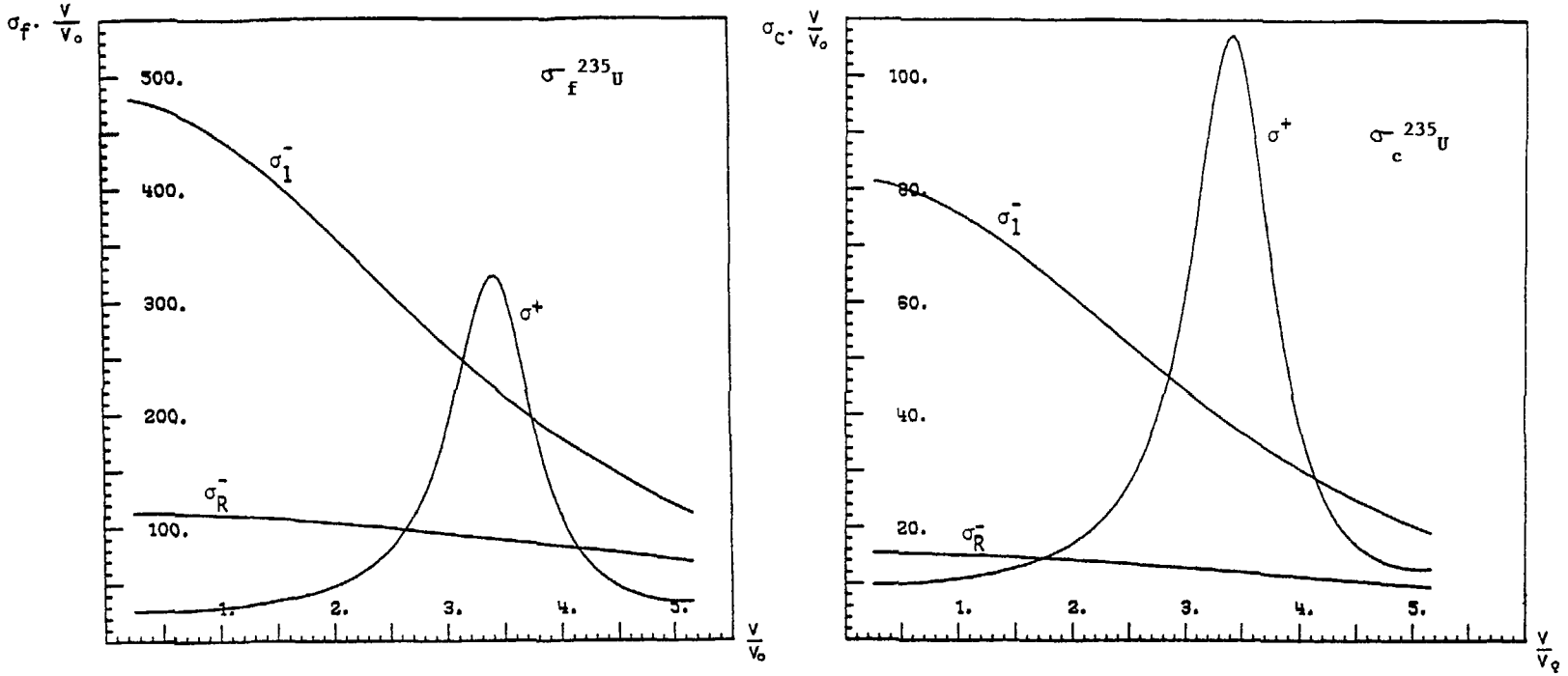

FIG. 23. Contribution of positive and negative resonances to the ^{235}U thermal cross-sections.

tion presented at the CHICAGO Conference /8/ (see figure 24) ; this new cross-section shape was supported a posteriori by the Oak-Ridge measurement /16/ and the Geel LINAC measurement /17/ (figures 24, 25). These rebuilt ^{235}U cross-section shapes are closer from the 1/v law than the ENDF/BV evaluation as shown in figure 25 : then, the corresponding $\alpha_{calc} - \alpha_{exp}$ comparison is improved by + 0.7 pcm/°C (LWR average effect in the 20-290°C temperature range).

In order to obtain a more positive RTC component, we introduce a small negative "capture" resonance close to the zero energy ; the resulting ^{235}U capture cross-section is graphed on figure 26 : our proposal is consistent with GWIN measurement inside the experimental uncertainty margins. The σ_{2200} cross-section level was adjusted in order to be consistent with ^{236}U build up in PWR lattices (GEDEON irradiation /18/ in Melusine reactor, Tihange and Fessenheim spent fuel analyses /19/ up to 50 Gwd.T^{-1}).

The negative resonance parameters corresponding to the proposed evaluation (figures 24, 26) are the following :

First small resonance (σ_0^- contribution) :

Γ_γ = 40 meV Γ_f = 10 meV g x Γ_n° = 1.6 x 10^{-4}

Large resonance σ_1^- (E_1^- = - 0.80 eV)

Γ_γ = 31 meV Γ_f = 230 meV g x Γ_n° = 0.34

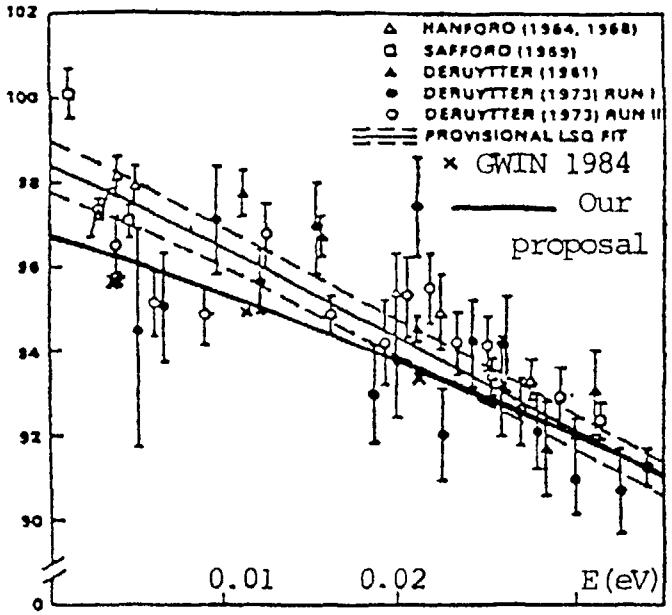

FIG. 24. $\sigma_f^{235}\sqrt{E}$.

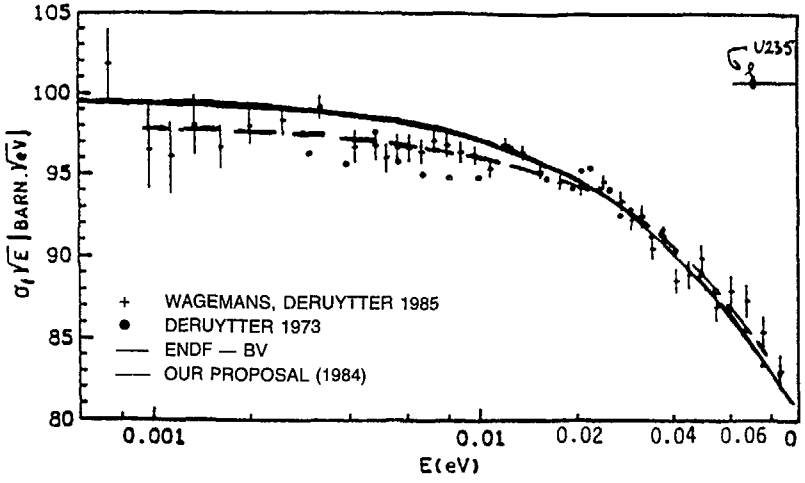

FIG .25. Thermal fission cross-section.

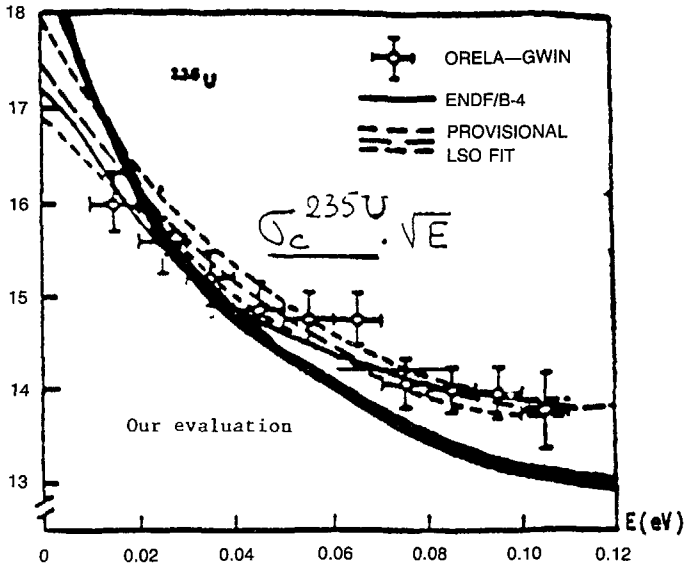

FIG. 26. ^{235}U thermal capture cross-sections.

Negative resonances : $E_n^- = -0.0$ eV $- n\langle D\rangle$ $\quad n = 2, 10$

$\Gamma_\gamma = 31$ mev $\quad \Gamma_f = 220$ meV.

Cross-section components, at the reference neutron velocity v = 2200 m/s, are as follow :

Components	Capture (b)	Fission (b)
Positive resonances σ^+	11.6	30
Small capture resonance σ_0^-	11.7	3
Large negative resonance σ_1^-	62.2	455
Other negative resonances σ_R^-	13.7	97
Total	**99.2**	**585**

We used a $^{235}\nu$ thermal flat shape ; this $^{235}\nu$ value was deduced from buckling measurements, mainly French LWR critical experiments perfor-

med in the EOLE reactor : in these 3 % ^{235}U enriched UO_2 lattices, the moderation ratio was varied from 0.45 /20/, 1.79 (CAMELEON /21/ PWR benchmark experiment), up to 5.46 in the ten CRISTO configurations /22/.

The resulting η^{235} value is graphed on figure 27, and compared with the usual flat shape deduced from fission and absorption cross-section measurements. Figure 27 points out that our proposal is in agreement with the direct η^{235} measurements of Palevsky.

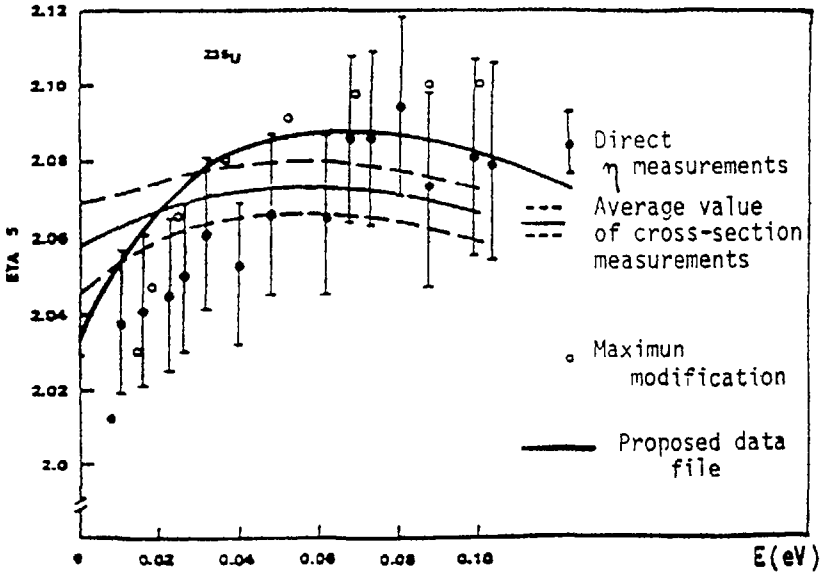

FIG. 27. Proposal and measurements for η_{235}.

6.3 ^{238}U capture cross-section

Our ^{235}U cross-section evaluation enabled us to cancel the Calc-Exp discrepancy in the RTC measurements performed in graphite moderated lattices. RTC calculations in LWR lattices are improved, but a 2 pcm/°C bias is still observed in "undermoderated" lattices with low enrichment fuel (BAPL/TRX, KRITZ ...). Figures 21 and 22 point out that ^{238}U thermal capture cross-section shape allows us to eliminate the Calc-Exp disagreement in this type of LWR lattice.

The modification of the ^{238}U cross section shape necessitates to define the first negative resonance in the range 0 - 0.01 eV : we shawn that the associated probability of this type of first resonance (the 2200 contribution of this resonance is necessary 0.2 barn) is 4 %. Our need for the ^{238}U data file corresponds to a resonance energy E = - 0.005 eV. The corresponding rebuilt capture cross-section is graphed on figure 28. Figure 20 points out that our proposal seems to be in agreement with measurements of MOXON, whereas EDENIUS adjustment (see figure 29) is not consistent with nuclear laws and with MOXON measurements in the 0.5 - 1 eV energy range.

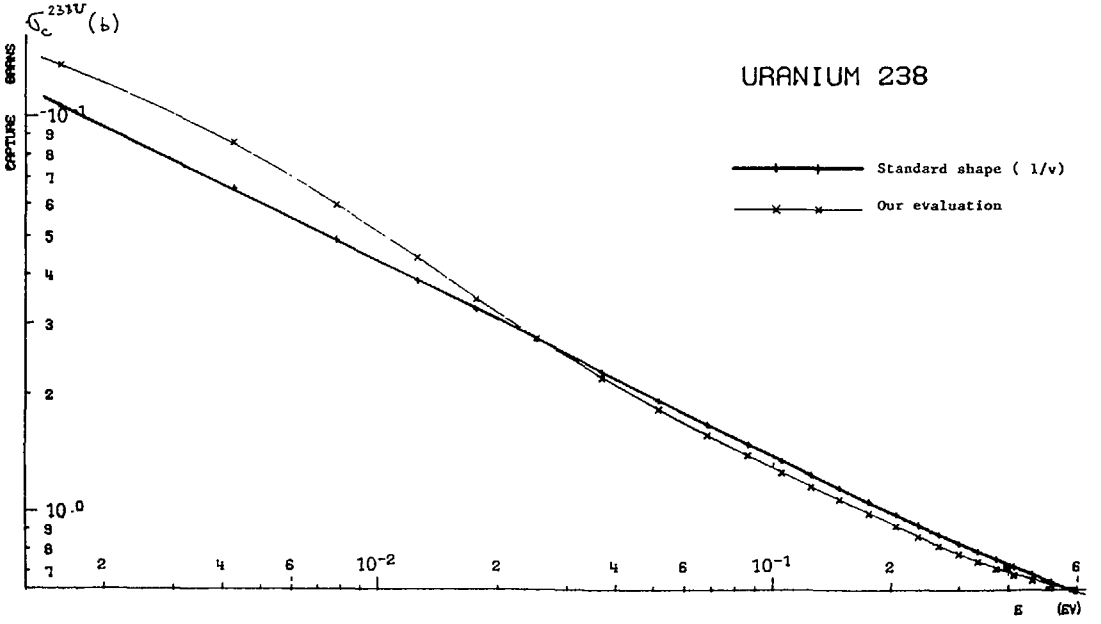

FIG. 28. Capture σ^8_{IR}.

6.4 Qualification of our ^{235}U and ^{238}U evaluations

The reinterpretation of all experiments on temperature coefficient has validated these new cross-sections.

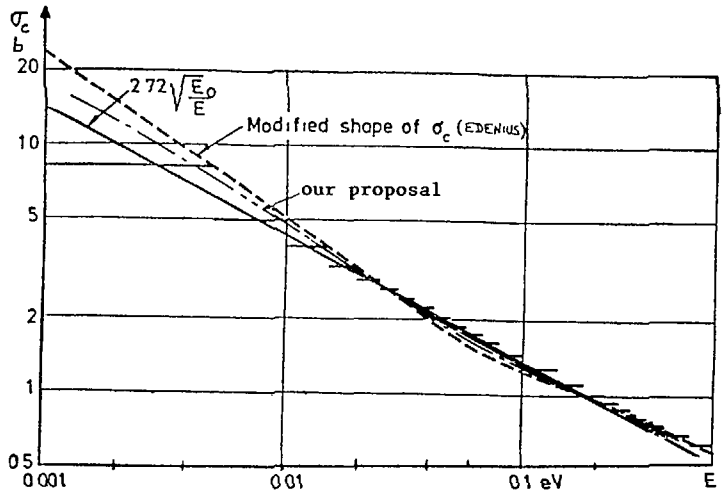

FIG 29 Comparison of EDENIUS adjustment and of our σ_c ^{238}U modified shape

The previous $\overline{\Delta\alpha}$ = - 5.7 ± 2.1 pcm/°C average discrepancy associated to the 17 isothermal RTC measurements below T = 90°C is now reduced to $\overline{\Delta\alpha}$ = - 2.0 ± 1.9 pcm/°C. The comparison between CREOLE (thermal effect) interpretations with the previous thermal cross-section and with the proposed set is given in table X : Calculation and Experiment are now in agreement within experimental uncertainty margins.

TABLE X α CALCULATION-EXPERIMENT COMPARISON IN THE RTC CREOLE EXPERIMENT (C-E in pcm/°C) EFFECT OF THE PROPOSED ^{235}U AND ^{238}U EVALUATION

$[T_{IN} - T_{FIN}]$	$\Delta\alpha$ "1979"	$\Delta\alpha$ "CEA 1986"	Correction U^{8}_{TH}	Correction U^{5}_{TH}	Correction Debye
20° - 90°	- 4.8 ± 2.0	- 1.7 ± 2.0	1 21	1.09	+ 0.80
90° - 190°C	- 2.6 ± 1.5	- 0.5 ± 1.5	0 86	0.73	+ 0.51
190° - 245°C	- 2.2 ± 1.5	- 0.7 ± 1.5	0 64	0.52	+ 0.32
245° - 300°C	- 2.1 ± 2.0	- 0.8 ± 2.0	0 54	0.36	+ 0.27

REFERENCES

/1/ P. REUSS
CEA/SERMA Report N° 2695 (1976)

/2/ J.R. ASKEW et al.
"Thermal reactor temperature coefficient studies in the U.K."
UKAEA Report, AEEW-R-886 (1973)

/3/ M. EDENIUS
"Studies of the reactivity temperature coefficient in light water reactors", AE-RF-76-3160, AB ATOMENERGY (1976)

/4/ A. KAVENOKY et al.
"APOLLO" Note CEA-N-1610

/5/ C. GOLINELLI et al.
"Temperature coefficient and Doppler effect measurements"
ANS Advances in Reactor Physics - Sun Valley (14-17 Sept. 80)

/6/ L. ERRADI
Ph. D. Thesis ORSAY, Feb. 1982

/7/ J. BOUCHARD et al.
"Besoins en donnees nucleaires pour les reacteurs a neutrons thermiques". International Conference on Nuclear Data for Science and Technology. ANVERS 6-10 Sept. 1982

/8/ A. SANTAMARINA et al.
"Temperature effect analysis in LWR lattices". ANS Topical Meeting Advances in Reactor Physics, CHICAGO Sept. 1984

/9/ A. SANTAMARINA, H. TELLIER
"Bibliotheque APOLLO CEA 86" Rapport CEA/DRE/SEN n° 86-294 Oct. 1986

/10/ A. SANTAMARINA, M. DARROUZET, L. MARTIN-DEIDIER
"Nuclear Data Qualification through French LWR integral experiments" International Conference on Nuclear Data SANTA-FE 13-17 Mai 1985

/11/ M. DARROUZET, G. GRANGET, L. MARTIN-DEIDIER, A. SANTAMARINA
CEA/SEN Report 091 (EURATOM n° 012-77-1-RPUF)

/12/ J. PEYTIER
EDF internal report

/13/ J.L. AVERTY
EDF internal report

/14/ B.C. HAYWOOD
J. Nucl. Energy 21, 249 (1967)

/15/ M.J. HALSALL
AEEW-R1492 UKAEA Report

/16/ R. GWIN et al.
Nucl. Science and Eng. 88, 37-55 (1984)

/17/ A.J. DERUYTTER, C. WAGEMANS
"Sub-thermal fission cross-section measurements".
International Conference in Nuclear Data SANTA-FE 13-17 May 1985

/18/ P. CHAUCHEPRAT, A. SANTAMARINA
"Qualification of the calculation of Gd poisoned PWR assemblies through the GEDEON experiment"
ANS Topical Meeting on Advances in Fuel Management. PINEHURST (USA) March 1986

/19/ P. GAUCHER, A. SANTAMARINA
"Interpretation of spent fuel analyses from French PNRs"
ANS Topical Meeting in Reactor Physics. SARATOGA-SPRINGS (1986)

/20/ A. SANTAMARINA
"The CRISTO III experiment" 24 th NEACRP Meeting (1982)

/21/ L. MARTIN-DEIDIER, A. SANTAMARINA et al.
Trans. Am. Nucl. Soc, 46, 755 (1984)

/22/ A. SANTAMARINA, L. MARTIN-DEIDIER
"Experimental qualification of high density fuel storage"
ANS Topical Meeting in Reactor Physics. KIAMESHA-LAKE (NY) (1982)

MEASURED DEPENDENCE OF EFFECTIVE CROSS-SECTIONS ON THERMAL NEUTRON TEMPERATURE

A. OKAZAKI, R.T. JONES
Reactor Physics Branch,
Chalk River Nuclear Laboratories,
Atomic Energy of Canada Limited,
Chalk River, Ontario, Canada

Abstract

The variation of effective cross sections with temperature of Maxwellian neutron distributions has been measured for fission in U233, U235 and Pu239, and for capture in U238, Th232, Cu63, In115, Lu176 and Au197. Foil activation methods were used. Mn55, which has a 1/v dependence, was used as the reference. The results agree within the estimated uncertainties with the ENDF/B-V data except for Lu176 and Au197.

---

1. Introduction

Integral or effective cross section measurements in well thermalized neutron spectra of different neutron temperatures can provide a check of the shape or energy dependence of reaction cross sections. We have made such measurements using activation foils in neutron spectra with Maxwellian temperatures from -195°C to 300°C and these have been reported in detail [1,2]. The results for U233, U235 and Pu239 fission and for capture in the fertile nuclides U238 and Th232 are summarized in this paper. Also included are the results for Cu63, In115, Lu176, and Au197 used for activation foil measurements in some lattice measurements.

2. Method

The reaction rate per unit mass in a well thermalized neutron spectrum of Maxwellian temperature T is given by,

$$R(T) = N \int_0^\infty \sigma(v)\, n_T(v)\, v\, dv$$

where N = number of atoms per unit mass
σ = neutron cross section
$n_T(v)$ = neutron density distribution of temperature T
v = neutron velocity.

In the thermal energy region most nuclides have reaction cross sections that vary as or close to 1/v. A convenient parameter to describe the deviation from 1/v dependence is the Westcott g-factor[3], which is defined by,

$$g(T) = \int_0^\infty \sigma(v)\, n_T(v)\, v\, dv \;/\; \sigma_o v_o \int_0^\infty n_T(v)\, dv$$

where v_o = 2200 m/s
σ_o = cross section at v_o
For a 1/v cross section g(T) = 1.

In this experiment pairs of activation foils, one of each pair containing the test nuclide and the other Mn55, which has a 1/v dependence, were irradiated simultaneously in two thermal neutron spectra of different temperatures T1 and T2. After the irradiation the gamma ray activity of the fission products or of the capture products is measured. The measured activity, A_i, of nuclide i is proportional to the number of reactions in the foil. The measured activities can be combined to yield

$$\frac{g_i(T1)}{g_i(T2)} = \frac{A_i(T1)}{A_i(T2)} \bullet \frac{A_{Mn}(T2)}{A_{Mn}(T1)}$$

It should be noted that the simultaneous irradiation in two different neutron spectra of both the test nuclide and Mn55 has the advantage that counter efficiencies and neutron densities need not be known.

3. Activation Foils

The measurements were made with thin circular activation foils about 11.5 mm diameter and less than 0.25 mm thick. The U233, U235, Pu239 and In foils were aluminum alloys, and the Th, U, Au and Cu foils were elemental metal. Lu-Mn-Al and Mn-Ni alloys were also used. All gamma activities from fission products and from capture products, except from Th foils, were counted with NaI detector systems. The 312 keV gamma rays accompanying the decay of Pa233 in the Th foils were counted with a Ge(Li) detector.

4. Experiment

The irradiations were made in the heavy water moderated ZED-2 reactor at two locations where the neutron spectrum was well thermalized. The core shown in Figure 1 consisted of 84 rods in a hexagonal array of 200 mm pitch arranged to give large rod free regions of heavy water at the center and on the perimeter of the core. Each fuel rod contained 32.5 mm diameter natural uranium metal cylinders stacked in an aluminum alloy tube 1 mm thick with an outside diameter of 34.9 mm.

The foils in the reference location in the heavy water reflector outside the core were at least 0.43 m from the nearest fuel rod. The neutron temperature (T2) at the reference location was assumed to be the same as the physical temperature of the reflector. The neutrons of different temperatures were provided by hot or cold moderator located in the well thermalized central heavy water region in the core where the minimum distance of the foils from the nearest fuel rod was 0.6 m. For measurements above 20°C the activation foils were placed in light water contained in a double-walled zirconium alloy assembly shown in Figure 2. The pressurized light water contained in the 103 mm ID pressure tube could be heated by means of a 3 kW electric heater to 300°C.

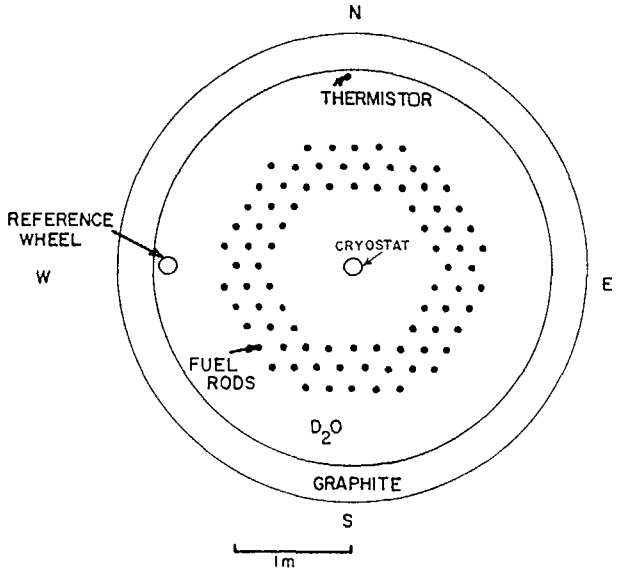

FIG. 1 Irradiation Locations

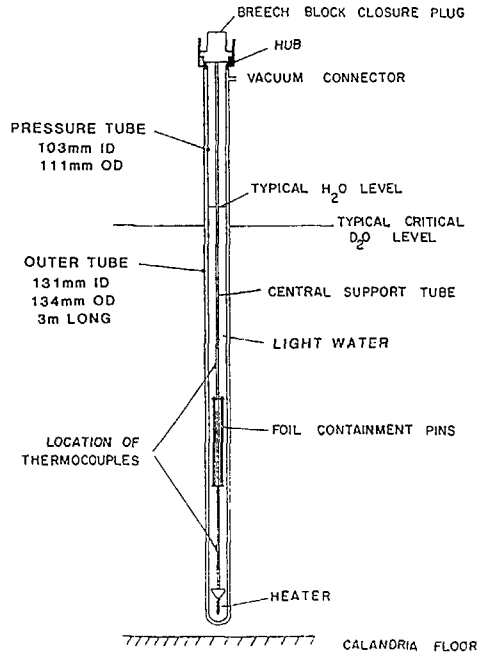

FIG. 2 Hot Moderator Assembly

For the cold measurements the cryostat shown in Figure 3 was used. The foils were placed at the center of a 50 mm ID, 112 mm OD, 225 mm high cylindrical block of paraffin wax cooled by liquid nitrogen. The temperature was measured with chromel-alumel thermocouples. The lowest temperature was -195°C. Measurements were also made at -110°C and -77°C by allowing the paraffin wax to warm up.

Measurements across the cold moderator of the ratio of Lu176 capture, which is strongly dependent on neutron temperature, to Mn55 capture showed that neutrons at the foil locations were rethermalized. Similar measurements had been made earlier [4] in hot light water moderator up to 269°C contained in a similar but smaller pressure tube, 82.5 mm vs 103 mm diameter. They showed that the neutrons were rethermalized.

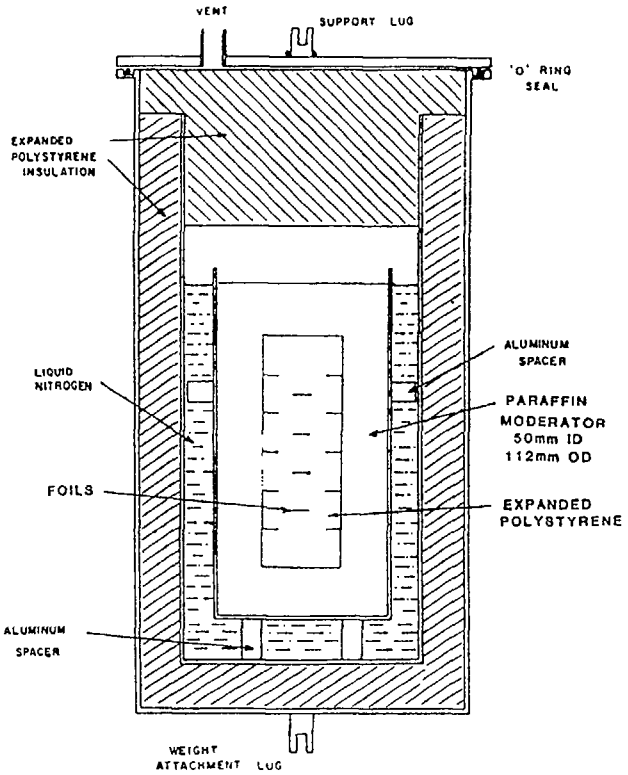

FIG. 3 Cold Moderator Assembly

5. Results

The measured activity ratios have been corrected for the following effects:

1. epithermal neutron activation
2. deviation of the reference temperature from 20°C
3. neutron self-shielding in the foils.

Cadmium ratio measurements made at the reference and test locations indicate that the correction for epithermal neutron activation was significant only for the In115, U238 and Au197 capture reactions and that it was largest (0.6%) for U238. The temperature of the heavy water moderator in the ZED-2 reactor differed for the various irradiations. The measured activity ratios were corrected to a reference temperature of 20°C. This correction was only important for Lu176 capture and Pu239 fission, which have a high sensitivity to neutron temperature, and was the largest for Lu176 at 0.4%/°C. The corrections for neutron self-shielding in the foils were less than 0.5%.

The results expressed as the ratio g(T)/g(20) as a function of neutron temperature are shown in Figures 4 to 8. The lines are obtained by integration of the ENDF/B-V [5] differential cross section data over the Maxwellian neutron distributions.

In general the results agree within the estimated uncertainties of 0.5% to 1.5% with the ENDF/B-V data. For U233, g(T) is almost constant whereas for U235 it varies by 10% over the measured temperature range. Pu239 has a marked dependence on neutron

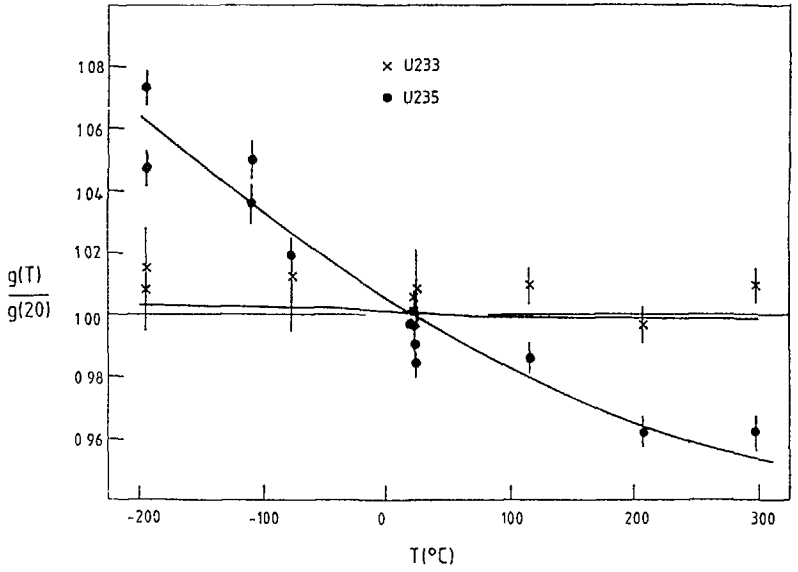

FIG. 4 U233 and U235 Fission

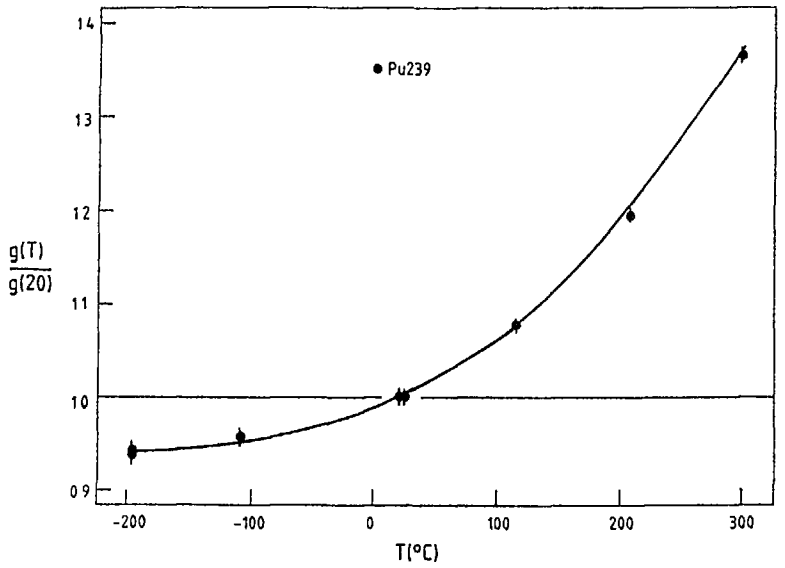

FIG. 5 Pu239 Fission

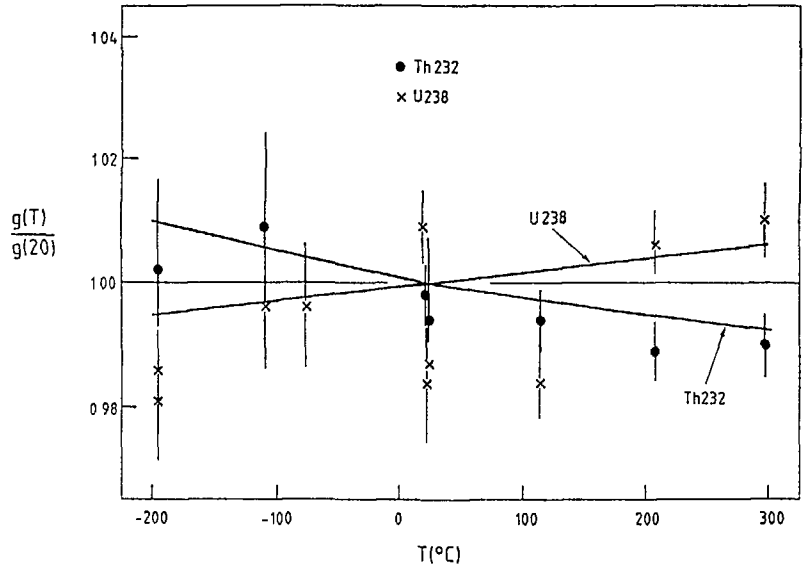

FIG. 6 U238 and Th232 Capture

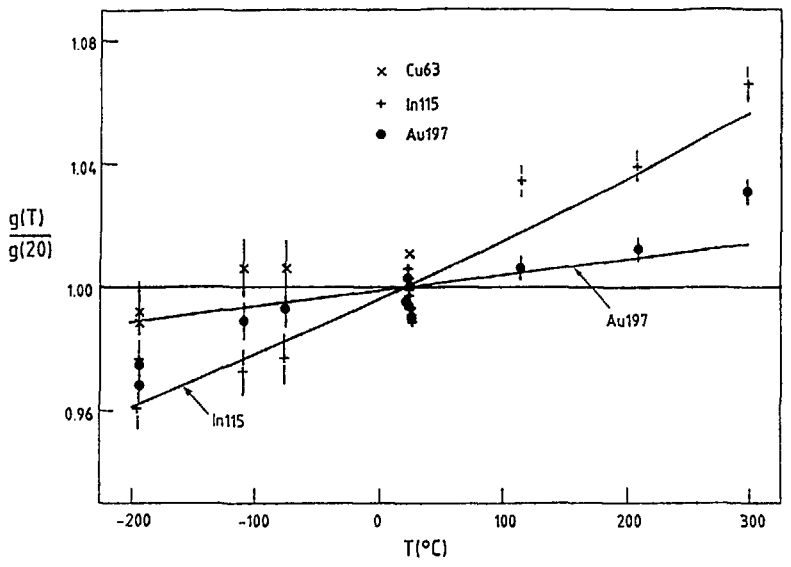

FIG. 7 Cu63, In115 and Au197 Capture

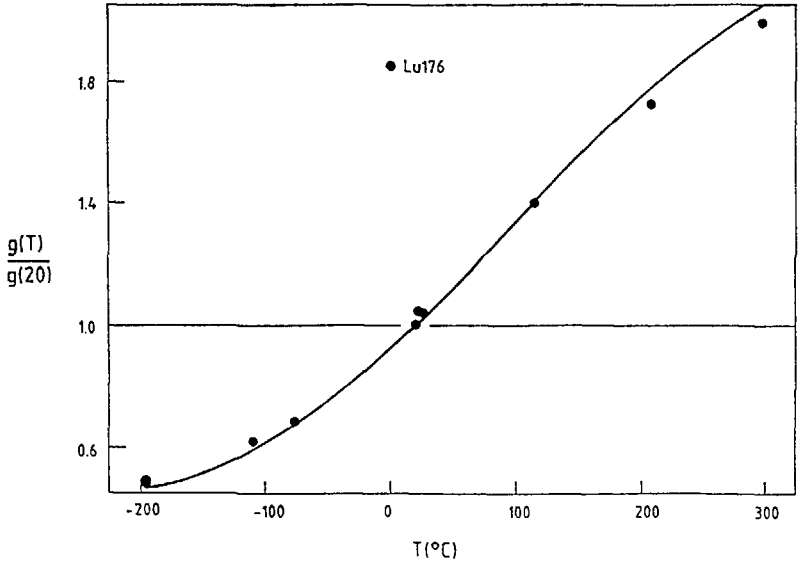

Fig. 8 Lu176 Capture

temperature. The measurements confirm the reduced neutron temperature dependence at low temperatures. For Th232 the average, 1.013±0.015, at -195°C agrees with 1.008±0.009 obtained by Green [6] using a similar method. The U238 results are consistent with ENDF/B-V data in which the cross section does not drop as fast as 1/v. However, they are not consistent with the cross section shape proposed [7] to reduce the discrepancy between measured and calculated light water reactor moderator temperature coefficients. The low and high temperature results for Au197 suggest a more steeply sloped line than that derived from ENDF/B-V data. The result 0.972±0.004 at -195°C agrees well with 0.969±0.004 obtained by Green. At temperatures above 100°C the Lu176 results are below the ENDF/B-V data.

REFERENCES

[1] Jones, R.T., Okazaki, A., "Dependence of Effective Cross Sections on Thermal Neutron Temperatures", Rep. AECL-6483, Atomic Energy of Canada Ltd. (1979)

[2] Jones, R.T., Okazaki, A., "Measured Dependence of Some Effective Cross Sections on Thermal Neutron Temperatures in the Range -195°C to 20°C", Rep. AECL-8844, Atomic Energy of Canada Ltd. (1985)

[3] Westcott, C.H., Walker, W.H. and Alexander, T.K., Effective Cross Sections and Cadmium Ratios for the Neutron Spectra of Thermal Reactors (Proc. 2nd UN Intl. Conf. Peaceful Uses Atomic Energy, Geneva, 1958), Vol. 12, 70.

[4] Bigham, C.B., Turner, R.B., Chidley, B.G., "Experimental Neutron Spectra in a Cylinder of Hot Moderator", Rep. AECL-1471, Atomic Energy of Canada Ltd. (1962)

[5] Garber, D.I., Brewster, C., "ENDF/B Cross Sections", Rep. BNL17100(ENDF-200), Brookhaven National Laboratory (1975)

[6] Green, L., Thermal Westcott g-factor Measurement for Thorium-232, Nucl.Sci.Eng. 66, 127 (1978)

[7] Santamarina, A., Golinelli, C., Erradi, L., American Nuclear Society Topical Meeting on Reactor Physics and Shielding, Chicago, Sept. 1984.

ANALYSIS OF INTEGRAL EXPERIMENTS BY THE MONTE CARLO METHOD

L.V. MAJOROV
I.V. Kurchatov Institute of Atomic Energy,
Moscow, Union of Soviet Socialist Republics

Abstract

Description of the MCU code, based on Monte Carlo method, is given. This code was used for calculation of the vapour effect of the reactor of Chernobyl nuclear power plant. In apppendix are given the results of verification of this code on the basis of integral critical experiments.

The MCU code [1,3] is a large general purpose Monte Carlo radiation transport code system. The structure of the code permits to simulate the abstract scheme of walking of abstract neutral particles of several various types in the multidimensional space of arbitrary dimension. The walking of a particle from the point of view of code structure is a random sequence of abstract events: generation of particle from an outward source or initial distribution, collisions flight between the two points of collision, crossing of the border of geometrical or score (registrarion) zones, death, birth of secondary particles of different types, changing of the weight, flight out of the system etc. Concretisation, that is physical meaning and algorithms of interpretation of these events, are realised using the modules belonging to the module library of the code. Module of MCU is a set of subroutines which has functional destination and interfaces strictly determined by the codes structure. Regarding their destination the modules are classified into following types:

C - control (governing) modules realising the certain abstract schemes of solution of radiation transport problems. To concrete these schemes it is necessary to include into the operating version of the code the concrete modules of the other types.

P - physical modules realising the treatment of collision and the other topics of interaction between the walking particles and the medium. The choice of P-type module is determined by the user's demand for precision of the physical models. Different P-modules can use the different nuclear data libraries.

G - geometry modules destined to model trajectories between collisions. Their choice is determined by the geometry of the assembly to study.

R - registration modules destined to estimate the necessary set of the functionals.

S - source modules destined to model the production of the primary particles from the sources.

N - nonanalog modules for realisation of different schemes of nonanalog calculations.

Besides, the code includes the preprocessor governing the process of compilation of the operating (working) version of the program from the choosen modules. The compilation means the realisation of the following formula:

$$WP = M + C + P + G + R + S + N$$

where M is monitor and C,P,G,R,S,N are the concrete names of the modules of the corresponding types.

The names of modules are defined by users as the initial data for code. All the modules of the same types are interchangeable.

The MCU code can be used on IBM, EC, BESM computers.

Below we shall explain some topics, which may be necessary to understand the analysis of the critical experiments with the MCU code. The code can operate with the several physical models and nuclear data libraries. The concept of the complex physical module is used for this purpose.

It is supposed that all the energy scale is divided into four intervals with the energy boundaries E_1, E_2, E_3, E_4. The collision model for every interval is realised with the help of special independent submodules of types P_i ($i = 1...4$). The submodule of type P_i is destined to imitate the interaction between the particles (neutrons) and matter for energy range $E_i \leq_1 E < E_i$.

The working version of the complex physical module (WPH) is defined by the following formula:

$$WPH = C_p + P_1 + P_2 + P_3 + P_4$$

where P_i are the concrete names of physical submodules of corresponding type, C_p - is control submodule.

The names are defined by user as initial data for variant. Below it would be reviewed some of the neutron submodules from the MCU library. The type of submodule is indicated in the brackets.

PFOR (P_1) - the submodule for energy range 100 keV<E<20 meV. It uses the evaluated data files in the special NEDAM [3,4] format. Two version of the NEDAM library can be used now: the 18 and 52 groups modifications.

PG (P_2) - submodule using 26 groups ABBN library [5] for energy range 0<E<10.5 MeV. It is used the pure group approximation to model the collisions.

PR (P_2) - submodule for energy range 0 - 10.5 MeV using the nuclear data libraries ABBN an LIPAR [6]. For all the range cross-sections are described by ABBN data except the region of resolved resonances. The resonance effects can be described by any of 3 models:

- f-factor formalism,
- subgroup formalism for unresolved and resolved resonances,
- "exact" calculation cross-sections by the resonance

formulas for every energy point when it is necessary (only for resolved resonances with parameters from LIPAR library). The version of description is choosed for every isotope by user.

From 10.5 MeV to 10 Kev the collision treatment is carried in the group approximation. Below 10 Kev energy of neutrons changes continiously as it is dictated by the kinematic formulas.

PT (P_3) - submodule for treatment of collisions in the normalisation region. Every isotope can be described by the one of the three models: heavy gas, free gas or "crystal". The crystal model means, that inelastic scattering cross-sections are described in the gaussian incoherent approximation and elastic scattering cross-sections are calculated with coherent corrections, if it is necessary. The absorbtion and fission cross-sections are used from TEPCON library, based on the evaluated data libraries KORT and LIPAR. The method of probability tables is used to describe the continious change of neutron energy after collision.

The results of testing the code MCU and data libraries are given here in Appendix, where the well known benchmark-experiments are considered. In these calculations it was used the next configuration of the complex physical moduled named by symbols RT:

$$RT = C_p + P_1 + PR + PT + P_4$$

Symbols P_1, P_4 designate the dummy submodules. The boundary of the thermalisation region (PT submodule) was used 1 eV.

The same modification of physical module RT was used in the wide series of calculations RBMK reactor after Chernobyl accident. The aim of these calculations was to analyse the vapour effect and its dependence from the additional safety measures. In these calculations were studied the supercells (4 * 4) for different states. The isotope structure temperature etc. were early calculated using the engineer codes of WIMS [7] type. In the MCU calculations the geometry of supercells was described without any approximations. The boundary conditions of Translation were considered.

The MCU code includes a large library of geometry modules of specialised and universal types. The set of ten specialised modules permits to describe the geometry of main types of reactors, constructed in the USSR (VVER, RBMK VTGR etc.). It is possible to calculate systems with double heterogeneousity - the sphere microcells. In the universal modules it is used the method of combinatorial geometry. Their possibilities are similar to CG and MARS modules of MORSE code [10]. In MORSM module of MCU code every element of the system must be necessarily described when it can't be produced from another element as a result of reproduction operation [8]. The description of every element needs the memory place.

The GDL module [9] similar to MARS of MORSE helps to economise not only the computer memory but the efforts of the user too (during the writing of initial data). It is achieved by using hierarchical scheme of descriptions and carrying out the operations of reproductions of the same projects.

The codes MCU permits to analyse the assemblies with the known buckling defined by vector $\vec{B}$ (B_x, B_y, B_z). It is possible to calculate the multiplication coefficient K_{eff} and the values of different functionals when $\vec{B}$ is known. For this purpose it solved the problem for one (central) cell of heterogeneous lattice with the following boundary conditions [11,12] for flux F(R,W,E):

$$F(\vec{R} \pm \vec{e}_\alpha, \vec{W}, E) = \exp(\pm \vec{B}\vec{e}_\alpha i)\ F(\vec{R}, \vec{W}, E)$$

$$(\vec{W}, \vec{n}_\alpha) > 0 \qquad (\vec{W}, \vec{n}_\alpha) < 0$$

where α = 1, 2, 3 - the numbers of cell surfaces, $\vec{e}_\alpha$ - the basic vectors of lattice, $\vec{B}$ - the vector of buckling, n - vector normal to surface of cell.

Three methods are usually recommended to calculate the density and temperature coefficients by Monte Carlo methods (besides direct methods)[13]:

- correlated sample method using the weights;
- correlated sample method using the same random numbers;
- calculation with using of importance function by perturbation theory method when it is necessary to simulate additional trajectories.

All these methods are not always efficient. So it is necessary to develop new approaches for perturbation calculations. It will be given one example demonstrated the difficulties of such calculations with application of standard technique. The example concerns calculation of vapour coefficient of supercell of reactor RBMK. During analysis of proposed measures to increase safety many calculations were made not only by direct methods but with nonanalog simulation also.

In the example considered below it was calculated K_{eff} for supercell with different densities of water (by E. Gomin, V. Brysgalov

and author). The simulation was realised for supercell with water density $\gamma = 0.5$ g/cm^3. All the same trajectories were used to calculate K_{eff} for supercells with the water densities: 0.78, 0.25, 0.51, 0.49, 0.01. Aslo the derivative $dK_{eff}/d\gamma$ was calculated using the same trajectories.

The standard algorithm of perturbation theory is:

1. It is supposed that the fission density is unchanged.
2. The values K_{eff} for supercell with water density 0.5 are estimated with collision estimator using the weight:

$$W_N = \prod_{n=1}^{N} e^{-\frac{\Delta\gamma}{\gamma_0}\tau_n}\left(1 + \varepsilon_n \frac{\Delta\gamma}{\gamma_0}\right)$$

where

$$\gamma_0 = 0.5; \quad \Delta\gamma = \gamma - \gamma_0$$

τ_n - optical length between n-1 and n collisions.
ε_n - 1, if collision has place inside water and 0 outside.

3. For derivative estimation the weight used is:

$$W_N = \sum_{n=1}^{N}\left(\frac{-\tau_n + \varepsilon_n}{\gamma_0}\right)$$

The values K_{eff} and $K'_{eff} = dK_{eff}/d\gamma$ are given in the table. They are fitted with the values calculated by direct methods well enough. However the statistical errors of nonanalog calculations are too large. This demonstrates that the choosen approach is not efficient for our example. The large errors for $\gamma = 0.25$ are understandable theoretically ($\gamma < \gamma_0/2$). But bad results for derivative have not so clear formal theory basis.

TABLE

RESULTS REACTIVITY CALCULATIONS FOR DIFFERENT WATER DENSITIES

N	39000	69600	82800	147000
K_{eff}	I,032±5.10^{-3}	I,034±4.10^{-3}	I,032±3,7.10^{-3}	I,028±0,003
K'_{eff}	-5.10^{-3}±5.10^{-3}	+5 10^{-3}±3 10^{-3}	0,042±0,03	0,023±0,026
$\gamma\downarrow$	ΔK_{eff}	ΔK_{eff}	ΔK_{eff}	ΔK_{eff}
0,78	-0,065±0,02	-0,01±0,02	0,005±0,04	0,008±0,027
0,51	-4,9.10^{-5}±5.10^{-4}	5.10^{-4}±3,5.10^{-4}	4.10^{-4}±3.10^{-4}	2,5.10^{-4}±2,5.10^{-4}
0,49	7,4.10^{-5}±5.10^{-4}	-4,8.10^{-4}± ±3,5.10^{-4}	-4.10^{-4}±3.10^{-4}	2,5.10^{-4} ±2,5.10^{-4}
0,25	0,02±0,06	0,001±0,04	-0,02±0,03	-0,01±0,02
0,01	-0,54±0,1	-0,58±0,06	-0,51±0,07	-0,5±0,06

N - histories

$K_{eff} = K_{eff}(0.5)$ - for water density, $\gamma = 0,5$

$\Delta K_{eff} = K_{eff}(\gamma) - K_{eff}(0.5)$

K'_{eff} - derivative for $\gamma = 0,5$.

APPENDIX

ANALYSIS OF EXPERIMENTS ON CRITICAL ASSEMBLIES FOR TESTING THE CONSTANT SUPPORT OF REACTOR CALCULATIONS*

E.A. Gomin, A.V. Kapitonova, S.L. Kononov,
L.V. Maiorov S.V. Marin, M.S. Yudkevich
I.V. Kurchatov Institute of Atomic Energy, Moscow, USSR

Yu. E. Vaneev
Scientific Research Institute of Atomic Reactors

The results of Monte-Carlo calculations are presented for critical assemblies with the following compositions: (^{235}U, ^{238}U, H_2O), (^{235}U, ^{238}U, D_2O), (^{239}Pu, U, H_2O), (^{233}U, ^{232}Th, H_2O).

The computer programs for nuclear reactor calculations with the constant support directly using the information contained in the evaluated neutron data files have been developed in a number of countries. Among programs of such a class in the MCU code 1 with the constant support on the basis of the neutron-physical constant support on the basis of the neutron-physical constant bank of I.V. Kurchatov Institute of Atomic Energy 2.

The sets of the MCU code physical modules simulating the interaction of neutrons with the medium nuclei are constructed so that the constants of neutron-nuclear interaction in a variety of energy ranges can be described in various detail up to the direct use of information from the evaluated neutron data files. Such an approach enables a reasonable compromise between the required accuracy and the computation time.

To test the accuracy of the MCU code constant support the calculations were performed. They are compared with the experimental data for critical assemblies and with the results of calculations on the programs involving the ENDF/B-5 library data [3]. The assemblies with ordinary and heavy water were selected. Most of them are acknowledged as benchmarks.

The selected assemblies are sensitive mainly to the cross-sections of fissile and fertile isotopes in the range of thermal and resonance neutron energies. The following data sources were used for these isotopes:

- ^{233}U, ^{235}U. The recommendations of the ENDF/B-5 library were accepted in the range of thermal neutron energies. The parameters of the allowed resonances were adopted from ref. [4];
- ^{238}U. The file evaluated by M.N. Nikolaev et al. 5 was used;
- ^{239}Pu, ^{240}Pu. The files with the evaluation of V.A. Konshin et al. [6] were used;
- ^{232}Th. The file evaluated by G.N. Manturov and M.N. Nikolaev [7].

The group constants and the subgroup parameters for all isotopes were taken from the ABBN system of constants [8].

The results of the calculations are presented in tables 1-8 and Fig. 1. Discussion and analysis of the results are not included in this report; only the brief comments and the general conclusion are given.

The following notation is accepted for the assemblies with ^{235}U and ^{238}U: K is the neutron multiplication constant; δ 25 is the ratio of the ^{235}U fission numbers above and below the cadmium cut-off E_{Cd}=0.626 eV, δ 28 is the ratio of the ^{238}U and ^{235}U fission numbers; δ 28 is the ratio of the ^{238}U capture numbers above and below the cadmium cut-off; ρ 28 is the ratio of the ^{238}U capture and ^{235}U fission numbers; P is the probability of neutron leakage. The analogous notation is used for the assemblies with ^{239}Pu and ^{238}U and those with ^{233}U and ^{232}Th.

TABLE 1. HOMOGENEOUS BENCHMARK: ^{235}U, H_2O

Assembly		Infinite medium [9]	ORNL-10 [10]	ORNL-1 [10]	L6 [11]	L5 [11]
$H/^{235}U$		2110±10	1835	1400	44,3	27,1
δ^{25}		0,013	0,018	0,019	0,458	0,805
P		0,0	0,070	0,18	0,46	0,45
K	MCU	1,002±0,002	1,001(3)	0,997(4)	1,010(4)	1,007(3)
	11	-	0,9988(15)	-	1,0104(23)	1,0093(28)

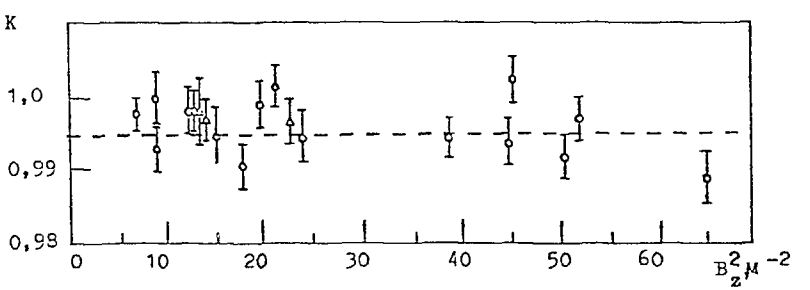

FIG.1. Criticality calculations for ZR-6 assemblies [15].

---

* This material was reported on the International Conference on Neutron Physics, Kiev, 1987.

TABLE 2. HETEROGENEOUS BENCHMARK: ^{235}U, ^{238}U, H_2O [10]

Assembly	K	δ^{25}	δ^{28}	ρ^{28}	C^*
TRX-1 exper.	1,0	0,0987(10)	0,0946(41)	1,320(21)	0,797(80)
V_3/V_5=2,35 MCU	0,992(2)	0,083(5)	0,0922(4)	1,348(7)	0,797(3)
$H/^5U$=250 [12]	0,996(1)	0,1003(16)	0,0987(15)	1,359(27)	0,798(9)
TRX-2 exper.	1,0	0,0614(8)	0,0693(35)	0,837(16)	0,647(6)
V_3/V_5=4,02 MCU	0,993(4)	0,0602(5)	0,0661(5)	0,840(9)	0,639(5)
$H/^5U$=430 [12]	0,998(4)	0,0614(11)	0,0699(10)	0,846(10)	0,642(5)
TRX-3 exper.	1,0	0,231(3)	0,167(8)	3,03(5)	1,255(11)
V_3/V_5=1,0 MCU	0,999(2)	0,232(4)	0,175(3)	2,98(4)	1,235(1)
$H/^5U$=105 [12]	-	-	-	-	-
BAPL-1 exper.	1,0	0,084(2)	0,078(4)	1,39(1)	-
V/V=1,43 MCU	0,994(3)	0,0823(4)	0,0737(4)	1,410(9)	0,809(6)
$H/^5U$=305 [12]	1,0028	0,0840	0,0762	1,414	0,810
BAPL-2 exper.	1,0	0,068(1)	0,070(4)	1,12(1)	-
V_3/V_5=1,78 MCU	0,996	0,0680(3)	0,0629(3)	1,169(8)	0,735(4)
$H/^5U$=385 [12]	1,0031	0,0680	0,0653	1,173	0,738
BAPL-3 exper.	1,0	0,052(1)	0,057(3)	0,906(1)	-
V_3/V_5=2,4 MCU	0,995(3)	0,0521(3)	0,0519(3)	0,912(5)	0,655(3)
$H/^5U$=510 [12]	1,0055	0,0525	0,0533	0,914	0,656

In the case of the heterogeneous assemblies with H_2O the calculation underestimates B by about 0.5%. This results from the group approximation in the energy range above the ^{238}U fission threshold.

TABLE 3. HETEROGENEOUS BENCHMARK: ^{235}U, ^{238}U, D_2O [10]

Assembly	K	δ^{25}	δ^{28}	ρ^{28}	C^*
MIT-4 exper.	1,000(2)	0,0865(16)	0,0459(13)	1,155(1)	1,007(8)
V_3/V_5=15,2 MCU	1,0010(3)	0,0783	0,0386	1,087	0,982
$D/^5U$ =2190 [13]	1,0016	0,0803	0,0389	1,071	0,975
MIT-5 exper.	1,000(2)	0,0371(12)	0,0326(10)	0,525(2)	0,740(7)
V_3/V_5=35,9 MCU	1,007(4)	0,0345	0,0277	0,494	0,722
$D/^5U$ =5170 [13]	1,0128	0,359	0,0278	0,487	0,720
MIT-6 exper.	1,000(2)	0,0222(24)	0,0291(18)	0,317(2)	0,647(2)
V_3/V_5=64,9 MCU	1,007(4)	0,0203	0,0243	0,289	0,628
$D/^5U$ =9350 [13]	1,0116	0,0210	0,0245	0,286	0,628

The calculated data for the MIT assemblies on the MCU code as well as with the ENDF/B-5 library constants differ strongly from the experimental results. The possible errors in the deuterium cross-section could not cause such a significant difference. The authors of this work are prone to think that the experiment is the reason here, but not the calculations.

TABLE 4. HOMOGENEOUS BENCHMARK: ^{239}Pu, H_2O [10]

Parameter		Infinite medium	PNL3	PNL5	PNL2
$H/^{239}Pu$		3695	1204	578	131
δ^{09}		0,009	0,025	0,046	0,187
P		0,0	0,319	0,373	0,388
K	MCU	1,005	1,003(3)	1,018(3)	1,028(4)
	12	1,000(1)	1,000(2)	1,011(2)	1,018(8)

TABLE 5. HETEROGENEOUS BENCHMARK: Pu, U, H_2O [10]

Paremeter	PNL30	PNL31	PNL33	PNL34	PNL35
V_3/V_5	1,19	1,19	2,52	3,64	3,64
$H/^{239}Pu$	184	184	390	562	562
K	1,008(3)	1,009(4)	1,020(3)	1,014(3)	1,014(3)

TABLE 6. CELLS: Pu, U, H_2O

Assembly		K	ε_{49}^{25}	δ^{49}	δ^{25}	ρ^{28}
PNL31	MCU	1,268	0,210	0,147	0,310	5,11
V_3/V_5=1,19; $H/^9Pu$=184	13	1,253	0,211	0,156	0,322	5,20
PNL33	MCU	1,185	0,220	0,082	0,150	2,61
V_3/V_5=2,52; $H/^9Pu$=390	13	1,179	0,220	0,085	0,155	2,60
PNL35	MCU	1,158	0,228	0,060	0,104	1,80
V_3/V_5=3,64; $H/^9Pu$=562	13	1,155	0,228	0,062	0,106	1,80

TABLE 7. HOMOGENEOUS BENCHMARK: ^{233}U, H_2O

Parameter	Infinite medium [9]	[9]	[14]	[14]
$H/^{233}U$	2260±20	1324	391	73
δ^{23}	0,034	0,062	-	0,719
P	0,0	0,177	-	0,515
K	1,0016±0,004	1,003(2)	1,005	1,021(2)

TABLE 8. HETEROGENEOUS BENCHMARK: ^{233}U, ^{232}Th, H_2O [10]

Assembly		K	δ^{25}	δ^{02}	ρ^{02}	c^*
BNL-1 $V_3/V_S=1,00$; $H/^{3}U=109$	exper MCU	1,0 1,002(3)	- 0,59	- 0,02	1,338(42) 1,32(5)	- 0,64
BNL-2 $V_3/V_S=1,38$; $H/^{3}U=151$	exper MCU	1,0 1,010(4)	- 0,44	- 0,02	0,903(38) 0,90(2)	- 0,59
BNL-3 $V_3/V_S=3,00$; $H/^{3}U=328$	exper MCU	1,0 1,015(5)	- 0,22	- 0,02	0,421(13) 0,41(1)	- 0,52

The BNL-THO_2 assemblies are exponential. The analytical calcuations revealed that they are not asymptotic (contrary to the recommendations of ref. 10). The difference of K form 1 is possibly connected with the error in measuring the constant of decay of the asymptotic neutron flux along height.

The analysis of the results obtained in the calculations carried out has shown that the level of knowledge about the neutron constants of ^{233}U, ^{235}U, ^{238}U and ^{232}Th isotopes satisfies principally the requirements to the accuracy of calculations of present-day thermal power nuclear reactors. The cross-section of ^{239}Pu requires refining in the range of resonance energies including the first resonance.

REFERENCES

1. L.V. Maiorov, M.S. Yudkevich, Vopr. Atomn. Nauk. i Techn. (Fiz. i Techn. Nucl. React.), 1985, No. 7, p. 54.

2. G.F. Liman, L.V. Maiorov, M.S. Yudkevich, ibid., 1985, N7, p. 21.

3. L.Z. Zahkharov, L.V. Markovski, A.D. Frank-Kamenetski, G.E. Shatalov, ibid., 1981, N8(21), p. 42.

4. L.Z. Zahkharov, L.V. Markovski, A.D. Frank-Kamenetski, G.E. Shatalov, ibid., 1981, N8(21), p. 57.

5. L.P. Abagjan, O.N. Bazazyanz, M.N. Nikolaev et al., Atomnaya Energia (Sov. Journ. of Atomic Energy), 1980, v. 48, N2, P. 117.

6. L.P. Abagjan, V.V. Tebin, M.S. Yudkevich. CROSS - a Package of Codes and Libraries to Calculate Cross-Sections in Resolved Resonance Range. Preprint IAE-4009/5, Moscow, 1984.

7. J.R. Askew, F.J. Fayers, P.B. Kemshell. "A General Description of the Lattice Code WIMS". JBNES, October 1966, p. 564.

8. V.I. Bryzgalov, M.I. Gurevich, A.S. Ilyashenko. Monte Carlo Methods in Computational Mathematics and Mathematical Physics, Novosibirsk, SO AN USSR, 1985, p. 196-198.

9. S.V. Ostashenko. Monte Carlo Methods in Computational Mathematics and Mathematical Physics, Novosibirsk, SO AN USSR, 1985, p. 199 - 201.

10. A Review of the Theory and Application of the Monte-Carlo Methods. Oak Ridge. ORNL/RSIC-44. 1980.

11. L.V. Maiorov, Atomnaya Energia (Sov. Journ. of Atomic Energy) v. 58, N2, p. 93.

12. V.G. Zolotukhin, L.V. Mayorov. Evaluation of Reactor Criticality Parameters with Monte Carlo Methods, 1984, Moscow, Energoizdat.

13. V.G. Zolotukhin, D.A. Usikov, Evaluation. Evaluation of Reactor Parameters with Monte Carlo Methods, 1979, Moscow, Atomizdat.

A GENERALIZED SUBGROUP APPROACH TO CALCULATING RESONANCE ABSORPTION OF NEUTRONS IN NUCLEAR REACTORS

V.V. TEBIN
I.V. Kurchatov Institute of Atomic Energy,
Moscow, Union of Soviet Socialist Republics

Abstract

The author formulates a subgroup kinetic equation and describes a method of obtaining subgroup parameters assuming constant collision density within a given subgroup.

1. Introduction

The commonest approach to engineering calculations of resonance absorption in thermal reactors is based on the theorem of equivalence of resonance absorption in homogeneous and heterogeneous media. When determining the void and temperature coefficients of reactivity in this way one can encounter certain problems - for instance, when it is essential to take into account the real distribution of temperature across a fuel slug, or to determine the effect of partial loss of water from the reactor core.

Around 1985 the Generalized Subgroup Approach (GSA) was developed [1]. Up to the present time, it has been used in a series of thermal reactor cell calculation engineering programmes [2, 3]. The main feature of this approach is the special consideration it gives to spatial migration of neutrons at different resonance cross-section values. Slowing-down effects at the resonances in absorber assemblies are thought to be less critical and can be taken into account by applying effective parameters.

The concept of a "subgroup" was first introduced in the article cited as Ref. [4]. The further development and use of the subgroup approach [5-8] has centred around a consideration of resonance self-shielding of cross-sections in the context of fast reactor design. In fast reactors, resonance effects occur, for the main part, in the high-energy region (the heavy isotope unresolved resonance region). Therefore, in obtaining subgroup parameters, an assumption was used which is justified for this energy range - the energy released during neutron scattering significantly exceeds the resonance width and the distance between resonances (narrow resonance approximation). Moreover, in obtaining subgroup parameters for fast reactor calculations, the basic criterion involved is the preservation of resonance self-shielding factors in a homogeneous medium in relation to the dilution cross-section.

Calculations performed specially for thermal heterogeneous systems [9] have shown that the use of subgroup parameters obtained for this kind of technology results in an error of ~ 10% in resonance absorption. For certain resonances the error may be as high as ~ 30%.

In the present paper, a subgroup neutron transport equation valid for resonances of arbitrary width is formulated. Certain problems in obtaining subgroup parameters are considered. Comparative calculations of resonance absorption are presented - by the Monte Carlo method, on the basis of the detailed cross-section energy dependence, and by the first collision probability method, based on GSA.

2. The Subgroup Equation

Let us divide the resonance region into intervals - groups. The boundaries of the groups will be determined just as in the normal group method, i.e. in such a way that, for the whole class of problems under consideration, neutron absorption and leakage do not result in a significant difference in the flux rates of slowing-down neutrons on the boundaries of the

group. It should be noted here that, for typical thermal reactor lattices, this condition is fulfilled whenever the group lethargy interval ΔU is of the order of 1.

The basic idea of the subgroup approach consists in attributing within the group the same spatial + angular distribution to all neutrons with energies such that the total cross-sections fall within the interval

$$\Delta\sigma_t^i = \{\sigma^{i-1}, \sigma^i\} \quad , \quad \sigma^0 = \min_{u \in \Delta u} \sigma_t(u) \quad ,$$

In the absorber elements of a heterogeneous thermal reactor, the spatial distribution of neutrons is determined primarily by single-collision neutrons, and the anisotropy of scattering on heavy resonance isotopes in the intermediate energy region is not great. Therefore, all neutrons in the group with energies for which the total cross-sections of the resonance isotopes are equal have roughly the same spatio-angular distribution. This fact makes the subgroup approach useful in resonance absorption calculations for heterogeneous thermal reactors.

Let us write out the integral neutron transport equation in the subgroup formulation. First of all, some definitions:

1. The neutron subgroup i of the isotope k (hereafter designated either (i,k) or i) consists of all neutrons in the group with energies such that the total cross-section of this isotope lies within the stipulated interval $\Delta\sigma_t^{(i,k)}$;
2. The subgroup neutron flux at point $\vec{r}$ in the direction $\vec{\Omega}$ – $\phi^{(i,k)}(\vec{r},\vec{\Omega})$ is the integral flux for subgroup (i,k) normalized to unit lethargy;
3. The neutron subgroup is characterized by the total subgroup cross-section – $\sigma_t^{(i,k)}$, and by a fraction of the subgroup within the group – $a^{(i,k)}$. The value of $\sigma_t^{(i,k)}$ within $\Delta\sigma_t^{(i,k)}$ is determined by averaging the total cross-section and for $\sigma^{i-1\to\sigma^i}$ is equal to σ^i. The subgroup fraction is the relative portion of the group lethargy interval where all neutrons belong to this subgroup, i.e. $\sum_{i=1}^{I} a^{(i,k)} = 1$, where I is the total number of subgroups in the group. Partial subgroup cross-sections are determined from the criterion of preservation of the number of processes for each reaction X in each subgroup:

$$\sigma^{(i,k)} = A_x^{(i,k)}(\vec{r},\vec{\Omega}) \Big/ \phi^{(i,k)}(\vec{r},\vec{\Omega}) \qquad (1)$$

4. The relative proportion of neutrons of subgroup (j,ℓ) also belonging to subgroup (i,k) is termed the correlation coefficient of subgroup j of isotope ℓ in relation to subgroup i of isotope k. It is designated $\alpha^{[(j,\ell),(i,k)]}$ or $\alpha^{[j,i]}$. From the definition it follows that $\sum_{j=1}^{J} \alpha^{[(j,\ell),(i,k)]} = 1$, and $\alpha^{[(j,k),(i,k)]} = 0$.

5. The probability of a neutron of subgroup (j,ℓ) after scattering on isotope ℓ belonging to subgroup (i,k) is called the scattering subgroup function. It is designated $\omega^{[(j,\ell),(i,k)]}$ or $\omega^{[j,i]}$.

Let us now formulate a balance correlation for neutrons of subgroup (i,k) in group n at point $\vec{r}$ moving in the direction $\vec{\Omega}$. Sources from other groups $Q^{(i,k)}(\vec{r},\vec{\Omega})$, and from the surface of the area under consideration $T^{(i,k)}(\vec{r}_s,\vec{\Omega})$, are taken as known. Following this line of reasoning,

just as when working out a normal transport equation, we get the following:

$$\Phi^i(\vec{r},\vec{\Omega})\Sigma_t^{\prime i} + \Phi^i(\vec{r},\vec{\Omega})\sum_{\ell\neq k}^{L}\sum_{j}^{J}\Sigma_t^{\prime i}\alpha^{[j,i]}(\vec{r},\vec{\Omega}) =$$
$$= \int_V d\vec{r}\, P^i(\vec{r}',\vec{r})\left\{\int d\vec{\Omega}'\sum_{\ell}^{L}\sum_{j}^{J}\Phi^j(\vec{r}',\vec{\Omega}')\Sigma_{s'}^{\prime j}\omega^{[j,i]}(\vec{\Omega}',\vec{\Omega},\vec{r}') + \right. \quad (2)$$
$$\left. + Q^i(\vec{r}',\vec{\Omega})\right\} + \int_S d\vec{r}_s\, P^i(\vec{r}_s,\vec{r})\, T^i(\vec{r}_s,\vec{\Omega})$$

Here the index of the group and of the isotope is omitted,

$$\Sigma_t^{\prime i} = \sigma_t^i \rho^k$$

ρ^k – concentration of isotope k;

Σ_s^j – macroscopic scattering cross-section in subgroup j of one of the isotopes ℓ, including k;

$P^i(\vec{r}',\vec{r})$ – probability of a neutron of subgroup (i,k), arising at point $\vec{r}^1$, undergoing its first collision at point $\vec{r}$.

On trying out all possible values of $1 \leq k \leq L$ and $1 \leq i \leq I$ we obtain a closed system of equations.

Determination of group functionals from values of subgroup fluxes involves calculating sums of the following type:

$$A_x(\vec{r},\vec{\Omega}) = \Delta u \sum_{\ell}^{L}\sum_{j}^{J}\sigma_x^j \rho^\ell(\vec{r})\Phi^j(\vec{r},\vec{\Omega})a^j \quad (3)$$

To solve equation (2), it is necessary to know the subgroup parameters, which are dependent in turn on the neutron spectrum. In this respect, the subgroup approach is no different from other methods of solving the transport equation by determinate methods, for example the group method and the microgroup method. Thus, taking into account general conformities within the class of problems under consideration, one must find a mass spectrum to obtain "universal" subgroup parameters for this class of problems.

3. Establishment of Subgroup Parameters

A long series of calculations was performed using the Monte Carlo method in order to establish the very general laws governing resonance neutron distribution in thermal reactor cells [10, 11, 12]. The results of these calculations confirmed that, over a widely varying range of cell parameters, the spatial distribution of the neutron collison density of one group is determined principally by the value of the total cross-section. For this reason, it was assumed, when deriving subgroup parameters, that the energy dependence of collision density is a function only of σ_t. The collision density dependence is approximated by a step function. The analysis was conducted using fixed group boundaries for a 26-group division, for inclusion in the existing BNAB libraries of constants [6].

The assumption of constant collision density within the subgroup allows subgroup boundaries to be obtained and all subgroup parameters to be determined. Details of the selection criteria for subgroup boundaries and the method of obtaining subgroup parameters are given in Ref. [12]. In Ref. [12], by reducing Peierls integral equation to subgroup form, conditions were obtained which must be satisfied by the subgroup parameters that will be used for heterogeneous thermal reactor calculation. Conversion to subgroup form is achieved by means of replacing the customary representation energy of cross-sections by a probabilistic one [4].

In brief, the conditions for obtaining subgroup parameters may be formulated in the following manner:

To achieve the stipulated accuracy in calculating resonance absorption (E), it is sufficient to select the number of subgroups and subgroup cross-sections in such a way that for each subgroup the following inequalities obtain:

$$\left| \left\langle \frac{\sigma_x}{\sigma_t} \right\rangle_i - \frac{\langle \sigma_x \rangle_i}{\langle \sigma_t \rangle_i} \right| \leq \delta_x(\varepsilon), \quad x = c, f, s, \tag{4A}$$

$$\left| \left\langle \exp\left(-\sigma_t \cdot t_{max}(\varepsilon)\right) \right\rangle_i - \exp\left(-\langle \sigma_t \rangle_i t_{max}\right) \right| < \delta_e(\varepsilon) \tag{4B}$$

where: $\langle\ \rangle_i$ – denotes averaging within the subgroup;

t_{max} – is the characteristic dimension (per cm^2) of areas with a resonance absorber.

In Ref. [12] an overview evaluation was obtained of the upper limits for values of δ_x, δ_e, t_{max} as a function of the stipulated accuracy for calculating resonance absorption – E.

Subgroup cross-sections and subgroup fractions are calculated using a combination of two methods: the moments method [7] and the method of direct integration for energy ranges corresponding to certain subgroups with closely related total cross-section values. Such a combination allows the number of subgroups to be reduced approximately by half by comparison with direct integration, and helps avoid computing difficulties when processing moments of widely varying orders. For example, a maximum of 8 subgroups in the group are sufficient to obtain an accuracy level in calculating resonance absorption of, at worst, 3% for the majority of isotopes of practical interest.

The boundaries of the subgroups in those parts of the total cross-section where the moments method is used are determined by numerical solution of the equation:

$$\int_{\sigma^{i-1}}^{\sigma^i} \sigma_t\, a(\sigma_t)\, d\sigma_t = a^i \sigma_t^i, \tag{5}$$

where $a(\sigma_t)$ is the probability distribution density for the total cross-section within a group.

If the boundaries of all subgroups are known, then it is not difficult to calculate correlation and inter-subgroup transport matrices, working directly from their definition in the approximation of constant collison density within the subgroup.

In order to take into account the influence of slowing-down effects on the neutron spectrum in the subgroup close to resonances which cannot be considered narrow, special adjustments are introduced for inconstant collison density in a resonance isotope – light moderator mixture [11]. These corrections for each group of individual isotope are presented in tabular form in the data library as a function of the atomic weight of the moderator, temperature and dilution cross-section. When solving subgroup equations, they are introduced in the form of a correction of the probability of transport to a subgroup of the resonance isotope after scattering on the light moderator.

The effect of these corrections is appreciable for large-scale units. For typical UO_2 units in water-water thermal reactors the effect is of the order of 2–3% in resonance absorption in ^{238}U.

The temperature dependence of subgroup cross-sections and subgroup fractions can be written with the help of two corrections:

$$\sigma_x^i(T) = \sigma_x^i(300^\circ K) + \Delta L_x^i b + \Delta S_x^i \sqrt{b}, \tag{6}$$

where b = T/300–1.

The correlation and inter-subgroup transport matrices are entered in the subgroup parameter library for several temperatures (usually four).

Although considerable in comparison with traditional data in group libraries, the volume of data on subgroup parameters does not complicate essentially computation on modern computers. Extension of the BNAB library [6] to include the GSA parameters has increased its volume from 1 megabyte to 2 megabytes (the extended BNAB library has been named BNAB/TR).

4. Results of comparative calculations

At the present time, a great deal of experience has been accumulated in calculating resonance absorption using GSA for cells of varying geometry and composition [1, 12]. Comparisons made with calculation results from precision programs have shown that, for reactor cells with a not very hard spectrum (> 0.2 probability of avoiding resonance absorption), the error level does not exceed the value laid down when obtaining subgroup parameters.

The following test gives the fullest picture of the capacity of GSA. Using the MCU [13] and SAPFIR [3] programs, the polycell depicted in Fig. 1 was calculated. The MCU program is based on the Monte Carlo method and, in the resolved resonance region, solves the transport equation without approximations. For the real calculations in the SAPFIR program, GSA and the first collision probability method were used in the resonance energy region. The reference information on the detailed energy dependence of neutron cross-sections in the MCU program, and that for obtaining subgroup parameters, was identical [14]. When obtaining subgroup cross-sections, E was determined with an accuracy of 3%.

The geometry of the test problem was typical for water-water power reactors. The absorber elements contained uranium dioxide of varying enrichment. The central element contained high-concentration ^{10}B.

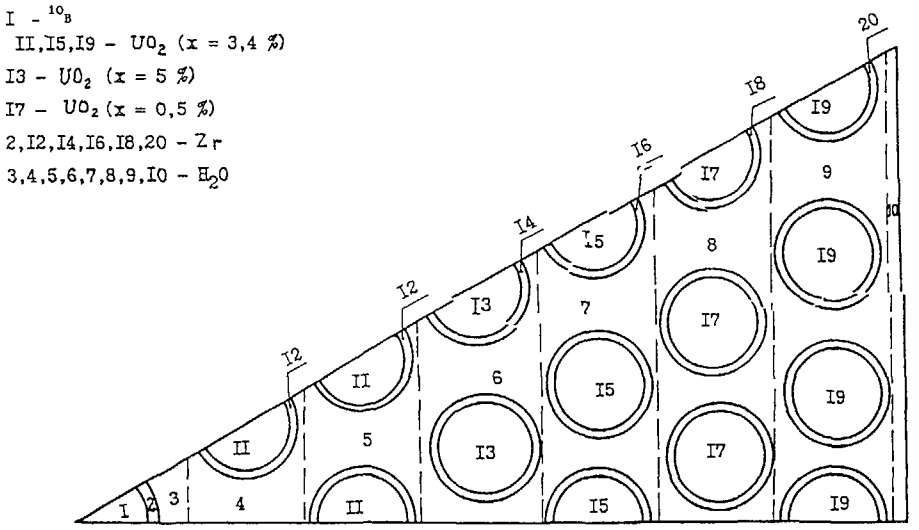

FIG.1. Geometry of a polycell.

Using the MCU program, a multiplication factor of 1.349 ± 0.004 was obtained for such a system, and using the SAPFIR program - 1.344. The total computing time for the SAPFIR program was 1/50 of that for the MCU program. The computing time required for a calculation in the resonance energy region (10 KeV-1 eV) for a computer with an operating speed of 1 Mflops was 7 minutes. A detailed comparison of results from the two programs in the resolved resonance region (100 eV-1 eV) is given in the table. In the table, one relative mean-squared deviation of the results calculated using the MCU program is given. $A_{c,f}^{5,8}$ is the number of reactions of the processes c, f for the isotopes ^{235}U and ^{238}U.

Statistical analysis of all test results obtained up to the present time has raised no doubts regarding the correctness of the conclusions formulated above on the accuracy of GSA.

TABLE: COMPARISON OF RESULTS FROM THE MCU AND SAPFIR PROGRAMS

Zone No.	Φ^{MCU}/Φ^{GSA}	$A_c^{8\,MCU}/A_c^{8\,GSA}$	$A_c^{5\,MCU}/A_c^{5\,GSA}$	$A_f^{5\,MCU}/A_f^{5\,GSA}$
I	1,033±0,029			
2	0,984±0,027			
3	0,998±0,025			
4	0,989±0,009			
5	1,008±0,006			
6	1,005±0,006			
7	1,004±0,005			
8	1,005±0,005			
9	1,010±0,005			
10	1,007±0,005			
11	0,989±0,012	0,992±0,038	0,980±0,022	0,995±0,017
12	0,985±0,012			
13	1,016±0,008	0,998±0,025	0,982±0,016	1,031±0,013
14	1,016±0,007			
15	1,005±0,007	0,970±0,014	0,972±0,014	1,017±0,012
16	1,007±0,007			
17	1,002±0,006	1,015±0,020	0,942±0,013	1,003±0,011
18	1,001±0,006			
19	1,008±0,006	1,008±0,016	1,006±0,013	1,029±0,010
20	1,011±0,006			

REFERENCES

[1] TEBIN, V.V., YUDKEVICH, M.S., Obobshchennyj podgruppovoj podkhod k raschetu rezonansnogo pogloshcheniya (Generalized subgroup approach to calculating resonance absorption), At. Ehnerg. 59 2 (1985) 96-101.

[2] GOMIN, E.A., OSIPOV, V.K., TEBIN, V.V., Annotatsiya programmy SCOCRT (Notes on the SCOCRT program), Voprosy atomnoj nauki i tekhniki, ser.: Fizika i tekhnika yadernykh reaktorov 4, TsNIIatominform, Moscow (1985) 52-53.

[3] Proekt paketa programm SAPFIR dlya resheniya zadach rascheta yachejki reaktora (Design of the SAPFIR program package to solve problems in reactor cell calculation), Voprosy atomnoj nauki i tekhniki, ser.: Fizika i tekhnika yadernykh reaktorov 4, TsNIIatominform, Moscow (1985) 68-71.

[4] NIKOLAEV, M.N., FILIPPOV, V.V., Izmerenie parametrov rezonansnoj struktury sechenij nekotorykh elementov v oblasti ehnergij nejtronov 0.3-2.7 MeV (Measurement of the resonance structure parameters of the cross-sections of certain elements in the neutron energy range 0.3-2.7 MeV), At. Ehnerg. 15 (1963) 493-498.

[5] NIKOLAEV, M.N., IGNATOV, A.A., ISAEV, N.V., KHOKHLOV, V.F., Metod podgrupp dlya ucheta rezonansnoj struktury sechenij v nejtronnykh raschetakh (The subgroup method for taking the resonance structure of cross-sections into account in neutron calculations), At. Ehnerg., Part I, 29 1 (1970) 11-16; Part II, 30 5 (1971) 426-430.

[6] ABAGYAN, L.P., BAZAZYANTS, N.O., NIKOLAEV, M.N., TSIBULYA, A.M., Gruppovye konstanty dlya rascheta reaktorov u zashchity (Group constants for reactor calculation and protection), Ehnergoizdat, Moscow (1981) 231.

[7] SINITSA, V.V., NIKOLAEV, M.N., Analiticheskij metod polucheniya podgruppovykh parametrov (An analytical method of obtaining subgroup parameters), At. Ehnerg. 35 5 (1973) 429-430.

[8] KOROBEJNIKOV, V.V., NIKOLAEV, M.N., Raschet ehffektov rezonansnoj geterogennosti metodom Monte-Karlo (Calculation of resonance heterogeneity effects using the Monte Carlo method), Voprosy atomnoj nauki i tekhniki, ser.: Yadernye konstanty 22, Atomizdat, Moscow (1976) 103-118.

[9] KOROBEJNIKOV, V.V., SBOEV, A.G., TEBIN, V.V., Modelirovanie metodom Monte-Karlo ehksperimentov po izmereniyu rezonansnogo integrala ^{238}U (Modelling of experiments to measure the resonance integral of ^{238}U using the Monte Carlo method), Voprosy atomnoj nauki u tekhniki, ser.: Yadernye konstanty 35 4, TsNIIatominform, Moscow (1979) 52-61.

[10] TEBIN, V.V., Rezul'taty rascheta rezonansnogo pogloshcheniya nejtronov metodom Monte-Karlo v nekotorykh reaktornykh yachejkakh s vodnym medlitelem (Results of neutron resonance absorption calculations,

using the Monte Carlo method, in reactor cells with a water moderator), Voprosy atomnoj nauki u tekhniki, ser.: Fizika i tekhnika yadernykh reaktorov 22 9, NIKIEhT, Moscow (1981) 19-59.

[11] TEBIN, V.V., YUDKEVICH, M.S., Uchet ehnergeticheskoj zavisimosti plotnosti stolknovenij, obuslovlennoj rezonansnym rasseyaniem, pri raschete gruppovykh sechenij (Taking into account the energy dependence of collision density due to resonance scattering when calculating group cross-sections), Voprosy atomnoj nauki u tekhniki, ser.: Yadernye konstanty 36 1, TsNIIatominform, Moscow (1980) 81-88.

[12] TEBIN, V.V., YUDKEVICH, M.S., "Podgruppovye parametry v oblasti razreshennykh rezonansov" (Subgroup parameters in the resolved resonance region), Moscow, Preprint IAEh-3395/5 (1981) 32.

[13] LIMAN, G.F., MAJOROV, L.V., YUDKEVICH, M.S., Paket programm dlya resheniya metodom Monte-Karlo zadach perenosa izlucheniya v reaktore (Program package designed to solve problems of radiation transport in a reactor using the Monte Carlo method), Voprosy atomnoj nauki i tekhniki, ser.: Fizika u tekhnika yadernykh reaktorov 7, TsNIIatominform, Moscow (1985) 27.

[14] TEBIN, V.V., YUDKEVICH, M.S., Raschet nejtronnykh sechenij po otsenennym rezonansnym parametram (Calculation of neutron cross-sections from evaluated resonance parameters), Voprosy atomnoj nauki u Tekhniki, ser.: Yadernye konstanty 29 2, TsNIIatominform, Moscow (1978) 2-7.

ADVANCED PWRs (APWRs) AND RELATED SAFETY CONSIDERATIONS

C.H.M. BROEDERS, H. KÜSTERS, A. MATEEVA*
Institut für Neutronenphysik und
Reaktortechnik,
Kernforschungszentrum Karlsruhe GmbH,
Karlsruhe, Federal Republic of Germany

Abstract

The paper describes the main characteristics of a tight lattice advanced pressurized water reactor (APWR) with mixed-oxide (MOX) fuel with emphasis to nuclear data sensitivities and calculational procedures. It is concluded that certain cross-section data of actinides and fission products are not yet known with sufficient accuracy, and some problems in the calculational procedures are identified.

1 Introduction

The performance of present day LWRs is very reliable The availability of KRAFT-WERKUNION nuclear power plants usually is about 90 % or more, e g the power station Grohnde with 1369 MWe reached in 1986 an availability of almost 93 % Any modification of these reactors to improve economy must not violate the proven safety behaviour

In order to improve the fuel utilization in conventional LWRs, an extension of core life and burnup ($\geq$ 50 GWd/t)has been studied to improve economy One of the limiting factors for further extension is the loss of stability of the cladding material zircaloy

Furthermore, the recycling of reprocessed plutonium in LWRs has been intensively studied since the mid-60s In the Federal Republic of Germany, thermal Pu-recycling has been demonstrated on a large scale in the power plants at Kahl (VAK), Gundremmingen (KRB-A) and Obrigheim (KWO) Since 1981 Pu-recycling has been carried out with mixed-oxide (MOX) fuel of improved fabrication

* From the Institute for Nuclear Research and Nuclear Energy, Bulgaria.

process at KWO, but also at the large power reactors Neckarwestheim (GKN) and Unterweser (KKU) In the Federal Republic of Germany the technical feasibility and economic use of reprocessed plutonium has been proven primarily for PWRs The programme is scheduled to include also BWRs in order to increase the recycle capacity No technical problems have arisen in the design and use of reprocessed uranium after enrichment (ERU) Strategy and current status of the recycling programme was presented in /1/ and /2/

For validation of the nuclear design methods and nuclear data the results of the experimental recycling demonstration programmes in the KWU reactor stations and special irradiation experiments are used /1, 2, 3, 4/ The insertion of MOX and ERU fuel assemblies shows that thermal recycling is feasible on an industrial scale and that common levels of reliability and safety can be achieved in reactor operation

About 1976 the idea came up to improve the fuel utilization in LWRs by increasing the conversion ratio to a value near to one If possible, this idea should be realized with standard LWR technology by replacing "only" the core, all other components should preferably stay unchanged

This investigation led to a core with a tight triangular lattice with MOX fuel in modern PWR designs One of the main problems then is to verify that the usual PWR safety criteria are kept valid in this tight lattice PWR concept (APWR)

This paper describes at first the main characteristics of such an APWR, then deals with the calculational procedures and nuclear data sensitivities A comparison with experiments, where available, will show the present day capabilities in calculating the nuclear characteristics of such a tight lattice advanced PWR

2 Present Status of APWR-Design Investigations

In this chapter a brief review of the efforts to design an APWR in the Federal Republic of Germany as a joint venture of the Nuclear Research Center Karlsruhe (KfK), KRAFTWERKUNION (KWU), and the Federal Swiss Institute for Reactor Research (EIR), is given

The objective to achieve a high conversion ratio in a Pu-fuelled LWR, can be realized by hardening the neutron spectrum e g by tightening the reactor lattice In the Shippingport Reactor /5/, a tight lattice movable seed and blanket core for $^{233}U/Th$ fuel was in operation to prove the feasibility of light water breeder reactors However, it is not prudent to develop high converting reactors without also developing reprocessing capabilities Therefore studies in Germany are examining the U/Pu cycle for LWR-high converters It has been shown /6/ that, if fast breeder reactors will be commercially available only with some delay, there is an incentive to develop such a high converting reactor to take an intermediate role until fast reactors are fully accepted

The present investigations for developing a tight lattice light water cooled high converter reactor are performed under the following constraints

(1) A high converting tight lattice core should directly replace a normal PWR core, such that the essential out-of-core components remain the same for the same reactor power

(2) The conversion ratio should preferably reach a value of CR $\approx$ 0 95

(3) The fissile inventory should be comparable with that of a fast reactor inventory of equal size

(4) The safety features of the reactor must be such that they can be accepted for licensing That is

- sufficient positive moderator density coefficient
- negative void-reactivity effect in all burnup states
- acceptable pin deformation behaviour in the tightly packed lattice
- proven emergency core cooling for off nominal conditions

The neutron physics investigations have begun with an assessment of the validity of the available calculational methods and data bases for tight lattice (MOX and uranium fuel) analysis /7/ The data and methods used at KfK are being improved up to the present day, the 1985 status can e g be found in Ref /8/ With such data and methods, an assessment of the following concepts was done

(a) homogeneous concept, the preferred solution for industry

(b) heterogeneous concept, seed and blanket solution with movable seeds for control and shut down

(c) heterogeneous module concept with fixed seed and control rods for shut down and control

(d) zonewise heterogeneous concept with rods for control and shut down (similar to FBR heterogeneous concepts)

In concept (a) the critical physics task is the clear identification of a negative void coefficient for an enrichment of about 7 0 % to 8 % Pu fissile (This allows a conversion ratio of about 0 95 to be obtained) In all the heterogeneous concepts the fissile Pu is about 12 % to 14 %, with low enriched Pu (≈ 5 %) breeder regions In the latter concepts the void coefficient seems sufficiently negative to allow licensing from this particular point of view, but the overall concept clearly is more complicated from the engineering aspect

From the various design possibilities the concepts (a) and (c) have been considered in more detail

Fig 1, taken from Ref 9, shows the reactivity change as a function of the in-core water density at EOC conditions at about 15 GWd/t for various pitch/diameter values, both for homogeneous and heterogeneous designs

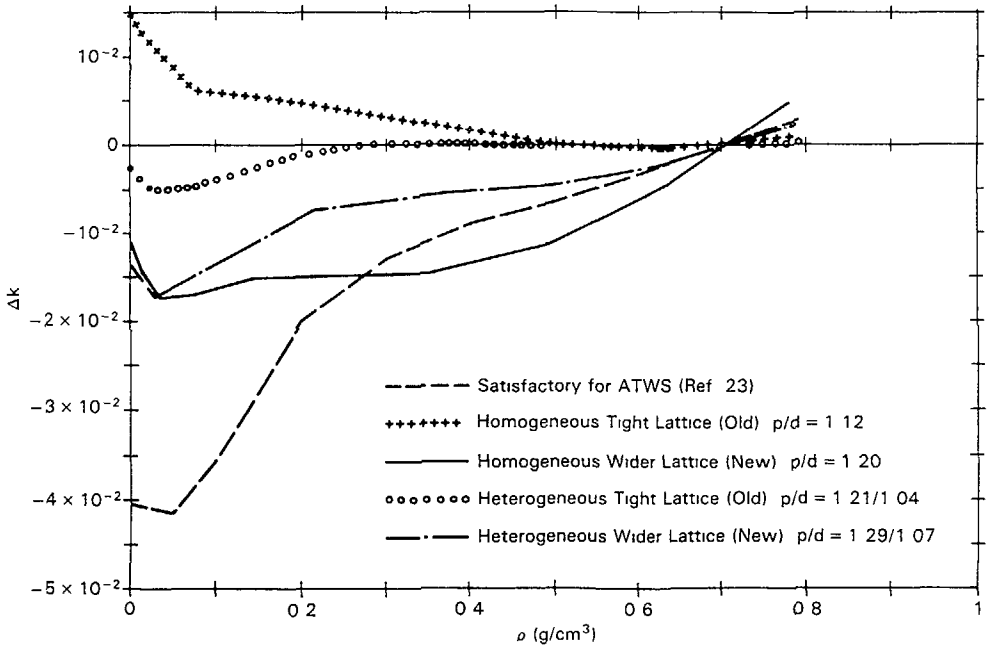

Fig 1 Reactivity change as a function of in-core water density at EOC conditions The calculation was performed with KARBUS

This analysis clearly shows that, on the basis of used methods and nuclear data, the tight core lattice should be widened to guarantee a negative void reactivity effect and an acceptable water density coefficient at the working point of normal reactor operation, i e water density ρ = 0 7 g/cm³

The widened lattice gives a conversion ratio of about 0 85 - 0 90 for the homogeneous system, and 0 90 to 0 95 for the heterogeneous APWR system The fissile inventory for both cases is about 8 tons of heavy metal, compared to about 3 tons of heavy metal in a standard PWR The Doppler coefficient in both cases is sufficiently negative (about -3 10 5, even a bit more negative than for PWRs) There seems to be no large advantage of the heterogeneous core design over the homogeneous one

The problem, still to be investigated, is whether the favourable findings for wider lattices still hold at a core burnup up to 70 000 MWd/t, which is also one of the desirable goals of an APWR

3 Important Influences of Nuclear Data Uncertainties and Methodical Aspects on the Void Reactivity Coefficient Δk of an APWR

From the discussion in chapter 2 it can be seen that the moderator density and the void reactivity coefficients are a very dominant parameters in the design investigations of an APWR Therefore the accuracy of the used nuclear data basis, of the processing codes to generate group constants, and of the reactor physics programmes is of high importance for a reliable determination of the void reactivity effect These aspects will be discussed in some detail in the following sections

3 1 Isotopic contribution to the void reactivity effect Δk

The neutron spectrum of an APWR has its maximum above the thermal energy region, i e between about 0 1 eV and 10 eV as can be seen from Fig 2 of ref /8/ This immediately has the consequence that uncertainties of the neutron capture and fission cross sections of the contributing isotopes in the resolved resonance region are of prime importance

The isotopic contribution to the void reactivity effect has been investigated by many authors As an example, here we reproduce a table from J Porta et al /10/ for a typical hexagonal APWR tight lattice It should be mentioned that the void

reactivity effect, Δk, is a combination of three effects (a) reduced absorption in the core in the voided case, giving a positive contribution, (b) increased leakage of neutrons, resulting in a negative contribution, and (c) spectral shift effects in the case of voiding, which can give a positive or negative contribution, depending on composition and size of the reactor The contributions of the single isotopes are listed in Table 1 /10/ (it should be noted that 1 pcm = 10^{-5} Δk/k)

Table 1 *Isotope Contribution to Voiding Effect (24 000 MWd/tonne)*

Isotope		Δρ Voiding (pcm)
^{235}U	1	−3 418
^{239}Pu		−68 865
^{241}Pu		−37 255
Sum 1		−109 538
^{238}U	2	+41 926
^{240}Pu		−36 084
^{242}Pu		+6 521
Sum 2		+84 531
Sum 1 + 2		−25 007
^{241}Am	3	−1 627
^{243}Am		+2 504
Other uranium, plutonium, americium, curium		+1 124
Sum 3		+5 255
Sum 1 + 2 + 3		−19 752
Fission products		+17 606
Structural materials + O_{16}		+5 576
Xenon		+1 087
Samarium		+2 020
Water		+1 068
Total		+7 605

As seen from Tab 1, the main fissionable isotopes give a strong negative contribution, while the fertile isotopes produce a slightly less, but almost an equally large positive contribution The minor actinides, the fission products and the structural materials give positive contributions These various contributions almost compensate and, as in the presented case, give a positive net reactivity effect upon voiding the APWR core

3 2 The effect of nuclear data uncertainties on the void reactivity coefficient

Already from Tab 1 of Sect 3 1 it is evident that due to the large compensating effects of the various contributing isotopes to the void reactivity coefficient one can expect large uncertainties originating from unsufficiently well known nuclear data In fast reactor physics development therefore nuclear data adjustment to integral experiments was and still is used in design calculations and in the interpretation of the results from recent integral experiments For the determination of the void reactivity effect of an APWR therefore one could use one of the many adjusted data sets for the fully voided core Meanwhile the reevaluation of the cross sections for most of the reactor materials have been improved and new data files have been established, e g ENDF/B-V and VI, JEF-1, JENDL-2

Therefore it is not unreasonable to assume that the deficiencies of the important nuclear data have been reduced Whether the same statement can be made for processing the basic data to multigroup constants, can not be detected so easily (this latter aspect will be discussed in section 3 3 to some detail) Thus at least it can be doubted, that the uncertainty of the void reactivity effect Δk still is as large as 0 04 % Δk/k per percent voidage /11/ As mentioned at the beginning of section 3 1, the APWR spectrum has essential parts in the resolved resonance range of the heavy isotopes It is clear that the spread in Δk-results can be very large, if old data files or group constant sets and, in addition, not suitable methods are used to calculate the void effect of an APWR As an example, this can be seen from some of the preliminary solutions of the NEACRP benchmark /12/ Part of the results will also be discussed by Y Ishiguro at this meeting /13/

Instead of performing a further sensitivity analysis on the uncertainties in the calculated Δk-value for voiding an APWR core, originating from nuclear data uncertainties, in chapter 4 theoretical results for some important reactor parameters, using modern nuclear data sets, are compared with experimental results of tight lattice configurations It is clear that the main uncertainties from nuclear data area come from the capture cross section of U238, capture and fission cross section of Pu239, the capture cross section of Pu240, and the fission cross section of Pu241

3 3 Some remarks on the processing of basic nuclear data to group constants

At Karlsruhe basic nuclear data in KEDAK format are processed to group constants with the processing code MIGROS /14/ The European nuclear data file JEF uses the ENDF/B format, therefore the processing code NJOY was adapted at KfK It was decided to keep the fundamental calculational basis used at KfK, therefore resonance selfshielding factors $f^g(T,\sigma_0) = \sigma^g_{eff}(T,\sigma_0)/\sigma^g_\infty$ were formally derived from NJOY (σ_0 is the background cross section representing the nuclides in the reactor mixture under consideration, and σ^g_∞ the corresponding cross section for infinite dilution) In applying this code to JEF, many irregularities were found /15/ For some materials overflows, underflows and divide checks appeared in different modules of NJOY

Following four items should be mentioned here

(a) For a number of heavy materials the resonance selfshielding factors became unacceptably larger than unity

(b) For some fission products the resonance selfshielding factors became negative, probably due to a large 'background' cross section in the ENDF/B format-data files this 'background' cross section usually is not flat with energy, so it would also require a 'selfshielding' treatment, which usually is not done

(c) NJOY produces resonance selfshielding factors even in the high energy region about 1 MeV without any resonances, probably near a threshold of a cross section Similar phenomena may and probably will occur in other energy regions also

(d) Some cross sections of isotopes having in JEF multilevel Breit Wigner representation of resonances and 'unphysical' resonance spins J, failed to be processed in NJOY

Some examples of these irregularities produced via cross section generation to group constants can be found in ref /15/ chapter 2 Similar findings as in ref /15/ have been reported also by D E Cullen /16/

Most of the mentioned irregularities have been removed at KfK, partly only formally /17/, or are being removed at present

Furtheron one has to consider, whether the formalism, introduced by Bondarenko et al and which has been taken over e g at Karlsruhe in the calculational scheme for fast reactors, is still valid if the group widths are narrowed and if then a resonance is cut by one or more group boundaries Then the Bondarenko formalism is not allowed anymore and will introduce certain errors in the results of reactor calculations This unsatisfactory situation is being improved at Karlsruhe at present

The accuracy of processing codes is mandatory Often the errors, produced by the processing codes, are simply attributed to possible deficiencies in the basic cross section data As a general rule, any adoption of larger code systems requires very intensive checking of the various procedures and code modules used It is not tolerable that in the end of the 1980ies, when the uncertainties in the basic cross sections seem to become acceptably small, the major non-negligible left uncertainty is then due to the processing systems, especially in the determination of resonance selfshielding (for instance in the unresolved resonance range)

The findings in this section will have also a definite effect on the value of the reactivity change upon voiding the tight lattice core But the uncertainty, related e g to unprecise or unphysical resonance selfshielding factors, are difficult to extract from the results of reactor calculations, because the reactor codes are designed as to operate e g with 'physical' resonance shielding factors $0<f\leq 1$

3 4 Influence of the weighting spectrum in calculating the void reactivity effect

In this section we will discuss the influence of the weighting spectrum, used for the generation of group constants, on the void reactivity effect of a tight lattice APWR configuration, proposed as a NEACRP benchmark, ref /12/

It is well known for many years that the weighting spectrum, used to generate group constants, can have a marked effect in fast reactor analysis Loosing the coolant from a tight lattice APWR, the maximum of the spectrum will be shifted from relatively low energies (between 0 1 and 100 eV) to a very fast spectrum in the high keV range Therefore, the voided core must be calculated with a group constant set, using a weighting spectrum for the voided configuration, while the normal configuration has to be calculated with the corresponding 'normal' weighting spectrum The results of this investigation have been presented in /18/ It was shown that the effect on Δk is relatively large for the HCLWR-benchmark The reactivity effect is reduced by about 50% compared to that value, which is determined by using the same APWR weighting spectrum in both the normal and the voided core lattice This effect is predominantly caused by the change in the out-of-group scattering characteristics of the medium weight nuclei (e g O16 gives almost 50% of the total effect)

3 5 Influence of using the fission spectra of all fissionable isotopes

It is also known from fast reactor investigations that the use of the fission spectra of the contributing fissionable isotopes (especially of Pu239 and Pu241) are of importance for some reaction rate ratios and for Δk The tight lattice APWR is also sensitive to the isotopic fission spectra /19/ In principle there exists no problem, because in modern data libraries the fission spectra of the important fissionable isotopes are stored as e g in JEF Sometimes reactor codes have to be modified to include all fission spectra

4 Test of Nuclear Data and Calculational Methods in Critical Experiments for APWRs

A tight lattice APWR has a neutron spectrum, which covers to an important part the energy region between 0 1 eV and 100 eV, i e the lower part of the resonance region of the heavy nuclides Neither thermal nor fast reactors are as sensitive as the epithermal APWR to uncertainties of cross sections (both basic nuclear data and resonance selfshielded effective cross sections) in the resonance range

Therefore a test of nuclear data and reactor physics methods on integral experiments is necessary to obtain confidence in the computed neutron characteristics of APWR desings

KfK started the qualification of data and methods together with KWU and the Technical University Braunschweig about 1980 in applying their codes and nuclear data to experiments, reported in the literature, with UO_2 tight lattices, wider lattices with MOX fuel, but relatively low PuO_2 content The results of these investigations are given in /7/ Since then experiments have been performed in Japan on UO_2-tight lattice fuel, on MOX fuel in Switzerland, Germany and France In this chapter we will examine, whether the steadily improved data and methods are able to describe these experiments, which cover both the normal (water-in) and partially or totally voided core configurations

4 1 Investigations in Germany and Switzerland (KfK, KWU, and EIR)

In a joint cooperation between KfK, KWU and EIR, in Wurenlingen (Switzerland) the PROTEUS facility is intensively used for evaluating the neutronic characteristics of tight lattice configurations Besides this effort in SNEAK-12 at Karlsruhe some experiments were performed The Phase I experiments in PROTEUS and in SNEAK-12 together with their interpretation were reported in 1986 /20/ In Table 2, taken from ref 20, experimental k_∞-results in a two rod lattice for three voidage ranges are compared with calculated results, using different data bases and different methods

Table 2 Comparison of Calculated[a] and Measured Values of the Net k_∞ Void Coefficient for the PROTEUS-LWHCR 6% fissile-Pu Test Lattice over Different Voidage Ranges (units 10^{-4}%)

Void Range	0 - 100 %	0 - 42.5 %	42.5 - 100 %
Experiment / Code. Lib.	- 14.4 ± 1.4	- 10.1 ± 3.5	- 17.5 ± 3.0
A. ENDF/B Data Basis			
EPRI-CPM	- 8.9	- 9.8	- 8.2
CASMO, E3LI69C	- 10.1	- 9.9	- 10.2
CASMO, E3LBI70	- 13.4	- 10.8	- 15.3
SRAC, ENDF/B-4	- 17.2	- 14.2	- 19.5
B. U.K. Data Basis			
WIMS-D, Std.	- 11.3	- 13.8	- 9.5
WIMS-D, 1981	- 11.4	- 10.4	- 12.1
WIMS-E	- 11.2	- 9.2	- 12.7
CASMO, UKLI69A	- 10.9	- 12.0	- 10.0
C. KfK Data Basis			
KARBUS, KEDAK-4	- 15.5	- 14.4	- 16.3
GRUCAH2, KFKINR	- 12.2	- 13.0	- 11.6
D. JAERI Data Basis			
SRAC, JENDL-2	- 15.6	- 13.5	- 17.1

[a] deduced from the corresponding k_∞ values as $\Delta k_\infty/\overline{k_\infty}\cdot\Delta v$, where Δv is the voidage change in %

From this table it can be seen that the net k_∞ void coefficient for the 100% void range, associated with the largest change in the neutron spectrum, CASMO/E3LBI70, KARBUS/KEDAK 4 and SRAC/JENL 2 agree with the experimental value within the given 1σ-error In the same ref 20, however, it is pointed out that the experimental breakdown of this net reactivity change shows larger discrepancies in those components which are related to the reaction rate ratios C8/F9 (= capture in U238/fission in Pu239) and F8/F9 For the KfK results it is known that

KEDAK-4 has too high capture data in U238, so that the negative contribution from C8/F9 becomes stronger negative, which then is partly compensated by the overestimation of the positive contributions to the void coefficient (F1/F9 and others)

As another example the results for the polystyrene removal experiments in SNEAK 12F1 and SNEAK 12F2 are shown in Table 3, taken again from ref 20 The calculational results are obtained with exact perturbation theory applied to a 2-dimensional diffusion theory in (r,z)-geometry for the whole reactor The results have been normalized to one of the experiments, viz III B

Table 3 Moderator Removal Experiments in SNEAK 12F1, 12F2

Experiment No., Description	Δρ(Expt. X) / Δρ (Expt. III.B)	
	Measured	Calculated by KARBUS / KEDAK-4
I. Voiding of Central Element[a] in 12F1		
A. over ± 20 cm	0.029±3%	0.029
B. over core (± 42 cm)	0.049±2%	0.047
C. over core & blanket (± 72 cm)	0.048±2%	0.047
II. Introduction of Central Zone[b] (12F1 ⟶ 12F2)	0.153±5%	0.195
III. Voiding of Central Zone[b] in 12F2		
A. 0 ⟶ 47 % void	0.643±2%	0.597
B. 0 ⟶ 100 % void (norm.)	1.00[c]	1.00

[a] 54 mm x 54 mm; [b] 326 mm x 326 mm; [c] absolute Δρ-value: - 1.474%

As in Tab 2 it can be seen that the net voidage effect is well represented with KARBUS/KEDAK-4 But one has to keep in mind that compensating effects may shadow inconsistencies in the components

Recent measurements in the PROTEUS-PHASE II experiments with a single rod lattice of 7 5% Pu fissile material show a similar trend Tab 4 gives the C/E-values for k_∞ and the reaction rates using WIMS D/81 and KARBUS/KEDAK-4 calculational schemes /21/

As in the case of PROTEUS-Phase I results we can observe an overprediction of the important void-reactivity components C8/F9 and F8/F9 with KARBUS/KEDAK-4 The strong misprediction of the relative capture in Pu242 (C2/F9) for the water-in-case with both WIMS and KARBUS comes mainly from a neglection of resonance selfshielding in the 2 67 eV resonance of Pu242 In this case a group boundary is cutting the resonance near the peak area

Table 4 Calculation/Experiment (C/E) values for k_∞ and reaction rate ratios measured in LWHCR-PROTEUS, Cores 1-8

Moderator	WIMS D, 1981			KARBUS, KEDAK 4		
	H_2O	Dowtherm	Air	H_2O	Dowtherm	Air
Single Rod Lattice, 7 5% Pu_{fiss}						
C_8/F_9	0 982		1 007	1 036		1 082
F_8/F_9	1 030		1 026	1 024		1 047
F_5/F_9	0 995		1 013	1 012		1 006
F_1/F_9	1 054		1 152	1 008		0 967
C_2/F_9	1 729		0 962	1 552		1 138
k_∞	1 012		1 037	0 986		0 984

The observed failures of the group cross sections and their resonance self-shielding are removed as far as possible at KfK at present

4 2 Investigations in Japan and France on a tight lattice APWR configuration

First physics experiments on HCLWR cores in Japan have been carried out in the FCA assemblies XIV-1, XIV-1 (45 V) and XIV-2 during 1986 and 1987 The cores operate in the test zone on enriched uranium, the U235 enrichment and the moderator to fuel-volume-ratio are varied It is reported /22/ that C/E values range from 0 994 to 1 001 for k_{eff} and from 0 988 to 0 993 for k_∞ The measured moderator (polystyrene) voidage reactivity change in k_∞ was well predicted by the calculation (C/E = 0 975) The calculations were based on JENDL-2 and the SRAC code system

Of international interest is the NEACRP-HCLWR benchmark, proposed by Y Ishiguro et al in 1986 /12/ Preliminary results of the various contributions show a large spread in the calculated reactivity change due to voiding the core, as reported by Ishiguro to this conference /13/ The final discussion of this benchmark will take place in April 1988 Then more definite conclusions can be drawn, very probably the spread of the results can be narrowed in that discussion

In France, experimental physics investigations on tight PWR lattices are done in the EOLE, MINERVE and MELUSINE reactors The program is described in /23/ Reactivity measurements, reaction rates, control rod worths, neutron capture in fission products and other reactor parameters are systematically studied in MOX-fuel lattices with various moderator to fuel volume ratios A comparison of measured and calculated reactor quantities is not distributed at present It is communicated that in general there is good agreement between calculations and measurements

5 Conclusions

From the important safety parameters for an advanced tight lattice PWR (APWR), the Doppler coefficient is sufficiently negative and the present uncertainty is not of primary concern for a design of such a reactor The reactivity change in an APWR upon voiding the tight lattice has to be sufficiently negative, too, but the required accuracy of this parameter is not yet fully achieved at present Although some codes with their associated data sets (e g KARBUS/ KEDAK-4) give agreement with experimental results for the net void effect, there exist larger differences in the important compensating components of this quantity The main reasons are summarized in the following

(a) Further improvement of the neutron capture data in the unresolved resonance region of U238 There has been considerable progress in the last years, but the problems seem to be not yet fully solved Also the inelastic cross section of U238 is fairly important, especially for the voided stage of an APWR, and should be carefully re-checked

(b) For Pu239 there exist still some discrepancies between total cross sections measured in Dubna and the earlier Saclay data Inconsistencies over the broader resonances should be resolved

(c) For Pu240 a re-investigation of the cross sections in the neighbourhood of the first resonance should be made

(d) For Pu241 not all discrepancies and inconsistencies have been removed yet

The recommendations (a) to (d) are taken from the summary of the Third Advisory Group Meeting on "Transactinium Isotope Nuclear Data", Uppsala 1984 (IAEA-TECDOC 336), and still hold for the data sets used in this contribution

(e) The capture data for important fission products need special attention They are important at EOL for a reliable determination of Δk (void)

(f) The current maximum difference in processing basic nuclear data with NJOY (IBM) to group constants reaches sometimes a value of about 20%, as found by Cullen in the processing code verification project of the IAEA Especially in the resonance region resonance selfshielding is sometimes unsatisfactorily determined, as reported in the present contribution

(g) Special attention has to be given to the use of effective group constants, given in the Bondarenko formalism, if the groups get narrow and a resonance is cut by one or more group boundaries

(h) The weighting spectrum to generate group constants is important in calculating the reactivity change upon voiding an APWR core The present situation seems to require two weighting spectra, one for calculating the properties of the normal water-in core or a core with a low void content, and one for highly or totally voided core regions

Further work is intended to remove the left deficiencies in basic data and processing procedures The re-evaluation of nuclear data for JEF-2 will hopefully be so successful that adjustment of the group constants on integral experiments will not be necessary as in the past for fast reactor analyses

ACKNOWLEDGEMENTS

The authors thank Dr H W Wiese for careful reading the manuscript and Mrs M Wesche and Mrs Ch Kastner for the effective typing

REFERENCES

/1/ G J Schlosser, S Winnik
Thermal Recycle of Plutonium and Uranium in the Federal Republic of Germany, Strategy and Present Status
IAEA-SM-294/33

/2/ H Roepenack, F U Schlemmer, G Schlosser
Development of Thermal Plutonium Recycling
Nuclear Technology 77, p 175 (1987)

/3/ M Peehs, G Schlosser
Prospects of Thorium-Fuel Cycles in a Standard Pressurized Water Reactor
Siemens Forsch - und Entwick -Bericht 15, p 199 (1986)

/4/ D Porsch, G Schlosser, W Stach, M Zimmermann
Uberwachung der Leistung von MOX-Brennelementen in DWR
Methoden und Verifikation
Jahrestagung Kerntechnik '87, p 47 (1987)

/5/ "Light Water Breeder Reactor Programme"
Environmental Assessment of a Conceptual Thorium-Uranium Fuel Cycle

/6/ H H Hennies and H Markl
Uberlegungen zur Modifizierbarkeit eines LWR im Hinblick auf eine bessere Uranausnutzung,
in Proc Jahrestagung Kerntechnik, Kerntechnische Gesellschaft, Berlin (1980), p 953

/7/ H D Berger et al
Uberprufung der Berechnungsverfahren fur enge Reaktorgitter von fortschrittlichen Druckwasserreaktoren (FDWR) an experimentellen Anordnungen,
KfK-Report 3389 (1982)

/8/ C H M Broeders
Neutron Physics Investigations for Advanced Pressurized Water Reactors,
Nucl Techn 71, No 1, p 96 - 110 (1985)

/9/ C H M Broeders and M Dalle Donne
Conceptual Design of a (Pu, U)O_2 Core with a Tight Lattice for an Advanced Light Water Reactor
Nucl Techn 71, No 1, p 82 - 95 (1985)

/10/ J Porta et al
Sensitivity Studies on High-Conversion Power Reactors, via Perturbation Methods and Information Conditioning,
Nucl Sci Eng 95, 266 - 281 (1987)

/11/ L Martin-Deidier et al
private communication (1985)

/12/ Y Ishiguro et al
Proposal of Benchmarks on Data and Methods to Calculate Reactor Characteristics in High Conversion Light Water Reactors,
NEACRP-A Report (1986)

/13/ Y Ishiguro
Resonance Absorption and Coolant Void Reactivity Coefficient in Tight Pitch Lattices,
this meeting (1987)

/14/ I Broeders, B Krieg et al , "MIGROS-3, A Code for the Generation of Group Constants for Reactor Calculations from Neutron Nuclear Data in KEDAK Format"
KfK-2388 (1977)

/15/ A Mateeva, H Kusters, Testing of JEF-1 Data on the Burnup Behaviour of PWR-Fuel up to 33 GWd/t
JEF-DOC (1987)

/16/ D E Cullen, Report on the IAEA Cross Section Processing Code Verification Project
INDC(NDS)-170/NI (1985)
and
D E Cullen, The Accuracy of Data Processing, Proc of the Intern State of the Art-Seminar on Nuclear Data, Cross Section Libraries and their Application in Nucl Technology

/17/ I. Broeders, B Krieg, "The KfK-Version of the Neutron and Photon Cross Section Generation Code NJOY Implementation, Verification and Modification of the Code"
Internal KfK-report and JEF-DOC (1987)

/18/ A Mateeva, Influence of the Weighting Spectrum in Calculating the Void Reactivity Effect in a Tight-Lattice-PWR Configuration
Contributed to the "Jahrestagung Kerntechnik", Travemunde (1988)

/19/ C H M Broeders, Contribution to the NEACRP-HCLWR-benchmark, to be discussed in April 1988

/20/ R Chawla and R Bohme, LWHCR Physics Experiments and their Interpretation
ANS Topical Meeting on Advances in Reactor Physics and Safety, Saratoga Springs, N Y (1986)

/21/ R Seiler et al , Investigation on the Void Coefficient and other Integral Parameters in the PROTEUS-LWHCR Phase II Programme
Nucl Techn 80, Nr 2, p 311-323 (1988)

/22/ T Osugi et al , private communication (1987)

/23/ G Gambie et al , Advanced Water Reactors in France Preliminary Design and R&D Programme
Int Top Meeting on Advances in Reactor Physics, Mathematics and Computation, Paris (1987)

94 RESONANCE ABSORPTION AND COOLANT VOID REACTIVITY COEFFICIENT IN TIGHTER PITCH LATTICES

Y. ISHIGURO
Japan Atomic Energy Research Institute,
Tokai-mura, Naka-gun, Ibaraki-ken,
Japan

Abstract

This paper reviews the present status of the nuclear data needed for analysis of high conversion light water reactors with tighter pitch lattice, through sensitivity analysis, cell burnup benchmark calculation and comparison of the conventional methods with Monte Carlo calculation.

1. INTRODUCTION

The realization of a commercial scale introduction of FBRs becomes distant from view, thus worldwidely accepted is the prospect of long-term utilization of LWR. Accordingly, plutonium is supposed to be increasingly produced in LWR, and the surplus of fissile plutonium is estimated to be about 100 tons by 2000 in Japan, for instance. The way to effectively utilize and preserve the surplus plutonium has been seeked and pursued in countries with nuclear programme. On the other hand, though the recent growth curves for expansion of LWR capacity are projected to be lower in a short-term aspect, there is still an anxiety that uranium shortage might be serious in a mid-/long-term aspect at the countries such as Japan without any practically available uranium resource. From these points of view, the development of innovative LWRs with a much better plutonium utilization and higher natural uranium saving is thought to be essential.

Recently much works have been done for the R and D of high conversion light water reactors (HCLWRs) with tighter pitch lattice. All the design efforts aim at achieving both high conversion and high burnup. The details of HCLWRs such as the concept and its advantages have been published and can be seen elsewhere[1]-[13]. The HCLWR design concepts so far proposed can be classified into two groups : The first group is the simple tight HCLWR (V_M/V_F = 0.5 ~ 0.75 ; KWU, KFK)[5]-[7], while the second is the quasi-tight one with spectral shift mechanism (V_M/V_F = 1.1 ~ 1.4 ; Framatome, CEA)[8],[9].

An HCLWR with tighter pitch lattice has the following two design features, compared with the conventional LWR : i) Reduced volume ratio of water to fuel (V_M/V_F) and ii) higher plutonium fissile enrichment. From the view point of reactor physics, the first feature brings an intermediate neutron spectrum in the core, while the second one likely does a positive void reactivity mainly provided with ^{240}Pu. These reactor characteristics are peculiar in the meaning that the intermediate energy region is quite important, and exist out of the range of experience.

One of the most critical problems in the design of HCLWR is the existence of the trade-off relation between the enhancement of the conversion ratio and the safety margin concerning coolant void coefficient[14],[15]. Hence, reliable data and methods for the reactor physics calculations will be essential to assess and confirm the HCLWR concept.

The conceptual designs so far proposed however seem to be based on insufficient accuracy of the data/methods in reactor physics. Taking this situation into consideration, a benchmark problem of tight lattice cell burnup calculation[16] was proposed at the 29th meeting of the Nuclear Energy Agency Committee on Reactor Physics (NEACRP), Sept., 1986. This benchmark problem aims to extract the problems included in the data/methods and to accelerate the developing works of the data/methods.

The preliminary report[17] of the benchmark calculations however shows that a large discrepancy is found in the k_∞, conversion ratio and void reactivity coefficients obtained by the participants. This discrepancy seems to be much larger than generally encountered on an existing LWR cell.

The 30th NEACRP Meeting, Sept.1987, recommended that a specialist meeting concerning the results of NEACRP HCLWR cell burnup benchmark problem should be convened in the week starting 18th April 1988 at the NEA Data Bank. Discussions among the experts of the HCLWRs and also of cell code were thought to be essential to grasp and clarify the physics problems included in the data/methods of HCLWRs.

In the present paper, the nuclear data involved in HCLWRs will be reviewed from the viewpoint of calculating the resonance absorption, burnup and coolant void reactivity coefficient, which are primarily important to evaluate the HCLWR core characteristics. The review will be grounded mainly upon the works made at Japan Atomic Energy Institute (JAERI). Under the light of the intermediate spectrum of HCLWR, various physics problems in the conventional data/methods will rise to the surface. The resulting understandings will be also useful to enhance accuracy of the data/methods for thermal and/or fast reactor.

2. GENERAL ASPECT OF HCLWR

Let us take a look at the general reactor physics aspect of HCLWR, before stepping into the details. Figure 1 compares an HCLWR spectrum with a typical PWR one, and figures 2 ~ 4 show the neutron spectrum and the energy distributions of capture and fission rates, respectively, for a hexagonal lattice with homogeneously mixed material of two fuel materials of PROTEUS-LWHCR Cores[12],[13] at EIR(See Fig.5). These figures were obtained by using SRAC system[18], of which the descriptions are somewhat given in APPENDIX 1. As seen from these figures, more than 40% of fission reaction and 70% of capture reaction take place in the resonance energy ($E \gtrsim 10$ KeV). Especially, most of capture reaction are due to the typical resolved resonances of major actinide isotopes.

Table I shows the contribution of different families of isotopes to the reactivity loss of an equilibrium cycle of a PWR and a plutonium fueled quasi-tight HCLWR[8]. Fission products are the most important part, contributing about 55% of the total, and minor actinides quite largely affect the isotopic evolution.

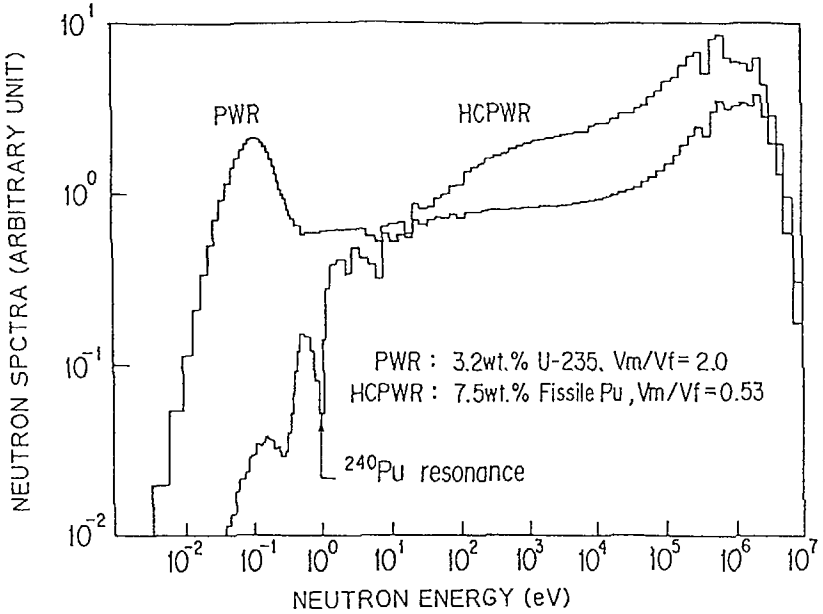

Fig.1 Neutron Spectra in PWR and HCLWR

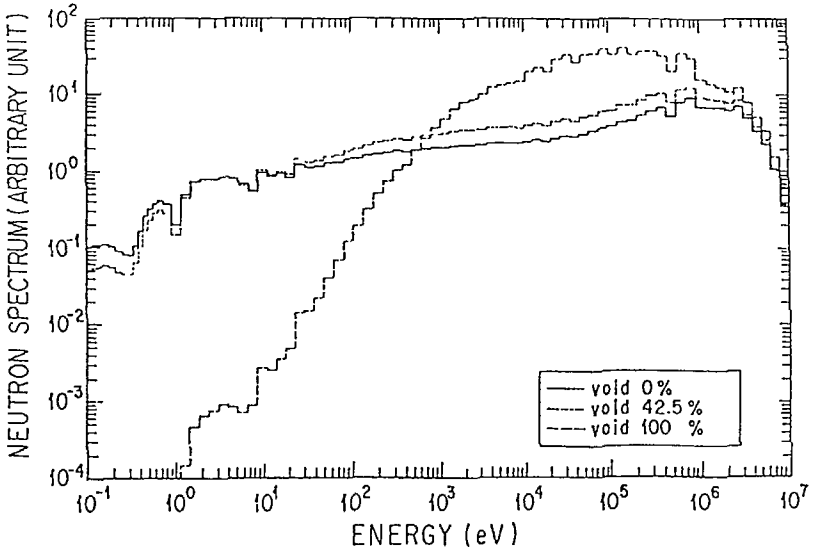

Fig.2 Neutron Spectra in Test Region of PROTEUS Cores

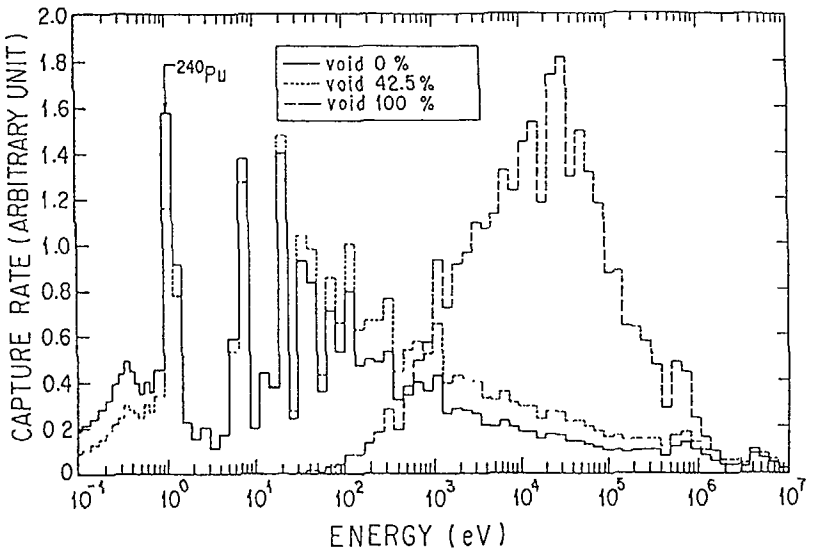

Fig.3 Macroscopic Capture Rate Distribution in Test Region of PROTEUS Cores

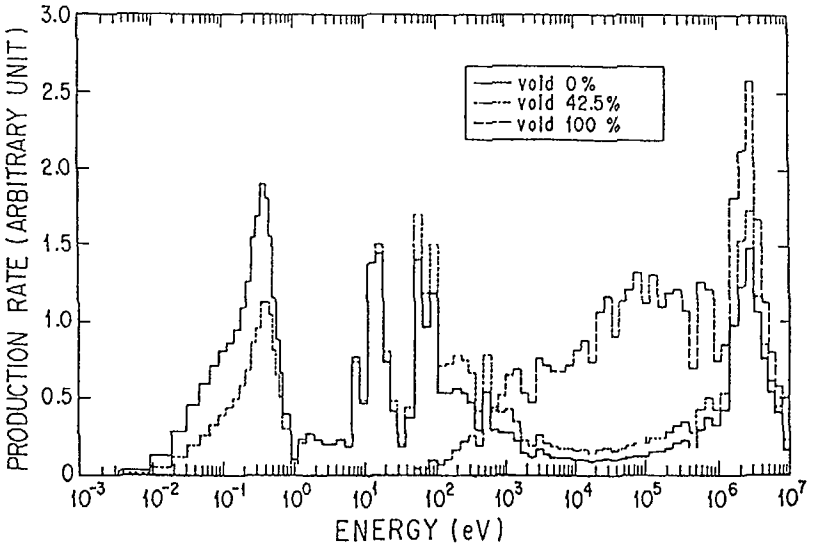

Fig.4 Macroscopic Fission Rate Distribution in Test Region of PROTEUS Cores

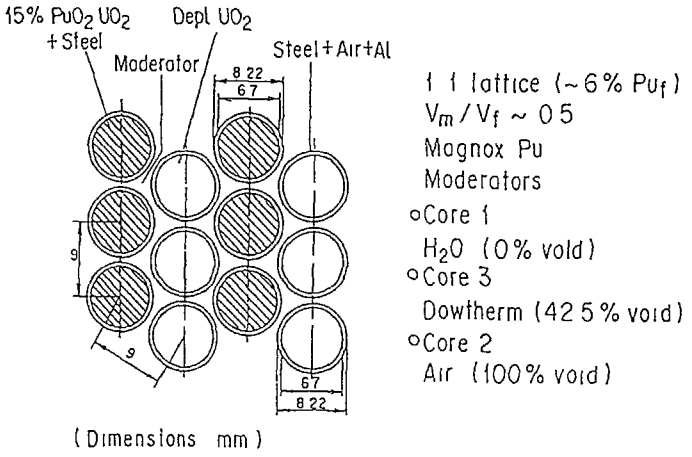

Fig 5 Test-Lattice for PROTEUS-LWHCR Cores 1-3

Table I Contribution of the main isotopes families to reactivity change / cycle

Reactivity Change/Cycle	PWR -14%	PU-HCLWR - 6%
Breakdown :		
Uranium Isotopes	-87	- 1
Plutonium Isotopes	+21	-26
Am, Cm Isotopes	- 2	-16
Fission Products	-32	-57
(norm.)	100	100

Figure 6 shows the variations of k_{eff} with void fraction in a simple tight HCLWR core of V_M/V_F=0 8[19] It should be noted that the void coefficient is considerably positive at the end of equilibrium cycle (35Gwd/t) This is due to the accumulation of fission products and minor actinides, though the positive contribution can mostly be attributed to the 1 05eV capture resonance of ^{240}Pu, which is the evil of HCLWR' Hence, their accurate nuclear data will be essential for the design of HCLWR core

Concerrned with the 1 05eV resonance of ^{240}Pu, it is well known that a precise treatment of this level is rather difficult from neutronic aspect, because it lies in half way between resonance and thermal energy regions.

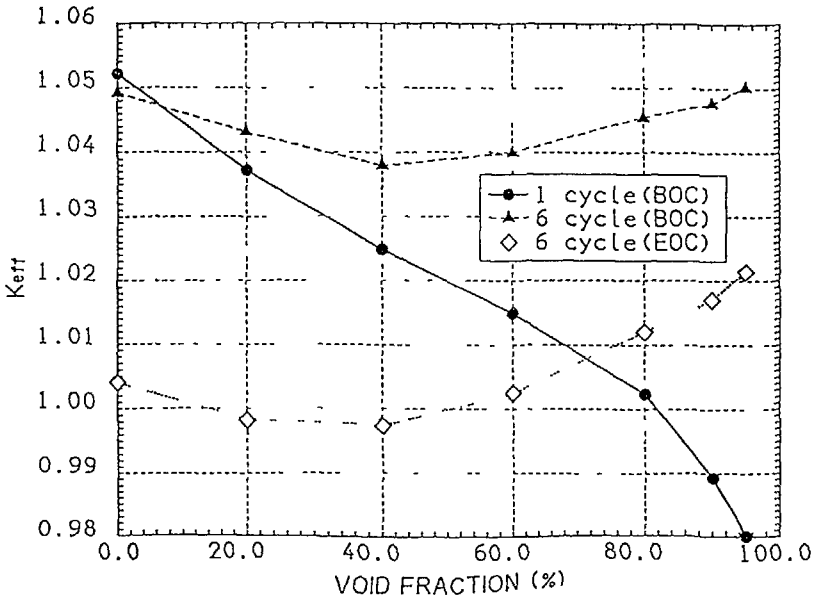

Fig 6 Void Variation of Keff in HCLWR Cores with V_M/V_F = 0 8

Recently, a new measurement of the resonance parameter was reported[20] The resulted resonance integral is reported to be higher by about 5% than that calculated with the ENDF/B-V parameters The void reactivity coefficient should be reevaluated using the new resonance parameters

3. STATUS OF ACCURACY OF CONVENTIONAL CELL CALCULATION METHODS

One of the fundamentals in analysis of nuclear physics characteristics is to estimate accurately the neutron spectrum in lattice cell Especially, an HCPWR core has a spectrum different from both of the LWR's and FBR's, which has not fully been studied The accuracy of calculated lattice spectrum is of course determined by the nuclear data used, while it depends not only on the way to calculate effective multigroup cross sections but also on the geometrical model for lattice representation

3.1 CALCULATION METHODS

In order to validate the accuracy of the conventional cell calculation methods in HCPWR lattice, a comparison study[21] was made for the effective cross sections, k_∞ and reaction rate ratios calculated by the SRAC system and the continuous energy Monte Carlo code VIM[22] This comparison study was made again for the hexagonal lattice of PROTEUS-LWHCR Cores[12] [13]. The both calculations were carried out by the libraries (T = 300°K) based on ENDF/B-IV[23] Here, the infinite dilution cross sections were also compared on multigroup level between the two libraries and proved to be

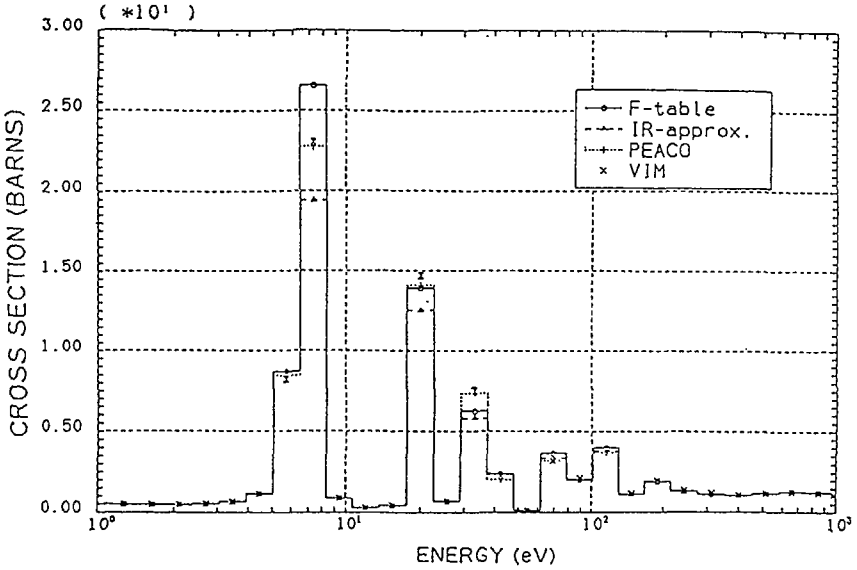

Fig.7 Comparison of Effective Capture Cross Sections Calculated by Various Methods (U-238)

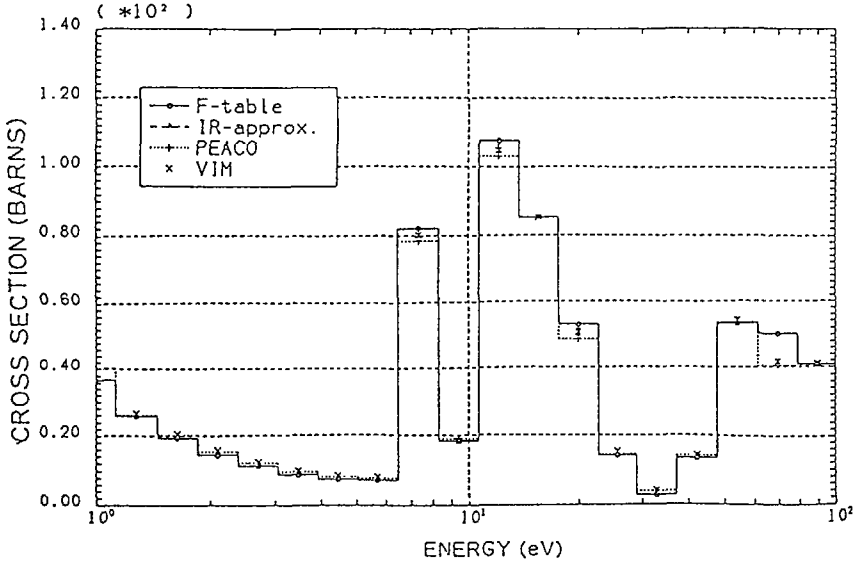

Fig.8 Comparison of Effective Fission Cross Sections Calculated by Various Methods (Pu-239)

consistent, where the values for the VIM code were obtained in a homogeneous medium consisting of hydrogen or carbon atoms where the absorber under consideration was infinitely diluted.

Figures 7 and 8 show the comparison of the effective cross sections, respectively, of ^{238}U capture and ^{239}Pu fission among the various calculation methods for the case of 0% void. The same tendency has been observed also for the cases of 42.5 and 100% void. These figures show that the effective cross sections in the important resolved resonance region should be calculated by in details solving the neutron slowing down equation. It should be noted that a higher accuracy can not be expected by use of either of the IRA or table-look-up method in the HCPWR analysis, which is an excellent approximation for thermal and fast reactor analysis, respectively.

Table II compares k_∞ and the the reaction rate ratios between the SRAC and the VIM code. This table shows that the table-look-up method and the IRA method considerably underestimate, respectively, k_∞ and the conversion ratio(C8/F9). These validation tests show that the conventional resonance treatments developed for the analysis of FBR and /or LWR are not always suitable for analizing an HCLWR core with intermediate spectrum.

Table II Comparison of reaction rate ratios between VIM and SRAC. (The values in parentheses are the ratio of SRAC values to VIM.)

<Calculational conditions>
Library : ENDF/B-IV, geometrical buckling = 0.0,
Lattice model : hexagonal cell

* Core 1 (Water) void 0 %

reaction rate ratio	VIM (100000 hist.)	SRAC F-Table	SRAC IR	SRAC PEACO
C8/F9	0.06739 ± 0.46%	0.06806 (1.010)	0.06489 (0.963)	0.06673 (0.990)
F8/F9	0.009648 ± 0.56%	0.009815 (1.017)	0.009641 (0.999)	0.009704 (1.006)
F5/F9	0.8389 ± 0.37%	0.8475 (1.010)	0.8434 (1.005)	0.8491 (1.012)
F1/F9	1.627 ± 0.34%	1.664 (1.023)	1.666 (1.024)	1.637 (1.006)
k_∞	1.0265 ± 0.35% (collision)	1.0148 (0.989)	1.0301 (1.004)	1.0240 (0.998)
	1.0306 ± 0.34% (analog)	(0.985)	(1.000)	(0.994)
	1.0273 ± 0.40% (track length)	(0.988)	(1.003)	(0.997)
	1.0281 ± 0.30% (average)	(0.987)	(1.002)	(0.996)

(to be continued)

Table II (continued)

* Core 2 (Air) void 100 %

reaction rate ratio	VIM (60000 hist.)	F-Table	SRAC IR	PEACO
C8/F9	0.1604 ± 0.18%	0.1598 (0.996)	0.1597 (0.996)	0.1597 (0.996)
F8/F9	0.01988 ± 0.96%	0.02058 (1.035)	0.02057 (1.034)	0.02057 (1.034)
F5/F9	1.118 ± 0.10%	1.118 (1.000)	1.118 (1.000)	1.119 (1.000)
F1/F9	1.450 ± 0.12%	1.444 (0.996)	1.444 (0.996)	1.444 (0.996)
k_∞	0.9056 ± 0.29% (collision)	0.8965 (0.990)	0.8967 (0.990)	0.8968 (0.990)
	0.8999 ± 0.45% (analog)	(0.996)	(0.996)	(0.997)
	0.9034 ± 0.33% (track length)	(0.991)	(0.992)	(0.992)
	0.9033 ± 0.24% (average)	(0.992)	(0.993)	(0.993)

* Core 3 (Dowtherm) void 42.5 %

reaction rate ratio	VIM (80000 hist.)	F-Table	SRAC IR	PEACO
C8/F9	0.08850 ± 0.40%	0.08949 (1.011)	0.08538 (0.965)	0.08804 (0.995)
F8/F9	0.01181 ± 0.33%	0.01228 (1.040)	0.01204 (1.019)	0.01217 (1.030)
F5/F9	0.9856 ± 0.35%	0.9892 (1.004)	0.9830 (0.997)	0.9968 (1.011)
F1/F9	1.781 ± 0.34%	1.780 (0.999)	1.786 (1.003)	1.765 (0.991)
k_∞	0.9706 ± 0.31% (collision)	0.9543 (0.983)	0.9697 (0.999)	0.9615 (0.991)
	0.9677 ± 0.38% (analog)	(0.986)	(1.002)	(0.994)
	0.9694 ± 0.42% (track length)	(0.984)	(1.000)	(0.992)
	0.9693 ± 0.30% (average)	(0.985)	(1.000)	(0.992)

3.2 ADAPTABILITY OF CROSS SECTION ADJUSTMENT METHODS

Figure 9 show the deviations of the infinite dilution and effective cross sections of ^{238}U based on the ENDF/B-IV from those on JENDL-2, where the effective cross sections are calculated for the lattice of PROTEUS-LWHCR Core 1. These evaluations were made to estimate the cross section uncertainty for use in a sensitivity analysis for the lattice system[24]. It is worth while noting that the deviations of the effective cross sections are much larger than those of the infinite cross section in the energy range from 4 KeV to 100 eV, which is just the resolved resonance region of ^{238}U. Moreover, the two deviations show even opposite sign each other below 1 KeV. This difference can be attributed to the difference of the resonance shielding effects calculated by the different sets of resonance parameters. As known from Fig.10, each resonance shielding factor obtained from a sequence of independently evaluated resonance parameters has a different value In fact, a large difference can be seen among the resonance parameters of ENDB/B-IV and JENDL-2, though they give almost the same values for the infinitely dilute cross section.

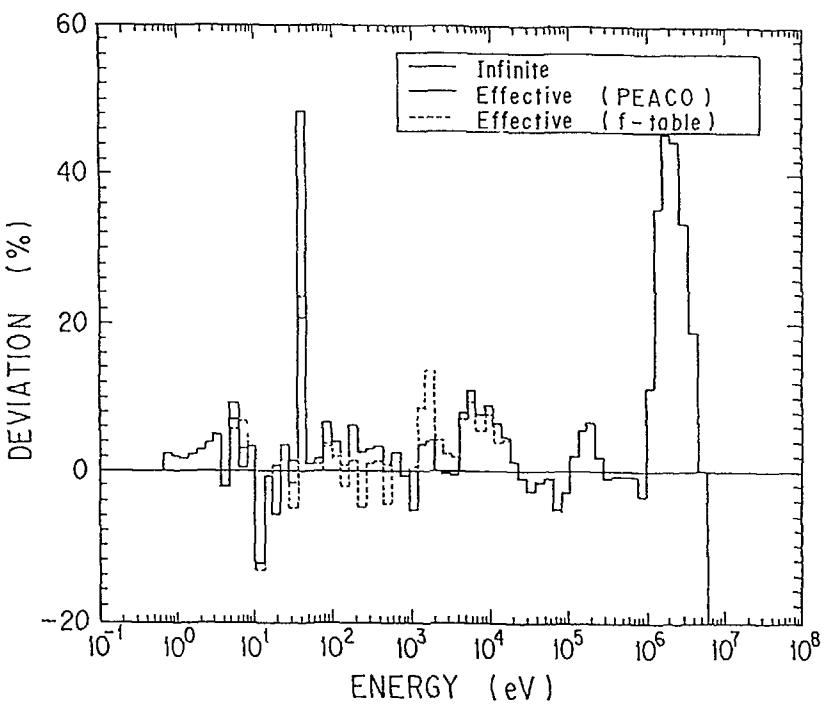

Fig.9 Deviation of U-238 capture cross section of ENDF/B-IV from JENDL-2

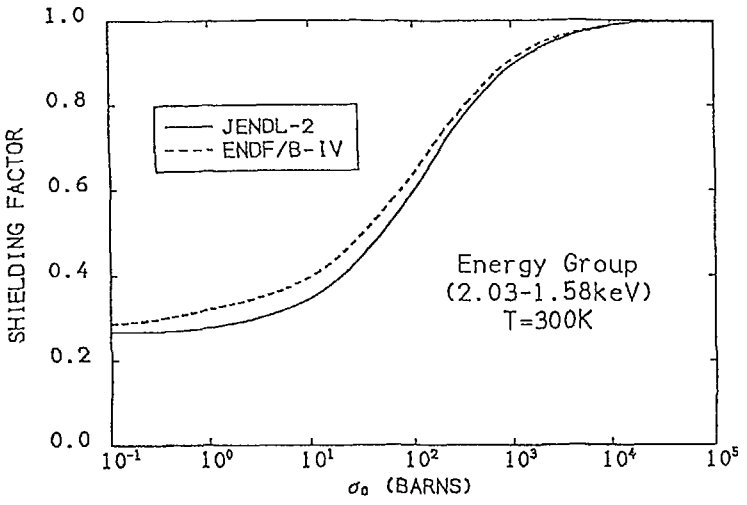

Fig.10 Self-shielding factor of U-238

This fact show that it will be quite difficult to define the cross section deviations of typical resonance nuclides in the resonance energy range to be used in a conventional sensitivity analysis. So, a cross section adjustment method based on multigroup scheme will be a question when applied to strong resonance nuclide such as ^{238}U. Here, it should be noted that the error originated from the calculational methods themself is generally not so large in the higher energy region. Nevertheless, a sensitivity method can tell us something useful. And the discussions made in this section will be applicable also to fast reactor analysis.

3.3 SENSITIVITY ANALYSIS

Sensitivity analysis is a useful tool to identify the nuclear data requirement and to assess the accuracy of calculated integral quantities in fission reactors. As pointed out in the previous subsection, it is generally difficult to assign cross section uncertainty in multigroup scheme, which depends on neutron energy and reaction. Hence, the resulting conclusions should be considered with caution.

A sensitivity analysis[24] using the cross section difference of Fig.9 was made to see its effect on the cell parameters of the PROTEUS core. The sensitivity coefficients were calculated by the SAINT code[25], which is based on the generalized perturbation theory and can treat the cell parameters with collision probability methods. Figures 11 and 12 show the group contributions of the ^{238}U capture cross section differences to k_{eff} and coolant void reactivity, respectively. These figures show that the uncertainty caused by use of the different set of the resonance parameters is predominant in the higher energy range (E > 100eV), while that by the different calculational methods is highlighted in the lower. Anyway, a reevaluation work will be essential for the resonance parameters of ^{238}U in the resolved resonance region.

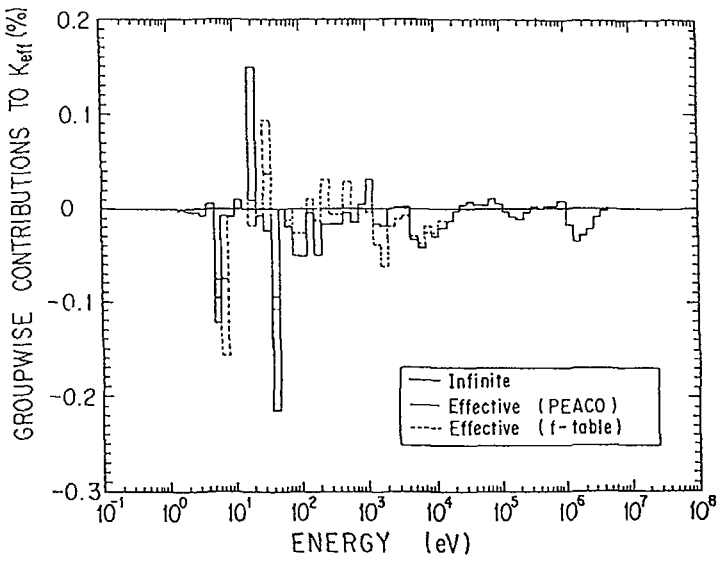

Fig.11 Groupwise contributions of U-238 capture cross section differences to multiplication factor

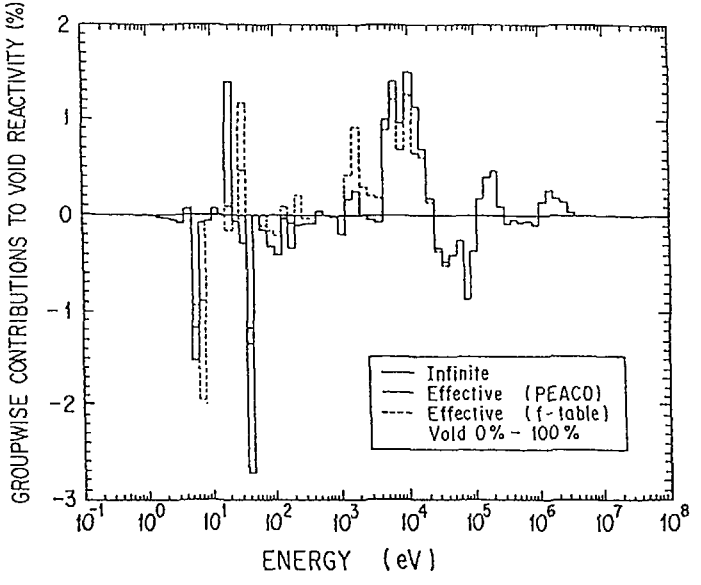

Fig.12 Groupwise contributions of U-238 capture cross section differences to void reactivity

Another overall sensitivity analysis[26] was made for typical HCLWR lattice. Tables III and IV show the results for the effect of the differences of the ^{238}U capture and ^{239}Pu fission cross sections resulted from calculation methods (the same cross section library) and those from cross section libraries (the same methods) on the cell parameters of the PROTEUS cores.

Table III Effect of change in group constants obtained from VIM and SRAC to cell parameters of PROTEUS core (%)

	k_∞		28C/49F		Void worth (0~42.5% void)
	0% void	42.5% void	0% void	42.5% void	
^{238}U capture					
Unresolved	−0.10	−0.14	0.32	0.47	0.96
Resolved	−0.36	−0.18	1.52	0.62	0.45
Total	−0.45	−0.32	1.84	1.09	1.41
^{239}Pu fission					
Unresolved	0.29	0.29	−0.41	−0.25	−2.23
Resolved	−0.13	0.12	−0.17	−0.13	−2.28
Total	0.16	0.41	−0.58	−0.39	−4.51
Total	−0.29	0.09	1.26	0.70	−3.10

1) The group constant differences were calcultated by $(\sigma_{VIM}-\sigma_{SRAC})/\sigma_{SRAC}$.

Table IV Effect of change in group constants obtained from ENDF/B-IV and JENDL-2 libraries (%) to cell parameters of PROTEUS cores (%)

Coolant void	k_∞			28C/49F		Void worth (0~42.5% void)
	0%	42.5%	100%	0%	42.5%	
^{238}U capture						
Fast	−0.09	−0.10	−0.12	0.28	0.16	0.08
Unresolved	−0.06	−0.11	−0.12	0.27	0.25	1.02
Resolved	−0.38	−0.35	−0.29	1.42	1.41	0.23
Thermal 2)	0.	0.	0.	0.	0.	0.
Total	−0.53	−0.56	−0.53	1.97	1.82	1.33
^{239}Pu fission						
Fast	−0.11	−0.18	−0.71	0.21	0.31	1.06
Unresolved	−0.31	−0.45	−0.96	0.57	0.84	3.25
Resolved	0.25	0.19	−0.01	−0.36	−0.29	0.75
Thermal	−0.08	−0.05	−0.00	0.10	0.09	−0.45
Total	−0.25	−0.49	−1.68	0.52	0.95	4.61
^{235}Pu capture	0.04	0.01	0.01	−0.01	0.01	0.32
^{240}Pu capture	0.04	0.08	0.08	0.02	0.00	−0.69
Total	−0.70	−0.96	−2.12	2.50	2.78	5.57

1) The group constant differences were calculated by $(\sigma_{ENDF/B-IV}-\sigma_{JENDL-2})/\sigma_{JENDL-2}$.
2) Same data is used for both libraries in this range.

Here, the cross section difference between calculational methods were defined as the deviation of the group cross section obtained by the SRAC code(ultrafine group option) from that by the VIM code. In addition to the above mentioned problems concerned with the ^{238}U capture cross section, the effect of the difference of the ^{239}Pu fission cross section between the libraries is large in the unresolved resonance region and increases with coolant void fraction, which brings a relatively large change in the void reactivity.

4. BURNUP CALCULATION, RELATED CROSS SECTIONS

A better conversion ratio is obtainable in tighter pitch lattices, but lower plutonium enrichment is allowed to avoid the positive void coefficient. This means that higher burnup is not achievable. Thus, there is a trade-off relation between effective fuel utilization and safety requirement. As shown in the section 2, the void reactivity coefficient become lesser negative with increase of burnup. Hence, it is quite important to forecast accurately the behaviour of the void characteristics in the case of coolant loss at any burnup stage.

4.1 BURNUP DEPENDENCE OF SENSITIVITY COEFFICIENTS

Changing the volume ratio V_M/V_F of HCLWR cell, investigations have been made for the burnup dependence of the sensitivity coefficients in order to identify the effect of the cross section uncertainty of minor actinides and fission products[26]. The sensitivity coefficients were calculated again with the SAINT code [25] by using the group constants calculated by the SRAC code equipped with the library based on JENDL-2.

Table V lists the sensitivity coefficients of k_∞ and coolant void worth at 0, 30 and 50 GWd/t for an HCLWR cell of the volume ratio V_M/V_F = 0.5 and of the Pu fissile enrichment = 8% (based on the Pu recovered from a PWR). As burnup proceeds, the sensitivities of k_∞ to ^{238}U, ^{239}Pu and ^{240}Pu capture cross sections decrease and, on the contrary, those to typical fission products increase with negative sign. *The void worth sensitivity coefficients* change the sign on the way of burnup because the void worth itself change its sign on the cell of V_M/V_F = 0.5. The sum of the sensitivity coefficients of fission products amounts to 0.98, hence has a large effect on the change in coolant void worth with burnup.

Table VI shows the sensitivities of minor actinides. The capture cross sections have larger sensitivity than fission cross sections for these nuclides. Especially, ^{243}Am and ^{241}Am have large sensitivities for k_∞. As shown later, if these nuclides are neglected in the burnup calculation of HCLWR, the k_∞ after 50 GWd/t burnup is overestimated by more than 1.5%. This reveals that accurate nuclear data of the minor actinides are required for evaluation of the burnup characteristics in an HCLWR.

4.2 FISSION PRODUCTS

Takano et al[27] made a detailed investigation for the effects of fission products on the burnup characteristics in HCLWRs. For this investigation, a typical hexagonal lattice of HCLWR was selected: 1.0-cm-diam fuel pin, 0.04-cm-thick stainless steel cladding, V_M/V_F = 0.74 and 8% enrichment of fissile plutonium. In addition to this lattice, another lattice of V_M/V_F = 1.4 with 0.064-cm-thick Zircaloy cladding was also considered complementarily.

Table V Burnup dependence of sensitivity coefficients for Case 1

		k_∞			Coolant void worth[1]	
Burnup (GWd/t)	0	30	50	0	30	50
	1.0858	0.9868	0.9444	−3.21E-3	9.67E-3	1.37E-2
^{238}U c[2]	−0.259	−0.240	−0.232	6.993	−2.016	−1.327
f	0.074	0.082	0.085	−3.014	0.960	0.692
^{235}U c	−0.003	−0.002	−0.001	−0.018	0.007	0.005
f	0.008	0.006	0.004	−0.244	0.043	0.022
^{239}Pu c	−0.143	−0.125	−0.119	−6.764	2.259	1.645
ν	0.635	0.617	0.608	7.376	−3.253	−2.496
f	0.383	0.397	0.400	−1.781	−0.386	−0.426
^{240}Pu c	−0.077	−0.070	−0.068	−6.569	1.990	1.396
f	0.020	0.024	0.025	−1.402	0.532	0.411
^{241}Pu c	−0.021	−0.020	−0.020	−0.999	0.365	0.274
ν	0.186	0.198	0.205	2.494	−1.311	−1.056
f	0.116	0.133	0.140	0.374	−0.561	−0.492
^{242}Pu c	−0.017	−0.014	−0.013	−1.502	0.503	0.362
f	0.003	0.003	0.003	−0.215	0.075	0.056
^{103}Rh c	0.	−0.003	−0.004	0.	0.080	0.081
^{109}Ag c	0.	−0.002	−0.003	0.	0.076	0.082
^{131}Xe c	0.	−0.005	−0.006	0.	0.096	0.099
^{135}Xe c	0.	−0.002	−0.002	0.	0.117	0.082
^{133}Cs c	0.	−0.004	−0.006	0.	0.075	0.076
^{147}Pm c	0.	−0.003	−0.003	0.	0.078	0.064
^{149}Sm c	0.	−0.006	−0.006	0.	0.338	0.268
^{151}Sm c	0.	−0.003	−0.003	0.	0.077	0.075
^{152}Sm c	0.	−0.002	−0.003	0.	0.062	0.069
^{154}Eu c	0.	−0.001	−0.002	0.	0.065	0.080

1) 0 ~ 50% void (Unit: $\delta k/kk'$) 2) c: capture, ν: ν-value, s: scattering, f: fission.

Table VI Sensitivity coefficients of higher actinides produced during burnup (after 50 GWd/t burnup)

		k_∞	Coolant void worth[1]
^{239}Np c[2]	−0.000	0.001
^{241}Am c	−0.006	0.115
f	0.001	0.011
^{242m}Am c	−0.000	0.002
^{242g}Am c	−0.000	0.000
^{243}Am c	−0.009	0.139
f	0.001	0.013
^{244}Cm c	−0.002	0.028

1) 0 ~ 50% void 2) c: capture, f: fission

Since a number of fission product nuclides have very large resonance capture cross sections, the resonance self-shielding effect on the reactivity change with burnup was shown to be very important. So, in the cell burnup calculations, the effective cross sections for the 65 fission products explicitly treated in the burnup chain were calculated at each burnup step by using the self-shielding factors.

Figure 13 shows the contribution of fuel isotopes and fission products to total absorption rate : The total fission product contributes about 10% of the total absorption at the burnup of 50GWd/t, while the fractional absorptions are about 0.8%, 1.4%, and 0.4%, respectively, for the minor actinides, ^{241}Am, ^{243}Am, and ^{244}Cm. Hence, the fission products are very important contributors to the reactivity change with burnup.

The contribution of individual fission product nuclides to total reaction absorption rate is shown in Fig.14 at burnup of 50 GWd/t. It is observed from this figure that the self-shielding effects of ^{131}X and ^{133}Cs are remarkable compared with other nuclides. The reactivity loss by burnup is reduced considerably when taking into account the self-shielding effects of fission products. Figure 15 shows that the effect of the self-shielding causes the differences of about 0.6% and 0.8% in k_∞ at the burnup of 50 GWd/t for the lattices of V_M/V_F = 0.74 and 1.4, respectively. As pointed out in the previous section, one of the major problems of the tight lattice reactors with MOX fuels is the void coefficient because it becomes positive with increasing plutonium enrichment and/or burnup. And the fission products play an important role in the prediction of the reactivity void coefficients. For example, the reactivities of the 90% void calculated with and without the self-shielding factors of fission products were −0.48% and +0.07% $\delta k/k$, respectively, for the lattice of V_M/V_F = 0.74. The coolant voiding makes the neutron spectrum harder, thus the self-shielding effect itself becomes innocent, while it is more reactive at the zero voiding stage.

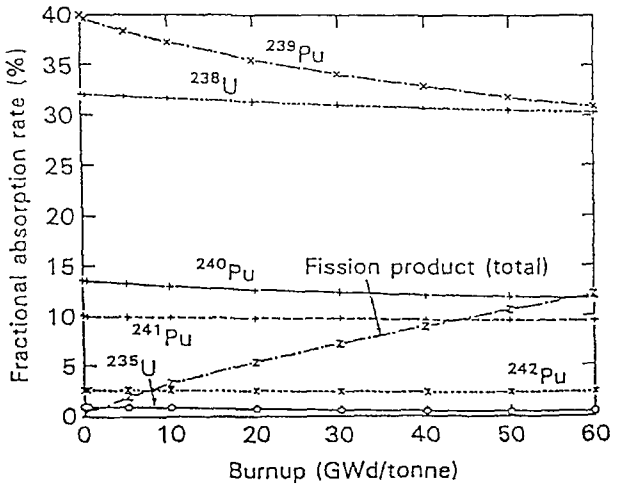

Fig.13 Contribution of fuel isotopes and total fission product to the total absorption

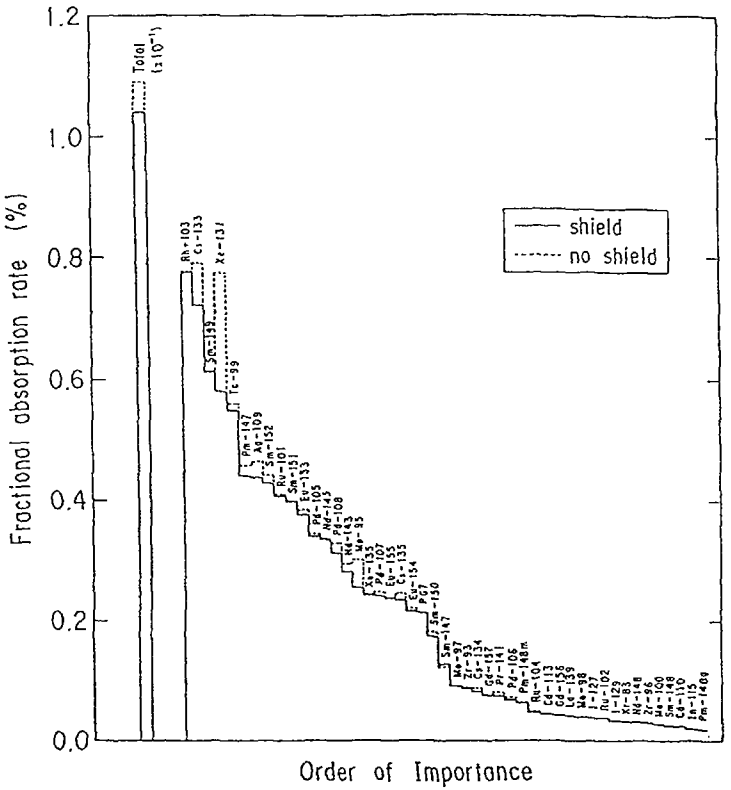

Fig.14 Contribution of individual nuclide to total absorption at the burnup stage of 50 GWd/t: The P67 stands for the pseudo fission product.

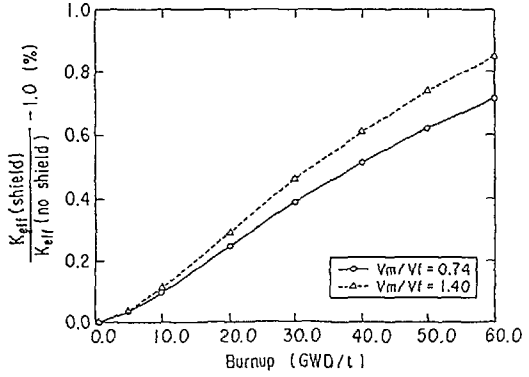

Fig.15 The effects of resonance self-shielding for fission products on the multiplication factors calculated for the moderator to fuel volume ratio of 0.74 and 1.4

Table VII Comparison of Thermal Cross Sections and Resonance Integrals (b)

Nuclide		JENDL-2	JENDL-1	ENDF/B-V	JEF-1
^{99}Tc	2200 m/s	19.8	17.7	19.5	19.0
	RI[1)]	319.2	207.0	351.0	359.0
^{103}Ru	2200 m/s	5.0		7.7	66.8
	RI	92.0		70.0	595.0
^{107}Pd	2200 m/s	1.9	10.0	10.0	1.9
	RI	101.0	120.0	76.4	103.7
^{108}Pd	2200 m/s	8.5		12.2	7.4
	RI	252.4		226.0	188.0
^{131}Xe	2200 m/s	85.0	88.0	90.1	85.5
	RI	900.0	904.0	891.0	1015.0
^{133}Cs	2200 m/s	29.0	29.0	29.6	29.0
	RI	437.2	398.0	405.0	383.0
^{145}Nd	2200 m/s	43.8	41.9	42.0	42.0
	RI	204.0	266.0	233.0	233.0
^{152}Sm	2200 m/s	206.0		207.0	206.0
	RI	2766.0		3001.0	2982.0
^{155}Eu	2200 m/s	4046.0	4040.0	4040.0	3647.0
	RI	18840.0	3218.0	1857.0	2178.0
^{155}Gd	2200 m/s	60890.0	61130.0	60930.0	61130.0
	RI	1548.0	2589.0	1555.0	2589.0

1) Resonance integral in the 0.5-eV to 10-MeV energy range.

Discrepancies among nuclear data of fission products are more remarkable than those of fuel materials. Table VII shows the comparison of the primary data; the cross sections at 2200m/s, and resonance integrals for typical fission product nuclides obtained from the evaluated nuclear data files JENDL-1, JENDL-2, ENDF/B-V, and JEF-1[28]. Large discrepancies are observed for these primary nuclear data. Especially for the resonance cross section data, the uncertainty is striking. As a typical example, the resonance cross sections for ^{155}Eu and ^{103}Ru are compared among the three evaluated files in Figs.16 and 17. From these figures, it can be observed that the discrepancies among the evaluated capture data for ^{155}Eu and ^{103}Ru are incredibly large. The same discrepancies can be found in those nuclides which have large discrepancy in the resonance integral (See Table VII).

In order to examine the effects of the nuclear data uncertainty of the fission products on burnup reactivity change, the cell burnup calculations were performed using the above four data files for the lattice of V_M/V_F = 0.75. Figure 18 compares the contributions of fractional absorption rates of the individual fission products nuclides calculated from JENDL-2, ENDF/B-V, and JEF-1. The differences among the absorption fractions are remarkably observed for several nuclides, ^{99}Tc, ^{105}Pd, ^{135}Cs, ^{103}Ru, and ^{155}Eu. The burnup reactivity changes are shown as the relative values to JENDL-2 in Fig.19. A considerable difference is observed between JENDL-2 and ENDF/B-V, while the difference between JENDL-2 and JEF-1 is very small. This situation is merely due to an accidental cancellation as seen from Fig.18.

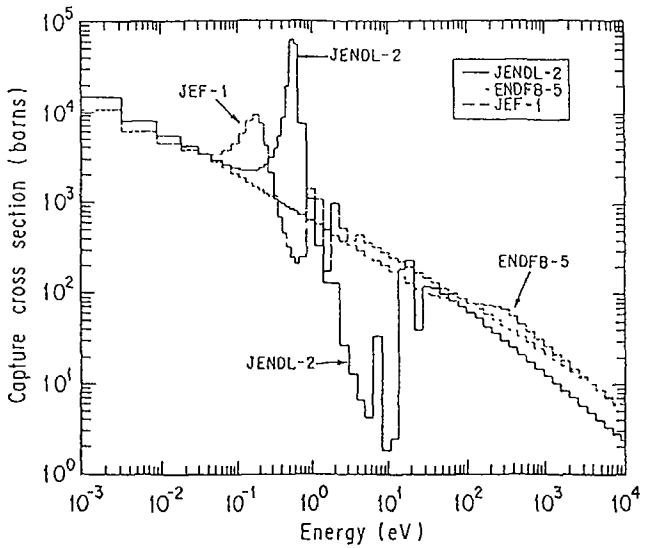

Fig.16 Comparison of capture cross sections of Eu-155 among the three nuclear data files: The cross sections of ENDF/B-4 are the same as those of ENDF/B-5.

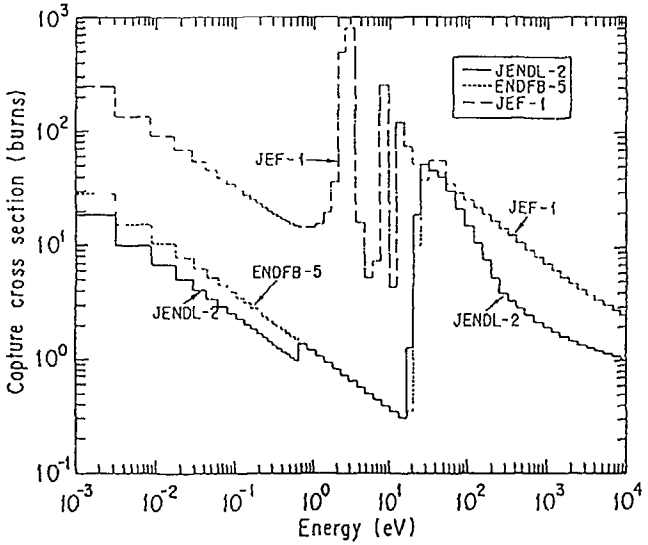

Fig.17 Comparison of capture cross sections of Ru-103 among the three nuclear data files: The cross sections of ENDF/B-4 are the same as those of ENDF/B-5.

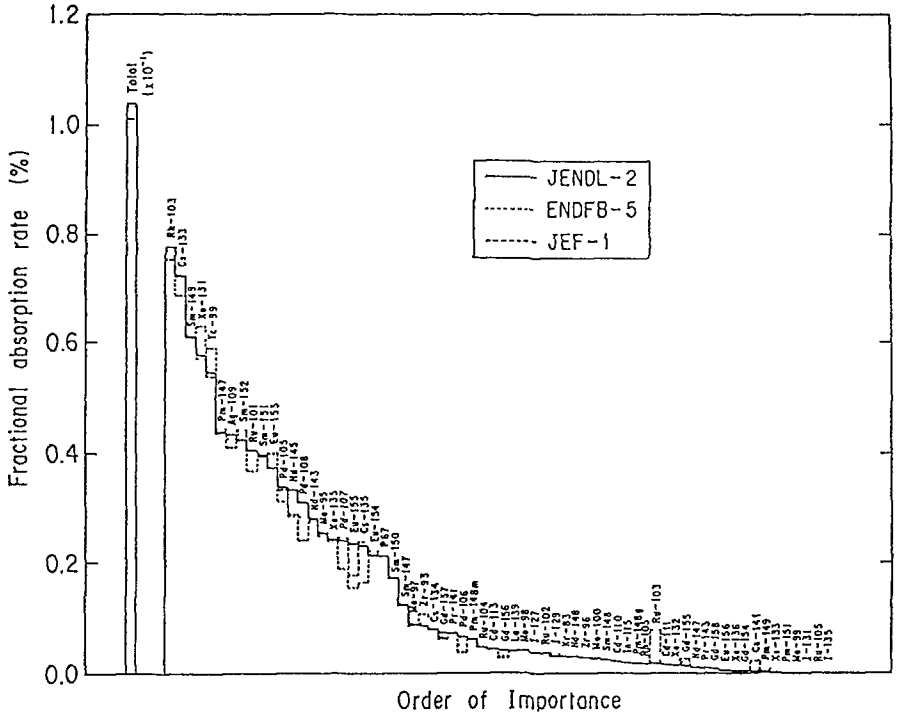

Fig.18 Contribution of individual nuclide to total absorption at the burnup stage of 50 GWd/t

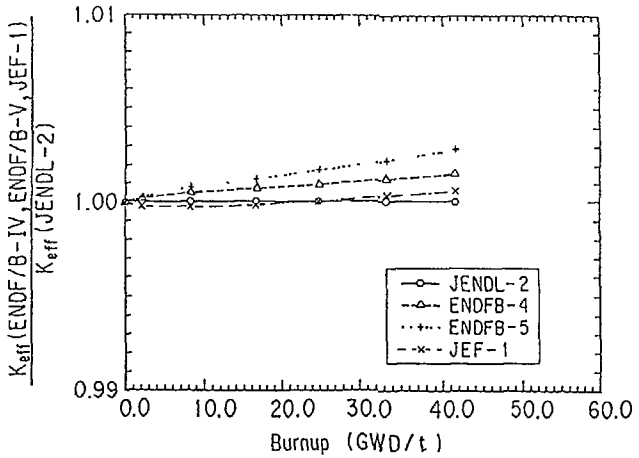

Fig.19 Burnup dependence of the ratios of the multiplication factors calculated with the other files to those obtained with JENDL-2

The mutual shielding effects between fission products and major actinides were also investigated with the ultrafine group methods, which can directly treat both the self-shielding and mutral shielding effects. The mutual shielding effects are observed for several nuclides. However, the difference between the total fractional absorptions calculated by the table-look-up and ultrafine methods is very small due to an accidental cancellation among the contributions of individual fission products.

It was shown that the fractional absorption rates for individual fission product nuclides are considerably scattered among the existing nuclear data files. The builtup of the fission products was also shown to affect the void reactivity characteristics. A consistent reevaluation of the nuclear data of the fission product is needed for a better estimate of HCLWR and/or LWR burnup characteristics.

4.3 MINOR ACTINIDES

As pointed out the previous subsections, the fission product and actinide nuclides play an important role in predicting burnup characteristics and burnup-dependent void reactivity coefficient. The prediction accuracy primarily depends on the quality of the nuclear data for these nuclides, the calculational methods of group cross sections and burnup chain model. A investigation has been made also on the effect of minor actinides on the burnup changes in HCLWRs[29].

Figure 20 shows the burnup reactivity changes for the lattice of V_M/V_F = 0.74. It will be seen that the contributions of ^{241}Am and ^{243}Am to the burnup reactivity loss is very large to be about 1.0% and 1.6%Δk/k, respectively, at the burnup 60 GWd/t. This effect of ^{241}Am and ^{243}Am is almost equal to reduce the burnup by about 10 GWd/t.

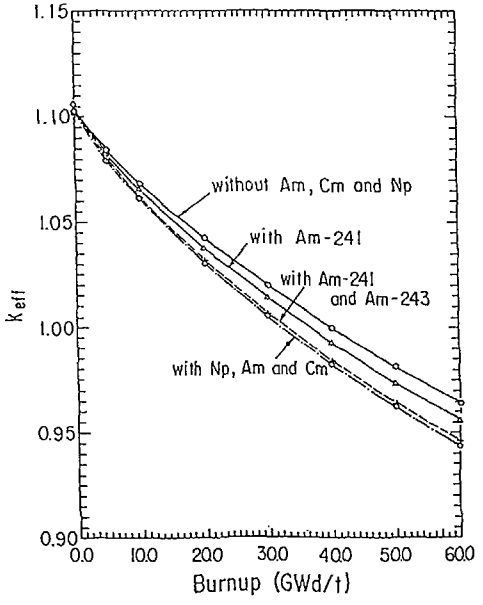

Fig.20 Comparison of burnup reactivity changes

Nuclear data uncertainties for minor actinides are usually larger than those of major ones such as ^{238}U and ^{239}Pu. The capture and fission cross sections are compared in Figs.21 and 22, respectively. Considerable discrepancies are found among the existing four nuclear data files, JENDL-2, JEF-1, ENDF/B-IV, and V. Figure 23 compares the fractional absorptions of minor actinides calculated by using the four different cross section data, where the total absorption in the lattice is normalized to 100%. The results obtained with ENDF/B-IV being older data seem to fairly deviate from others, which are in good agreement with each other.

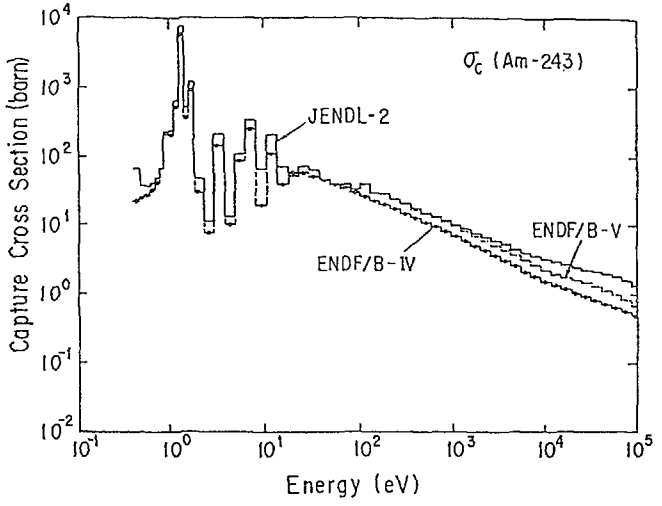

Fig.21 Comparison of capture cross sections of Am-243

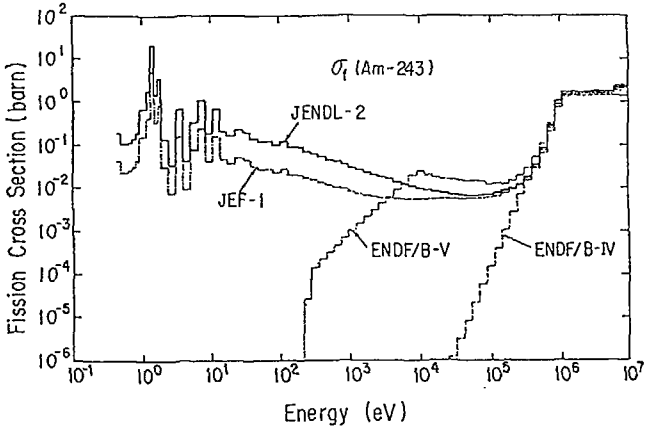

Fig.22 Comparison of fission cross sections of Am-243

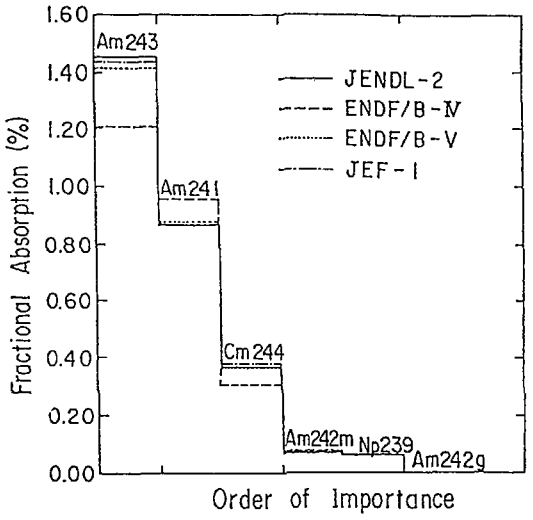

Fig.23 Comparison of fractional absorptions for minor actinides at the burnup stage of 50 GWd/t: The total absorption in cell is normalized to 100%

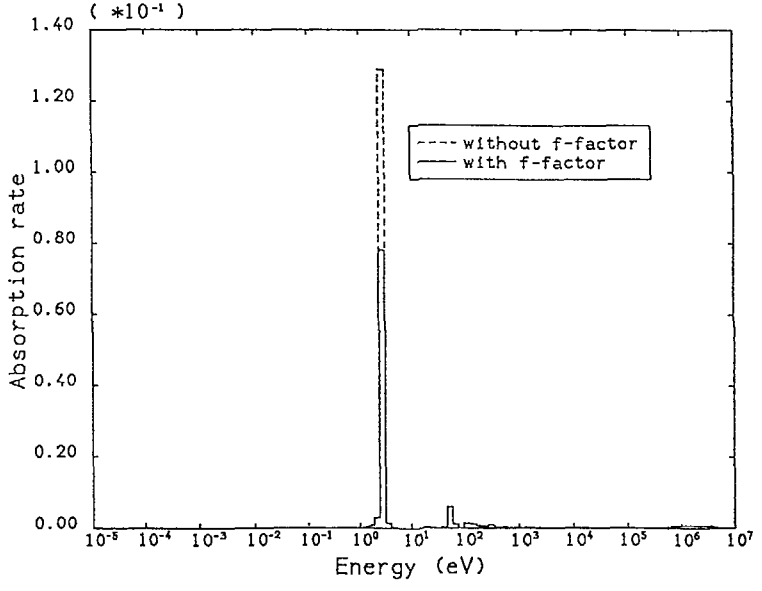

Fig.24 Groupwise absorption rates of Pu-242

The 2.67eV resonance of ^{242}Pu plays an important role in void reactivity change as well as the 1.06eV resonance of ^{240}Pu. The neutron absorption by this resonance is often calculated with infinitely dilute cross section, because of its lower atomic number density compared with other Pu isotopes. The resonance absorption cross section is however very large, hence the self-shielding effect is also to be significant. This effect on the HCLWR neutronic characteristics was examined by cell calculations[30].

Figure 24 compares the group-wise absorption rates of ^{242}Pu calculated with and without the self-shielding effect. The neutron absorption by ^{242}Pu is about 4% of total absorption when the self-shielding is ignored. If the shielding effect is taken into account, the absorption rate decreases by 2.8%, and k_∞ becomes larger by 1.4%. For the case of V_M/V_F = 0.6, this effect is reduced to about 1% due to the harder spectrum. Figure 25 shows the dependence of k_∞ on void fraction. The self-shielding effect on k_∞ decreases with increase of void fraction by spectrum hardening, which results in the increase of negative void coefficient.

Concerned with the minor actinides, the nuclear data seem to be fairly satisfactory for the analysis of the HCLWR core characteristics, considering Kusters's review[31].

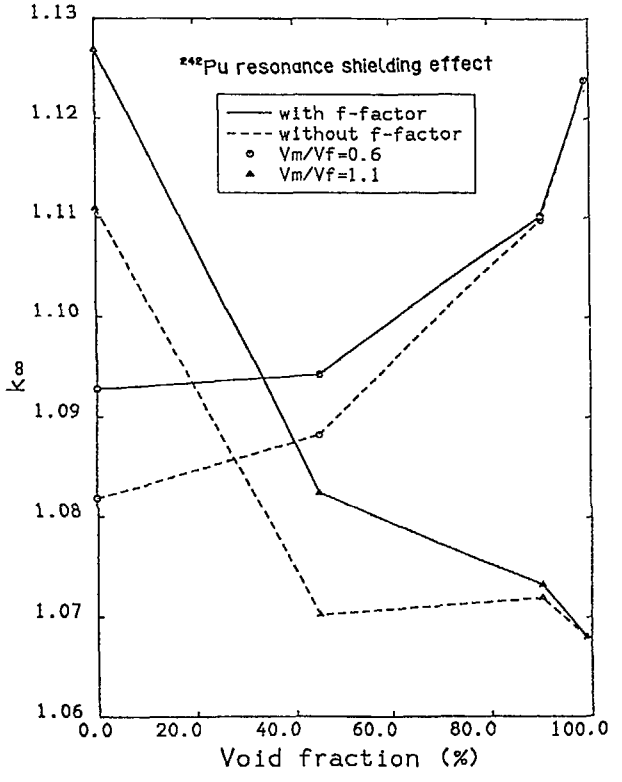

Fig.25 Dependence of k_∞ on void fraction

5. PRELIMINARY RESULTS OF NEACRP HCLWR CELL BURNUP BENCHMARK

As supposed from the previous discussions, the presently proposed designs seem to be based on insufficient accuracy of data and methods in neutronic calculations. According to the international comparison of lattice calculations for the PROTEUS-LWHCR reviewed by Chawla[32], descrepancies among the integral papameters calculated with standard LWR methods and data sets were much larger than generally encountered for an LWR lattice. Taking this situation into consideration, a benchmark of tight lattice cell burnup calculation[16] was approved at the 29th meeting of the Nuclear Energy Agency Committee on Reactor Physics (NEACRP), Sept. 1986. This benchmark problem aims to extract the problems included in the data/methods and to accelerate the developing works of the data/methods. The proposed benchmark problem is shown in Appendix 2.

Thirteen organizations from seven countries(Australia, West Germany, Japan, Sweden, Switzerland, UK and USA + probably France) participated in the present benchmarks. These organizations submitted the sixteen benchmark results obtained using different computer codes and data libraries. Though the major problem requested for participants was to calculate nuclear characteristics for a tight lattice cell with moderator to fuel volume ratio(V_m/V_f) of 0.6, thirteen results for the additional case of V_m/V_f=1.1 were also participated. The integral data requested to be calculated were the multiplication factors, conversion ratios, fractional reactions and coolant void reactivities at each burnup time.

A wide variety of data and methods were used by the participants in the present benchmark calculations: The basic nuclear data files were ENDF/B-IV, ENDF/B-V, JENDL-2, WIMS and KEDAK. The neutron spectrum were calculated by the collision probability, Sn transport and Monte Carlo methods. A preliminarily arranged report[17] was submitted to the 30th NEACRP Meeting, Sept.,1978. Several typical results are presented in Figs. from 26 to 35.

By intercomparing these preliminary solutions, the conclusions obtained can be summarized as follows:

- A relatively large discrepancy is found in the k_∞, conversion ratio and void reactivities obtained among participants.
- Discrepancy in k_∞ is caused mainly by the difference in ^{239}Pu production rate. On the other hand, the conversion ratios are scattered depending on the dispersion among the absorption rates of both fertile(^{238}U and ^{240}Pu) and fissile(^{239}Pu) nuclides.
- Burnup reactivity change is strongly influenced by the change of ^{241}Pu reaction rates, while the reaction rates for ^{239}Pu and whole fission products are of some importance.
- Absorption rate by ^{242}Pu plays an important role in k_∞ and the void reactivity change. Production rate of ^{239}Pu is also important for the void reactivity change especially in the condition of high void fraction. Difference in void reactivity is caused, in some cases, by that of ^{240}Pu absorption rate.
- Most of discrepancies among the reaction rates of ^{241}Pu and ^{242}Pu can be attributed to the resonance self-shielding effect being considered or not. The shielding effect of ^{242}Pu results in more than 1% $\Delta k_\infty / k_\infty$.

Moreover, through arrangement of the results submitted and in view of the outcomes so far surveyed, the followings were found:

- o Uncertainty for any quantity could be reduced to half probably excepting conversion ratio , if the imperfection of the codes, including lack of consideration of the rsonance shielding factors of ^{241}Pu and ^{242}Pu, were removed.
- o There seems to be still a large difference among the effective cross sections of ^{238}U, of which the studies have the longest history in reactor physics.
- o Though none of the results might show truth, it is certain that any abnormally deviated result has its definite cause.

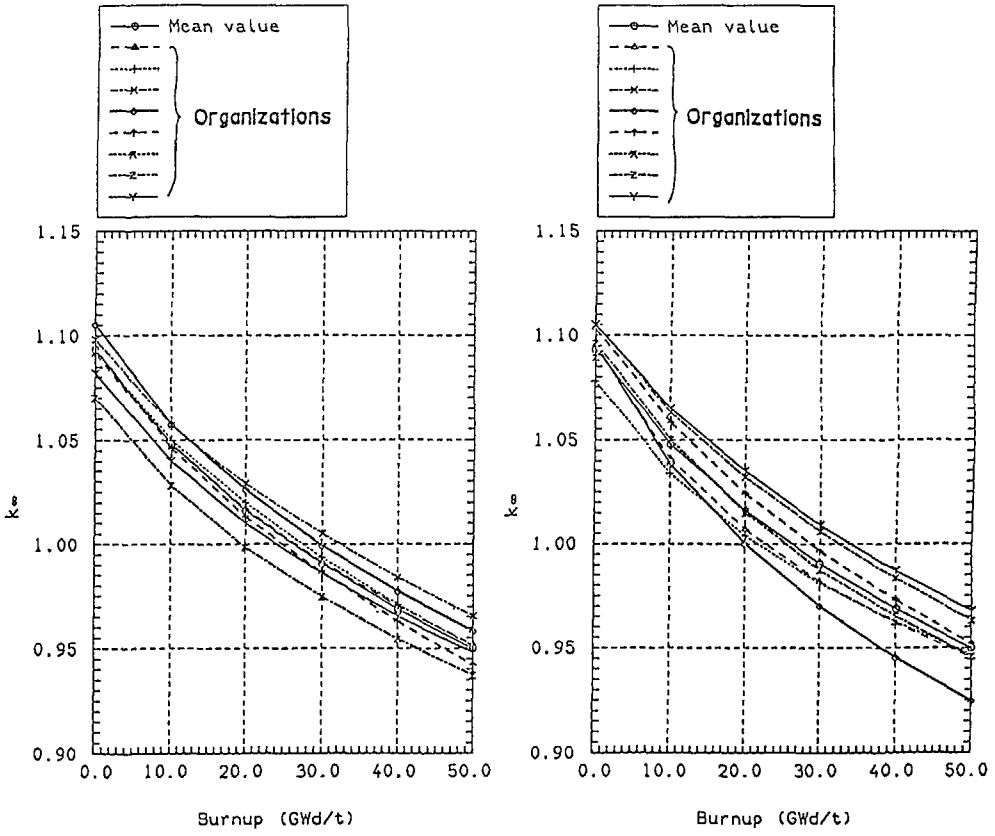

Fig.26 Burnup dependence of k_∞: V_M/V_F = 0.6, enrich. = 8%

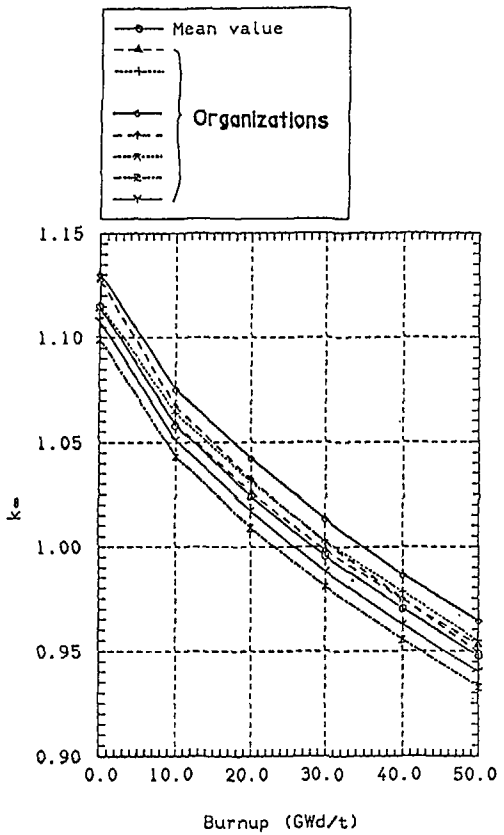

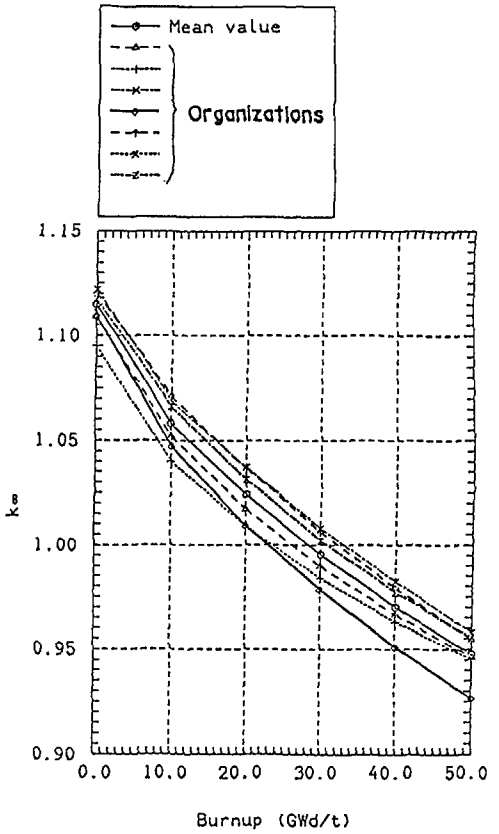

Fig.27 Burnup dependence of k_{eff}: V_M/V_F = 1.1, enrich. = 7%

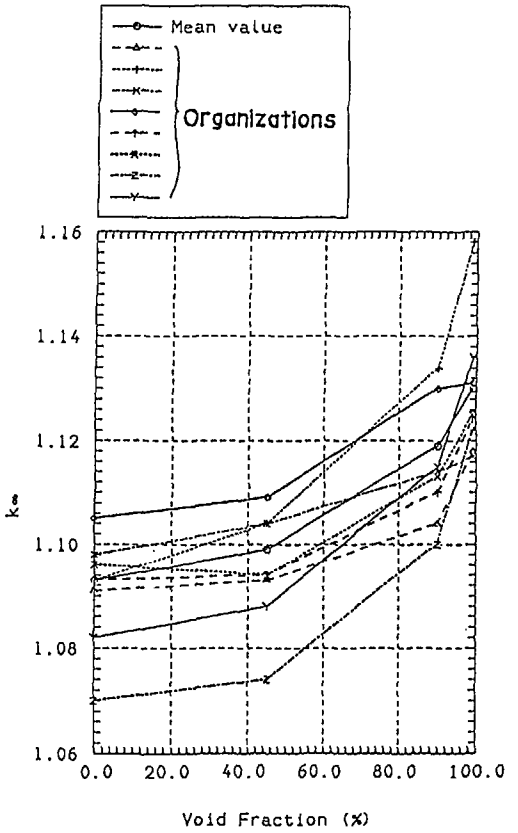

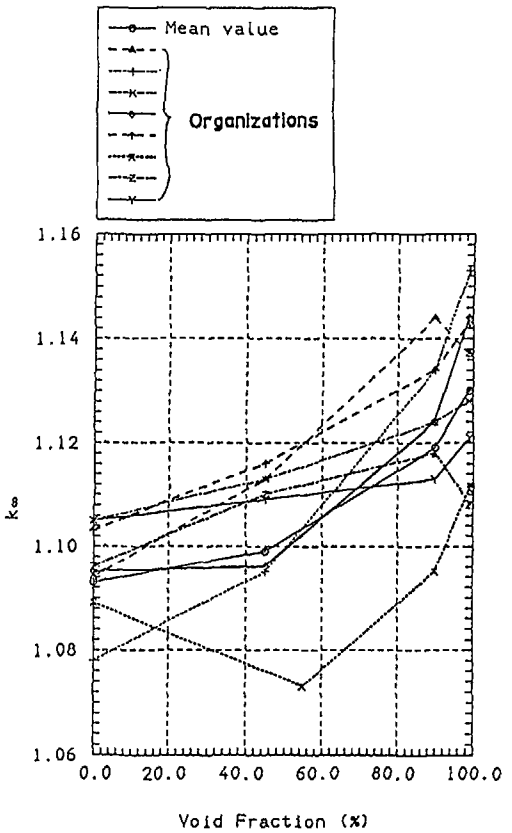

Fig.28 Dependence of k_{eff} on void fraction: V_M/V_F = 0.6, 0GWd/t

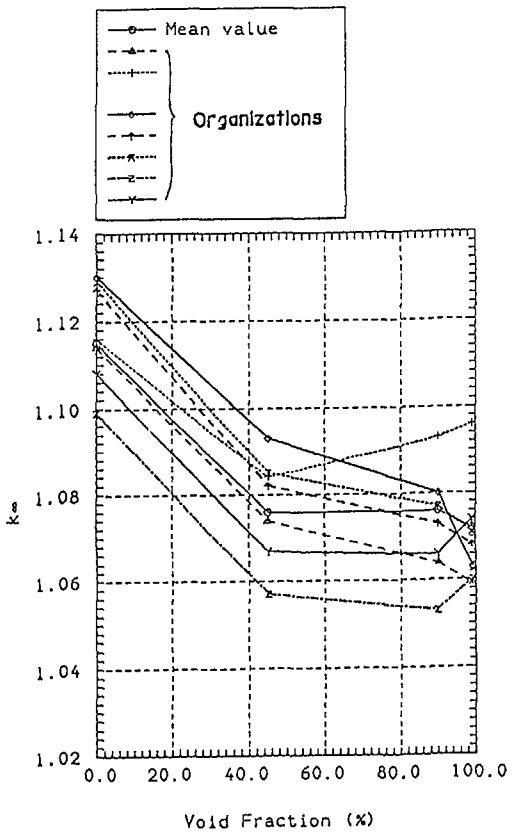

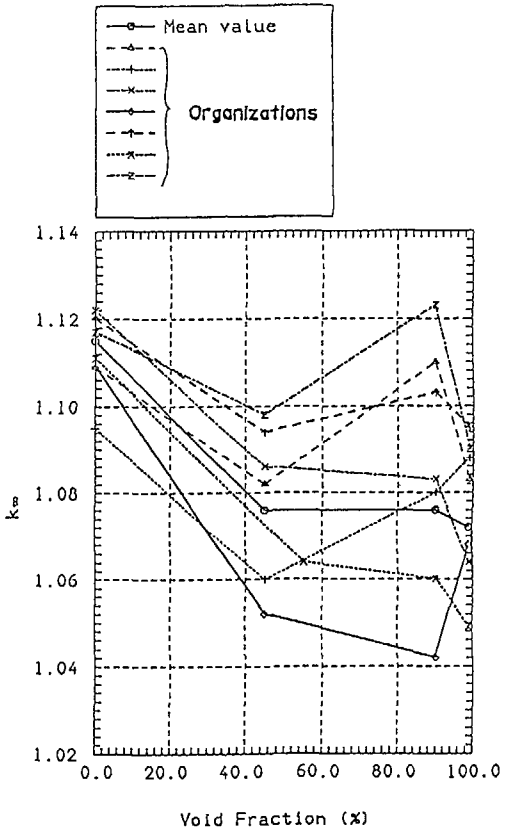

Fig.29 Dependence of k_{eff} on void fraction: V_M/V_F = 1.1, 0GWd/t

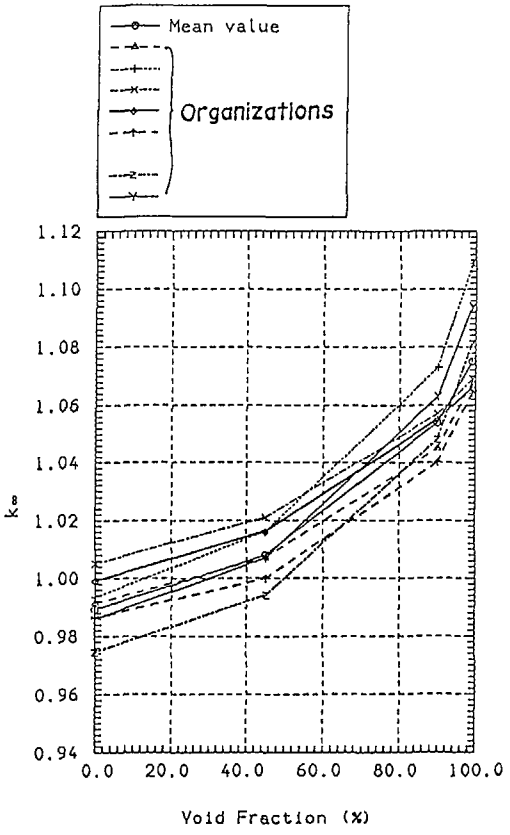

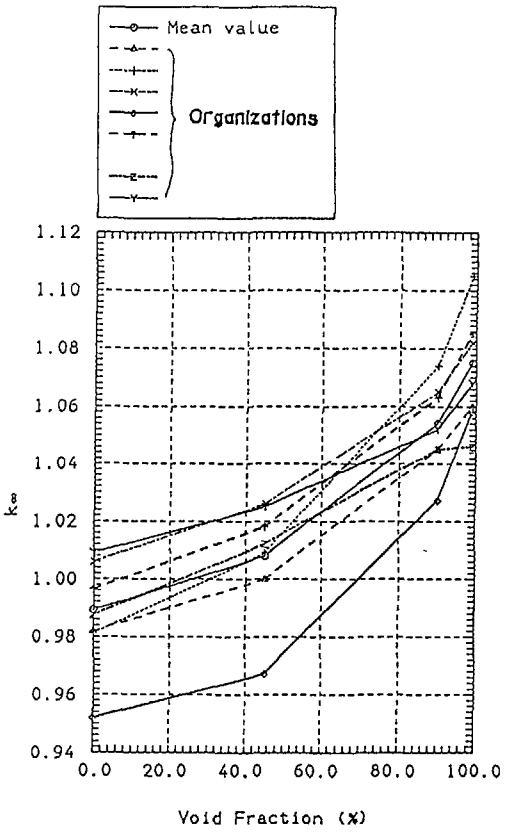

Fig.30 Dependence of k_{eff} on void fraction: V_M/V_F = 0.6, 30GWd/t

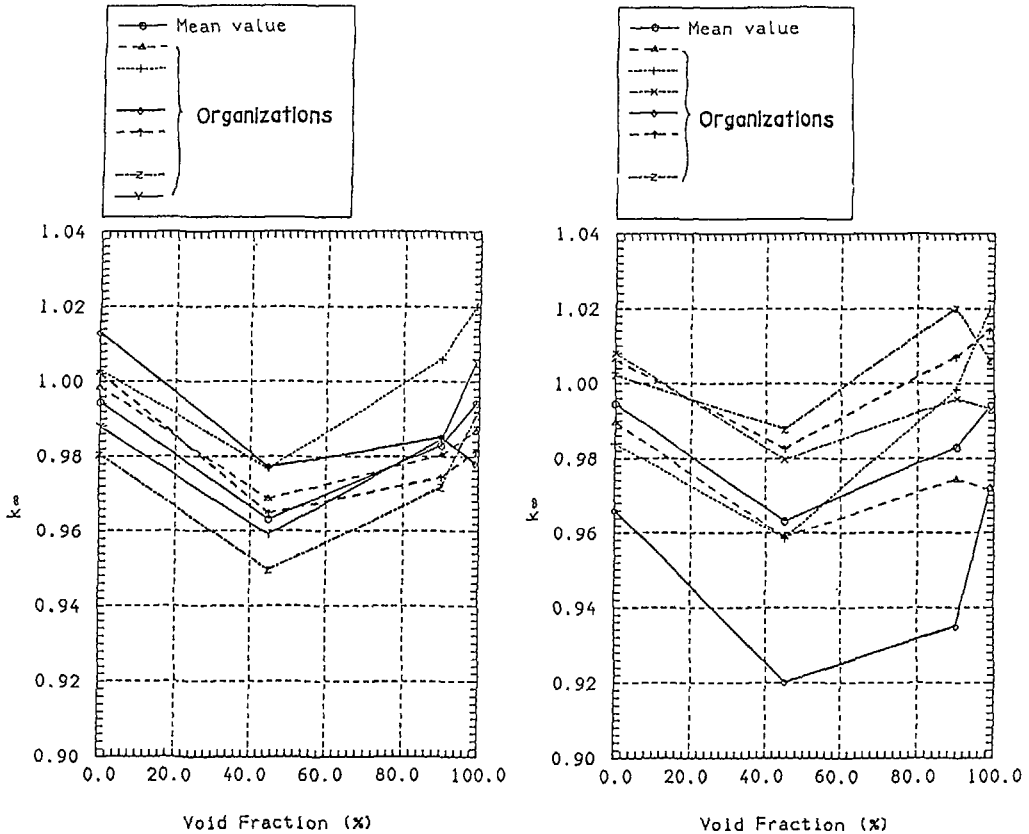

Fig.31 Dependence of k_{eff} on void fraction: V_M/V_F = 1.1, 30GWd/t

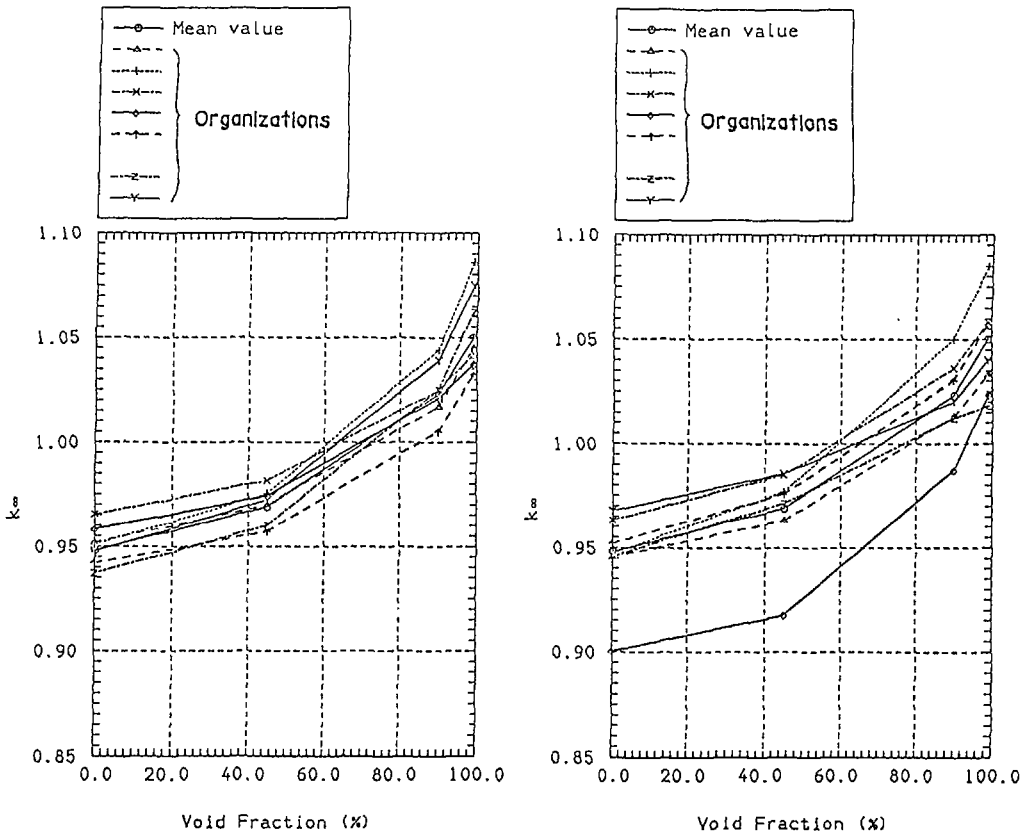

Fig.32 Dependence of k_{eff} on void fraction: V_M/V_F = 0.6, 50GWd/t

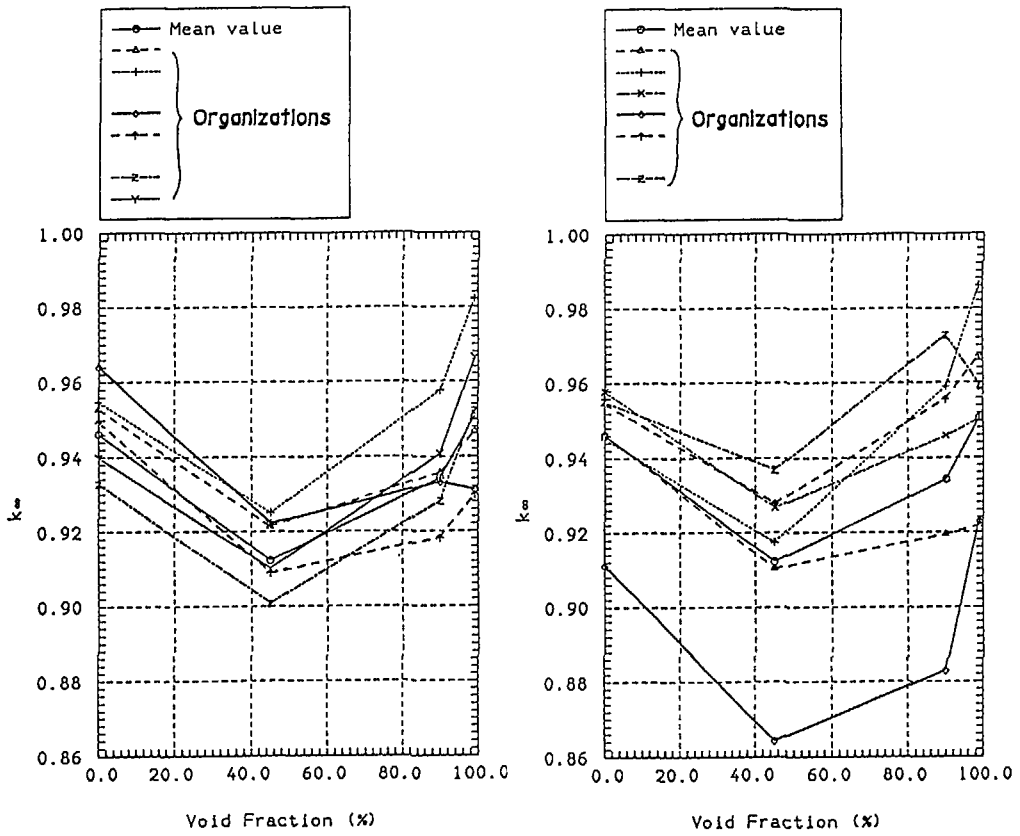

Fig.33 Dependence of k_{eff} on void fraction: V_M/V_F = 1.1, 50GWd/t

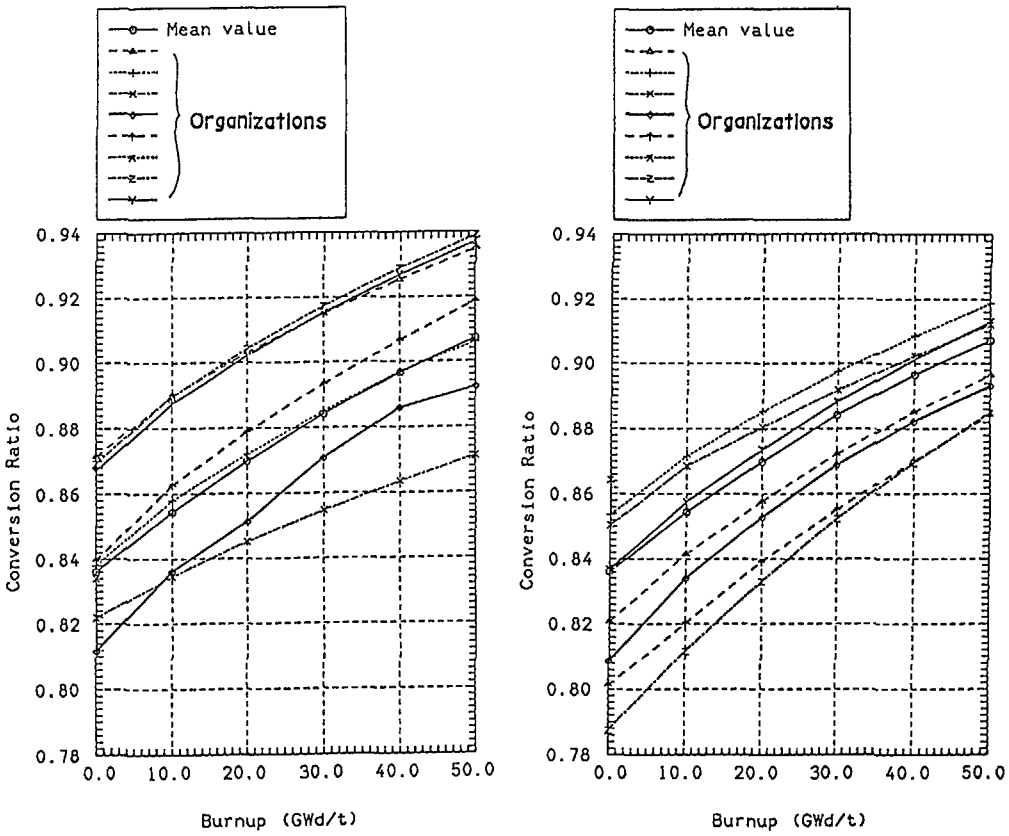

Fig.34 Burnup dependence of conversion ratio: V_M/V_F = 0.6, enrich. = 8%

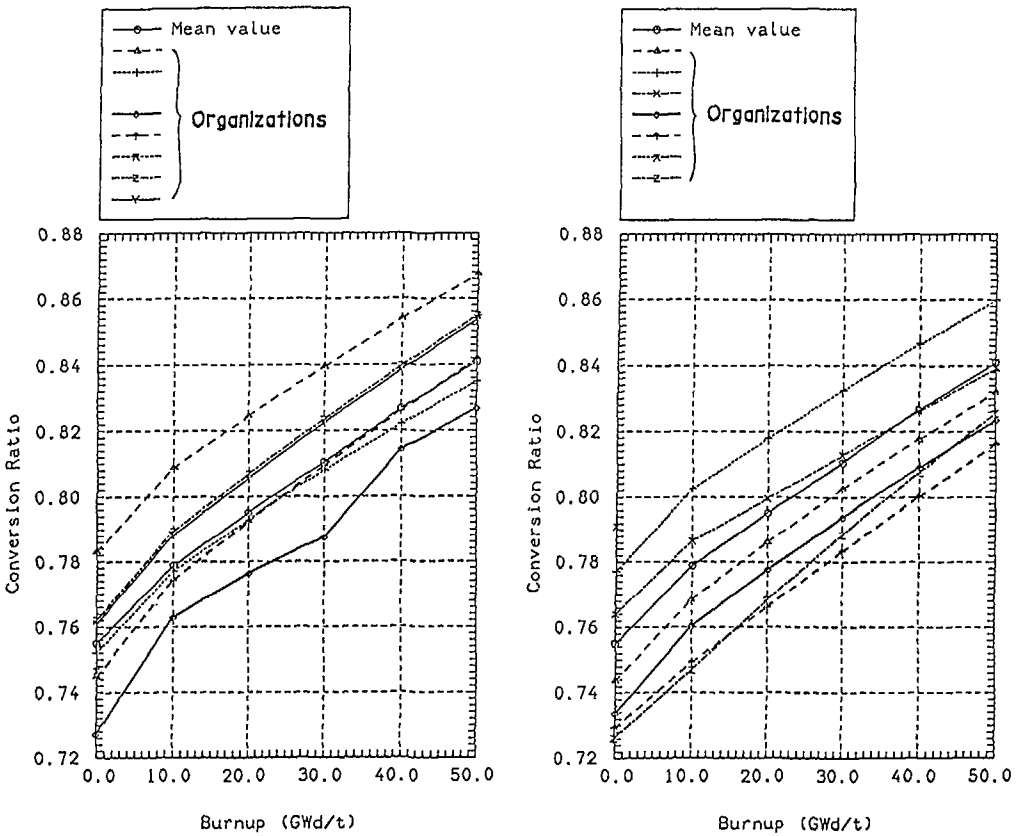

Fig.35 Burnup dependence of conversion ratio: V_M/V_F = 1.1, enrich. = 7%

6. CONCLUSION

Much efforts have been devoted to conceptual design of HCLWRs. The presently proposed designs however seem to be based upon insufficient accuracy of the data/methods in reactor physics. As for HCLWRs, the key problem concerned with "reactivity coefficients" is the coolant void reactivity coefficient.

Uranium 238 being the largest contributor of negative void coefficient still has a large uncertainty in the resonance parameters, while the uncertainty due to the calculation methods of the effective cross section is highlighted in the lower energy region. A reevaluation work will be essential for the resonance paramcters of ^{238}U.

The fissile nuclides ^{239}Pu and ^{241}Pu have also large sensitivity coefficient to the void coefficient. Integral experiments in the intermediate spectra will offer useful imformation to evaluate the nuclear data.

As for ^{240}Pu which is the major positive contributor to the void coefficient, uncertainty analysis of the nuclear data is left made in future.

The accumulation of the fission products nucides was shown to greatly affect the void reactivity characteristics of HCLWRs. A large difference was found in the absorption cross sections of several nuclides, ^{99}Tc, ^{108}Pd, ^{135}Cs, ^{103}Ru, and ^{155}Eu among the existing nuclear data files.

Concerned with the minor actinides important for the HCLWR characteristics, the nuclear data seem to be comparatively satisfactory for their effect on reactor parameters.

Fortunately, the preliminary results of the NEACRP cell burnup benchmark calculation show that the descrepancies among the calculated void coefficients are not so large as expected and may at least be reduced in near future.

APPENDIX 1. DATA AND METHODS IN SRAC SYSTEM

The fundamental cross section library of the SRAC system consists of the fast group library of 62 groups(10 MeV $\geq E \geq$ 1.855 eV with Δu = 0.5), epithermal one of 12 groups (1.855 eV $\geq E \geq$ 0.42399 eV with Δu = 0.125), and thermal one of 33 groups(E $\leq$ 0.41399 eV with the equal velocity width of 270m/sec.). The resonance shielding factors are prepared for all heavy resonance nuclei in the resonance energy region, which is divided into two energy ranges, i.e., the first resonance range above 275.36 eV and the second one from 275.36 to 0.41399 eV.

The shielding factors are calculated by solving the following slowing down equation assuming the narrow resonance approximation to moderator slowing-down:

$$\{\sigma_t(u,T) + \sigma_0\}\varphi(u;T,\sigma_0) = K(\sigma_s\varphi) + \sigma_0 \qquad (-1-)$$

where K is the slowing down operator of the resonance nuclide under consideration, and T and σ_0 are, respectively, temperature and background cross section, and other notation is conventional. Here, it should be noted

that the neutron slowing down of the resonance nuclide is exactly taken into account. The resulting shielding factors are tabulated into the Bondarenko type cross section set using the two parameters T and σ_0.

In the first resonance range, the effective cross sections are obtained by the table-look-up method, where the heterogeneity is treated by well known equivalence theorems between heterogeneous and homogeneous mixtures. The cross sections in the second range are calculated by either of of the table-look-up method (the combined use of the intermediate resonance(IR) approximation and the table-look-up method) or the direct numerical method using ultrafine groups(Δu = 0.00125). Here, in the last method, the neutron slowing-down equations are solved to calculate the ultrafine spectrum using the collision probability method as follows:

$$V_i \Sigma_i(u) \varphi_i(u) = \sum_j P_{ij}(u) V_j S_j(u) \qquad (-2-)$$

where $S_j(u)$ is the slowing down source, and other notation is conventional. The effective cross sections and averaged neutron fluxes are given for each spatial region following the group structure specified by the user. This calculation is made in the PEACO routine incorporated in the SRAC system.

The neutron slowing-down equations of multigroup scheme are solved using the effective cross sections to obtain the spatial fine structure and the homogenized cross sections. The fine structure thus obtained is renormalized by use of homogeneous P_1 or B_1 spectrum to take account of neutron leakage. Through this procedure, a correction is made to the discontinuity of neutron spectrum due to the different calculation methods among the first and second resonance ranges and the thermal energy region.

The SRAC system is equipped with two sets of multigroup libraries, respectively, mainly based on JENDL-2 and ENDF/B-IV. The usage of the libraries leaves to the choice of the SRAC user.

Appendix 2. Benchmark Specification

Burnup characteristics

Burnup calculations should be made for the infinite cell (geometrical buckling Bg^2 equals to zero) with Vm/Vf value of 0.6 described in Fig.A-1, Tables A-I and A-II. Results for the cell of volume ratio of 1.1 are also received. No control is needed to keep multiplication factor k=1.0. The following integral data are required:

<< k_∞ and conversion ratio >>

The multiplication factor k_∞ and the conversion ratio at the burnup stages of 0, 10, 20, 30, 40 and 50 GWD/t.

The conversion ratio is defined as follows:

$$C.R \approx \Sigma_c^{fer}(t) / \Sigma_a^{fis}(t) \ ,$$

where $\Sigma_c^{fer}(t)$ and $\Sigma_a^{fis}(t)$ stand for the one group macroscopic cross sections for capture of U-238 and Pu-240, and for absorption of U-235, Pu-239 and Pu-241, respectively at any burnup time t.

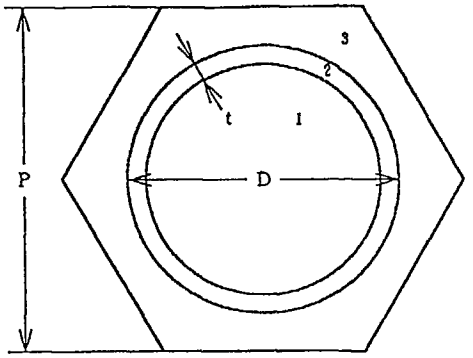

1. $PuO_2 + UO_2$
2. Stainless steel or Zr
3. H_2O

Fig.A-1 Unit cellmodel

Table A-I Specification of fuel cell model

Moderator/fuel volume ratio (Vm/Vf)	0.6	1.1
Cell pitch P (cm)	1.0883	1.2204
Fuel (PuO_2+DUO_2)		
Pu fis. (%)	8.0	7.0
Temperature (K)	900	900
Cladding	Stainless steel	Zr
Outer diameter D (cm)	0.95	0.95
Thickness t (cm)	0.065	0.065
Temperature (K)	600	600
Moderator (H_2O)		
Temperature (K)	600	600
Linear power (W/cm)	160	160

Table A-II Atomic number densities. ($\times 10^{24}/cm^3$)

Fuel	8% Pu fis.	7% Pu fis.
U-235	6.094×10^{-5}	6.194×10^{-5}
U-238	2.025×10^{-2}	2.058×10^{-2}
Pu-239	1.563×10^{-3}	1.367×10^{-3}
Pu-240	6.872×10^{-4}	6.009×10^{-4}
Pu-241	2.765×10^{-4}	2.418×10^{-4}
Pu-242	2.108×10^{-4}	1.844×10^{-4}
O	4.610×10^{-2}	4.608×10^{-2}
Cladding	Stainless steel	Zr
Zr (natural)	-	3.702×10^{-2}
Fe (natural)	4.831×10^{-2}	-
Cr (natural)	1.570×10^{-2}	-
Ni (natural)	7.648×10^{-3}	-
Mn-55	1.486×10^{-3}	-
Moderator		
H	4.744×10^{-2}	
O	2.372×10^{-2}	

<< Cross sections >>
One-group and three-group effective microscopic cross sections (absorption, fission and production) of fuel materials at 0, 30 and 50 GWD/t, and of structural materials at zero burnup are required for the nuclides shown in Table A-III. The three group structure is shown in Table A-IV.

<< Reaction rates >>
One-group and three-group fractional reaction rates for fuel and fission product nuclides at the burnup of 0, 30 and 50 GWD/t.

In this calculation, the total absorption rate in a cell is normalized to unity. The absorption, fission and production rates are required for the fuel nuclides(Table A-III), and the absorption rates for the 23 fission products (Table A-III) and the total F.P. which is the summation of all fission products considered.

<< Number densities >>
Number densities of fuel isotopes at the burnup of 30 and 50 GWD/t.

Table A-III Nuclides to calculate one- and three-group cross sections and/or reaction rates

Fuel	U-235, U-238, Pu-239, Pu-240, Pu-241, Pu-242, Am-241, Am-243, Cm-244
Fission Product	Mo-95, Tc-99, Ru-101, Rh-103, Pd-105, Pd-107, Pd-108, Ag-109, Xe-131, Xe-135, Cs-133, Cs-135, Nd-143, Nd-148, Pm-147, Sm-147, Sm-149, Sm-150, Sm-151, Sm-152, Eu-153, Eu-154, Eu-155
Structure	Zr (Zr cladding) Fe, Cr, Ni, Mn-55 (Stainless steel cladding)

Table A-IV Three-group energy structure

	energy range
fast	10 MeV - 9.118 keV
resonance	9.118 keV - 4 eV
thermal	4 eV - 0.0 eV

Void reactivity

Further calculations should be performed for each cell in moderator voidage state at several burnup stages of the burnup calculations. Following results are needed :

<< k_∞ and reaction rates >>
k_∞ and reaction rates when void fractions of moderator are changed from 0% to 45%, 90% and 99% at the burnup of 0, 30 and 50 GWD/t.

In these calculations, density of moderator should be reduced to 55%, 10% and 1% according to the void fraction. The one- and three-group fractional reaction rates should be calculated for the fuel isotopes and the total F.P.

ACKNOWLEDGEMENTS

The author appreciates the helpful discussions with Dr.H. Takano. He is also very grateful to Miss A. Yokota for her typing of this report.

REFERENCES

1) EDLUND, M.C., Ann. Nucl. Energy, 2, 801 (1975).
2) EDLUND, M.C., Trans. Am. Nucl. Soc., 24, 508 (1976).
3) UOTINEN, V.O., et al., EPRI NP-1833, Electric Power Research Institute (May 1981).
4) OGURA, S., TOYODA,Y., SHIMADA,S., IWAI,S., IAEA-TECDOC-344, p.21, International Atomic Energy Agency (1984).
5) BERGER, H.D., OLDEKOP, W., ZEGGEL, W., IAEA-TECDOC-344, p.84, International Atomic Energy Agency (1984).
5) BROEDERS, C.H.M., DALLEDONNE, M., Nucl. Technol., 71, 82 (1985).
6) GOETZMANN, C., BROGLI, R., KUCZERA, B., Proc. 4th European Nuclear Conf. Geneva, Switzerland, June 1-6, 1986, Vol. 2, p. 493 (1986).
7) VALLE, A., MILLOT, J.P., BRUNA, G., Proc. 4th European Nuclear Conf. Geneva, Switzerland, June 1-6, 1986, Vol. 2, p. 477 (1986).
8) BARRE, B., COURTAUD J.M., DARROUZET, M., GOLINELLI, C. at al, Proc. 4th European Nuclear Conf., Geneva, Switzerland, June 1-6, 1986, Vol.2, p.487 (1986).
9) JOHANSSON, E., Nucl. Technol., 68, 263 (1985).
10) BROEDERS, C.H.M., Nucl. Technol., 71, 96 (1985).
12) CHAWLA, R. et al., Nucl. Technol., 67, 360 (1984).
13) CHAWLA, R., GMUER, K., HAGER, H., PILLER, G. et al., Proc. 4th European Nuclear Conf., Geneva, Switzerland, June 1-6, 1986, Vol. 2, p.567 (1986).
14) AXMANN, J., CHENG, X., OLDEKOF, W., Atomkernenergie-Kerntechnik 48, 209(1986).
15) AKIE, H., ISHIGURO, Y., IDO, M., Parameter Survey for Burnup of High Conversion Light Water Reactor Lattice, JAERI-M-86-197,Japan Atomic Energy Research Institute(1987).
16) ISHIGURO, Y., AKIE, H., TAKANO, H., Proposal of Benchmarks on Data and Methods to Calculate Reactor Characteristics in High Conversion Light Water Reactor, NEACRP-A-798, NEA Data Bank(1986).
17) AKIE,H., ISHIGURO, Y., TAKANO, H., Preliminary Report of HCLWR Cell Burnup Benchmarch Calculations, NEACRP-A-849, NEA Data Bank(1987).
18) TSUCHIHASHI, K., TAKANO, H., HORIKAMI, K., ISHIGURO, Y., SRAC: JAERI Thermal Reactor Standard Code System for Reactor Design and Analysis, JAERI-1285, Japan Atomic Energy Research Institute (1983), and TSUCHIHASHI, K., ISHIGURO, Y., KANEKO, K., IDO, M., Revised SRAC Code System, JAERI 1302, Japan Atomic Energy Research Institute (1986).
19) OKUMURA, K., ISHIGURO, Y., Core Burnup Calculation for HCLWR, JAERI-M 87-126, p.88, Japan Atomic Energy Research Institute (1987).
20) SPENCER, R.R., HARVEY, J.A., HILL, N.W., WESTON, L.W., Nucl. Sci. Eng.,96,318(1987).
21) ISHIGURO, Y., TSUCHIHASHI, K., SASAKI, M., Physics Problems on Analysis of High Conversion Pressurized Water Reactor (HCPWR) with Tight Pitch Lattices, JAERI-M84-180, Japan Atomic Energy Research Institute(1984), and ISHIGURO, Y., AKIE, H., KANEKO, K., SASAKI, M., Physics Problems on Analysis of High Conversion Light Water Reactor (II), JAERI-M86-039, Japan Atomic Energy Research Institute(1986).
22) LEVITT, L. B., LEVIS, R.C. VIM-1, A Non-Multigroup Monte Carlo Code for Analysis of Fast Critical Assemblies, AI-AEC-12951, Atomic International(1970), and Milton L.J. VIM User's Guide, ANL, Argonne National Laboratory, January(1980)
23) ENDF/B Summary documentation, BNL-NCS-17541(ENDF-201), 1st. Edition, compiled by D. GARBER, available from the National Data Center, BNL, New York(1973) , and ibid., 2nd. Edition(1975)
24) TAKANO, H., NAGATANI, M., Sensitivity Analysis of Cell Parameters in the PROTEUS Cores, JAERI-M 87-126, p.17, Japan Atomic Energy Research Institute(1987).
25) TAKEDA, T., NAKANO, M., J. Nucl. Sci. Technol., 23, 681(1986).
26) NAKANO, M., TAKEDA, T., TAKANO, H., J. Nucl. Sci. Technol., 24, 610(1987).
27) TAKANO, H., KANEKO, K., AKIE, H., ISHIGURO, Y., The effects of Fission Products on Burnup Characteristics in High Conversion Light Water Reactors, to be appeared in Nucl. Technol., Jan. (1988).
28) JEF Report 3, NEA Data Bank (1985).
29) TAKANO, H., AKIE, H., J. Nucl. Sci. Technol., 24, 501(1986).
30) AKIE, H., TAKANO, H., Self-Shielding Effect of ^{242}Pu 2.67 eV Resonance on Neutronic Characteristics in HCLWRs, JAERI-M 87-126, p.20, Japan Atomic Energy Research Institute(1987).
31) KÜSTERS, H., Testing of Evaluated Transactinides Isotope Neutron Data and Remaining Data Requirements, IAEA-TECDOC-336, p.9, International Atomic Energy Agency (1984).
32) CHAWLA, R., A review of Lattice Calculations for the PROTEUS-LWHCR Phase-I Experiments, NEACRP-A-726, NEA Data Bank(1985).

RECENT DIFFERENTIAL LOW ENERGY CROSS-SECTIONS AND THERMAL EVALUATIONS

A.J. DERUYTTER*, C. WAGEMANS**, F. CORVI*,
E.J. AXTON*, P. SCHILLEBEECKX*
*Central Bureau for Nuclear Measurements,
Joint Research Centre,
Commission of the European Communities,
Geel

**Centre d'étude de l'énergie nucléaire (SCK/CEN),
Mol, Belgium

Abstract

Shapes of the fission cross-sections of ^{235}U, ^{239}Pu and ^{233}U were measured in the thermal and sub-thermal neutron energy regions, down to 2 meV, at the Geel linear electron accelerator, making use of a liquid nitrogen cooled methane moderator. For ^{235}U also a relative fission cross-section measurement was done at the Very Cold Neutron Source of the ILL at Grenoble. Preliminary results of these measurements are reported, and Westcott g_f factors based on these results are calculated.

Also the shape of the $^{238}U(n,\gamma)$-reaction was measured at the Geel Linac in the same experimental conditions, and preliminary results are reported.

Recent evaluations of the thermal parameters for ^{233}U, ^{235}U, ^{239}Pu and ^{241}Pu and the fission neutron yield of ^{252}Cf are briefly commented, and the difference between evaluation results with and without Maxwellian data discussed.

---

1. INTRODUCTION

Measurements of neutron cross-sections of the common fissile nuclides in the thermal and subthermal energy regions have been extremely scarce in the period after 1975. Some evaluation effort on the thermal constants of ^{233}U, ^{235}U, ^{239}Pu and ^{241}Pu and the fission neutron yield of ^{252}Cf continued at Brookhaven National Laboratory (BNL) by Stehn, Divadeenam and Holden[1][2] and at the Central Bureau for Nuclear Measurements (CBNM), Geel by Axton[3][4]. These evaluations will be briefly discussed and some comments on the difference between the Maxwellian average and differential data sets will be given.

At the International Conference on Nuclear Data for Science and Technology at Antwerp in 1982 Bouchard, Golinelli and Tellier[5] drew the attention to a discrepancy existing between the calculated temperature coefficient of reactivity for light water reactors and measured values obtained in integral experiments. Santamarina et al.[6] proposed that the energy dependence of certain differential nuclear data in the subthermal neutron energy region be modified with respect to the evaluated Data File ENDF/B-5 within their experimental uncertainties, in order to remove this discrepancy. The quantities concerned are the fission cross-section, σ_f, and the number of fission neutrons emitted per neutron absorbed, η, of ^{235}U as well as the capture cross-section, σ_γ, of ^{238}U. In this respect the shapes of the cross-sections and not the absolute values were considered responsible. As a consequence it was requested by French and British reactor physicists (NEANDC/NEACRP High Priority Request List) to remeasure these quantities.

In order to perform these measurements under reliable experimental conditions, a liquid nitrogen (77K) cooled methane moderator has been installed at the Geel electron linear accelerator (GELINA), which yields about five times more neutrons below 20 meV than with the usual water-beryllium moderator at room temperature. In these experimental conditions measurements were performed of 1) the shapes of the fission cross-sections of ^{235}U, ^{239}Pu and ^{233}U, also with the goal of obtaining values for the Westcott g_f-factors; 2) the capture cross-section of 238U and 3) the number of fission neutrons emitted per neutron absorbed in ^{235}U, all in the energy range from about 2 meV up to 100 meV.

The results of the fission cross-section shape measurements will be reported and discussed and a short account will be given of the preliminary results obtained for the capture cross-section of ^{238}U.

The preliminary results of η of ^{235}U for subthermal energies, as measured at the Geel-Linac, will be reported separately at the meeting, by H. Weigmann[7].

The measurements of σ_f ^{235}U will be completed by measurements at the Very Cold Neutron Source of the Institut Laue-Langevin (ILL) at Grenoble, and first results will be reported here. The measurements of η will also be repeated at ILL, Grenoble, with the use of a pulsed monoenergetic neutron beam, enabling a much more reliable background subtraction.

2. LOW ENERGY FISSION CROSS-SECTION SHAPE MEASUREMENTS

2.1. Measurement of the shape of the fission cross-section of ^{235}U.

Preliminary results of a first measuring campaign at GELINA were reported by Wagemans and Deruytter[8] at the Santa Fé Conference on Nuclear Data for Basic and Applied Science. These measurements were performed at a well-collimated 8.2 m flight-path of GELINA. The accelerator was operated at a 40 Hz repetition frequency with 2 µs burst widths and with an average electron current of 15 µA. Until now three measuring campaigns have been performed. In the first two campaigns, a 25 µg/cm² ^6LiF layer and in the third one an 8 µg/cm² ^{10}B layer were used for the neutron flux determination in a back-to-back arrangement with a 53 µg/cm² $^{235}UF_4$ layer for the fission detection, mounted in the centre of a vacuum chamber with 50 cm diameter. The $^6Li(n,\alpha)t$, respectively $^{10}B(n,\alpha)^7Li$ reaction particles and the fission fragments were detected in a low geometry with two 20 cm² large surface barrier detectors placed outside the neutron beam. The neutron energy scale in the meV-region was verified by means of the prominent Bragg-reflection cuts at 5.24 and 6.84 meV in the Be transmission spectrum. The background was determined using the black resonances of Cd, Rh, Au and W. The background due to neutrons from overlapping bursts was checked by operating GELINA at 20 Hz. In Fig. 1 the $^{235}U(n,f)$ and the $^6Li(n,\alpha)t$ counting-rate spectra are shown with the corresponding background curve (lower full lines), obtained via a polynomial fit through the (normalized) black resonance counting-rates. The ratio of the

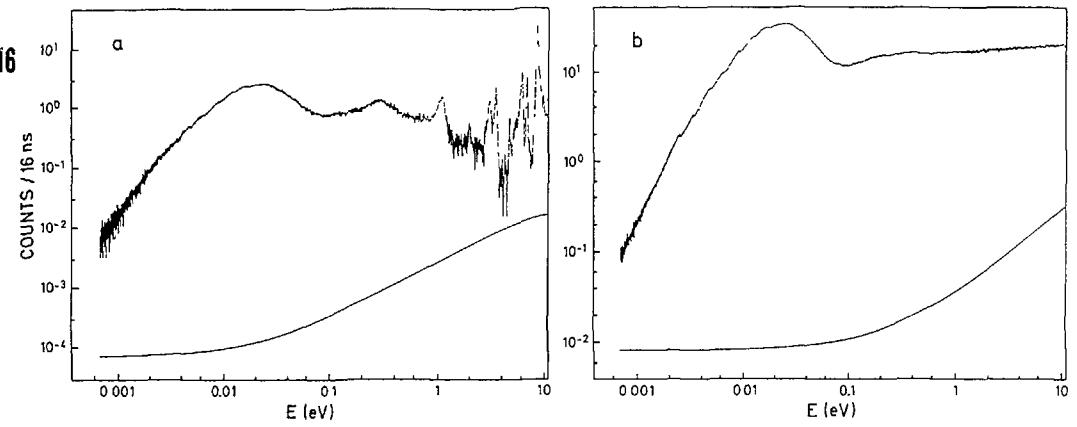

Fig. 1.

(a) $^{235}U(n,f)$ counting-rate spectrum; the lower full line represents a polynomial fit through the background points
(b) idem for $^{6}Li(n,\alpha)t$.

background-corrected fission and $(\alpha+t)$ respectively $(\alpha_0+\alpha_1)$ counting rates, yields under the assumption of a $1/v$ dependence for the two standard reaction cross-sections the $\sigma f\sqrt{E}$ shape for the $^{235}U(n,f)$ reaction. Results from the three campaigns were normalized to the σ_f° value proposed for ENDF/B-6 equal to 584.25b (±0.19%)(9) and averaged. In Fig. 2 these data are shown together with the ENDF/B-5 curve in the energy range 2 meV to 1 eV. An exploded view of the low energy part from 2 to 100 meV is shown in Fig. 3. Within the experimental error the experimental data and the evaluated file agree. Below 10 meV the experimental data are somewhat lower, but the deviation is smaller than

reported in (8). Also the value of

$$\int_{7.8\,eV}^{11.eV} \sigma_f(E)\,dE = 243 \pm 4 \text{ b.eV},$$

calculated from the present $\sigma_f(E)$ data agrees with the value of this integral recommended for use with ENDF/B-6, which has a value of 246.5 ±1 b .eV, which gives a control of the normalisation of the data. The $\sigma_f(E)$ values reported here are in very good agreement in the overlapping energy region with the results of Gwin et al. (10)

Okazaki and Jones (11) reported at the Santa Fé Conference on Nuclear Data that integral or effective cross-section measurements in well thermalized neutron spectra of different neutron temperatures indicate that the ENDF/B-5 shape describes the fission cross-section shape for 235U adequately.

We then measured the shape of the $^{235}U(n,f)$ cross-section at very low energies at the Very Cold Neutron Source of the Institut Laue-Langevin at Grenoble. For this purpose a slow chopper (operated at 300 and 600 rotations per minute) has been installed at the end of the 'very cold' neutron guide. A 3 μg/cm² ^{6}LiF layer and an 11 μg/cm² $^{235}UF_4$ layer were mounted back to back in a vacuum chamber at a distance of 58.1 cm from the chopper. The $^{235}U(n,f)$-fragments and the $^{6}Li(n,\alpha)t$-particles were detected in a low geometry with 30 cm² surface barrier detectors. The $^{6}Li(n,\alpha)t$

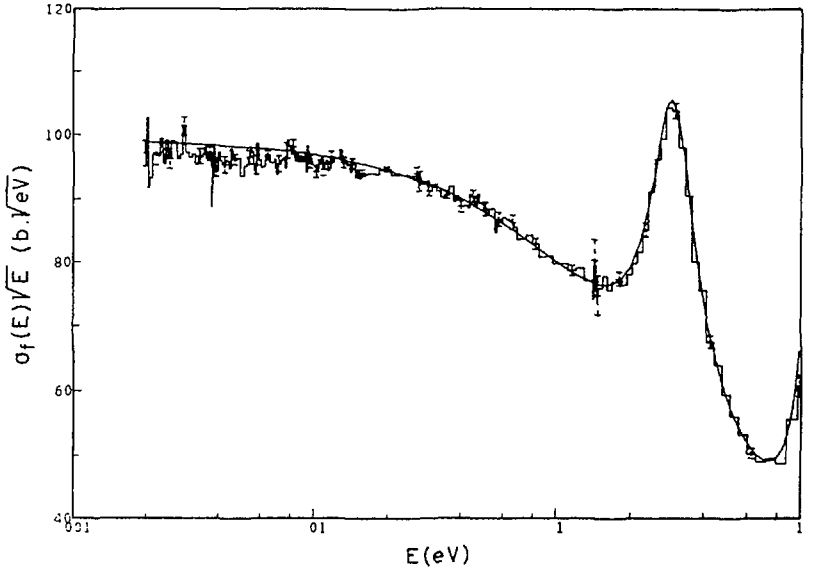

Fig. 2.

The measured fission cross-section shape for ^{235}U (broken line) compared to ENDF/B 5 (continuous line) in the neutron energy range from 2 meV to 1 eV.

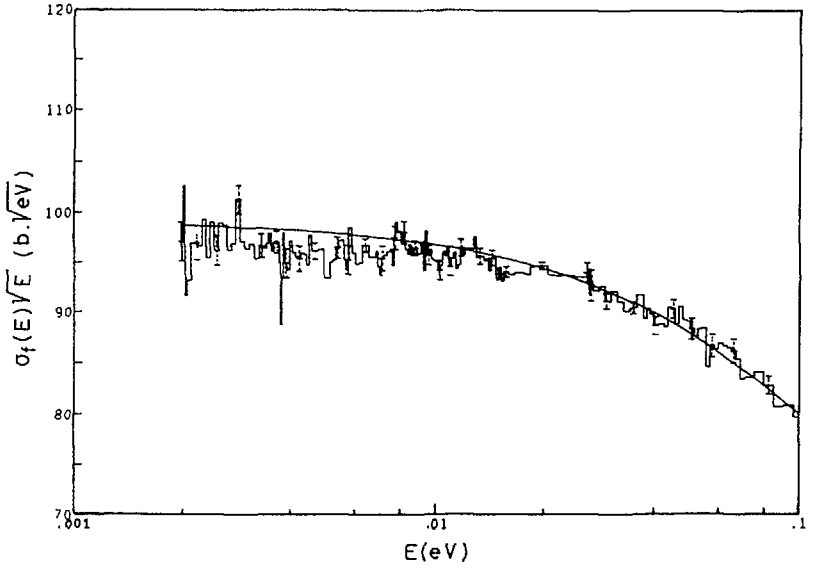

Fig. 3.

The measured fission cross-section shape for ^{235}U (broken line) compared to ENDF/B 5 (continuous line) in the neutron energy range from 2 meV to 0.1 eV.

counting rate as function of neutron energy is shown in Fig. 4. From the $^{235}U(n,f)$ and the corresponding $^{6}Li(n,\alpha)t$ counting-rates, $K\sigma_f\sqrt{E}$ was calculated, again adopting a 1/v-behaviour of the $^{6}Li(n,\alpha)$ cross-section. These results are also shown in Fig. 4. Within the precision, these results do not show a significant deviation of the ^{235}U fission cross-section from a 1/v shape. So it is believed that a 1/v-extrapolation of σ_f to zero energy (below 2 meV) is justified.

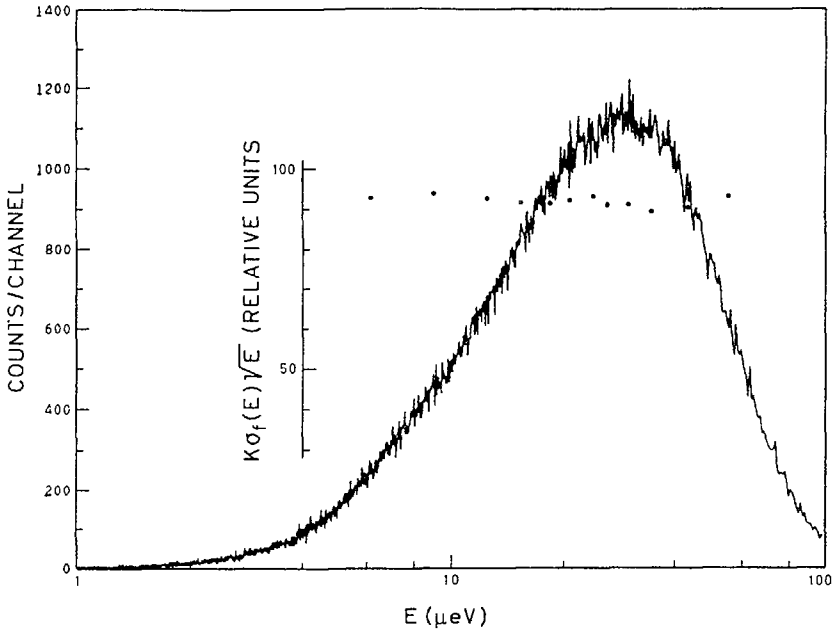

Fig. 4.

The measured neutron flux spectrum at the Very Cold Neutron Source of ILL. Dots give value of K $\sigma_f\sqrt{E}$ (relative units) for ^{235}U, in the neutron energy range from 6 μeV up to 60 μeV.

2.2. Measurements of the shape of the fission cross-section of ^{239}Pu.

Similar measurements were performed at GELINA for the fission cross-section of ^{239}Pu in the low energy region, where a $^{239}PuF_3$ target of 30 μg/cm² thickness was used in back-to-back geometry with the same 25 μg/cm² ^{6}LiF target. Linac parameters were identical. The quality of the $^{6}Li(n,\alpha)t$ and $^{239}Pu(n,f)$ reaction particle spectra is illustrated in Fig. 5. The respective counting-rates are treated in the same way as for ^{235}U and result in $\sigma_f\sqrt{E}$ values as a function of neutron energy. The results in the neutron energy range from 2 meV up to 1 eV are shown in Fig. 6 and an exploded view of the low energy part from 2 meV to 100 meV in Fig. 7. The curve is normalized to the σ_f°-value suggested for use with ENDF/B-6, i.e. 748.0 barn (± 0.25%).

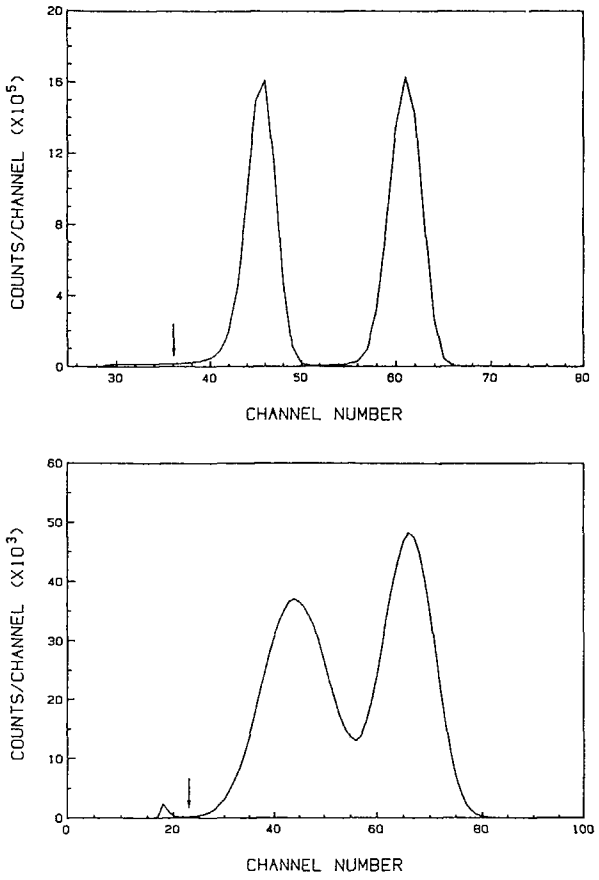

Fig. 5.

Pulse height spectra for (a) a 25 μg/cm² ^{6}LiF target and (b) a 30 μg/cm² $^{239}PuF_3$ target. Both are taken for Linac low energy fission cross-section measurements.

2.3. Fission cross-section shape for ^{233}U

The shape of the fission cross-section neutron energy dependence was measured again in the same experimental conditions. For the fission detection a $^{233}UF_4$-layer with thickness 40 μg/cm² was used. The 25 μg/cm² ^{6}LiF-layer was used for the neutron flux determination. After identical treatment of the data as described above for ^{235}U, and normalisation to the σ_f° value suggested for use with ENDF/B-6, i.e. 531.14 barn (± 0.25%), the $\sigma_f\sqrt{E}$ values in the neutron energy range 2 meV to 1 eV are obtained and plotted on Fig. 8.

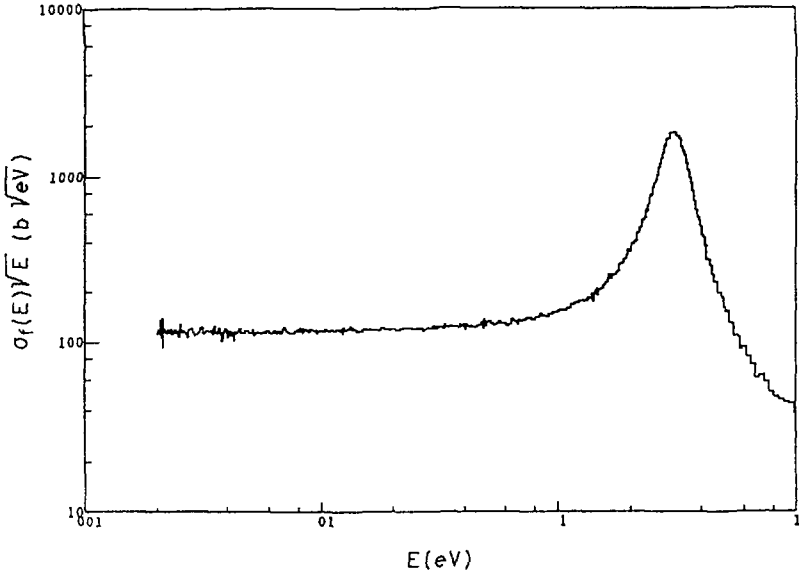

Fig. 6.

The measured fission cross-section shape for ^{239}Pu in the neutron energy range from 2 meV to 1 eV.

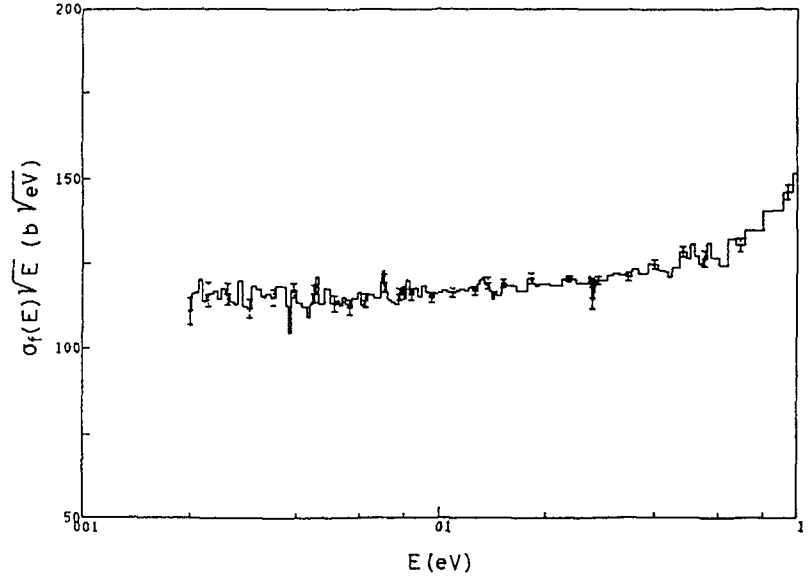

Fig. 7.

The measured fission cross-section shape for ^{239}Pu in the neutron energy range from 2 meV to 0.1 eV.

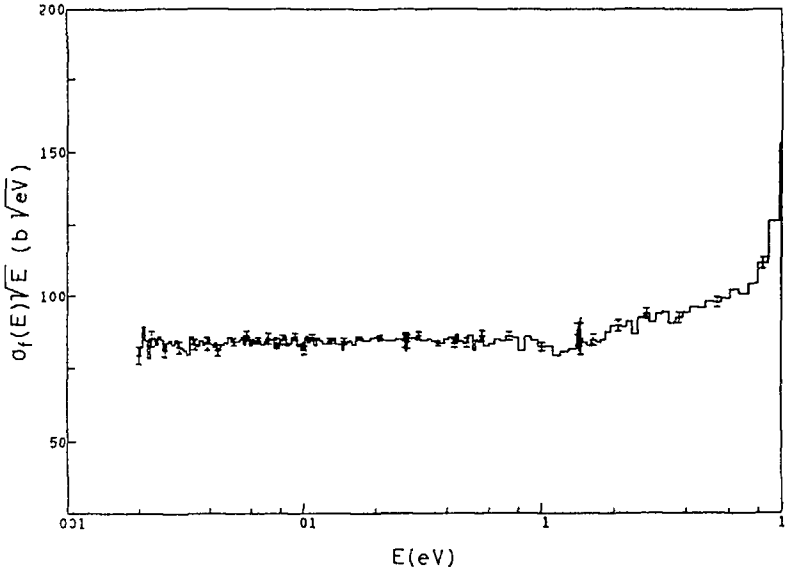

Fig. 8.

The measured fission cross-section shape for ^{233}U in the neutron energy range from 2 meV to 1 eV.

3. CAPTURE CROSS-SECTION OF ^{238}U

Two measurement campaigns were performed until now for the determination of the shape of the ^{238}U capture cross-section in the subthermal and thermal neutron energy range at GELINA. The Linac parameters were the same as for the fission cross-section shape measurements, and the flight distance to the capture sample was 8.68 m.

In the first campaign a foil of 13.78 g of highly enriched (99.999% ^{238}U) uranium metal was used. The sample surrounded by a 6 mm thick metallic ^{6}Li sleeve was viewed by four C_6D_6 liquid scintillators housed in a large shielding facility with walls made of 14 cm lead and 25 cm borated wax. Best signal-to-background conditions were obtained by counting coincidences between pulses from any two detectors.

The time-dependent background was measured by replacing the sample by an equivalent graphite scatterer. The neutron flux at the position of the uranium sample was measured in a separate run by replacing the ^{238}U with a 0.6 mm thick ^{10}B slab and recording the 480 keV γ-rays with the same detectors. The constancy of the flux during the various runs was checked by a double gridded ionization chamber placed in the beam before the shielding and loaded with back-to-back deposits of ^{10}B of 5 $\mu g/cm^2$ thickness.

In the second measurement campaign the metallic sample was replaced by a 60 g sample of U_3O_8 enriched to 99.999% ^{238}U. This material was measured immediately after a chemical purification carried out by the CBNM Sample Preparation Group, so that the amounts of radioactive decay products, in particular the thorium, were strongly reduced with respect to

the secular equilibrium case. As a consequence, the constant background due to sample activity decreased accordingly as compared with the first campaign. However, this was partly compensated by an increase of the energy dependent background caused by multiple scattering from the oxyde sample, and the neutron capture in the aluminium container.

The results of the two campaigns were in reasonable agreement. The present preliminary results for the uranium-oxyde sample are shown in Fig. 9, for the energy range 2 meV to 0.1 eV. The present data agree with a flat energy dependence of $\sigma_\gamma\sqrt{E}$, meaning a 1/v-dependence (ENDF/B 5) and not with the shape suggested by Santamarina et al.(6)

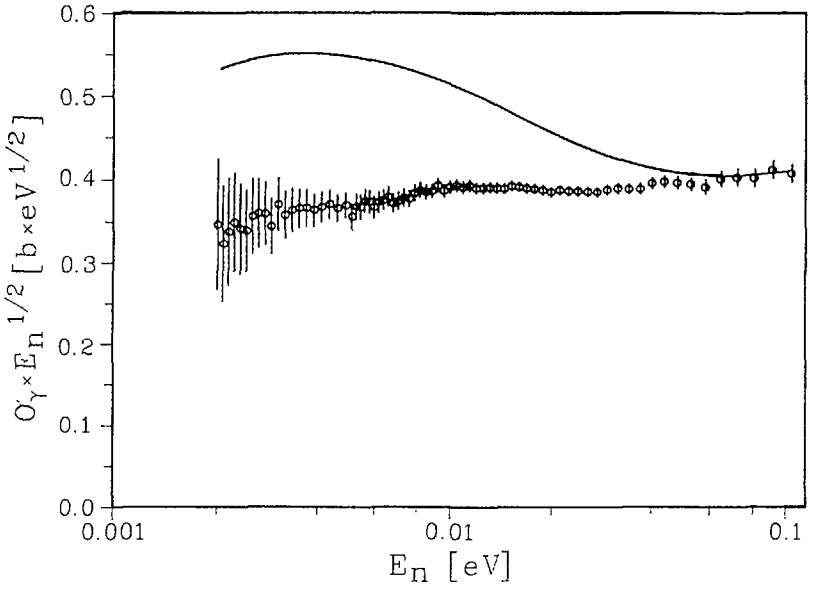

Fig. 9.

Preliminary experimental results for the cross-section of $^{238}U(n,\gamma)$ compared to the curve suggested by Santamarina et al. (6).

4. WESTCOTT g_f FACTORS

The dependence of the measured fission cross sections on neutron energy can be used to calculate Wetscott g_f factors, which can be compared with existing evaluated values.

Westcott(12) defined the effective cross-section $\hat{o}(T)$ for neutrons having a pure Maxwellian energy distribution with absolute temperature T as the product of the cross-section at thermal energy σ_o and the so-called g-factor:

$$\hat{o}(T) = \sigma_o g(T)$$

This g-factor is a function of temperature and may be calculated from the cross-section curve $\sigma(E)$ in the low energy region via the following expression:

$$g(T) = \frac{1}{\sigma_o\sqrt{E_o}} \int_o^\infty \sigma(E)\sqrt{E}\, n(E)\,dE$$

with

$$n(E) = \frac{2n\sqrt{E}}{(nkT)^{3/2}} \exp[-E/kT]$$

$$\text{and} \int_o^\infty n(E)\,dE = 1$$

k being the Boltzmann constant, E_0 = 0.025298 eV and T the absolute temperature.

In the case of a fission reaction at room temperature (T = 293.60 K) the Westcott g_f factor is then given by

$$g_f = \frac{2}{\sigma_f^\circ \sqrt{n E_o}(293.6\,k)^{3/2}} \int_o^\infty \exp[-E/293.6\,k] \cdot \sigma_f(E)\,E\,dE$$

This g_f factor is important for the physics of thermal reactors and especially important for the interpretation of measurements done with neutrons having a Maxwellian energy distribution or with a reactor spectrum with a similar shape. The value of g_f is determined by the shape of $\sigma_f(E)$ below 1 eV. The σ_f data below 20 meV even contribute with about 30% to the total g_f value. As the available differential data in the neutron energy region $0 \le E_n \le 20$ meV are scarce and sometimes discrepant, better data in this low energy region will improve the accuracy of the g_f factor.

New g_f-calculations were done, making only use of the present fission cross-section results for ^{233}U, ^{235}U and ^{239}Pu in the energy region 2 meV $\le E_n \le$ 1 eV, discussed above. In these calculations, the extrapolated part ($0 \le E_n \le 2$ meV) contributed only with about 1.5% to the g_f-value. The measurement of the fission cross-section shape for ^{241}Pu in the same neutron energy region is planned, but in the meantime we refer to the value for g_f for ^{241}Pu of 1.046 ± 0.004 reported by Wagemans and Deruytter (13).

The resulting values for g_f at T = 20 ·44°C are given in Table 1. They are compared with the proposed values for ENDF/B6 (9) and the results of recent evaluations by Axton(4) and by Divadeenam and Stehn(2) and the values of evaluations quoted in (2).

5. THERMAL CONSTANTS OF ^{233}U, ^{235}U, ^{239}Pu and ^{241}Pu

In recent years two evaluations of the thermal constants of ^{233}U, ^{235}U, ^{239}Pu and ^{241}Pu and the fission yield of ^{252}Cf were performed. The first one by Divadeenam and Stehn(2), used all available information up to 1983, and employed a least-squares fitting programme LSF, to obtain a best overall fit and provide an estimate of the sensitivity of the parameters to the quoted uncertainties in experimental data. The second one was done

Table 1. Westcott g_f-factors at t = 20.44°C

Reference	^{233}U	^{235}U	^{239}Pu	^{241}Pu
Hanna (1969)	0.9950 ± 0.0021	0.9766 ± 0.0016	1.0548 ± 0.0030	1.0486 ± 0.0053
Steen (1972)	0.9966	-	-	-
Leonard (76/81)	-	0.9775 ± 0.0011	1.0535 ± 0.0015	-
Lemmel (75/82)	0.9967 ± 0.0017	0.9762 ± 0.0012	1.0555 ± 0.0024	1.0442 ± 0.0048
Divadeenam (1984)	0.9955 ± 0.0015	0.9761 ± 0.0012	1.0558 ± 0.0023	1.0440 ± 0.0049
Axton (1986)	0.9955 ± 0.0014	0.9774 ± 0.0008	1.0555 ± 0.0022	1.0445 ± 0.0055
ENDF/B 5	0.9966	0.9775	1.0582	1.0452
ENDF/B 6	0.9955 ± 0.0014	0.9771 ± 0.0008	1.0563 ± 0.0021	1.0450 ± 0.0053
Present work	0.994 a) ± 0.003	0.976 a) ± 0.002	1.055 a) ± 0.003	1.046 b) ± 0.004

a) preliminary result

b) Ann. Nucl. En. 2 (1975) 541

Table 2. Least-squares fit of 2200 m s^{-1} constants (Divadeenam and Stehn, 1984)

Quantity	^{233}U	^{235}U	^{239}Pu	^{241}Pu
σ_s(b)	12.6 ± 0.3	14.0 ± 0.5	7.3 ± 0.4	9.1 ± 1.0
σ_a(b)	574.7 ± 1.0	680.9 ± 1.1	1017.3 ± 2.9	1369.4 ± 7.7
σ_f(b)	529.1 ± 1.2	582.6 ± 1.1	748.1 ± 2.0	1011.1 ± 6.2
σ_γ(b)	45.5 ± 0.7	98.3 ± 0.8	269.3 ± 2.2	358.2 ± 5.1
g_a	0.9996 ± 0.0011	0.9788 ± 0.0008	1.0784 ± 0.0024	1.0442 ± 0.0020
g_f	0.9955 ± 0.0015	0.9761 ± 0.0012	1.0558 ± 0.0023	1.0440 ± 0.0049
η	2.2957 ± 0.0040	2.0751 ± 0.0033	2.1153 ± 0.0052	2.1686 ± 0.0080
α	0.0861 ± 0.0015	0.1687 ± 0.0015	0.3600 ± 0.0032	0.3543 ± 0.0057
$\bar{\nu}_t$	2.4933 ± 0.0039	2.4251 ± 0.0034	2.8768 ± 0.0057	2.9369 ± 0.0073

^{252}Cf $\bar{\nu}_t$ = 3.7675 ± 0.0040; $t_{1/2}$ (233) = 1.5913 ± 0.0016 × 10^5 years; $t_{1/2}$ (234)= 2.4575 ± 0.0050 × 10^5 years; $t_{1/2}$ (239) = 2.4101 ± 0.012 × 10^4 years.

by Axton[4], who performed a similar evaluation, but used for the first time, a full covariance matrix to describe the correlations in the uncertainties of the input data.

Divadeenam and Stehn concluded that their recommended set of fissile thermal parameters now constitute a self-consistent set and that problems encountered in earlier evaluations were not significant in casting any doubt on the consistency of certain types of input data (such as nubar measurements and observations made in pile and Maxwellian spectra) with the main body of input data.

In the evaluation by Axton, the uncertainties in the fitted parameters are slightly larger than those of Divadeenam due to the inclusion of more correlations (cfr. Tables 2 and 3). The correlations in the uncertainties of the fitted values are significantly greater in the case of Axton's results, e.g. for each nuclide the average correlation between σ_a, σ_f and eta is 86% and between σ_c, and α even 95%. It is believed that the inclusion of the input covariance matrix places the estimates of the output uncertainties on a more realistic basis. Also Axton concludes that the complete set of data is internally consistent. It has a χ^2 value of 103 for 129 degrees of freedom. Among the weighted residuals, which are calculated from the fit to all data used, only 35 have an absolute value greater than unity, compared with an expectation figure of 53. There is no weighted residual with an absolute value greater than 2, whereas between 7 and 8 would be expected. It can be concluded that the uncertainties of the input data have not been underestimated.

Axton also performed an evaluation excluding Maxwellian data (cfr. Table 4). Differences occur, e.g. the ~9% difference in σ_c and α for ^{233}U, a much smaller (~ 2%) difference in σ_c and α for ^{235}U, and a 2.5 b difference in σ_f for ^{235}U. However, these differences must not be confused with discrepancies. The distributions of residuals obtained with the complete data set reveals a reasonably normal distribution (see above) and the above differences should not be regarded as discrepancies. Likewise the difference between some $\bar{\nu}_T$ measurements for ^{252}Cf cannot be regarded as discrepant. It follows naturally from the assumption of a normal distribution of input uncertainties. One could say that the agreement between important subsets of the data is at the 0.5% level, whereas internal consistency of the subsets would be 0.2%. In the present situation of the data set and evaluation any individual effort (measurement) is only likely to create an additional value with no sizeable influence on the present accuracy unless a new revolutionary

Table 3. Results with all Data (Axton 1986)

Parameter	Fitted	Uncertainty	Relative Uncertainty %
SCA 33	12.1861	.6681	5.483
SCA 35	15.9828	1.1051	6.914
SCA 39	7.8966	.9739	12.333
SCA 41	12.1878	2.6168	21.470
SCR 33	10.9169	.8788	8.050
SCR 35	14.2071	1.2671	8.919
SCR 39	6.8000	1.7494	25.726
SCR 41	11.1717	3.6126	32.337
ABS 33	576.2174	1.3000	.226
ABS 35	681.8303	1.3099	.192
ABS 39	1018.9667	2.8747	.282
ABS 41	1373.2025	9.0860	.662
FIS 33	530.6953	1.3424	.253
FIS 35	582.7836	1.1442	.196
FIS 39	747.6236	2.0105	.269
FIS 41	1011.8730	6.5974	.652
CA 33	45.5221	.6990	1.535
CA 35	99.0467	.7432	.750
CA 39	271.3431	2.1340	.786
CA 40	289.3296	1.3933	.482
CA 42	18.5144	.4001	2.161
CA 41	361.3294	4.9387	1.367
CAP 34	95.8369	1.9849	2.071
NUB 33	2.4950	.0040	.161
NUB 35	2.4334	.0036	.147
NUB 39	2.8822	.0051	.177
NUB 41	2.9463	.0058	.196
NUB 52	3.7676	.0047	.126
ETA 33	2.2979	.0041	.180
ETA 35	2.0799	.0035	.167
ETA 39	2.1147	.0051	.243
ETA 41	2.1710	.0077	.353
ALPHA 33	.0858	.0014	1.634
ALPHA 35	.1700	.0013	.792
ALPHA 39	.3629	.0031	.841
ALPHA 41	.3571	.0049	1.376
WGA 33	.9995	.0011	.107
WGA 35	.9789	.0008	.084
WGA 39	1.0782	.0024	.227
WGA 41	1.0442	.0020	.190
WGF 33	.9955	.0014	.142
WGF 35	.9774	.0008	.083
WGF 39	1.0555	.0022	.212
WGF 41	1.0445	.0055	.527
F3ETA 33	742.2525	2.3692	.319
F3ETA 35	718.5735	2.2183	.309
F3ETA 39	1175.7377	5.5862	.475
F3ETA 41	1679.8787	14.2078	.846

The value of X^2 is 103. There are 167 measurements, and 38 unknown parameters, leading to 129 degrees of freedom.

Table 4. Results with Maxwellian Data Omitted (Axton 1986)

Parameter	Fitted	Uncertainty	Relative Uncertainty %
SCA 33	12.3204	.6999	5.681
SCA 35	16.2388	1.1994	7.386
SCA 39	7.8966	.9776	12.380
SCA 41	11.9740	2.5857	21.595
SCR 33	11.1480	.9083	8.147
SCR 35	14.5259	1.3723	9.448
SCR 39	6.8131	1.7462	25.630
SCR 41	10.8285	3.8599	35.646
ABS 33	575.2391	1.8484	.321
ABS 35	681.1651	1.6956	.249
ABS 39	1018.8813	3.6895	.362
ABS 41	1382.1872	14.9131	1.079
FIS 33	533.2694	2.4363	.457
FIS 35	585.0603	1.6181	.277
FIS 39	748.5181	2.5460	.340
FIS 41	1020.5836	11.4887	1.126
CA 33	41.9697	1.7551	4.182
CA 35	96.1049	1.7408	1.811
CA 39	270.3632	3.1728	1.174
CA 41	361.6036	6.1868	1.711
NUB 33	2.4856	.0054	.218
NUB 35	2.4261	.0046	.188
NUB 39	2.8794	.0060	.207
NUB 41	2.9406	.0065	.220
NUB 52	3.7644	.0050	.132
ETA 33	2.3042	.0062	.271
ETA 35	2.0838	.0053	.255
ETA 39	2.1153	.0066	.311
ETA 41	2.1713	.0087	.399
ALPHA 33	.0787	.0035	4.494
ALPHA 35	.1643	.0032	1.962
ALPHA 39	.3612	.0046	1.280
ALPHA 41	.3543	.0059	1.668
WGA 33	.9988	.0012	.120
WGA 35	.9787	.0009	.092
WGA 39	1.0767	.0029	.269
WGA 41	1.0444	.0020	.191
WGF 33	.9966	.0020	.201
WGF 35	.9778	.0009	.092
WGF 39	1.0562	.0029	.275
WGF 41	1.0452	.0070	.670
F3ETA 33	746.4586	5.0978	.683
F3ETA 35	721.2735	3.6582	.507
F3ETA 39	1179.4821	9.4998	.805
F3ETA 41	1693.1349	30.0340	1.774

The value of X^2 is 48. There are 101 measurements, and 38 unknown parameters, leading to 63 degrees of freedom.

highly accurate technique is introduced in measurement or analysis. The use of beam-guides, e.g. at the ILL Grenoble reactor could improve substantially the background problems of earlier differential low energy measurements.

Some comments were received by Axton following the publication of his evaluations. It was observed that the higher value for σ_f^o of the 2200 m/s evaluation compared to the complete evaluation was in better agreement with criticality experiments. A careful diagnostic study of the Maxwellian input data revealed that these measurements were reasonably distributed and that there were not one or more highly accurate values that stood out.

Table 5. Preliminary 2200 m/s values for ENDF/B-6 evaluation (1987)

Nuclide	Parameter	Fitted Value	Uncertainty (%)
^{233}U	g_a	0.9996	0.11
	g_f	0.9955	0.14
	σ_s(b)	12.1309	5.48
	σ_f(b)	531.1396	0.25
	σ_c(b)	45.5096	1.50
	$\bar{\nu}_t$	2.4946	0.16
^{235}U	g_a	0.9790	0.08
	g_f	0.9771	0.08
	σ_s(b)	15.4557	6.87
	σ_f(b)	584.2522	0.19
	σ_c(b)	98.9649	0.75
	$\bar{\nu}_t$	2.4320	0.15
^{239}Pu	g_a	1.0782	0.22
	g_f	1.0563	0.21
	σ_s(b)	7.8835	12.30
	σ_f(b)	747.9861	0.25
	σ_c(b)	271.4266	0.79
	$\bar{\nu}_t$	2.8815	0.18
^{241}Pu	g_a	1.0440	0.19
	g_f	1.0450	0.53
	σ_s(b)	12.1738	21.50
	σ_f(b)	1012.6840	0.65
	σ_c(b)	361.2900	1.37
	$\bar{\nu}_t$	2.9453	0.20
^{252}Cf	$\bar{\nu}_t$	3.7676	0.13

In the data set there are no arguments to leave the Maxwellian data out of the evaluation. Later on it transpired[14] that the function K_1 provided a better criterion for judging the output data. The quantity $K_1 = (\hat{\eta} - 1)\hat{\sigma}_a$ which is the same as $\bar{\nu}\hat{\sigma}_f - \hat{\sigma}_a$, has a value of 718.57 ± 2.22 in Table 3 (all data) and a value of 721.27 ± 3.66 in Table 4 (without Maxwellian data) and the value deduced from criticality experiments is 722.7 ± 3.9 in better agreement with the value of Table 4. The same comment is valid for K_1 (^{233}U). In the Tables K1 is called F3 ETA 35.

A second comment at the UK Nuclear Data Forum 1984 by Brissenden[15] concerned the value of eta for ^{239}Pu, which is 2.115 ± 0.005 in Table 3 and which is considered too high compared to a value of 2.091, in harmony with the criticality experiments. Again it turned out that the value of K1 is more important. But in the ^{239}Pu case the evaluation without Maxwellian data yields a value of 2.115 ± 0.007 which is in agreement with the evaluation of the total data. In all diagnostic tests which have been carried out so far, the value of eta has never changed substantially from 2.115.

In the standards evaluation for ENDF/B-6 the evaluation of Axton without the use of Maxwellian data was used as input and resulted in the values shown in Table 5, which are suggested as 2200 m/s values for this standards evaluation.

REFERENCES

(1) Stehn, J., Divadeenam, M., Holden, N., Proceedings International Conference on Nuclear Data for Science and Technology, Evaluation of the thermal neutron constants for ^{233}U, ^{235}U, ^{239}Pu and ^{241}Pu, (Böckhoff K.H., Editor) Reidel Publishing Company (1983), 685.

(2) Divadeenam, M. and Stehn, J., same title, Annals of Nuclear Energy, 11 (1984), 375.

(3) Axton, E.J., Evaluation of the thermal neutron constants of ^{233}U, ^{235}U, ^{239}Pu and ^{241}Pu and the fission neutron yield of ^{252}Cf, European Applied Research Reports, Vol. 5, Nr. 4 (1984).

(4) Axton, E.J., same title, Report CBNM GE/PH/01/86 (1986).

(5) Bouchard, J., Golinelli C., Tellier, H. Besoins en données nucléaires pour les réacteurs à neutrons thermiques, Proceedings International Conference on Nuclear Data for Science and Technology(Böckhoff K.H., Editor), Reidel Publishing Company (1983), 21.

(6) Santamarina, A., Golinelli, C., Erradi, L., ANS Topical Meeting on Reactor Physics, Chicago (1984).

(7) Wartena, J.A., Weigmann, H., Bürkholz, C., Preliminary results on η of ^{235}U for sub-thermal neutron energies, This Meeting (1987).

(8) Wagemans, C., Deruytter, A.J., Sub-Thermal fission cross-Section measurements, Proceedings International Conference on Nuclear Data for Basic and Applied Science, Radiation Effects 93, (1986), 163.

(9) Carlson, A., Hale, G., Peelle, R., Poenitz, W., Memo to Dunford, C.; Private Communication to Axton, E.

(10) Gwin, R., Spencer, R., Ingle, R., Todd, J., Scoles, S., Fission Cross Sections of ^{235}U and ^{239}Pu, Nucl. Sci. Eng., 88 (1984), 37.

(11) Okazaki, A., Jones, R.T., Measured dependence of some effective cross-sections on thermal neutron temperatures in the range - 195°C to 297°C, Proceedings International Conference on Nuclear Data for Basic and Applied Science, Radiation Effects 93, (1986), 541.

(12) Westcott, C., Journal Nuclear Energy 2 (1955), 9.

(13) Wagemans C., Deruytter A.J., The Westcott gf-factor as a function of the temperature for ^{241}Pu, Annals of Nuclear Energy, Vol. 2, (1975), 541.

(14) Hardy, J., Private Communication to E.J. Axton, memo dated June 18, 1985.

(15) Brissenden, R.J., Report UKNDC (1985), p. 12, 19, AERE Harwell.

PRELIMINARY RESULTS ON η OF ^{235}U FOR SUB-THERMAL NEUTRON ENERGIES

J.A. WARTENA, H. WEIGMANN, C. BÜRKHOLZ
Central Bureau for Nuclear Measurements,
Joint Research Centre,
Commission of the European Communities,
Geel

Abstract

An experiment has been set up to measure the shape of η, the relative number of fission neutrons emitted per neutron absorbed, for ^{235}U in the sub-thermal neutron energy range. A ^{235}U sample which is "black" for neutrons in the energy range of interest is exposed to a collimated neutron beam from the cooled moderator of the Geel electron linac, and a liquid scintillation detector with pulse shape discrimintation is used for detection of the fission neutrons. The neutron flux is monitored with parallel plate proportional counters loaded with ^{6}Li or ^{10}B and ^{235}U. In separate runs the thick U sample is replaced by a thick ^{10}B slab used to measure the shape of the neutron flux.
Preliminary results of the experiment are given.

1 INTRODUCTION

A discrepancy is known to exist between the calculated temperature coefficient of reactivity for light water reactors and measured values obtained in integral experiments, which is of the order of 3 to 5 pcm/°C. The commonly accepted goal for the accuracy with which this parameter should be known is 1 pcm/°C (1). It has therefore been proposed by Santamarina et al. (2) that the energy dependence of certain differential nuclear data in the sub-thermal neutron energy region be modified with respect to ENDF/B-V within their experimental uncertainties, in order to remove most of this discrepancy.

One of the data sets thus modified is η, the number of fission neutron emitted per neutron absorbed, of ^{235}U. In fact, there are very few direct measurements of this quantity in the sub-thermal range, the most extensive data set being the one of Palevsky et al. (3) from 1956. An experiment has therefore been set up at the Geel linac to measure the energy dependence of η of ^{235}U in the sub-thermal neutron energy region.

2. EXPERIMENTAL METHOD

The principle method to measure the energy dependence of η is simple: A "black" ^{235}U sample which is sufficiently thick to absorb all neutrons with energies of interest, is exposed to a neutron beam, and the relative number of fission neutrons emerging from this sample is measured together with the flux of incoming neutrons.

The liquid methane moderator of the Geel electron linac was used as a white source of sub-thermal neutrons. A beam of neutrons from this source is defined by a 3.5 m long collimation system and passes first through two parallel plate proportional counters (PPP) used to monitor the shape of the neutron flux. In a first series of measurements, the first PPP was loaded with a 162 $\mu g/cm^2$ ^6LiF(95.65% ^6Li) evaporated onto an 100 μm/thick Al backing. In a second run, a 3.6 $\mu g/cm^2$ ^{10}B layer (90% ^{10}B), evaporated onto an identical backing, was used instead. In both runs, the second PPP was loaded with 279 $\mu g/cm^2$ UF_4 (97 6% ^{235}U), evaporated onto a gold coated mylar foil of 3.5 μm thickness. Both fission fragments were detected in coincidence in two separate halves of the PPP.

About 80 cm downstream from the flux monitors, the neutron beam hits a "black" metallic U sample. The transmission of the 4.59 g/cm^2 thick sample is almost zero for neutron energies below 0.1 eV. Fission neutrons emerging from this sample are detected by a 5 cm ⌀ and 5 cm thick NE213 liquid scintillation detector. Pulse shape discrimination (PSD) is used to distinguish fission neutrons from γ-rays. The energy of the neutron which initiated a fission event is determined from its time-of-flight along the 8.8 m flight path from the moderator to the ^{235}U sample.

The shape of the neutron flux at the position of the black U sample will not be the same as at the position of the flux monitors because of two reasons: Depending on neutron energy, a different fraction of the neutron beam is scattered in the exit window of the PPP and in the about 70 cm of air in between the PPP and the black U sample. Moreover, both detectors may view slightly different parts of the moderator which may yield neutrons with different flux shapes. Therefore, the actual measurement of the neutron flux shape is done by replacing the black U sample by a 0.11 g/cm^2 thick ^{10}B slab. Since also this slab is practically black for neutrons in the energy range of interest, the shape of the neutron flux is directly obtained from the yield of 480 keV γ-rays from the $^{10}B(n,\alpha)^6Li^*$ reaction. These γ-rays have been detected with the same liquid scintillation detector used also for the fission neutron detection in part of the measurements, or with a hydrogene free C_6F_6 liquid scintillation detector in another part. The PPP flux monitors are used only to record possible changes of the neutron flux shape between the fission measurements with the black U sample and the flux measurements with the ^{10}B slab.

Signals from the three detectors (the two PPP flux monitors and the liquid scintillator detector) are fed into a time-to-digital converter (TDC) and a routing unit. In case of the measurement with the black U sample, only signals from the NE213 liquid scintillator which have been indentified as "neutron" by the PSD circuit, are accepted. From the output of the TDC and the routing unit, three 4k time-of-flight spectra are constructed in a Nuclear Data ND6600 analyser. A fourth 4k spectrum is also constructed from signals fed into the TDC and the routing unit from a random pulse generator. This spectrum checks the dead-time of the analyser as a function of time-of-flight. No analyser dead-time effects of more than 0.2% have been recorded in the final measurements.

Apart from the analyser dead-time, the dead-time of the PSD circuit has to be considered. Every signal which is analysed by the PSD circuit produces a dead-time of this circuit of about 2 μs, also if the event is rejected as being due to a γ-ray. The rate of γ-ray events is rather high, especially at short flight times. The effect of this dead-time as a function of time-of-flight is estimated from spectra obtained from the liquid scintillator detector when all pulses are accepted by the PSD. Corrections necessary due to the PSD dead-time are smaller than 1% for neutron energies below 0.3 eV, but become considerably larger above that energy. The PSD dead-time is one of the factors limiting the useful energy range in the present experiment.

3 DATA ANALYSIS AND RESULTS

The first step in the analysis of the data is to correct the individual time-of-flight spectra for dead-times as described above and to subtract the backgrounds. The determination of the background presents a major problem in the present experiment. It is discussed in some detail below. Further, the data have to be corrected for incomplete absorption and scattering on the incident slow neutrons in the "black" U sample and in the ^{10}B slab. The multiple scattering of the fission neutrons produced in the "black" U sample, the relative number of secondary fission events induced by these neutrons, and the fraction of all fission neutrons that are detected in the liquid scintillator, must be taken into account. The latter fraction depends on the spatial distribution of primary fission events within the "black" U sample, and thereby on the energy of the incident slow neutrons. Finally, the self-absorption of the 480 keV γ-rays in the ^{10}B slab has to be considered. These corrections have been calculated by approximate analytical expressions as well as by Monte-Carlo techniques.

The energy dependence of η of ^{235}U resulting from the measurements at the Geel linac and including all above-mentioned corrections, is shown in figure 1 together wit the "reference shape" as well as the modification proposed by Santamarina et al.. The experimental data have been normalized to an average value of 2.075 between 20 and 30 meV neutron energy. An earlier analysis of the present data which seemed to indicate a flat shape below 20 meV did not include the multiple scattering corrections mentioned above in a complete manner.

The error bars as shown in figure 1 include both, statistical as well as systematic uncertainties. However, the largest contribution is due to the uncertainties in the determination of backgrounds (at low energies) and in the calculation of the correction factors (at high energies). Thus the data uncertainties are highly correlated.

The main experimental problem with the measurement of η at the linac white neutron source is connected with the determination of the background in the measurement of the fission neutrons. The number of neutrons per time-of-flight interval in the neutron beam at times corresponding to energies above about 20 meV is two orders of magnitude larger than at 2 meV. Essentially each of these neutrons hitting the black U sample produces 2.4 fission neutrons which may be slowed down in the surroundings of the sample and eventually initiate a background fission event in the sample at a later time when the foreground due to a much smaller incident flux is to be measured. A Cd or similar filter may be inserted into the neutron beam for background measurements. However, it will remove not only the foreground but a part of the background source as well. Thus the background determined that way will be too small. The undetected background component due to the mechanism described, can only roughly be estimated, and it is therefore essential to keep the background as small as possible. The main steps to reach this goal were to insert the black U sample into a cylindrical ^6Li sleave in order to protect it against backscattered neutrons, and to place a 2 cm thick Be filter in the neutron beam which

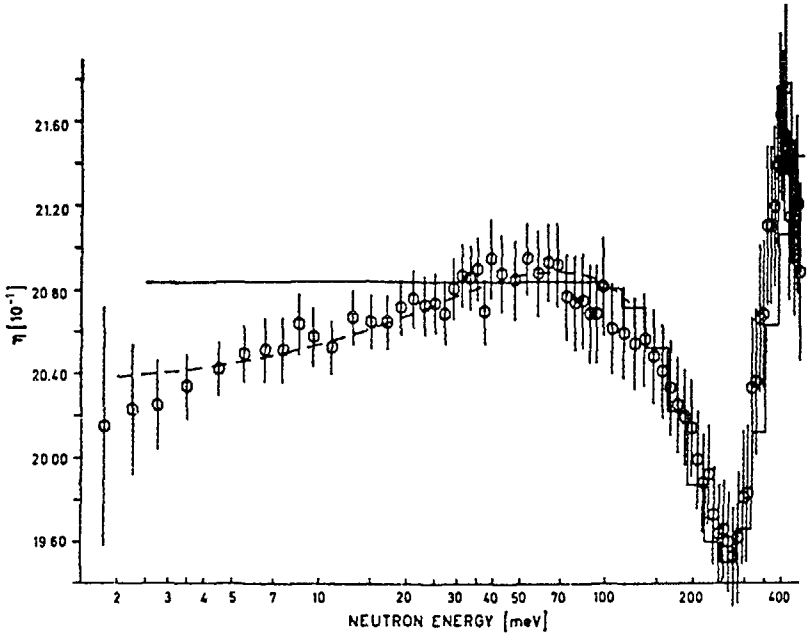

Fig. 1 . The measured energy dependence of eta of ^{235}U compared to the reference shape (—) and the modification (-----) proposed by Santamarina et al.[1]

reduces the neutron flux above 6.8 meV energy by about a factor of 4 while having only a small effect on the flux at lower energies.

Much better experimental conditions for the measurement of η will be met at a cold neutron guide of the ILL reactor at Grenoble: The flux of subthermal neutrons of interest is much larger, and there are only few neutrons with higher energies which may give rise to backgrounds. Since neutrons with energies above 0.2 eV are practically absent, one is able to use a double chopper installation to produce a pulsed monoenergetic beam. With this most of the background due to backscattered neutrons will be separated in time from the foreground and can thus be easily subtracted.

The aim of the planned experiment at ILL is:

- to check the results obtained at the Geel linac for possible undetected systematic errors in the backgound treatment, and
- to reduce the systematic uncertainty of the data in the most interesting energy region (below about 20 meV) by a factor of two (for 2 meV $< E_n <$ 20 meV) to four (for $E_n <$ 2 meV). Such error margins would be sufficiently small that their effect on the precision with which the tempeature coefficient can be calculated is in accord with the required 1 pcm/°C.

REFERENCES

(1) J. Bouchard, C. Golinelli and H. Tellier, Proc. Int. Conf. on Nuclear Data for Science and Technology, Antwerp 1982; D. Reidel, Dordrecht 1983; p. 814

(2) A. Santamarina, C. Golinelli and L. Erradi, ANS Topical Meeting on Reactor physics, Chicago 1984.

(3) H. Palevsky, D.J. Hughes, R.L. Zimmerman and R. Eisberg, J. Nucl. Energy 1 (1956) 177.

126 DOPPLER BROADENING EFFECTS IN LOW ENERGY RESONANCES

M.C. MOXON, M.G. SOWERBY
Harwell Laboratory,
United Kingdom Atomic Energy Authority,
Harwell, Didcot, Oxfordshire,
United Kingdom

Abstract

The gas model of Döppler broadening is used both when resonance parameters are extracted from measurements of nuclear data and when these parameters are converted to the cross-sections needed for reactor calculations. A brief review is made of the available information on the adequacy of the gas model for low energy resonances ($\lesssim$10 eV), as these are particularly significant for thermal reactors. It is found that the gas model with an effective temperature is not always an adequate prescription.

1. INTRODUCTION

The nuclear data in the resolved resonance range which are used for reactor calculations are based on cross-sections calculated from resonance parameters. In the calculations to convert the parameters to cross-sections the gas model of Doppler broadening is invariably used. (The same model is also used to extract the parameters from measured nuclear data (i.e. transmission, capture, fission, scattering and self-indication data).) This short paper makes some comments on the adequacy of the model for the low energy range which is important for thermal reactor calculations.

2. DOPPLER BROADENING

In the interaction of neutrons with nuclei the shape of a resonance in a cross-section is affected by the thermal motion of the nuclei. The resultant broadening of the resonances, which is known as Doppler broadening, increases with temperature and is important in reactor calculations because for thick samples of materials it results in reaction rates being temperature dependent.

Doppler broadening is a subject that has been considered widely in the literature. Bethe and Placzek [1] first called attention to Döppler broadening and developed a theory assuming the thermal motion of target nuclei to be that of an ideal gas. Lamb [2] refined the theory to include the effects of nuclei bound in a crystal lattice. He demonstrated that for sufficiently weak binding the resonance shape is the same as that obtained for an ideal gas but the temperture used in the calculation is not the real temperature T but an effective temperature T_{eff}. The theory was extended to arbitrary materials by Nelkin and Parks [3] who showed that Lamb's gas model is applicable if either the binding effect is "weak" or the nuclear recoil energy is large. On the assumption that the crystal may be treated as a Debye continuum Lamb showed that T_{eff} is related to the thermodynamic temperature T and the Debye temperature Θ_D by the equation

$$T_{eff}/T = 3(\Theta_D/T)/8 + 3(T/\Theta_D)^3 \int_0^{\Theta_D/T} (x^3/(e^x-1))dx \qquad (1)$$

In the "weak binding" limit ($\Gamma + \Delta \gg 2k\Theta_D$) T_{eff} is close to T (Δ is the Döppler width defined below). For medium binding where the atom is more tightly bound ($\Gamma + \Delta \sim \Theta_D$) fine structure should appear in the broadened resonance shape. In the extreme of strong binding a peak with no Doppler broadening together with a broadened peak at higher energies is expected. When the nuclear recoil energy is large, solid state effects are not expected to be important because the recoiling nucleus breaks free from the lattice.

In the gas model it is assumed that the nuclei have a distribution of velocities in the direction of the neutron beam given by the Maxwell-Boltzmann formula. It can then be shown (see for example Lynn [4]) that the effective cross-section σ_{eff} is given by

$$\sigma_{eff}(E_{lab}) = (1/\Delta\sqrt{\pi}) \int_{-\infty}^{+\infty} dE_t \exp(-(E_t-R)^2/\Delta^2)\, \sigma(E_{lab}-E_t) \qquad (2)$$

where $E_t = E_{lab}-E$
E = the energy in the centre of mass system
$R = mE_{lab}/(M + m)$
m = mass of the neutron
M = mass of the target nucleus
$\Delta = (4RkT_{eff}M/(M + m))^{1/2}$
$\sigma(E_{lab} - E_t) = \sigma(E)$ = value of the cross-section at energy E without Doppler broadening
k = Boltzmanns constant

In thermal reactors the low energy resonances are especially important. Table 1 due to Tellier [5] shows the importance of the low energy resonances in the absorption of neutrons by U-238 in a thermal reactor (U-238 is very important in calculating the neutron balance as ~20% of all neutron absorptions occur in it). Doppler broadening effects are significant for these resonances as the effective capture resonance integral between 2.76 eV and 37 keV increases by ~10% when the temperature changes from 20 to 700°C [5]. Since the gas model is invariably used for the reactor calculations the following questions arise

(1) Is the gas model correct for low energy resonances or should it only be applied above a certain energy?

(2) If it does apply what values of T_{eff} should be used?

Table 1

Absorption rate in the first resonances of U-238 relative to the total resonance absorption

Resonance eV	6.67	20.9	36.7	66	80.7	102.6 116.4 189.6
Absorption %	27.7	15.2	11.9	5.2	2.8	6.7

For U-238 the first (6.67 eV) and possibly the second (20.9 eV) resonances do not meet the "weak binding" limit and it is not surprising that a number of experimenters have found that transmission (total cross-section) data for the 6.67 eV resonance are not well fitted by the gas model with an effective temperature. Jackson and Lynn [6] found that the observed transmission results were consistent with the gas model for uranium metal samples at 297 and 77 K but were not well fitted for uranium metal at 4 K and U_3O_8 at 293, 77 and 4 K. Similar inconsistencies have been found for a variety of uranium compounds including UO_2 and the gas UF_6 by Bowman and Schrack [7] and Meister et al [8].

It would also be expected that the 1.057 eV resonance in Pu-240 and the 0.433 eV resonance in Ta-180 would exhibit solid state effects. Harvey et al [9] measured the transmissions of a Pu-Al alloy containing 0.726% of Pu-240 and a rolled Ta metal sample but no evidence of solid state effects was observed. Fig. 1 shows the observed transmission of Pu-240 with calculated curves obtained using the gas model of Doppler broadening based on a Debye temperature of 175 K. There is no evidence of a recoiless peak in either set of data. Though it is not a topic of this paper it is worth noting that Harvey et al observed much structure in the total cross-section of many different materials in the thermal energy range. This of course depends on the sample orientation but structure in this energy range is not normally taken into account in reactor calculations. An example of the observed structure is shown in Fig. 2 where data for a rolled Ta sample are displayed.

The above results on the gas model may at first sight appear to be contradictory as the gas model works for some materials and not for others. The qualitative explanation is that the detailed broadening function in the few eV energy range varies from compound to compound depending on the detailed properties of the matrix containing the isotope being investigated. In consequence in some cases the gas model with an effective temperature appears to be satisfactory while in others it is not. Obtaining the effective temperature from the Debye temperature is a poor approximation particularly for compounds because the phonon frequency spectra will be element dependent. In consequence for example for UO_2 the Debye temperature obtained from specific heat data gives information on the "average atom" in UO_2 rather than on the uranium.

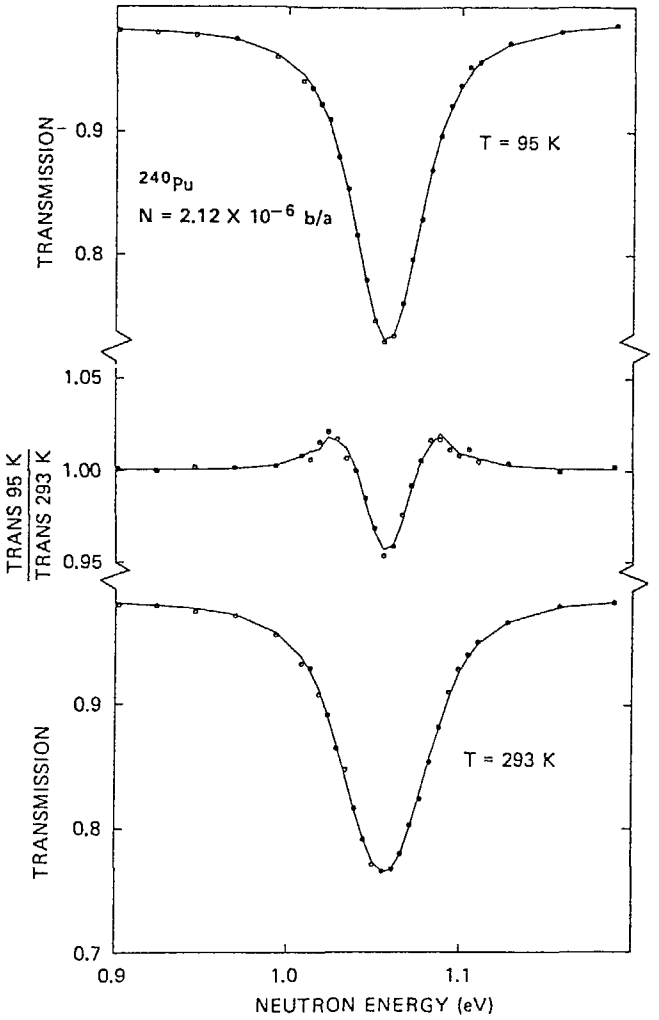

FIG. 1.

Transmission of the ^{240}Pu sample at 95 K (top), transmission at 293 K (bottom) and ratio (middle). The statistical uncertainties in the region of the resonance are 0.2% for the transmissions and 0.3% for the ratio.

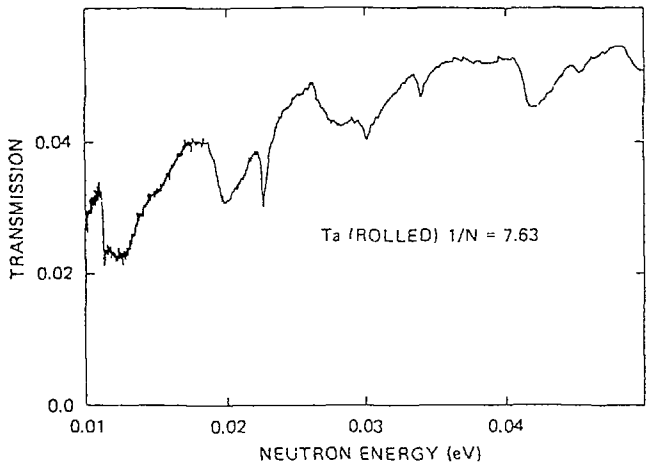

FIG. 2. Total cross section of rolled Ta.

It has been shown above that the gas model with an effective temperature is not always satisfactory at low neutron energies but does it apply at higher energies? In addition is the gaussian shape of the broadening function (see equation 2) correct? These points can be examined by investigating the shape of resonances observed in high resolution experiments.

Though resonances have been analysed on thousands of occasions, the number of analyses that have specifically checked the adequacy of the Doppler broadening formalism is really very small (because (1) most analyses use the area method, (2) the Doppler width Δ is often obtained in the analyses because it cannot be obtained accurately from other data and (3) the experimental conditions do not enable the formalism to be checked). One experiment due to Haste and Sowerby [10] is particularly important because it was made on UO_2 at room temperature and above. They measured the neutron transmission of UO_2 and determined the temperature of the samples by fitting the shape of the resonances. Table 2 gives the results obtained; the effective temperature was related to the absolute temperature by using the relationship derived by Butland [11] (see equation (3) below). Fig. 3 shows some shape fits to the 80.8 eV resonance at different temperatures. At both temperatures the figures obtained are internally consistent from resonance to resonance. The agreement between the fitted and measured temperatures is good at 1800K but only fair at 1100K. (The slight difference at the lower temperature was possibly due to a deposit on the viewing window or to a systematic error in the measuring instrument (optical pyrometer) which was working near the bottom of its usable range). However, the generally good agreement indicates that the gas model of Doppler broadening combined with the multilevel R-matrix description of the cross-sections provides a good description of the cross-section close to the resonances at elevated temperatures for solid UO_2. However, on the resonance wings the situation may not be so good as Haste and Sowerby

Table 2

Temperature determination of hot uranium dioxide samples by resonance shape fitting (errors in parentheses)

E_r (eV) (from uranium dioxide measurements)	Γ_n (meV)	Γ_γ (meV)	Fitted temperature (K) (nominal 1100K sample)	Fitted temperature (K) (nominal 1800K sample)
20.8711 (0.0064)	10.17 (0.10)	22.44 (0.43)	1121 (59)	1792 (169)
66.0556 (0.0177)	25.64 (0.66)	23.46 (0.87)	1130 (22)	1785 (66)
80.7616 (0.0048)	1.794 (0.058)	24 (assumed)	1121 (59)	1785 (89)
89.218 (0.046)	0.0847 (0.0051)	24 (assumed)	1127 (84)	1807 (153)
	Weighted mean (effective temperature)		1128 (19)	1788 (48)
	Absolute temperature from shape fitting		1125 (19)	1786 (48)
	Mean pyrometer reading		1096 (9)	1792 (12)

investigated Döppler broadened transmission data and therefore did not test the adequacy of the gas model on the wings of the broadening function. To do this the resonance shapes of measured capture cross-section data need to be investigated as a function of temperature under conditions where the Doppler width dominates over the resolution and resonance widths. This has not specifically been done but the analysis of Moxon [12] for room temperature Fe capture data can be used to give some confidence in the wings of the function. Fig. 4 shows a comparison of the measured and calculated capture yields for the 1.15 keV Fe-56 resonance and it can be seen that there are no significant errors in the wings of the broadening function. Further work needs to be done on this topic.

Another type of experiment has thrown some doubt about the adequacy of the gas model when uranium is melted. Brugger and Aminfar [13] measured the effective average total cross-sections (EATCS) for samples of various thicknesses of U-238 in the chemical forms of solid metal, liquid metal, U_3O_8, UO_2 and UC for beams of filtered neutrons with bands of energies about 2, 24 and 144 keV. In the context of this note the results shown in Fig. 5 are most important. It can be seen that there is a step in EATCS when uranium metal is melted and this cannot be explained by the gas model of Doppler broadening. (Brugger and Aminfar introduce an effective mass M_{eff} to obtain agreement but the value of 100-150 amu is not physical.) As a similar step was also observed when Sn was melted [14] it is clear that further measurements to investigate the effect are highly desirable as the results may be the manifestation of some effect which is not currently taken into account.

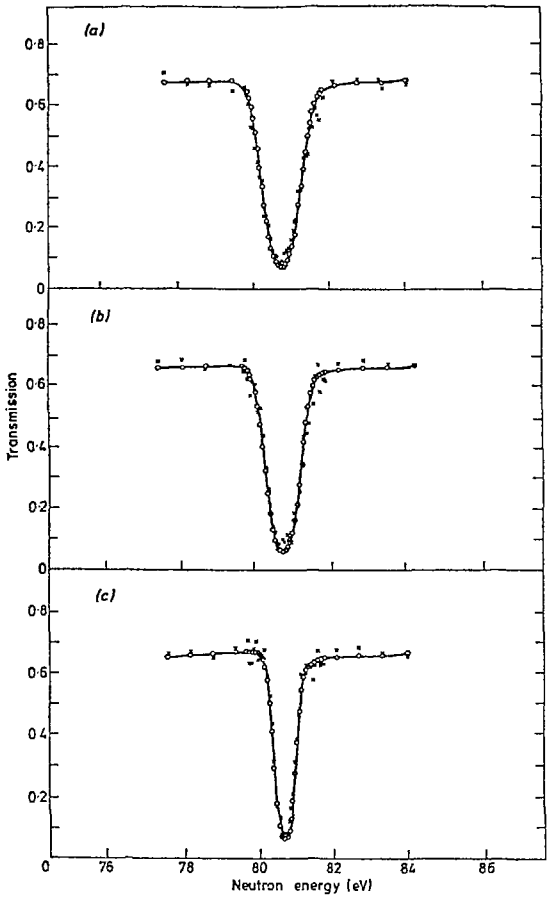

FIG. 3.

Shape fits to the 80·8 eV resonance for the 10 mm data at three different temperatures: (*a*), $T=1785\pm89$ K; (*b*), $T=1135\pm26$ K; (*c*), $T=293$ K. $E_r=80{\cdot}762\pm0{\cdot}005$ eV; $\Gamma_n=1{\cdot}794\pm0{\cdot}058$ eV; $\Gamma_\gamma=24$ meV. Sample thickness (cold)=0·0238 atoms ^{238}U/barn. ×, observed, O, calculated.

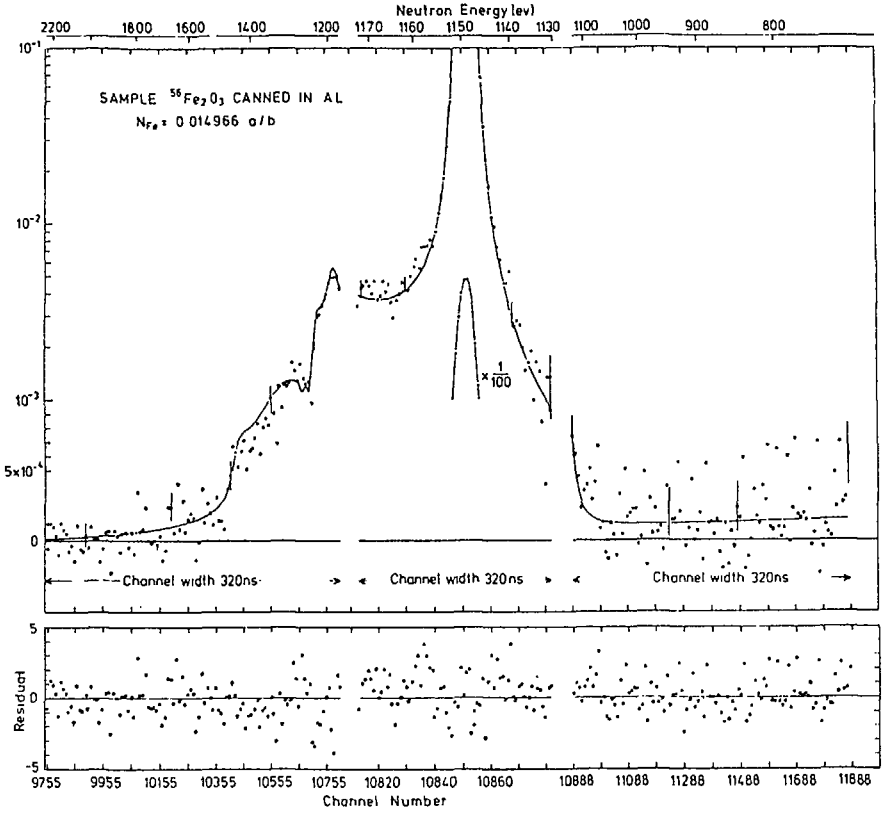

FIG. 4.

Least squares fit to the neutron capture yield in the energy region of the 1.15 keV resonance of ^{56}Fe. The derived parameters are:

E_R 1148.812±0.010 eV

Γ_n (56.64±0.13)x10^{-3} eV

Γ_γ (0.5678±0.0070) eV

Background adjustment -(5.22±0.95)x10^{-5}

Effective temperature (28.87±0.34)x10^{-3} eV

where the errors quoted are obtained only from the fit to the data.

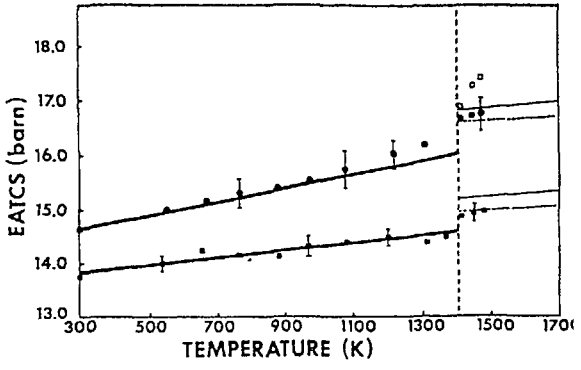

FIG. 5.

The EATCS of ^{238}U metal for 2keV neutrons. The points ● are for n=0.23 nuclei/barn, ■ are for n=0.059 nuclei/barn and □ are for n=0.022 nuclei/barn. The lines are from U3R calculations where —— is for M_{eff}=238amu, - - - is for M_{eff}=150amu and —— is for M_{eff}=100amu. The vertical dashed line is the melting point of U metal.

Though the gas model with an effective temperature is not particularly well validated experimentally and further work needs to be done, it appears reasonably satisfactory with some reservations above the few eV energy range. The selection of the effective temperature is a problem particularly for compounds though at the operating temperatures in power reactors T_{eff} is closer to the thermodynamic temperature than it is at room temperature. It is usually assumed that in a simple compound such as an oxide (e.g. Fe_2O_3) the effective temperature of each constituent element is close to that for the pure element [6]. This is not always quite correct as the effective temperature deduced in Fig. 4 for Fe_2O_3 is equivalent to a Debye temperature of 520±25 K while the value from the specific heat is 464 K. Moxon [15] has also determined T_{eff} by analysis of the 17.6 eV hafnium resonance for metal and oxide (HfO_2) samples. The values obtained were 298.2±5.8 and 305.7±11 K respectively so agreement is achieved in this case.

For UO_2 Butland [11] has made a careful analysis of a variety of data and recommends for uranium that

$$T_{eff} = T(1 + 3110/T^2)\ K \qquad (3)$$

This formula fits the resonance data of Haste and Sowerby and is equivalent to a Debye temperature of ~260 K. The Debye temperature of UO_2 deduced from X-ray diffraction data is 620 K. In addition Gollinelli et al [16] concluded that using a Debye temperature of 620 K for UO_2 improves the interpretation of thermal reactor Doppler experiments made in MINERVE and Brugger and Aminfar [13] deduced a value of 590 K. (In the case of Brugger and Aminfar a value of M_{eff} of 600 (M + m in equation 2) was also deduced and this produces more significant differences [for T = 293 K $\Delta = 0.0141\ \sqrt{E_{lab}}$ as compared with $\Delta = 0.0209\ \sqrt{E_{lab}}$ for T_{eff} from Butland with M = 238]). However, the Doppler effect measurements of Yusada et al [17] do not appear to be consistent with a Debye temperature of 620 K.

In view of these problems and differences it was decided to deduce the effective temperature for uranium metal for the first few resonances in U-238. The transmission data of Olsen et al [18] were therefore analysed with the code REFIT [19] and values of the neutron (Γ_n) and capture (Γ_γ) widths and T_{eff} obtained. The results are given in Table 3 and shown in Fig. 6 - the errors quoted are the values given by the code and do not take full account of systematic errors. It was found in obtaining these results that the fits to the first resonance (6.67 eV) and to a lesser extent to the second resonance were not good (χ^2 per degree of freedom high). At higher energies the fits were good and this suggests that solid state effects are effecting the Doppler broadening for the first two resonances. The average value of T_{eff} is 305.7±0.63 K which corresponds to a Debye temperature of 284±7 K which is inconsistent with the values obtained from specific heat (180-200 K) and X-ray diffraction (210 K) data. It, however, agrees with the value obtained by Brugger and Aminfar (Θ_D = 260, M_{eff} = 238). For U-238 metal in a liquid form Brugger and Aminfar also obtained Θ_D = 260 but with M_{eff} = 100-150.

Table 3

Fitted parameters for low energy resonances in U-238*

Resonance energy (eV)	Capture width (Γ_γ) (meV)	Neutron width (Γ_n) (meV)	Effective temperature (T_{eff}) (meV)	(K)
6.6741	22.997±0.042	1.4926±0.0023	26.461±0.065	307.05±0.7
20.8735	22.911±0.040	10.258±0.0093	26.320±0.082	305.43±0.81
36.6849	22.890±0.048	34.129±0.023	26.117±0.110	303.11±1.16
66.0382	23.364±0.121	24.605±0.041	26.587±0.134	308.44±1.51
80.7521	24.985±0.577	1.865±0.022	26.108±0.275	302.99±3.37
102.5677	23.416±0.195	71.704±0.195	26.211±0.233	304.27±2.79
116.9077	22.995±0.261	25.486±0.093	26.134±0.240	303.22±2.67
145.6713	19.086±8.58	0.8470±0.042	28.181±1.53	327.01±17.75
165.3107	25.763±2.94	3.367±0.0075	26.664±0.71	309.37±8.12
189.6853	22.378±0.403	173.2±0.32	26.094±0.39	302.87±4.41
208.5244	23.937±0.31	51.11±0.20	25.641±0.31	297.54±3.71

*The errors are the values given by the code and do not take full account of systematic errors.

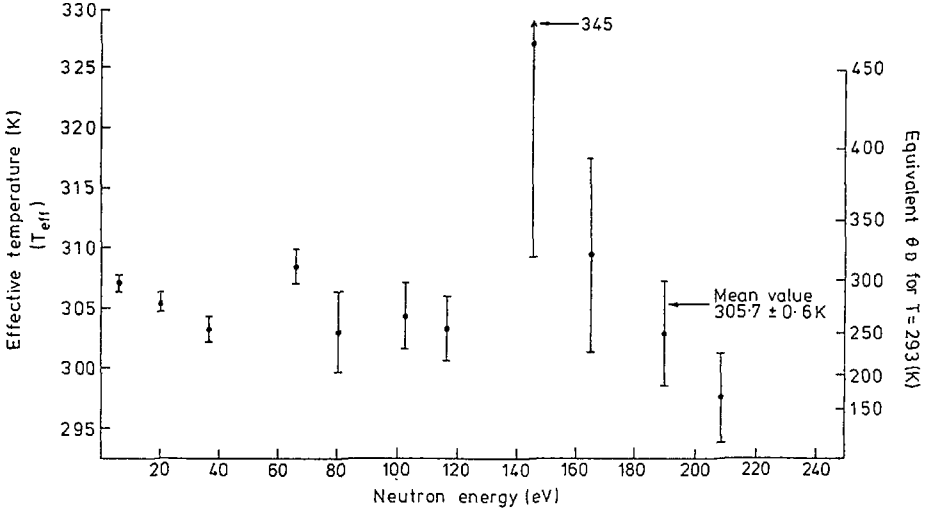

FIG. 6.

EFFECTIVE TEMPERATURE OBTAINED FOR U METAL SAMPLES BY RESONANCE SHAPE ANALYSIS

3. CONCLUSIONS

A short review has been made on the adequacy of the gas model of Doppler broadening for low energy resonances and the following conclusions drawn:

(1) In the energy range below a few eV the gas model of Doppler broadening with an effective temperature is not a reasonable approximation for all materials as solid state effects occur. In particular there is some evidence that it does not apply for UO_2.

(2) Above the few eV energy range the gas model appears to be a reasonable approximation though there are specific problems such as the change in the effective average total cross-section when uranium is melted and the need to confirm the shape of the broadening function particularly on its wings.

(3) The deviation of T_{eff} for use with the gas model is not well founded as the method based on the Debye temperature appears to be incorrect for some samples and in particular for compounds.

(4) For UO_2, however, it is clear from measurements of U-238 resonances that the formula of Butland (equation 3) should be used.

ACKNOWLEDGEMENTS

The authors wish to acknowledge the support and encouragement of Dr. M. S. Coates, Dr. A. T. G. Ferguson and Dr. J. E. Lynn. The work described in this paper was undertaken as part of the Underlying Research Programme of the UKAEA.

REFERENCES

[1] BETHE, H. A. AND PLACZEK, G., Phys. Rev. 51 (1937) 450.
[2] LAMB, W. E., Phys. Rev. 55 (1939) 190.
[3] NELKIN, M. S. AND PARKS, D. E., Phys. Rev. 119 (1960) 1060.
[4] LYNN, J. E., "The Theory of Neutron Resonance Reactions", p.24, Clarendon Press, Oxford (1968).
[5] TELLIER, H., INDC(NDS)-129/GJ, p.47 (1981).
[6] JACKSON, H. E. AND LYNN, J. E., Phys. Rev. 127 (1962) 461.
[7] BOWMAN, C. D. AND SCHRACK, R. A., Proc. Conf. on Neutron Physics and Nuclear Data for Reactors and Other Applied Purposes, Harwell, Sept. 1978, p.736.
[8] MEISTER, A., MITTAG, S., PAPST, D., PILZ, W., SEELIGER D., SEIDEL, K., TSCHAMMER, H., TSCHAMMER, R. AND HERMSDORF, D., Nuclear Data for Science and Technology (EUR 8355) p.968 (1983).
[9] HARVEY, J. A., MOOK, H. A., HILL, N. W. AND SHAHAL, O., Ibid, p.961 (1983).
[10] HASTE, T. J. AND SOWERBY, M. G., J. Phys. D: App. Phys. 12 (1979) 1203.
[11] BUTLAND, A. T. D., Ann. Nuc. Sci. and Eng. 1 (1974) 575.
[12] MOXON, M. C., AERE-PR/NP 28, p.9 (1981).
[13] BRUGGER, R. M. AND AMINFAR, H., INDC(NDS)-129/GJ, p.271 (1981).
[14] BRUGGER, R. M. AND TSANG, F. Y., Proc. Conf. on Neutron Physics and Nuclear Data for Reactors and Other Applied Purposes, Harwell, Sept. 1978, p.343.
[15] MOXON, M. C., Unpublished.
[16] GOLINELLI, C. ET AL., ANS Topical Meeting on Reactor Physics and Shielding, Sun Valley, p.243 (1980).
[17] YUSADA, H., AKINO, F., TAKEUCHI, M. AND KANEKO, Y., J. Nucl. Sci. and Tech. 24 (1987) 431.
[18] OLSEN, D. K., DE SAUSSURE G., PEREZ, R. B., SILVER, E. G., DIFILIPPO, F. C., INGLE, R. W. AND WEAVER, H., Nucl. Sci. and Eng. 62 (1977) 479.
[19] MOXON, M. C., Neutron Data for Structural Materials for Fast Reactors, Edited by K. H. Böckhoff (Pergamon Press, Oxford 1979) p.644.

LIST OF PARTICIPANTS

G. AMBROSIUS
Kraftwerk Union AG
Dept. Manager ST 121
P.O. Box 3220
D-8520 Erlangen
Federal Republic of Germany

C.H.M. BROEDERS
Institut für Neutronenphysik
und Reaktortechnik
Kernforschungszentrum Karlsruhe
Postfach 3640
D-7500 Karlsruhe 1
Federal Republic of Germany

A.J. DERUYTTER
Joint Research Centre
Central Bureau of Nuclear Measurements
Steenweg naar Retie
B-2440 Geel, Belgium

M. HALSALL
Atomic Energy Establishment
Winfrith, Dorchester
Dorset, DT2 8DH, United Kingdom

Y. ISHIGURO
Japan Atomic Energy Research
Institute (JAERI)
Tokai-mura, Naka-gun
Ibaraki-ken 319-11, Japan

M.W. JANKOWSKI
(part-time)
International Atomic Energy Agency
Division of Nuclear Safety
Wagramerstr. 5, P.O. Box 100
A-1400 Vienna, Austria

E. JOHANSSON
Studsvik Energiteknik AB
S-611 82 Nyköping, Sweden

V.A. KONSHIN
(part-time)
International Atomic Energy Agency
Division of Physical and Chemical Sciences
Wagramerstr. 5, P.O. Box 100
A-1400 Vienna, Austria

H.D. LEMMEL
(Scientific Secretary)
IAEA Nuclear Data Section
Wagramerstr. 5, P.O. Box 100
A-1400 Vienna, Austria

L.V. MAIOROV
Institut Atomnoi Energii
I.V. Kurchatova
Ploschad Kurchatova
SU-123182 Moscow D-182, U.S.S.R.

D.R. MATHEWS
Eidgenossisches Institut
für Reaktorforschung
CH-5303 Würenlingen, Switzerland

M. MOXON
UK Atomic Energy Authority
Atomic Energy Research Establishment
Harwell, Didcot
Oxfordshire OX11 ORA, United Kingdom

A. OKAZAKI
Atomic Energy of Canada Limited
Chalk River Nuclear Laboratories
Chalk River, Ontario koJ 1JO, Canada

J.L. ROWLANDS
(Chairman)
Fast Reactor Physics Division
Room 220, Building B.21
Atomic Energy Establishment
Winfrith, Dorchester
Dorset, DT2 8DH
United Kingdom

A. SANTAMARINA
Dept. des Reacteurs a Eau, SEN
Centre d'Etudes Nucléaires de Cadarache
B.P. No. 1
F-13115 Saint-Pual-Lez-Durance, France

J.J. SCHMIDT
(part-time)
IAEA Nuclear Data Section
Wagramerstr. 5, P.O. Box 100
A-1400 Vienna, Austria

V.V. TEBIN
Institut Atomnoi Energii
I.V. Kurchatova
Ploschad Kurchatova
SU-123182 Moscow D-182, U.S.S.R.

H. TELLIER
Centre d'Etudes Nucléaires de Saclay
Service d'Etudes de Reacteurs et de
de Mathematiques Appliquées
F-91191 Gif-sur-Yvette, France

WANG DAHAI
(part-time)
IAEA Nuclear Data Section
Wagramerstr. 5, P.O. Box 100
A-1400 Vienna, Austria

H. WEIGMANN
Central Bureau of Nuclear Measurements
Steenweg naar Retie
B-2440 Geel, Belgium

89-00249